UniversitätsSpital Zürich

Direktion Forschung und Lehre

Programm

17th Day of Clinical Research

17. Hartmann Müller Gedächtnisvorlesung 2018
Georg-Friedrich-Götz-Preisverleihung 2018

Zurich, April 5, 2018

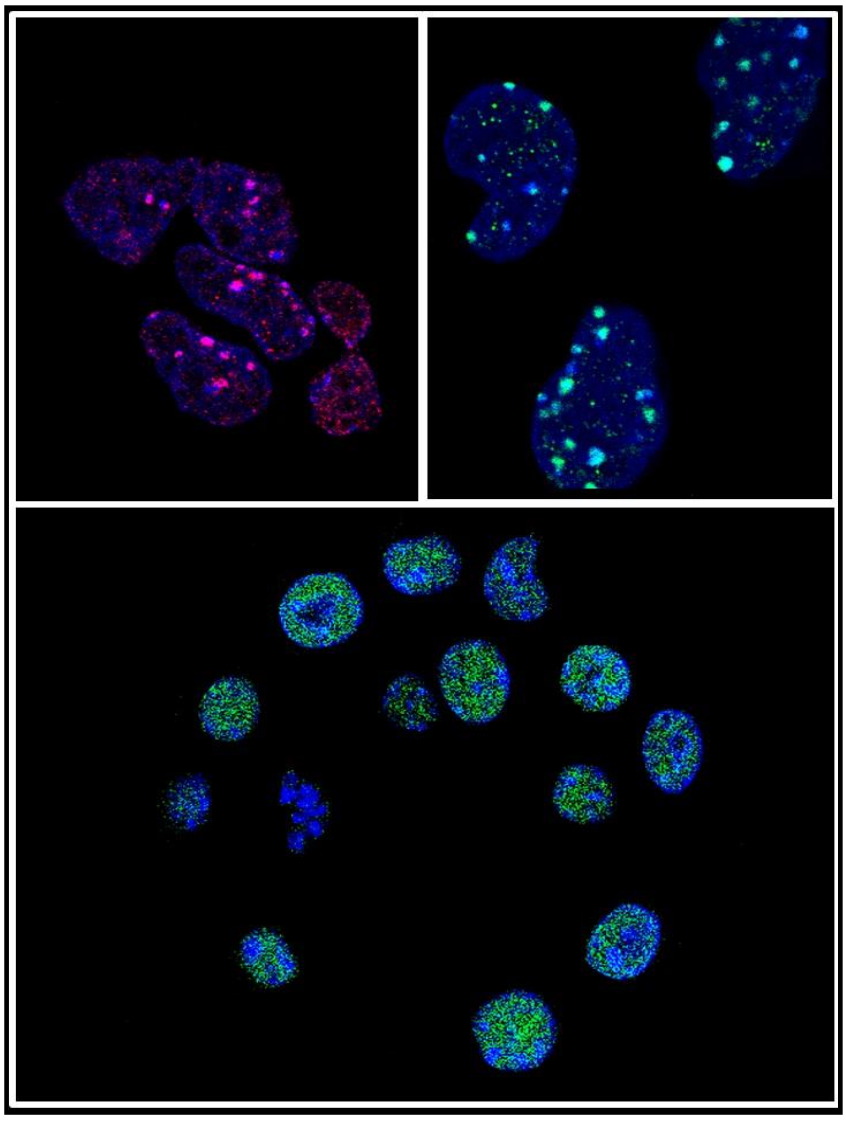

Universität Zürich[UZH]

Assoziierte Kliniken
Universitätsklinik Balgrist
Kinderspital Zürich
Psychiatrische Universitätsklinik Zürich
Zentrum für Zahnmedizin

Committee Day of Clinical Research

Prof. Dr. A. Aguzzi
Prof. Dr. O. Distler
Prof. Dr. R. Graf
Prof. Dr. H. Moch
Prof. Dr. G. Senti
Prof. Dr. R. Speck
Prof. Dr. M. Weller
Prof. Dr. A. von Eckardstein
PD Dr. Mira Katan Kahles
PD Dr. Paolo Cinelli
Robin Schneider, MBA

Table of contents

Bild Vorderseite: PD Dr. med. Paolo Cinelli & Dr. sc. nat. Urs Graf, UniversitätsSpital Zürich

Programm – Donnerstag, 5. April 2018

Grosser Hörsaal Ost

08.15 **Eröffnung**
Prof. Dr. med. Gabriela Senti
Direktorin Forschung und Lehre, UniversitätsSpital Zürich

08.20 **Begrüssung**
Prof. Dr. med. Jürg Hodler
Ärztlicher Direktor, UniversitätsSpital Zürich

08.25 **Begrüssung**
Prof. Dr. med. Claudia Witt
Prodekanin Interprofessionalität und Vorsitzende Fachbereich Internistische Fächer, Universität Zürich

Session 1: Cardiovascular Diseases/Metabolics/Endocrinology
Chairpersons: Prof. Dr. phil. Giovanni Camici / Prof. Dr. sc. nat. Thorsten Hornemann

08.35 Wissenschaftliches Hauptreferat
Heart Failure Moving Center Stage in Cardiology: A Tale of Drugs, Devices and Interventions
Prof. Dr. med. Frank Ruschitzka, Klinikdirektor, Klinik für Kardiologie, UniversitätsSpital Zürich

08.55 **Protective effect of obeticholic acid on obesity-induced cardiomyopathy**
C. Li, Y. Li, C. Hiller, G. Kullak-Ublick, Z. Gai

09.05 **Comprehensive molecular profiling in acute aortic dissection: seeking diagnostic biomarkers**
J. Gawinecka, H. Reiser, F. Schönrath, E. Arvaniti, C. Matter, V. Falk, M. Claassen, A. von Eckardstein

09.15 **Prognostic value of copeptin dynamics over 5 days after onset of ischemic stroke**
R. Senn, A.R. Luft, M. Christ-Crain, M.S. Katan

09.25 **Coffee Break**

Session 2: Hematology/Oncology
Chairpersons: PD Dr. med. Alessandra Curioni / Prof. Dr. med. Nicolaus Andratschke

09.40 Wissenschaftliches Hauptreferat
Life science improves survival- the melanoma experience
Prof. Dr. med. Reinhard Dummer, Stv. Klinikdirektor, Dermatologische Klinik, UniversitätsSpital Zürich

10.00 **Treatment of AML with immunotherapies**
R. Myburgh, J. Kiefer, S. Pfister, M. Wilk, N. Russkamp, C. Magnani, S. Alexander, A. Müller, M. Van Den Broek, B. Becher, D. Neri, M. Manz

10.10 **WNT-dependent regulation of SOX10 expression in melanoma development**
R. Uka, C. Britschgi, C. Matter, A. Kraettli, D. Mihic, M. Okoniewski, M. Levesque, R. Dummer, O. Shakhova

10.20 **Interim analysis of intervention trial evaluating focal therapy using high intensity focused ultrasound for the treatment of prostate cancer**
A. Mortezavi, J. Krauter, J. Sonderer, O. Donati, A. Gu, J. Bruhin, O. Gross, S. Kedzia, T. Sulser, D. Eberli

Session 3: Regenerative Medicine and Advanced Technologies
Chairpersons: PD Dr. med. Maurizio Calcagni / Prof. Dr. med. Roland Martin

10.35 Wissenschaftliches Hauptreferat
How the brain builds new nerve cells throughout life
Prof. Dr. med. Sebastian Jessberger, Direktor, Institut für Hirnforschung, Universität Zürich

10.55 **Healing-triggering biomaterials for the minimal-invasive treatment of iPPROM**
E. Avilla Royo, M. Ehrbar

11.05 **Development of an Off-the-Shelf Tissue Engineered Sinus Valve for Transcatheter Pulmonary Valve Replacement: A Proof-of-Concept Study**
S. Motta, E. Fioretta, P. Dijkman, V. Lintas, L. Behrendt, S. Hoerstrup, M. Emmert

11.15 **Quantitative Characterization of Bone Marrow Stroma Using Deep Learning**
A. Gomariz, P. Helbling, S. Isringhausen, U. Suessbier, A. Becker, A. Boss, G. Paul, G. Székely, S. Stoma, S. Nørrelykke, O. Goksel, M. Manz, C. Nombela-Arrieta

11.30 **Verleihung 17. Hartmann Müller Gedächtnisvorlesung**
Einführung und Preisverleihung durch Prof. Dr. phil. Bruno Weber, Präsident Hartmann Müller-Stiftung,
Institut für Pharmakologie und Toxikologie, Universität Zürich

11.40 **Vorlesung des Preisträgers**
Prof. Jeffrey D. Rothstein, MD, PhD, Neurologie, Johns Hopkins University, Baltimore, USA

12.20 **Lunch/Poster viewing**

12.20 **Verleihung Georg Friedrich Götz-Preis 2017**
mit anschliessendem Apéro Riche

Session 4: Infection/Immunity/Inflammation
Chairpersons: Prof. Cesar Nombela Arrieta / Prof. Dr. med. Annelies Zinkernagel

14.15 Wissenschaftliches Hauptreferat
Value of inflammatory parameterst o assest he clinical course after severe trauma
Prof. Dr. med. Hans-Christoph Pape, Klinikdirektor, Klinik für Traumatologie, UniversitätsSpital Zürich

14.35 **Validation of a novel xenograft mouse model for intestinal fistulas**
R. Bruckner, N. Marsiano, E. Nissim-Eliraz, E. Nir, M. Leutenegger, C. Gottier, S. Lang, M. Spalinger, G. Rogler, S. Yagel, M. Scharl, NY. Shpigel

14.45 **Mechanisms of adaptive resistance to cancer immunotherapy**
D. Sahin, N. Arenas-Ramirez, D. Zingg, L. Sommer, O. Boyman

14.55 **The effect of donor-recipient weight mismatch on kidney graft function – demand defines supply**
A. Figurek, L. Hapouja, V. Luyckx, T. Müller

Session 5: Neurosciences/Pharmacology

Chairpersons: Prof. Dr. Magdalini Poymenidou / Prof. Dr. Andreas Lutterotti

15.10 Wissenschaftliches Hauptreferat
Neuroimaging in translational stroke research
Prof. Dr. med. Susanne Wegener, Oberärztin, Klinik für Neurologie, UniversitätsSpital Zürich

15.30 **Reconstruction of the entire vascular web of the mouse brain by novel tissue clearing and imaging approaches**
D. Kirschenbaum, F. Voigt, A. Gomariz Carillo, M. Smith, C. Nombela Arrieta, F. Helmchen, A. Aguzzi

15.40 **The globular domain of the prion protein induces prion neurotoxicity through decreased rigidity of its b2a2 loop**
K. Frontzek, M. Bardelli, US. Herrmann, T. Sonati, R. Reimann, M. Carta, C. Zhu, S. Hornemann, L. Varani, A. Aguzzi

15.50 **Preoperative embolization of meningioma: inferior neurological outcome, increased risk of cardiovascular complications and shorter time to recurrence?**
H-G. Wirsching, J. Richter, F. Sahm, C. Morel, N. Krayenbühl, E. Rushing, A. Von Deimling, A. Valavanis, M. Weller

16.00 **Coffee Break**

Session 6: Klinische Forschungsschwerpunkte KFSP

16.15 **Präsentation**
KFSP: Viral Metagenomic profiling
Prof. Dr. med. Nicolas Müller, Leitender Arzt, Klinik für Infektionskrankheiten und Spitalhygiene, UniversitätsSpital Zürich

16.35 **Präsentation**
KFSP: Sleep and Health
Prof. Dr. med. Christian Baumann, Leitender Arzt, Klinik für Neurologie, UniversitätsSpital Zürich

17.00 **Verleihung Day of Clinical Research Preis**

17.15 **Apéro**

Cardiovascular Diseases / Metabolics / Endocrinology

Basic Research

3921
J. Von Spiczak, M. Mannil, B. Peters, T. Hickethier, R. Manka, D. Maintz, H. Alkadhi
Photon Counting CT with Dedicated Sharp Convolution Kernels: Tapping the Potential of a New Technology for Stent Imaging

3922
J. Von Spiczak, R. Manka, M. Mannil, S. Oebel, S. Hamada, K. Higashigaito, F. Ruschitzka, H. Alkadhi
3D Fusion of Coronary CT Angiography and CT Myocardial Perfusion Imaging: Intuitive Assessment of Morphology and Function

3968
D. Schoenenberg, G. Osterhoff
CT-based evaluation of volumetric bone density in fragility fractures of the pelvis – a matched case-control-analysis

3974
Z. Gai, C. Hiller, I. Alecu, S. Youhanna, M. Lone, T. Hornemann, G. Kullak-Ublick
FXR activation protects liver from nonalcoholic fatty liver disease through decreasing sphingolipid levels

3997
C. Li, Y. Li, C. Hiller, G-A. Kullak-Ublick, Z. Gai
Protective effect of obeticholic acid on obesity-induced cardiomyopathy

4009
J. Hutmacher, S. Brandt, N. Samartzis, I. Ihnenfeld, A. Noske, D. Fink, P. Imesch, E. Samartzis
ARID1A expression is ubiquitously retained in adenomyosis in contrast to endometriosis

Translational Research

3945
J. Gawinecka, H. Reiser, F. Schönrath, E. Arvaniti, C. Matter, V. Falk, M. Claassen, A. Von Eckardstein
Comprehensive molecular profiling in acute aortic dissection: seeking diagnostic biomarkers

3951
M. Mannil, J. Von Spiczak, R. Manka, H. Alkadhi
Texture Analysis and Machine Learning for Detecting Myocardial Infarction in Non-Contrast Low Dose CT: Unveiling the Invisible

3952
M. Mannil, J. Von Spiczak, T. Hermanns, H. Alkadhi, C. Fankhauser
Predicting the Success to Shock Wave Lithotripsy: Added Value of 3D Texture Analysis and Machine Learning on CT Images of Urinary Stones

3979
D. Gero, R. Steinert, H. Hosa, D. Cummings, M. Bueter
Appetite, Glycemia, and Entero-Insular Hormone Responses Differ Between Oral, Gastric-Remnant, and Duodenal Administration of a Mixed Meal Test After Roux-en-Y Gastric Bypass

4001
E. Fioretta, A. Ksiazek, M. Putti, A. Fallahi, T. Mes, A. Bosman, C. Cesarovic, E.Caliskan, H. Rodriguez, P. Dankers, C. Bouten, S. Hoerstrup, M. Emmert
Developing a Biodegradable Polymer-based Transcatheter Aortic Valve for the Young: a Proof-of-concept Study in Sheep

4013
M. Hashimoto, O. Lauk, M. Friess, W. Weder, I. Schmitt-Opitz
Poor nutritional status is a poor prognostic factor in a patient candidate for multimodal treatment for malignant pleural mesothelioma

4070
M. Yalcinkaya, M. Cardner, S. Goetze, M. Hunjadi, A. Ritsch, J. Hartung, U. Landmesser, G. Liebisch, B. Wollscheid, N. Beerenwinkel, L. Rohrer, A. Von Eckardstein
A Systems Biological Approach to the Anti-Atherogenicity of High Density Lipoproteins

4073
S. Bengs, I. Burger, C. Lohmann, M. Messerli, A. Becker, V. Treyer, M. Schwyzer, D. Benz, A. Giannopoulos, K. Kudura, C. Gräni, O. Gämperli, A. Pazhenkottil, R. Büchel, P. Kaufmann, C. Gebhard
Age- and Sex-dependent Changes in Sympathetic Activity of the Left Ventricular Apex Assessed by 18F-DOPA PET Imaging

4086
M. Baláz, E. Luca, M. Yalcinkaya, M. Cardner, S. Goetze, L. Rohrer, J. Hartung, U. Landmesser, G. Liebisch, B. Wollscheid, N. Beerenwinkel, J. Krützfeldt, C. Wolfrum, A. Von Eckardstein
A Systems Biological Approach to the Anti-Diabetogenicity of High Density Lipoproteins

4101
M. Kölling, C. Genschel, T. Kaucsar, A. Hübner, S. Rong, R. Schmitt, I. Soerensen-Zender, G. Haddad, A. Kistler, H. Seeger, J. Kielstein, D. Fliser, H. Haller, R. Wüthrich, M. Zörnig, T. Thum, J. Lorenzen
Hypoxia-induced long non-coding RNA Malat1 is dispensable for renal ischemia/reperfusion-injury

4107
M. Kölling, H. Seeger, G. Haddad, A. Kistler, A. Nowak, R. Faulhaber-Walter, H. Haller, D. Fliser, T. Mueller, R. Wüthrich, J. Lorenzen
Circular RNAs in critically ill patients with acute kidney injury

Clinical Trials

3966
A. Schneider, A. Rickenbacher, L. Frick, D. Cabalzar-Wondberg, S. Käser, P-A. Clavien, M. Turina
Insurance status influences the use of minimally invasive surgical techniques, but does not affect the rate of postoperative complications

3972
M. Gagesch, P. Chocano-Bedoya, J. Kanis, B. Vellas, R. Rizzoli, H. Bischoff-Ferrari
Physical Frailty and Quality of Life – Baseline data from a large European Multi-Centre Trial (DO-HEALTH)

3978
R. Peterli, B. Wölnerhanssen, T. Peters, D. Vetter, D. Kröll, Y. Borbély, B. Schultes, C. Beglinger, J. Drewe, M. Schiesser, P. Nett, M. Bueter
Effect of laparoscopic sleeve gastrectomy vs laparoscopic Roux-en-Y gastric bypass on weight loss in patients with morbid obesity: a randomized clinical trial

4042
P. Lanz, K. Fischer, H. Bischoff-Ferrari
Association of cognitive function and mental health with quality of life in seniors with severe knee osteoarthritis undergoing total knee replacement surgery

4049
R. Senn, A. Luft, M. Christ-Crain, M. Katan
Prognostic value of copeptin dynamics over 5 days after onset of ischemic stroke

4068
A. Figurek, V. Luyckx, T. Müller
Renal functional reserve in living kidney donors: Do we know enough?

Hematology / Oncology

Basic Research

3961
D. Vuong, M. Bogowicz, M. Huellner, P. Veit-Haibach, N. Andratschke, J. Unkelbach, M. Guckenberger, S. Tanadini-Lang
Robustness study on radiomic features in [18F]-FDG PET/CT and [18F]-FDG PET/MR

3964
B. Pouymayou, O. Riesterer, M. Guckenberger, J. Unkelbach
A Bayesian network model for personalized elective CTV definition in head & neck cancer

3986
N. Russkamp, R. Myburgh, J. Kiefer, A. Müller, M. Van Den Broek, B. Becher, D. Neri, M. Manz
Generation of mouse CAR T-cells for the depletion of cKIT-positive hematopoietic cells

3993
Y. Chang, D. Ignatova, D. Kollmann, T. Schweiger, S. Schwarz, G. Lewik, S. Schoppmann, W. Hoetzenecker, W. Klepetk, K. Hoetzenecker, E. Guenova
PD1-positive tumor-infiltrating lymphocytes are associated with poor clinical outcome after pulmonary metastasectomy for colorectal cancer

3996
D. Ignatova, D. Kollmann, J. Jedamzik, YT. Chang, G. Jomrich, A. Baierl, D. Kazakov, M. Michal, W. Hoetzenecker, T. Schatton, L. French, R. Asari, M. Preusser, M. Gnant, S. Schoppmann, E. Guenova
PD-L1 expression is an independent predictor of favorable outcome in patients with localized esophageal adenocarcinoma

4003
T. Kazimova, M. Pruschy
Identification of Biologically Active Factors in Ionizing Radiation Regulated Secretome

4005
A. Okonska, S. Bühler, V. Rao, M. Ronner, M. Blijlevens, I. Van der Meulen-Muileman, R. De Menezes, E. Smit, W. Weder, R. Stahel, L. Penengo, V. Van Beusechem, E. Felley-Bosco
Whole-genome RNAi Screen Reveals a Potential Therapy Depending on BAP1 Status in Malignant Pleural Mesothelioma

4022
L. Kovtonyuk, H. Takizawa, M. Manz
Intrinsic and Extrinsic Determinants of Hematopoietic Stem Cells Aging

4041
A. Papachristodoulou, R. Signorell, B. Werner, D. Brambilla, M. Rudin, J. Grandjean, E. Martin, M. Weller, J. Leroux, P. Roth
Overcoming temozolomide resistance in experimental gliomas: MRI-guided focused ultrasound-mediated blood-brain barrier opening facilitates the local delivery of liposome encapsulated MGMT inhibitors

4043
G. Spaltro, L. Kovtonyuk, M. Manz
Dissecting Mechanisms that Drive Hematopoietic Stem Cells to Quiescence

4045
L. Roth, E. Breuer, R. Graf, A. Gupta, P.-A. Clavien, K. Lehmann
The impact of HIPEC (chemotherapy plus hyperthermia) treatment on the immunogenicity of cancer cells

4046
S. Steiner, G. Wanner- Seleznik, T. Reding, A. Gupta, D. Lenggenhager, K. Endhardt, R. Graf
Identification of Gastrokine, a gastric tumor suppressor, in pancreatic carcinogenesis

4047
A. Krättli, R. Uka, M. Levesque, R. Dummer, O. Shakhova
The role of SOX10 in melanoma resistance

4048
R. Myburgh, J. Kiefer, S. Pfister, M. Wilk, N. Russkamp, C. Magnani, S. Alexander, A. Müller, M. Van den Broek, B. Becher, D. Neri, M. Manz
Treatment of AML with immunotherapies

4052
C. Yang, M. Gualandi, N. Jauquier, J. Joseph, K. Balmas Bourloud, A. Mühlethaler-Mottet, O. Shakhova
The Metastatic Role of SOX9 in Neuroblastoma

4053
U. Süssbier, HC. Wong, A. Gomariz, S. Isringhausen, P. Helbling, T. Nagazawa, M. Manz, A. Müller, C. Nombela-Arrieta
Functional and structural dynamics of the bone marrow stromal microenvironment after cytoreductive therapies

4059
H. Rehrauer, L. Wu, W. Blum, L. Pecze, T. Henzi, V. Serre-Beinier, C. Aquino, B. Vrugt, M. De Perrot, B. Schwaller, E. Felley-Bosco
How asbestos drives tumor development: YAP activation, macrophage and mesothelial precursor recruitment, RNA editing and somatic mutations

4061
M. Meerang, J. Kreienbühl, V. Orlowski, M. Kirschner, W. Weder, I. Opitz
Role of Cullin4 Ubiquitin Ligase in Malignant Pleural Mesothelioma

4062
D. Cabalzar-Wondberg, D. Birrer, A. Rickenbacher, S. Käser, M. Schneider, M. Turina
Rate of inapparent pathology in clinically inconspicuous specimens following routine hemorrhoidectomy

4071
M. Healy, Y. Boege, M. Hodder, F. Boehm, A. Scherr, M. Malehmir, J. Muhic, C. Klose, A. Macpherson, B. Koehler, M. Heikenwalder, A. Weber
MCL-1 is a tumor suppressor ensuring intestinal mucosal integrity and stem cell homeostasis independent of microbiota-driven inflammation

4075
LV. Isenegger, R. Zuber, P. Bode, T. Van Cann, C. Pauli, A. Wozniak, U. Camenisch, C. Matter, B. Bode, H. Moch, M. Manz, O. Shakhova, P. Schoeffski, C. Britschgi
Therapeutic Targeting of Clear Cell Sarcoma

4080
P. Helbling, S. Isringhausen, A. Gomariz-Carillo, U. Suessbier, T. Nagasawa, T. Yokomizo, M. Manz, C. Nombela-Arrieta
Identification of key niche cell types supporting expansive extramedullary hematopoiesis in the fetal liver.

4082
H. Honcharova-Biletska, M. Egger, F. Bohm, Y. Boege, M. Healy, J. Schmidt, S. Comtesse, R. Davis, M. Heikenwalder, A. Weber
A role of JNK signaling for biliary tract formation

4085
M. Gualandi, AE. Serra Roma, C. Yang, A. Baggiolini, L. Sommer, O. Shakhova
Dissecting the cellular origin of neuroblastoma: Characterization of new progenitor cell populations in the sympathetic nervous system.

4098
J. Kresoja-Rakic, A. Szpenchcinski, F. Cerciello, M. Kirchner, M. Ronner, R. Stahel, W. Weder, E. Felley- Bosco
Circulating non coding RNAs in liquid biopsies before and after chemotherapy reveals two groups of malignant pleural mesothelioma patients

4103
JH. Jang, M. Haberecker, A. Curioni , F. Janker, A. Soltermann, W. Weder, W. Jungraithmayr
The expression pattern of CD26/DPP4 in human lung cancer

4115
HC. Wong, S. Isringhausen, M. Manz, C. Nombela-Arrieta, A. Müller
Characterization of Bone Marrow GVHD post Allogeneic Hematopoietic Cell Transplantation in Mice

Translational Research

3930
A. Curioni Fontecedro, P. Tallon de Lara, V. Cecconi, S. Hiltbrunner, H. Yagita, M. Friess, B. Bode, I. Schmitt-Opitz, B. Vrugt, W. Weder, E. Felley- Bosco, R. Stahel, V. Tischler, D. Soldini, H. Moch, M. Van den Broek
Gemcitabine synergizes with immune-checkpoint inhibitors: from a preclinical model to mesothelioma patients

3994
M. Kirschner, B. Vrugt, M. Friess, M. Meerang, P. Wild, N. Van Zandwijk, G. Reid, W. Weder, I. Opitz
A combined microRNA-clinical Score as prognostic factor for malignant pleural mesothelioma

3998
V. Lysenko, N. Wildner, K. Zimmermann, P. Schürch, C. Fritz, L. Calabresi, A. Vannucchi, R. Flavell, P. Wild, M. Manz, A. Theocharides
Enhanced support of myelofibrosis stem cells in next generation humanized mice

4012
P. Busenhart, L. Hering, K. Atrott, E. Patsenker, F. Stickel, K. Bäbler, B. Weder, A. Wyss, G. Rogler, M. Spalinger, M. Scharl
Pharmacologic inhibition of integrin αvβ6 causes tumor shrinkage in the DSS/AOM mouse colon tumor model

4016
C. Corrò, M. Healy, S. Engler, P. Schraml, B. Bodenmiller, A. Weber, I. Frew, M. Rechsteiner, H. Moch
Renal cancer stem cells are characterized by IL8 and CXCR1 expression.

4017
T. Wildschut, P. Schürch, M. Van Oostrum, E. Milani, B. Wollscheid, A. Theocharides
The Consequence of CALR Mutations on Proteostasis in Myeloproliferative Neoplasms

4050
H. Bolck, C. Corrò, A. Von Teichman, C. Pauli, P. Schraml, H. Moch
A critical evaluation of in vitro renal cancer cell models for translational studies

4055
J. Friemel-Bauersfeld, I. Torres, E. Brauneis, A. Schäffer, M. Gertz, T. Ried, A. Weber, K. Heselmeyer-Haddad
Single cell-based assessment of copy number changes in nonalcoholic fatty liver disease (NAFLD), nonalcoholic steatohepatitis (NASH) and NASH-induced hepatocellular carcinoma (HCC).

4063
R. Uka, C. Britschgi, C. Matter, A. Kraettli, D. Mihic, M. Okoniewski, M. Levesque, R. Dummer, O. Shakhova
WNT-dependent regulation of SOX10 expression in melanoma development

4064
A . Batavia, M. Lukamowicz-Rajska, J. Kuipers, P. Schraml, N. Beerenwinkel, H. Moch
Characterising renal cell cancer with wild type VHL clear cell renal cell cancers as a focal point.

4069
Y. Zhang, V. Orlowski, B. Vrugt, M. Friess, W. Weder, I. Opitz, M. Kirschner
Identification of microRNAs as chemosensitivity-related biomarkers in MPM patients
4081
F. Meier-Abt, S. Amon, L. Gillet, W. Wolski, S. Dimitrieva, A. Theocharides, M. Manz, R. Aebersold
Transcriptome-Proteome Correlation in Human Hematopoietic Stem and Progenitor Cells

4084
P. Cheng, S. Freiberger, N. Pornputtapong, A. Irmisch, M. Khan, R. Halaban, R. Dummer, P. Wild, M. Krauthammer, M. Levesque
Melarray - a new sequencing platform for detecting genomic mutations and copy number changes in melanoma

4087
I. Grgic, N. Borgeaud, A. Gupta, P.-A. Clavien, M. Guckenberger, R. Graf, M. Pruschy
Tumor reoxygenation and image-guided SBRT for the treatment of hypoxic tumors

4088
S. Ehrbar, A. Jöhl, M. Kühni, M. Meboldt, E. Ozkan Elsen, O. Goksel, Ch. Tanner, S. Klöck, J. Unkelbach, M. Guckenberger, S. Tanadini-Lang
DELPHI: Dynamically deformable liver phantom for real-time adaptive radiotherapy treatments

4095
P. Schürch, T. Wildschut, E. Milani, B. Wollscheid, A. Theocharides
Functional differences between CALR mutations in the pathogenesis of Myeloproliferative Neoplasms

4114
AE. Serra Roma, M. Gualandi, A. Siebenhuener, M. Manz, O. Shakhova
Generation of neuroendocrine organoids

4118
Ph. Knobel, M. Pruschy
The BioID method: Opportunity for translational research

Clinical Trials

3923
A. Mortezavi, J. Krauter, J. Sonderer, O. Donati, A. Gu, J. Bruhin, O. Gross, S. Kedzia, T. Sulser, D. Eberli
Interim analysis of intervention trial evaluating focal therapy using high intensity focused ultrasound for the treatment of prostate cancer: safety, functional, psychological and oncological outcome 6 months after treatment

3929
K. Slankamenac, A. Neuenschwander, D. Keller
Need for early identification of palliative patients in the Emergency Department to decide best supportive strategies

3995
O. Lauk, K. Brüstle, M. Friess, T. Nguyen, T. Frauenfelder, R. Stahel, W. Weder, I. Opitz
Preoperative addition of anti-angiogenic bevacizumab to standard inductioncisplatin/pemetrexed does not increase the risk of acute postoperative bleeding after surgery for malignant mesothelioma

4008
R. Brun, E. Spoerri, L. Schäffer, R. Zimmermann, C. Haslinger
Induction of labor and postpartum blood loss

4014
D. Franke, J. Zepf, T. Burkhardt, P. Stein, R. Zimmermann, C. Haslinger
Impact of the etiology behind retained placenta on postpartum blood loss

4030
M. Müller, A. Rickenbacher, M. Schneider, D. Cabalzar-Wondberg, S. Käser, M. Turina
Young patients with colorectal cancer present with more advanced tumors and lymph node metastases

4033
M. Kahr, R. Brun, R. Zimmermann, C. Haslinger
Validation of a quantitative System for real-time Measurement of postpartum Blood Loss: A prospective Cohort Study in the daily Obstetric Setting

4034
M. Kahr, D. Franke, R. Brun, J. Wisser, R. Zimmermann, C. Haslinger
Blood Group 0: A novel Risk Factor for increased Postpartum Blood Loss?

4036
E. Kapfhammer, T. Pfammatter, D. Balsyte, R. Zimmermann, C. Haslinger
Success rate and long-term effects of embolization of pelvic arteries for the treatment of postpartum hemorrhage

4078
S. Angori, A. Kahraman, R. Ohashi, F. Prutek, S. Dettwiler, P. Schraml, H. Moch
Chromosomal Profiling of papillary Renal Cell Carcinoma

Regenerative Medicine and Advanced Technologies

Basic Research

3970
A. Gomariz, P. Helbling, S. Isringhausen, U. Suessbier, A. Becker, A. Boss, G. Paul, G. Székely, S. Stoma, S. Nørrelykke, O. Goksel, M. Manz, C. Nombela-Arrieta
Quantitative Characterization of Bone Marrow Stroma Using Deep Learning

3981
D. Gero, B. File, J. Justiz, A. Spector, M. Bueter
A drinkometer to analyze microstructure of drinking in humans: a proof of concept study in healthy adults

4004
D. Canepa, E. Casanova, V. Tosevski, B. Eggerschwiler, E. Arvaniti, M. Claassen, HC. Pape, P. Cinelli
Dissecting the Mesenchymal Stem Cells Heterogeneity for Clinical Applications

4006
U. Blache, Q. Vallmajo-Martin, V. Milleret, M. Ehrbar
3D cell biology meets synthetic materials: Microvascular network formation by endothelial cells in ECM-free hydrogels

4011
T. Maeyashiki, S. Arni, I. Iskender, W. Weder, I. Inci
The impact of perfusion temperature during ex vivo lung perfusion in donation after circulatory death donors

4020
E. Avilla Royo, M. Ehrbar
Healing-triggering biomaterials for the minimal-invasive treatment of iPPROM

4024
L. Reissner, G. Fischer, P. Giovanoli, M. Calcagni
Kinematic analysis of the hand during opening a jar and yoghurt

4025
L. Reissner, G. Fischer, P. Giovanoli, M. Calcagni
Wrist and Finger motion: A comparison of goniometric and 3D motion capture technique

4026
L. Reissner, G. Fischer, P. Giovanoli, M. Calcagni
Gender difference in kinematic analysis of hand movements during opening a yoghurt

4037
I. Iskender, T. Maeyashiki, S. Arni, M. Lipiski, S. Fehlings, T. Frauenfelder, M. Krafft, D.Spahn, W. Weder, I. Inci
Treatment of donor lungs with perfluorocarbon based oxygen carrier during ex vivo lung perfusion in uncontrolled donation after cardiac death

4108
P. Pagella, C. Cantù, G. Russo, M. Schwab, T. Mitsiadis
Nogo-A is a gate-keeper of stem cell niches

4110
A. Eijkenboom, L. Ebert, J. Plock, R. Schweizer, P. Kamat
Automated vessel recognition and vessel wall analysis in tissue sections using deep learning

4117
E. Malagola, R. Chen, M. Bombardo, E. Saponara, T. Reding, R. Graf, S. Sonda
Deiodinase type 3 (DIO3) limits acinar cell proliferation following acute pancreatitis

Translational Research

3937
W. Baumgartner, L. Otto, SC. Hess, WJ. Stark, S. Märsmann, M. Calcagni, P. Cinelli, J. Buschmann
Biomimetic Cartilage/ Bone Interface

3938
N. Cohrs, K. Schulz-Schönhagen, D. Mohn, W. Stark, P. Wolint, G. Meier Bürgisser, J. Buschmann
Modification of silicone elastomers with Bioglass 45S5® increases in vivo tissue biointegration

3944
I. Schneider, W. Baumgartner, O. Gröninger, W. Stark, S. Märsmann, M. Calcagni, P. Cinelli, P. Wolint, J. Buschmann
Impact of cultivation condition and cell format of human adipose-derived stem cells: 3D-microtissues versus single cells seeded on an electrospun nanocomposite in a perfusion bioreactor or static cell culture

3950
C. Greis, C. Zürcher, V. Djamei, A. Moser, S. Lautenschlager, A. Navarini
Unmet digital Health Service Needs in Dermatology Patients

3985
A. Leblond, R. Casanova, M. Rechsteiner, P. Wild, A. Jones, D. Heintze, A. Ciftlik, A. Soltermann
Assessment of predictive biomarkers in cancer tissues using micro-immunohistochemistry followed by DNA sequencing

4021
Q. Vallmajo-Martin, M. Lütolf, M. Ehrbar
Deciphering hematopoietic stem cell niche factors in bioengineered human bone marrow models in vivo

4056
N. Sanchez Macedo, M. McLuckie, L. Gruenherz, R. Lorenzini, D. Rittirsch, S. Uyulmaz, P. Giovanoli, N. Lindenblatt
Nanofat: novel tissue regeneration factors and molecular profiling

4083
V. Lintas, E. Fioretta, P. Dijkman, E. Caliskan, H. Rodriguez, N. Cesarovic, S. Hoerstrup, M. Emmert
Human cell derived off-the-shelf Tissue Engineered Heart Valves for next generation Transcatheter Aortic Valve Replacement: a proof-of-concept study in adult sheep

4105
S. Motta, E. Fioretta, P. Dijkman, V. Lintas, L. Behrendt, S. Hoerstrup, M. Emmert
Development of an Off-the-Shelf Tissue Engineered Sinus Valve for Transcatheter Pulmonary Valve Replacement: A Proof-of-Concept Study

Clinical Trials

4028
O. Politikou, T. Giesen, R. Guggenberger, S. Wirth, P. Giovanoli, M. Calcagni
Free vascularised corticoperiosteal medial femoral condyle flap for ankle and midfoot reconstruction; efficiency and donor site morbidity.

4035
A. Vent, Ch. Surber, N. Graf, J. Jürg
Painless local anesthesia with bicarbonate admixture in a ratio of 3:1: A phase II, monocentric, double blind, randomized, placebo controlled trial

4104
I. Besmens, M. Calcagni, T. Giesen
Reducing the immobilization period after DIP arthroplasty through a new dorsal approach

4106
I. Besmens, T. Giesen, O. Politikou, M. Calcagni
Finger reconstruction with dorsal metacarpal and dorsal finger flaps based on the dorsal branches of the palmar digital arteries. 40 consecutive cases.

Infection / Immunity / Inflammation

Basic Research

3924
C. Vulin, N. Leimer, M. Huemer, M. Ackermann, A. Zinkernagel
Prolonged lag time results in Small Colony Variants and reflects persisters in vivo

3931
V. Jeger, M. Arrigo, C. Schaer, F. Hildenbrand, M. Arras, G. Schoedon-Geiser, D. Spahn, D. Bettex, A. Rudiger
Heart rate elevations during early sepsis predict death in fluid resuscitated rats with faecal peritonitis

3932
R. Bruckner, N. Marsiano, E. Nissim-Eliraz, E. Nir, M. Leutenegger, C. Gottier, S. Lang, M. Spalinger, G. Rogler, S. Yagel, M. Scharl, N. Shpigel
Validation of a novel xenograft mouse model for intestinal fistulas

3939
M. Schwarzfischer, M. Morsy, C. Stanzl, K. Atrott, S. Lang, G. Rogler, M. Scharl, M. Spalinger
Heat shock protein GP96 is essential for self renewal of the intestinal epithelial barrier

3940
A. Özcan, D. Bunton, G. Macluskie, M. McAteer, T. Coulter, Y. Ding, U. Peral, O. Boyman, A. Kolios
Topical MTX-GNPs reduce IMQ-induced inflammation in mice

3946
A. Wyss, T. Raselli, G. Schmelczer, M. Spalinger, K. Atrott, I. Frey-Wagner, A. Sailer, M. Scharl, G. Rogler, B. Misselwitz
Role of EBI2 and Oxysterols in the Development of Intestinal Lymphoid Structures and Colitis

3948
M. Spalinger, M. Schwarzfischer, A. Geirnaert, C. Gottier, S. Lang, C. Lacroix, G. Rogler, M. Scharl
Loss of PTPN22 abrogates the beneficial effect of fecal microbiota transfer

3949
M. Spalinger, M. Schwarzfischer, L. Hering, A. Geirnaert, C. Gottier, S. Lang, C. Lacroix, G. Rogler, M. Scharl
Presence of an autoimmunity-associated variant in PTPN22 promotes chronic colitis in a microbiota dependent manner

3958
L. Hering, C. Gottier, S. Lang, B. Becher, G. Rogler, M. Scharl, M. Spalinger
Loss of PTPN2 in dendritic cells promotes T cell activation and expression of co-stimulatory molecules

3963
S. Isringhausen, U. Süssbier, N. Kräutler, L. Kovtonyuk, A. Gomariz-Carillo, P. Helbling, HC. Wong, M. Manz, A. Oxenius, C. Nombela-Arrieta
Chronic viral infections induce major disruption of bone marrow stromal cell networks and persistent loss of hematopoietic stem cell function

3969
C. Muller, C. Fenwick, G. Pantaleo, C. Münz, R. Speck
In vivo control of HIV-1 infection by broadly neutralzing antibodies in humanized mice

3971
N. Keller, J. Woytschak, E. Marques-Maggio, O. Boyman, A. Norrby-Teglund, A. Zinkernagel
Streptococcal DNase interferes with migration and type I IFN secretion of plasmacytoid dendritic cell

3973
C. Maeyashiki, H. Melhem, K. Baebler, S. Lang, M. Scharl, G. Rogler, C. De Valliere
Activation of pH-Sensing Receptor OGR1 (GPR68) Induces ER Stress and Autophagy in an Intestinal Epithelial Cell Model

3975
M. Gruenbach, G. Schreiber, E. Schlaepfer, S. Bredl, B. Escher, M. Schlapschy, A. Skerra, R. Speck
Do different IFN-α subtypes have distinct biological activities?

3983
V. Dengler Haunreiter, N. Leimer, D. Wipfli, C. Rachmühl, Y. Achermann, S. Benussi, R. Zbinden, A. Zinkernagel
In vivo evolution of Staphylococcus epidermidis in a patient with pacemaker-associated endocarditis

3987
D. Heinzer, M. Avar, M. Pfammatter, L. Irpinio, R. Moos, B. Kuhn, S. Mauerhofer, U. Rosenberg, A. Aguzzi, S. Hornemann
A screen for prion decontaminants to enhance safety of surgical instrument reprocessing

3988
K. Baebler, C. Maeyashiki, P. Busenhart, M. Schwarzfischer, K. Atrott, S. Lang, M. Spalinger, M. Scharl, G. Rogler, C. De Vallière
A novel OGR1 (GPR68) inhibitor attenuates inflammation in a murine model of acute colitis

3989
YT. Chang, M. Ziegler, D. Ignatova, P. Ivanov, R. Profanter, K. Kerl, J. Hafner, R. Clark, R. Dummer, E. Contassot, L. French, S. Misailovic, A. Cozzio, M. Vechev, W. Hoetzenecker, E. Guenova
HLA I shield tumor skin T lymphocytes from NK-cell-mediated elimination

3992
D. Ignatova, YT. Chang, A. Cozzio, R. Dummer, L. French, W. Hoetzenecker, E. Guenova
Malignant T cells inhibit anti-cancer immunity in cutaneous T cell lymphoma

4000
M. Raeber, R. Rosalia, D. Schmid, O. Boyman
IL-2-driven activation and expansion of dendritic cells

4007
R. Higgins, A. Jensen, C. Has, L. Bruckner-Tuderman, R. Spiegel, H. Traber, J. Achermann, M. Schaller, B. Fehrenbacher, M. Röcken, D. Ignatova, Y. Chang, L. French, W. Hoetzenecker, R. Hornung, A. Malzacher, A. Cozzio, A. Navarini, E. Guenova
Uniparental inheritance of junctional epidermolysis bullosa through a novel mutation of the ITGA6 gene and trisomic rescue.

4018
R. Higgins, M. Theiler, A. Smith, R. Wälchli, L. Weibel
Genetic Architecture of Linear Localized Scleroderma

4051
D. Impellizzieri, Y. Yamada, Y. Yamada, T. Nguyen, J. Jang, U. Karakus, I. Inci, C. Benden, W. Weder, W. Jungraithmayr, O. Boyman
Induction of tolerance by interleukin-2 complexes in experimental lung transplantation

4079
T. Turk, N. Bachmann, C. Kadelka, J. Böni, S. Yerly, V. Aubert, T. Klimkait, M. Battegay, E. Bernasconi, A. Calmy, M. Cavassini, H. Furrer, M. Hoffmann, H. Günthard, R. Kouyos
Assessing the danger of self-sustained HIV epidemics from phylogenetic cluster analysis

4096
S. Chaudron, K. Metzner, A. Marzel, J. Böni, S. Yerly, T. Klimkait, R. Kouyos, H. Günthard
A molecular epidemiology approach to identify HIV-1 superinfection in the Swiss HIV Cohort study

4099
D. Heuberger, A. Franchini, R. Schüpbach
Monitoring of proinflammatory mediators NF-κB and IL-8 in a human overexpression system

4116
R. Chen, Th. Hornemann, W. Yu, S. Camarago, R. Graf, S. Sonda,
1-Deoxy-Sphingolipids, novel biomarkers of diabetes, are cytotoxic for exocrine pancreatic cells

4119
C. Pothmann[1]; H.-C. Pape[1], H.-P. Simmen[1], V. Neuhaus[1]
Does the immunosuppressive therapy influence postoperative fracture healing after organ transplantation?

Translational Research

3934
HA. Mbunkah, A. Marzel, S. Schmutz, YL. Kok, O. Zagordi, M. Shilaih, N. Nsanwe, E. Mbu, L. Besong, B. Sama, E. Orock, R. Kouyos, H. Günthard, K. Metzner
Low Prevalence of Transmitted HIV-1 Drug Resistance Detected By a Dried Blood Spot Based NGS Method in Newly Diagnosed Individuals in Cameroon in the Years 2015/16

3935
P. Kamat, B. Kollar, R. Schweizer, J. Plock
Assessment of the vascular glycocalyx and the endothelium during graft vasculopathy following vascularized composite allotransplantation

3942
M. Brüggen, V. Djamei, E. Contassot, K. Kabashima, P. Romanelli, S. Oro, P. Wolkenstein, L. French
IRTEN - an international registry for toxic epidermal necrolysis

3984
V. Strouvelle, V. Vongrad, H. Günthard, K. Metzner
48 hours in the life cycle of patient-derived HIV-1 isolates in primary CD4+ T cells

4031
R. Schweizer, H. Klein, N. Fuchs, M. Waldner, B. Kollar, P. Kamat, F. Lehner, A. Taddeo, S. Salemi, D. Eberli, P. Giovanoli, J. Plock
Adipose-derived Stromal Cells attenuate Acute Rejection and Graft Vasculopathy in Rodent Vascularized Composite Allotransplantation

4032
R. Schweizer, M. Waldner, H. Klein, N. Fuchs, F. Lehner, S. Salemi, D. Eberli, A. Taddeo, P. Giovanoli, J. Plock
Evaluation of a Novel Conditioning Regimen including Belatacept, Cylophosphamid and Adipose-derived Stromal Cells in Rodent Vascularized Composite Allotransplantation

4038
I. Iskender, M. Schuurmans, S. Hillinger, I. Opitz, D. Schneiter, C. Benden, W. Weder, I. Inci
Survival after lung retransplantation: A single-center experience over 25 years

4039
I. Inci, M. Schuurmans, I. Iskender, S. Hillinger, I. Opitz, D. Schneiter, C. Caviezel, C. Benden, W. Weder
The incidence of chronic lung allograft dysfunction after cadaveric lobar lung transplantation is comparable to conventional lung transplantation

4058
P. Schreiber, V. Kufner, K. Hübel, O. Zagordi, S. Schmutz, C. Bayard, M. Greiner, A. Zbinden, R. Capaul, J. Böni, T. Müller, N. Mueller, A. Trkola, M. Huber
Virus transmission during kidney transplantation assessed by virome analysis of living donor and recipient

4077
D. Sahin, N. Arenas-Ramirez, D. Zingg, L. Sommer, O. Boyman
Mechanisms of adaptive resistance to cancer immunotherapy

4113
U. Karakus, J. Lam, O. Boyman
Development of Treg cell-stimulating IL-2/anti-IL-2 antibody complexes

Clinical Trials

3954
A. Plate, A. Anagnostopoulos, J. Glanzmann, L. Stadler, L. Weigelt, R. Sutter, A. Zinkernagel, P. Zingg, Y. Achermann
Synovial C-reactive protein for diagnosis of periprosthetic joint infection (PJI)

3955
A. Plate, L. Stadler, R. Sutter, A. Anagnostopoulos, D. Frustaci, R. Zbinden, S. Fucentese, A. Zinkernagel, P. Zingg, Y. Achermann
Inflammatory disorders mimicking periprosthetic joint infections may result in false positive α-defensin

4027
S. Halvachizadeh, H-C. Pape, V. Neuhaus
Does the time of the day of surgery influence perioperative complications – a nationwide database analysis in 31'692 patients

4029
O. Politikou, T. Giesen, C. Erling, M. Calcagni
Arthroscopic mid-carpal partial wrist arthrodesis. Early experience on eleven cases.

4057
L. Peterer, K. Jensen, G. Osterhoff, L. Mica, H-P. Simmen, H-C. Pape, K. Sprengel
Implementation of new standard operating procedures: What are the benefits for geriatric trauma patients with multiple injuries.

4072
L. Hapouja, A. Figurek, V. Luyckx, T. Müller
The effect of donor-recipient weight mismatch on kidney graft function – demand defines supply

4074
A. Figurek, K. Hübel, C. Oberkofler, O. De Rougemont, T. Müller
The kidney donor profile index (KDPI) is associated with early kidney transplant function

Neurosciences / Pharmacology

Basic Research

3920
P. Jirkof, M. Arras, N. Cesarovic
Tramadol:Paracetamol in drinking water for treatment of post-surgical pain in laboratory mice

3925
K. Frontzek, M. Bardelli, U. Herrmann, T. Sonati, R. Reimann, M. Carta, C. Zhu, S. Hornemann, L. Varani, A. Aguzzi
The globular domain of the prion protein induces prion neurotoxicity through decreased rigidity of its b2a2 loop

3926
K. Dockheer, C. Bockisch, A. Tarnutzer
Effects of optokinetic stimulation on verticality perception are domain-specific and restricted to vision-based paradigms

3933
M. Durst, P. Jirkof, M. Arras, K. Schmidt-Bleek, F. Buttgereit, A. Lang
Evaluating analgesia in mouse osteotomy: Tramadol and Buprenorphine applied via the drinking water

3936
R. Reimann, A. Assunta, C. Caflisch, I. Irpinio, H. Hornemann, S. Schneider, A. Aguzzi
The structural basis of prion-associated neurodegeneration

3941
I. Zygoula, C. Schori, C. Grimm, D. Barthelmes
Plasma levels of hypoxia-regulated factors in patients with age-related macular degeneration

3943
C. Scheckel, M. Marigona, A. Adriano
Systematic Profiling of Molecular Changes during Prion Disease Progression

3947
B. Weder, C. Mamie, G. Rogler, S. Clarke, B. McRae, P. Ruiz, M. Hausmann
BCL2 regulates differentiation of intestinal fibroblasts

3953
A. Lakkaraju, R. Marpakwar, U. Hermann, P. Liberski, A. Ballabio, A. Aguzzi
Identifying the determinants of spongiform phenotype in prion infections

3956
A. Magalhaes, M. Emmenegger, A. Kerschenmeyer, A. Aguzzi, S. Hornemann
Establishment of a high-throughput microELISA screen for naturally occurring human tau autoantibodies

3957
F. Scholkmann, T. Karen, S. Kleiser, D. Ostojic, H. Isler, D. Bassler
Brain oxygenation in preterm neonates measured with a novel NIRS oximeter: Preliminary findings of a new study

3965
A. Henzi, A. Senatore, A. Lakkaraju, S. Hornemann, R. Moos, K. Airich, A. Aguzzi
A Novel Tool for the Treatment of Peripheral Demyelinating Neuropathies

3967
D. Kirschenbaum, F. Voigt, A. Gomariz Carillo, M. Smith, C. Nombela Arrieta, F. Helmchen, A. Aguzzi
Reconstruction of the entire vascular web of the mouse brain by novel tissue clearing and imaging approaches

3976
S. Sorce, M. Nuvolone, G. Russo, A. Chincisan, P. Schwarz, A. Aguzzi
RNA sequencing of prion-infected mice uncovers early-onset, progressive derangement of

transcription and splicing

3977
S. Sorce, M. Nuvolone, P. Schwarz, P. Pelczar, E. Rushing, A. Aguzzi
The role of the prion protein in the development of muscular pathology

3980
C. Zhu, P. Schwarz, A. Aguzzi
Deficiency of Progranulin (PGRN) results in accelerated prion diseases

3982
J. Schaffenrath, M. Neidert, L. Regli, A. Keller
Determining the protein atlas of normal human blood-brain barrier and glioblastoma blood-brain barrier – towards understanding glioblastoma biology and improved therapies

3991
O. Török, B. Schreiner, A. Keller
The role of brain pericytes in the regulation of leukocyte trafficking under homeostatic and pathological conditions

3999
Y. Zarb, D. Kirschenbaum, D. Kindler, J. Klohs, A. Aguzzi, A. Keller
Ossifying environment accompanies brain capillary calcification in the mouse model of primary familial brain calcification

4002
Y. Liu, A. Aguzzi
Lymphocyte activation gene 3 (Lag3) is upregulated after prion infection without significant contribution to prion disease pathogenesis

4010
A. Senatore, M. Hermann, M. Nuvolone, P. Schwartz, J. Guo, S. Sahl, P. Pelczar, A. Aguzzi
Therapeutic approach against genetic prion diseases linked to insertion mutation in the octapeptide repeat region of PrP

4023
D. Pease
Identifying Novel Roles of MicroRNAs in PrPc Biosynthetic Regulation via miRNA Screening

4044
M. Wulf, J. Guo, K. Frontzek, A. Aguzzi
Electrophysiological Alterations in Hippocampal Neurons induced by Anti-PrPc antibodies

4065
A. Moncsek, M. Al-Suraih, C. Trussoni, S. O'Hara, P. Splinter, C. Zuber, E. Patsenker, A. Weber, J. Kirkland, G. Gores, B. Müllhaupt, N. LaRusso, J. Mertens
Combined targeting of senescent cholangiocytes and activated stromal fibroblasts with a Bcl-xL inhibitor ameliorates liver fibrosis in Mdr2-/- mice

4066
K. Frauenknecht, M. Emmenegger, A. Chincisan, A. Aguzzi
Detection of human antibodies against the TREM2 cleavage site

4076
T. Fedele, J. Niediek, L. Stieglitz, P. Hilfiker, K. König, F. Mormann, J. Sarnthein
Multi-unit activity underlies epileptic fast ripple EEG in the mesial temporal lobe

4090
E. Krajnc, Z. Gai, M. Visentin, G-A. Kullak-Ublick
Nefazodone effects on aerobic and anaerobic ATP production in liver cells

4091
K. Airich, K. Luk, D. Pease, M. Emmenegger, A. Aguzzi, S. Hornemann
High-throughput small RNA screens to identify modifiers of alpha-synuclein aggregation

4093
E. Boran, T. Fedele, L. Stieglitz, P. Hilfiker, T. Grunwald, J. Sarnthein
Persistently active neurons in human hippocampus support verbal working memory network.

4094
V. Eckhardt, B. Li, E. Schaper, J. Jérôme, P. Goloubinoff, A. Aguzzi
Elucidating the role of chaperones in prion biosynthesis and replication by siRNA mediated high-throughput screening

4102
F. Romano, D. Straumann, G. Bertolini
The role of visual inputs on vestibular Cross-coupling stimulus

4109
F. Romano, D. Straumann, G. Bertolini
Impact of alcohol on self-motion perception and reflexive eye movements

4111
F. Feldmann, G. Natalucci
Association between development of early cortical activity on amplitude integrated EEG and 5-years neurodevelopmental outcome in the preterm infant

4112
G. Natalucci, A. Adams
Two-year outcome of extremely preterm infants < 26 weeks of gestation born in Switzerland: is intensity of perinatal care associated with increased neurodevelopmental impairment?

Translational Research

4015
N. Binder, M. El Amki, R. Steffen, H. Schneider, R. Luft, M. Weller, B. Imthurn, G. Merki-Feld, S. Wegener
Contraceptive drugs against stroke? Mechanisms of progestin-induced neuroprotection in an Oxygen Glucose Deprivation/Reperfusion (OGD/R) Model

4054
S. Santos, C. Haslinger, M. Hamburger, M. Mennet, O. Potterat, M. Schnelle, U. Von Mandach, AP. Simões-Wüst
In vitro effect on myometrial contractility of a combination of Bryophyllum pinnatum press juice and nifedipine

4067
M. Emmenegger, A. Chincisan, G. Meisl, K. Frontzek, E. Schaper, R. Müller, A. Rosati, J. Domange, N. Wuillemin, T. Sonati, I. Xenarios, L. Saleh, A. Von Eckardstein, S. Hornemann, A. Aguzzi
High-throughput immune profiling for diagnostic and therapeutic antibodies in an ultra-large unselected hospital cohort

4092
P. Beeler, M. Cheetham, E. Battegay
Depression is independently associated with an increased length of stay in hospitalized patients

Clinical Trials

3919
R. Omary, R. Kardon, C. Bockisch, K. Landau, K. Weber
Buzzing Sympathetic Nerves: A New Test to Enhance Reflex Pupil Dilation in Suspected Horner Syndrome

3928
K. Slankamenac, C. Steinmann, D. Keller
Emergency department visits and risk factors for in-patient care in acute drug intoxication

3960
G. Traber, M. Kanku, S. Sele, G. Jaggi, U. Held, K. Landau
Assessment of cyclotorsion using SLO fundus imaging in patients with and without forth nerve palsy

3962
A. Bicvic, N. Scherrer, J. Schneider, A. Luft, M. Katan
Identification of a Novel Blood Biomarker Panel Index for Improved Mortality Prediction in Acute Ischemic Stroke

4089
H. Wirsching, J. Richter, F. Sahm, C. Morel, N. Krayenbühl, E. Rushing, A. Von Deimling, A. Valavanis, M. Weller
Preoperative embolization of meningioma: inferior neurological outcome, increased risk of cardiovascular complications and shorter time to recurrence?

4100
A. Van Ransbeeck, A. Budilivski, D. Spahn, L. Macrea, F. Giuliani, K. Maurer
Pain Assessment Discrepancies: A Cross- Sectional Study Highlights the Amount of Underrated Pain

3919

R. Omary[1], R. Kardon[2], C. Bockisch[1], K. Landau[1], K.P. Weber[1]

Buzzing Sympathetic Nerves: A New Test to Enhance Reflex Pupil Dilation in Suspected Horner Syndrome

University Hospital Zürich[1], University of Iowa and Veteran Medical Center[2]

Introduction:
Patients with suspected Horner syndrome and equivocal pupil dilation lag and pharmacologic testing might undergo unnecessary MR imaging. Our purpose was to increase the diagnostic sensitivity of pupillometry by accentuating sympathetic innervation to the iris dilator by surface electrical stimulation of the median nerve using a standard electromyography machine. We hypothesized that any difference in sympathetic innervation to the right and left eye would be accentuated.

Methods:
Seven healthy volunteers tested before and after monocular instillation of brimonidine 0.2% to induce pharmacological Horner syndrome were compared to two patients with proven Horner syndrome. Pupillary responses were measured with binocular pupillometry (DP-2000, Neuroptics; Irvine, CA) in response to sympathetic activation by electrical stimulation (0.2ms, 50mA) of the median nerve in darkness and at various times after extinction of a 3log lux light stimulus (1 vs. 4 seconds). Sudomotor sympathetic responses from the palm were recorded simultaneously.

Results:
In subjects with Horner syndrome or pharmacologically induced unilateral sympathetic deficit, electrical stimulation in combination with the extinction of light greatly enhanced the anisocoria during the evoked pupil dilation and was well tolerated. The asymmetric sympathetic response was greatest when the electrical stimulus was given 1-2s after termination of the light. Two discernible reflex dilation responses appeared; an initial symmetric dilation due to central inhibition of the Edinger-Westphal nucleus followed by an accentuated asymmetric dilation due to enhanced peripheral sympathetic stimulation.

Conclusion:
Electrical sympathetic stimulation given at the termination of a short light stimulus appears to greatly enhance the sensitivity for diagnosing asymmetric pupil dilation due to Horner syndrome. This strategy may improve upon the ability to rule in or rule out a unilateral oculosympathetic deficit, especially if the results of topical pharmacological testing are inconclusive.

3920

P. Jirkof[1], M. Arras[1], N. Cesarovic[1]

Tramadol:Paracetamol in drinking water for treatment of post-surgical pain in laboratory mice

Division of Surgical Research, University Hospital, Zurich[1]

Introduction:
In the search for stress-free analgesia administration for laboratory mice suffering pain, oral delivery of Tramadol:Paracetamol (T:P) shows great promise.

Methods:
Here, we monitored the analgesic efficacy and side effects of a T:P combination administered solely in the drinking water of female C57BL/6J mice after moderate-impact surgery (sham embryo transfer), using clinical and behavioral pain and recovery parameters. Animals underwent anesthesia and surgery with T:P treatment (OP +T:P), received no pain relief after surgery (OP), underwent anesthesia only with T:P treatment (An +T:P) or T:P treatment only (T:P). Indicators of pain and constraint were assessed at several time points during 24 h after surgery.

Results:
T:P-containing drinking water was consumed readily in amounts to assure sufficient drug levels. No obvious detrimental side effects of analgesia were observed. General condition of animals differed only slightly and non-significantly between treatment groups, with comparable post-procedural weight loss, water and food intake as well as home cage activity. Mean nest scores differed significantly between T:P and both surgery groups ($p = 0.002$, $p < 0.0001$) but revealed no significant difference between OP and OP+ T:P groups. Nevertheless, pain scores showed significant differences between the treatment groups at 1, 3 and 6 h after surgery ($p = 0.001$, $p = 0.014$, $p = 0.003$). OP animals scored highest, while scores of OP+T:P animals were comparable or lower than scores of the AN+T:P group. Same was true for burrowing latency that was significantly increased in OP animals compared to An +T:P and OP+T:P ($p = 0.032$, $p = 0.019$), but comparable between An +T:P and OP+ T:P. These results hint on a clear post-surgical pain effect after surgery that could be significantly reduced with T:P treatment towards a level of the control group receiving anesthesia and T:P only.

Conclusion:
In conclusion, we assume that orally administered T:P offers pain relief with no obvious side effects after mild-to-moderate impact surgery in female C57BL/6J mice.

3921

J. Von Spiczak[1], M. Mannil[1], B. Peters[1], T. Hickethier[2], R. Manka[1], D. Maintz[2], H. Alkadhi[1]

Photon Counting CT with Dedicated Sharp Convolution Kernels: Tapping the Potential of a New Technology for Stent Imaging

Institute of Diagnostic and Interventional Radiology, University Hospital Zurich, Zurich, Switzerland[1], Department of Radiology, University Hospital of Cologne, Cologne, Germany[2]

Introduction:
To assess the value of dedicated sharp convolution kernels for photon counting detector (PCD) computed tomography (CT) for coronary stent imaging and to evaluate to which extent iterative reconstructions (IR) can compensate for potential increases in image noise.

Methods:
For this in-vitro study, a phantom simulating coronary artery stenting was prepared including 18 different coronary stents expanded in plastic tubes (3 mm diameter). Tubes were filled with diluted contrast agent, sealed, and immersed in oil calibrated to an attenuation of -100 HU simulating pericardial fat. The phantom was scanned in a 128-slice research dual-source CT scanner equipped with a PCD detector. Image data was acquired using a tube voltage of 100 kVp and tube current time product of 100 mAs. Images were reconstructed using a conventional convolution kernel for stent imaging with filtered back projection (B46) and IR at SAFIRE level 3 ($I46_3$). For comparison, a dedicated sharp convolution kernel with filtered back projection (D70) and iterative reconstruction at SAFIRE level 3 ($Q70_3$) and level 5 ($Q70_5$) was used. Two independent, blinded readers evaluated subjective image quality (scale 0 – 3, 3 = excellent), in-stent diameter difference, in-stent attenuation difference, mathematically defined image sharpness, and noise of each reconstruction. Interreader reliability was calculated using Goodman and Kruskal's gamma and intraclass correlation coefficients. Differences in image quality were evaluated using a Wilcoxon signed-rank test. Differences in intraluminal stent diameter, in-stent attenuation, image sharpness, and image noise were tested using a paired sample t-test.

Results:
Interreader reliability was excellent ($\gamma = 0.953$ and ICCs = 0.952 – 0.999). Reconstructions using the dedicated sharp convolution kernel yielded significantly better results regarding image quality (B46: 0.4 ± 0.5 vs. D70: 2.9 ± 0.3, $p < 0.001$), intraluminal in-stent diameter difference (1.5 ± 0.3 vs. 1.0 ± 0.3 mm, $p < 0.001$), and image sharpness (728 ± 246 vs. 2069 ± 411 CT-numbers/voxel, $p < 0.001$). Regarding in-stent attenuation difference, no significant differences were observed between the two kernels (151 ± 76 vs. 158 ± 92 CT-numbers, $p = 0.627$). Noise was significantly higher in all sharp convolution kernel images, but could be reduced applying SAFIRE levels 3 and 5 (B46:16 ± 1, D70: 111 ± 3, $Q70_3$: 65 ± 2, $Q70_5$: 46 ± 2 CT-numbers, $p < 0.001$ for all comparisons).

Conclusion:
A dedicated sharp convolution kernel for PCD CT imaging of coronary stents yields superior qualitative and quantitative image characteristics compared to conventional reconstruction kernels. Resulting higher noise levels can be reduced with iterative reconstruction techniques.

3922

J. Von Spiczak[1], R. Manka[1], M. Mannil[1], S. Oebel[1], S. Hamada[1], K. Higashigaito[1], F. Ruschitzka[2], H. Alkadhi[1]

3D Fusion of Coronary CT Angiography and CT Myocardial Perfusion Imaging: Intuitive Assessment of Morphology and Function

Institute of Diagnostic and Interventional Radiology, University Hospital Zurich, Zurich, Switzerland[1], Department of Cardiology, University Heart Center, University Hospital Zurich, Zurich, Switzerland[2]

Introduction:
The objective of this work was to support three-dimensional fusion of coronary CT angiography (coronary CTA) and CT myocardial perfusion (CT-Perf) data visualizing coronary artery stenoses and corresponding stress-induced myocardial perfusion deficits for diagnostics of coronary artery disease.

Methods:
Twelve patients undergoing coronary CTA and CT-Perf after heart transplantation were included (56±12 years, all males). CT image quality was rated. Coronary diameter stenoses >50% were documented for coronary CTA. Stress-induced perfusion deficits were noted for CT-Perf. A software was implemented facilitating 3D fusion imaging of coronary CTA and CT-Perf data. Coronary arteries and heart contours were segmented automatically. To overcome anatomical mismatch of coronary CTA and CT-Perf image acquisition, perfusion values were projected on the coronary CTA left ventricle. Three resulting datasets (coronary tree/heart contour/perfusion values) were fused for combined three-dimensional rendering. 3D fusion was compared to conventional analysis of coronary CTA and CT-Perf data and to results from catheter coronary angiography.

Results:
CT image quality was rated good – excellent (3.5 ± 0.5, scale 1 – 4). 3D fusion imaging of coronary CTA and CT-Perf data was feasible in 11/12 patients (92%). One patient (8%) was excluded from further analysis due to severe motion artifacts. 2/12 patients (17%) showed both stress-induced perfusion deficits and relevant coronary stenoses. Using 3D fusion imaging, the ischemic region could be correlated to a culprit coronary lesion in one case (1/2=50%) and diagnostic findings could be rectified in the other case (1/2=50%). Coronary CTA was in full correspondence with catheter coronary angiography.

Conclusion:
A method for 3D fusion of coronary CTA and CT-Perf is introduced correlating relevant coronary lesions and corresponding stress-induced myocardial perfusion deficits.

3923

A. Mortezavi[1], J. Krauter[1], J. Sonderer[1], O. Donati[2], A. Gu[1], J. Bruhin[1], O. Gross[1], S. Kedzia[1], T. Sulser[1], D. Eberli[1]

Interim analysis of intervention trial evaluating focal therapy using high intensity focused ultrasound for the treatment of prostate cancer: safety, functional, psychological and oncological outcome 6 months after treatment

Klinik für Urolgie, Universitätsspital Zürich[1], Institut für Diagnostische Radiologie, Universitätsspital, Zürich[2]

Introduction:
In this interim analysis of a prospective trial we evaluate safety, functional, psychological and oncological outcome 6 months after true focal treatment of prostate cancer (PCa) with high intensity focused ultrasound (HIFU).

Methods:
Men with low to intermediate risk localised PCa (Gleason score [GS] ≤4 + 3, PSA ≤15 ng/ml) with no prior treatment were eligible for this prospective trial. After identifying tumours on multiparametric (mp) MRI and on extended transperineal prostate mapping biopsy (TPMB) patients received focal therapy using HIFU (Focal One, EDAP) delivered to significant PCa lesions with a safety margin of 8 mm. Urinary symptoms, erectile function and psychological outcome was assessed 6 months after the HIFU treatment by using established questionnaires. We performed an mpMRI 6 months after HIFU followed by TPMB. Clinically significant PCa (csPCa) was defined as GS 7 or higher.

Results:
Between May 2014 and October 2017 72 men (mean age 64y SD ±6) received focal HIFU therapy. A majority of patients (n=63, 91.7%) had a GS 7. Overall, 13 patients (18.0%) experienced complications in the follow-up period: five (6.9%) had a urinary retention after catheter removal, four (5.5%) had a urinary tract infection, two (2.7%) had diarrhoea and two (2.7%) patients needed a transurethral intervention due to an infravesical obstruction.

Follow-up biopsy after 6 months was performed in 60 patients while five men declined any intervention. A total of 36 (55.4%) men were free of any csPCa. TPMB detected csPCa in 24 patients (36.9%); of these men nine (37.5%) underwent a re-focal HIFU treatment and six (25.0%) underwent salvage radical prostatectomy. Eight (33.3%) patients with very low tumour volume opted for active surveillance. One patient was lost to follow-up.

Mean EPIC urinary incontinence and bowel symptoms scores showed no changes (non-significant, ns), whereas mean IPSS and IIEF-15 decreased significantly between baseline ([mean ±SD] 8.1 ±6 and 47.0 ±17.9) and 6 months (5.4 ±4 and 37.1 ±18.7, $p=0.027$ and $p<0.05$). The pad-free rate after 6 months was 96.7%. HADS and FACT-P scores did not show any change after 6 months while the three MAX-PC subscales indicated low and decreasing PCa anxiety (ns).

Conclusion:
Focal therapy with HIFU is safe and leads to an acceptable rate of genitourinary side effects and very low rate of psychological distress. TPMB detected a significant number of patients with csPCa during follow-up. Although most patients had a very low tumour burden which could be managed by re-HIFU or surveillance, salvage prostatectomy was indicated in a notable number of patients. Therefore, an early TPMB after focal HIFU is strongly recommended.

3924

C. Vulin[1], N. Leimer[3], M. Huemer[2], M. Ackermann[1], A. Zinkernagel[2]

Prolonged lag time results in Small Colony Variants and reflects persisters in vivo

Department of environmental systems science, ETH Zurich, Zurich[1], Division of infectious diseases and hospital epidemiology, University Hospital Zurich, Zurich[2], Antimicrobial Discovery Center, Department of biology, Northeastern University, Boston[3]

Introduction:
Staphylococcus aureus small colony variant (SCV) is a colony phenotype associated with chronic infections. Aiming to study the link between the observed phenotype and the relation to persisters or other growth-arrested bacteria, we focused on the bacteria-to-bacteria variability in a recovered population, and survival after antibiotic challenge.

Methods:
We recently showed that SCVs are selected by varying environmental factors including acidity. Thus, we assessed single cell fate at the microscopic and macroscopic level after low pH challenge including low pH media, intracellular localization and abscess material from both mice and patient. We followed bacterial growth over time using single-cell microscopy and automated agar plate imaging. We quantitatively compared the lag time and antibiotic challenge survival of previously stressed bacteria as compared to unstressed bacteria.

Results:
We found that previously stressed bacteria formed colonies with a wide range of colony radius, whereas the colony radius of previously unstressed bacteria had a smaller variability. By comparison of the lag time and growth rate distributions, we conclude that the small colony radius of bacteria surviving acidic stress resulted from delayed growth and not from slow growth or colony size limitation, a clear distinction from stable SCVs that are slow-growing due to auxotrophic defects. The proportion of bacteria with a long lag time correlated with the proportion of bacteria surviving an antibiotic challenge. Antibiotics further delayed first division time in stressed bacteria but not in control bacteria.

Conclusion:
Macroscopically observed heterogeneous *Staphylococcus aureus* populations as well as cell-to-cell variation observed after stress are due to delayed growth. This growth delay then leads to increased antibiotic tolerance and survival.

3925

K. Frontzek[1], M. Bardelli[2], U. Herrmann[1], T. Sonati[1], R. Reimann[1], M. Carta[1], C. Zhu[1], S. Hornemann[1], L. Varani[2], A. Aguzzi[1]

The globular domain of the prion protein induces prion neurotoxicity through decreased rigidity of its b2a2 loop

Neuropathology, University Hospital of Zurich, Zurich[1], IRB Bellinzona[2]

Introduction:
Antibodies and single-chain variable fragment (scFv) targeting certain epitopes of the prion protein PrP^C are acutely neurotoxic. Transcriptional and proteomic analyses indicate that their toxicity closely recapitulates that of prion infections, suggesting that these antibodies mimic the docking of prions to PrP^C. Toxicity is mediated by the flexible tail of PrP^C, implying that antibody binding triggers an allosteric transition within PrP^C. Here we report that scFvPOM1 imposes a spatial relaxation on the flexibility of the β2-α2 loop of PrP^C without appreciably distorting its overall structure.

Methods:
To assess the functional consequences of this structural irregularity, we replaced with alanine each one of the scFvPOM1 residues showing significant interaction with PrP^C in molecular dynamics simulations (MDS) resulting in 11 different scFvPOM1 mutants. Cerebellar organotypic slice cultures (COCS) from *Tga20* mice overexpressing the prion protein were used as *ex vivo* system faithfully reproducing prion pathology. Expression of PrP^C mutants important in mediating alterations of the β2-α2 loop was undertaken by transduction of adeno-associated viruses harboring wild-type and mutated PrP^C in COCS from *Prnp*$^{0/0}$ (Zurich 3) mice.

Results:
The resulting 11 individual scFvPOM1 mutants were found to be either toxic, innocuous or protective to naïve and prion-infected cerebellar organotypic slice cultures (COCS). Toxic mutants induced acute neuronal loss and astrogliosis that, as with their parental antibody POM1, was prevented by treatment with the antibody scFvPOM2, directed against the amino terminus of PrP^C. Protective mutants attenuated the production of reactive oxygen species and the unfolded protein response, and suppressed the toxicity of both scFvPOM1 and infectious prions. MDS showed that protective scFvPOM1 mutations led to a relaxation of the β2-α2 loop. Altered binding patterns of the PrP^C residues Tyr127 and Arg207 after POM1-PrP^C interaction in MDS led to the generation of the purportedly protective PrP^C mutants Tyr127Phe and Arg207Ala, both mutants did not show overt cell toxicity after transduction in *Prnp*$^{0/0}$ COCS.

Conclusion:
Besides implying loop rigidity as a mediator of prion toxicity, these investigations have led to the discovery of dominant-negative immunoreagents binding to PrP^C and quenching prion toxicity. *In vivo* experiments using osmotic minipumps will demonstrate the efficacy of these immunoreagents against prion disease *in vivo*. Identification of important PrP^C point mutations involved in toxicity will lead to a high-resolution map of prion pathogenesis. These structural insights provide a well-defined pathway towards the development of efficacious antiprion drugs.

3926

K. Dockheer[1], C. Bockisch[2], A. Tarnutzer[1]

Effects of optokinetic stimulation on verticality perception are domain-specific and restricted to vision-based paradigms

Department of Neurology, University Hospital Zurich, Zurich[1], Departments of Neurology, Otorhinolaryngology and Ophthalmology, University Hospital Zurich, Zurich[2]

Introduction:
Verticality perception as assessed by the subjective visual vertical (SVV) is significantly biased by a rotating optokinetic stimulus. The underlying mechanisms of this effect remain open. Potentially, the optokinetic stimulus induces a shift of the internal estimate of the direction of gravity. Thus, this hypothesis predicts a shift of perceived vertical using other, non-vision dependent, paradigms as well. Alternatively, an optokinetic stimulus may only induce a shift of visual orientation, and so would be task-specific.

Methods:
To test these predictions, both vision-dependent (SVV) and vision-independent (subjective haptic vertical, SHV) paradigms were applied. In a total of 12 healthy human subjects perceived vertical in different roll positions (up to ±120°, steps=30°) while presenting a clockwise or counter-clockwise rotating optokinetic stimulus was measured. For comparison, baseline trials were collected in darkness. Paired t-tests with Bonferroni-correction were applied for statistical analysis.

Results:
Optokinetic stimulation resulted in significant shifts ($p \leq 0.002$) of the SVV compared to baseline in all roll-tilt orientations except upright and 120° left-ear-down (clockwise optokinetic stimulation). In contrast, offsets of the SHV were significant ($p<0.05$) only in one (60° left-ear-down) and two (90° left-ear-down, 120° left-ear-down) roll orientations, for clockwise and counter-clockwise optokinetic stimulation, respectively. Compared to the SHV, the SVV showed significantly ($p<0.001$) larger shifts of perceived vertical when presenting a clockwise (12.4±5.8° vs. 1.3±2.8°, median±1 median absolute deviation) or counter-clockwise ((-11.7±5.0° vs. -2.7±3.0°) rotating optokinetic stimulus.

Conclusion:
The effect of optokinetic stimulation on verticality perception was restricted to the vision-dependent paradigm. This speaks against the hypothesis that optokinetic stimulation results in a shift of the internal estimate of direction of gravity and favors a vision-related mechanism.

3928

K. Slankamenac[1], C. Steinmann[1], D. Keller[1]

Emergency department visits and risk factors for in-patient care in acute drug intoxication

Institut für Notfallmedizin[1], UniversitätsSpital Zürich

Introduction:
In Switzerland, few reports exist about comprehensive data of acute drug intoxication (ADI) and the abuse of novel psychoactive substances (NPS). Therefore, the aim was to investigate the prevalence of ADI, epidemiology of psychoactive substances and risk factors needing an in-patient care.

Methods:
In a retrospective analysis, we enrolled consecutively patients who presented with symptoms of an ADI in the emergency department (ED) of a tertiary care hospital between April 2014 and August 2016.

Results:
We identified 186 of 89,576 ED patients (0.2%) with an ADI. Patients presented in the ED with one or more symptoms: somnolence (50.5%), agitation with aggression (38.7%), confusion (10.8%), psychosis (10.2%), chest pain (9.1%), seizure (3.2%) and cardiac arrhythmia (1.1%). In 65.6%, alcohol was combined with psychoactive substances. Patients consumed most often cocaine (37.6%) and cannabis (31.7%). NPS (2.2%) were rarely consumed.

Fifty-eight patients (31.2%) had to be admitted in-house. Patients presenting in the ED with acute psychosis (RR 5.1, 95%-CI 1.7-15.1, p=0.003), aggression (RR 3.2, 95%-CI 1.6-6.6, p=0.001) or with pre-existing schizophrenia (RR 4.9, 95%-CI 1.4-16.7, p=0.011) had to be admitted most frequently.

Conclusion:
NPS intoxication is rare in Switzerland. Even though the prevalence of acute drug intoxication is low, almost a third of these ED patients need in-patient care and therefore trigger health care costs. Identifying symptoms such as psychosis and aggression as well as pre-existing schizophrenia as risk factors for in-patient care may encourage future preventive strategies.

3929

K. Slankamenac[1], A. Neuenschwander[1], D. Keller[1]

Need for early identification of palliative patients in the Emergency Department to decide best supportive strategies

Institut für Notfallmedizin[1], UniversitätsSpital Zürich

Introduction:
Although the Emergency Department (ED) is not the ideal place to begin palliative care, in realty, it is frequent that palliative care patients present in the ED and need urgent care. Therefore, the aim of this study is to investigate the median overall survival of ED patients who need palliative care, their risk of in-hospital mortality and intensive care unit referral.

Methods:
In a retrospective analysis, we enrolled consecutively ED patients who needed inpatient care due to an end-stage disease and were transferred from the ED to the palliative care unit in a tertiary care hospital between April 2014 and March 2016.

Results:
We identified 194 ED patients who were in a palliative situation when admitted to the ED. Fifty-four patients (27.8%) did not know about their palliative situation. Of those, 21 patients knew about their underlying disease but not about the end-stage situation. Thirty-three patients (17%) received the initial diagnosis during the ED presentation.

The median overall survival was 27 days (IQR 11–96 days). There was no survival benefit knowing about the palliative situation when admitted to the ED (HR 1.1, 95% CI 0.7-1.5, p=0.75).

54.6% of patients (106 of 194) died during the same course of hospital stay. The multivariate logistic regression analysis showed a significantly increased risk for in-hospital mortality in ED patients presenting with abdominal pain or distension (RR 5.0, 95% CI 1.3–18.4, p=0.016). Patients who did not know about their palliative situation, showed an increased risk of in-hospital mortality if they were older than 67 years (RR 7.0, 95%CI 1.8–26.8, p=0.005) or presented to the ED with dyspnea (RR 6.7, 95% CI 1.4–31.6, p=0.017). They also had a significantly increased risk to be referred to the intensive care unit compared to those patients who knew about the palliative situation (RR 11.0, 95% CI 4.1-29.8, p<0.001).

Conclusion:
More than half of ED patients in a palliative situation died within one month after ED admission. Patient presenting with abdominal pain or distension, dyspnea and increased age are at high risk for in-hospital mortality during the same course of hospital stay. Therefore, there is a need to initiate promptly best supportive treatment strategies in cooperation with palliative care physicians, patients and their relatives during the ED stay, to avoid unnecessary ICU referrals and to ensure fast transferal to the palliative care unit.

3930

A. Curioni Fontecedro[2], P. Tallon de Lara[1], V. Cecconi[1], S. Hiltbrunner[1], H. Yagita[4], M. Friess[3], B. Bode[5], I. Schmitt-Opitz[3], B. Vrugt[5], W. Weder[3], E. Felley- Bosco[3], RA. Stahel[2], V. Tischler[5], D. Soldini[5], H. Moch[5], M. Van den Broek[1]

Gemcitabine synergizes with immune-checkpoint inhibitors: from a preclinical model to mesothelioma patients

Experimental Immunology, University of Zurich, Switzerland[1], Hematology and Oncology, University Hospital Zurich[2], Thoracic Surgery, University Hospital Zürich[3], Department of Immunology, Juntendo University School of Medicine, Tokyo, 113-8421, Japan[4], Institute of Pathology and Molecular Pathology, University Hospital Zurich and University of Zurich, Zurich, Switzerland[5]

Introduction:
Combination of immune checkpoint inhibitors with chemotherapy is under investigation for cancer treatment. We investigated the rationale of such combination for treating mesothelioma, a severe malignant disease with limited treatment options.

Methods:
Human tumor samples: 251 full diagnostic sections from 145 mesothelioma patients were analysed. Post-chemotherapy tumor samples were collected after three cycles of treatment. Out of 251 samples, 118 samples were collected before and 133 after chemotherapy. From this cohort of 145 patients, matching samples of 80 patients before and after chemotherapy were available. Anti-PD-L1 staining with E1L3N antibody diluted as 1:1000. Biopsies were considered PD-L1$^+$ when >1% of tumor cells were stained positive with anti-PD-L1. Tumor-specific OS in humans was determined from the date of histological diagnosis of mesothelioma to the date of death from the same cancer up to 5 years' follow-up. Mice C57BL/B6 mice were injected subcutaneously (s.c.) with 10^6 RN5 cells in 100 µl PBS. Tumor growth was monitored with a caliper every 2-3 days in two dimensions (length and width). When tumors reached a size of 40-50 mm^2 mice were randomized into treatment groups based on tumor size and treatment was started. The death event was defined as tumor size reaching the legally acceptable limit of 225 mm^2. Treatment included Gemcitabine given intraperitoneally (i.p.) once per week at a dose of 120 mg/g body weight; anti–CTLA-4 and anti-PD-1 administered i.p. once per week at 250 µg/100 µl PBS; dexamethasone administered orally once per week at 0.3 mg/kg body weight. All treatments were given on the same day. This experiment was repeated three times with at least 6 mice/group. Resected tumors from mice were processed for FFPE and 4-µm-thick sections were stained for IHC for PD-L1 (Lifespan LS-B9795), FoxP3 (Novus Biologicals, NBP1-18319) and CD3 (RMAB005, clone SP7, DBiosystem). For mice, tumor-specific OS was determined from the date of randomization and the death event was defined as tumor size reaching the legally acceptable limit of 225 mm^2. Two patients with advanced mesothelioma, resistant to both gemcitabine and pembrolizumab as monotherapy, were treated with combination of gemcitabine (1000mg/m2) weekly and pembrolizumab (200mg) every three weeks. Response to treatment was evaluated with Computer tomography 9 weeks after start of this combinatorial treatmen

Results:
We detected PD-L1 expression in 14% of primary mesothelioma samples and identified it as negative biomarker for survival. The expression of PD-L1 varied upon chemotherapy comparing matching tumor samples from before and after treatment. The combination of gemcitabine and immune checkpoint inhibitors outperformed monotherapy with regard to tumor control and survival in a pre-clinical mesothelioma model. The use of dexamethasone together with gemcitabine plus immune checkpoint inhibitors, however, nullified the synergistic clinical response. Treatment with gemcitabine plus anti-PD-L1 resulted in an objective clinical response of two mesothelioma patients, who were resistant to gemcitabine or anti-PD1 as monotherapy.

Conclusion:
Treatment of mesothelioma with a combination of gemcitabine with immune checkpoint inhibitors is feasible and results in synergistic clinical response compared to single treatment.

3931

V. Jeger[1], M. Arrigo[4], C. Schaer[1], F. Hildenbrand[2], M. Arras[5], G. Schoedon-Geiser[2], D. Spahn[1], D. Bettex[1], A. Rudiger[3]

Heart rate elevations during early sepsis predict death in fluid resuscitated rats with faecal peritonitis

Institute of Anesthesiology, University and University Hospital Zurich, Zurich, Switzerland[1], Department of Internal Medicine, University and University Hospital Zurich, Zurich, Switzerland[2], Institute of Intensive Care Medicine, University and University Hospital Zurich, Zurich, Switzerland[3], Department of Cardiology, University and University Heart Center, University Hospital Zurich, Zurich, Switzerland[4], Department of Surgery, University and University Hospital Zurich, Zurich, Switzerland[5]

Introduction:
In sepsis, early outcome prediction would be very useful to separate adaptive *mechanisms of survival* from maladaptive *mechanisms of death*. The aim of this study was to test if telemetry derived changes in heart rate during early sepsis could predict outcome in a long-term rat model of fecal peritonitis.

Methods:
Male Wistar rats (n = 24) were instrumented with a venous line for the administration of fluids, antibiotics and analgesics. A telemetry transmitter continuously collected ECG signals. Sepsis was induced by the intra-peritoneal injection of fecal slurry, and the observation time was 48 hours. Nalbuphine was administered continuously i.v. to comply with animal welfare requirements. Additional animals underwent arterial cannulation at baseline (n = 9), 4 (n = 16) or 24 hours (n = 6) for physiology and laboratory measurements.

Results:
Mortality of the sepsis model was 33% (8/24), and all deaths occurred between 4 and 22 hours. The septic animals were characterized by lethargy, fever, tachycardia, positive blood cultures, and elevated cytokine (IL-6, TNF) and B-type natriuretic peptide levels. An increase in heart rate of ³ 50 bpm during the first 4 hours of sepsis predicted death with a good sensitivity and specificity of 88 % each (p=0.001). The analysis of heart rate variability (HRV) demonstrated autonomic dysfunction during early sepsis in non-survivors.

Conclusion:
Telemetry derived changes of heart rate during early sepsis prognosticated outcome in research animals. HRV analysis identified autonomic dysfunction during early sepsis as a potential mechanism of death. This animal model allows the study of underlying mechanisms and the testing of novel therapies in sepsis.

Grant Acknowledgment:

This work was supported by a research grant from the *Privatdozenten-Stiftung* of the University of Zurich (2016) attributed to AR. VJ's preclinical sepsis research is supported by the "Forschungskredit" of the UZH (2017).

3932

R. Bruckner[1], N. Marsiano[2], E. Nissim-Eliraz[2], E. Nir[2], M. Leutenegger[1], C. Gottier[1], S. Lang[1], M. Spalinger[1], G. Rogler[1], S. Yagel[3], M. Scharl[1], N. Shpigel[2]

Validation of a novel xenograft mouse model for intestinal fistulas

Department of Gastroenterology and Hepatology, Universital Hospital Zurich, and University of Zurich, Zurich[1], Koret School of Veterinary Medicine, Hebrew University of Jerusalem, Rehovot[2], Department of Obstetrics & Gynecology, Hadassah University Hospital, Jerusalem[3]

Introduction:
Fistulas are a frequent, relapsing complication in Crohn's disease (CD), affecting up to 50% of patients at least once. Surgical resection is regularly required, as medical treatment outcome with conventional drugs is often insufficient. Previously, we demonstrated that epithelial-to-mesenchymal transition (EMT) plays a critical role for fistula development in CD patients. We found particular cytokines and their receptors upregulated along the tracts, supporting fistula development via the stimulation of EMT. Despite some progress in understanding the pathogenesis, there is still an urgent need for more effective medical treatments for CD patients with fistula formation. Due to a lack of a reliable *in vivo* model, new drug developments are complicated. Here, we validated a promising new human gut xenograft (XGR) mouse model of intestinal fistulas, clearly resembling the human situation.

Methods:
12-18 weeks (w) old human fetal small intestine was transplanted subcutaneously onto the backs of SCID mice. After 12–16w, ~15% of the mature xenografts spontaneously developed enterocutaneous fistulas. Using systemic LPS treatment followed by mild skin irritation adjacent to the transplant, we established a reproducible model system, resulting in enterocutaneous fistulas 2-4w later. XGR samples were analysed by immunohistochemistry staining (IHC) for EMT-, immune cell- and cell death markers.

Results:
IHC stainings of the XGR fistulas showed similar expression patterns for various EMT markers (e.g. SNAIL1) like in human CD fistula samples. The overexpression of the mesenchymal marker α-smooth muscle actin confirmed the hypothesis that EMT plays a critical role for the fistula development in the XGR mouse model, too. Moreover, collagen staining showed that the inflammatory regions were associated with fibrosis suggesting extracellular matrix remodeling.

The inflammatory response up- and downstream to the XGR fistula tracts mainly consisted of human CD45+ cells, but only very few murine CD45+ cells. Further characterization revealed CD4+ T cells as predominant cell type in the fistulating samples. We could confirm CD3+ cells from the human fetal guts proliferate and expand during the development *in situ*. Also strong expression levels of human CD68+ cells were found in the XGR fistulas. The overexpression of TNFα in the XGR fistulas samples emphasizes the importance of this mouse model, since this most likely represents a novel platform for the evaluation of new therapies for CD fistulas *in vivo*.

Positive TUNEL and cleaved caspase-3 IHC stainings in the XGR fistula samples suggest apoptosis playing a role here, too.

Conclusion:
Our data demonstrate that the *in vivo* model recapitulates both morphologically and mechanistically, human CD-associated fistulas. Establishing this novel *in vivo* platform, could improve identifying unique treatment targets and help to evaluate new therapies.

3933

M. Durst[2], P. Jirkof[2], M. Arras[2], K. Schmidt-Bleek[3], F. Buttgereit[1], A. Lang[1]

Evaluating analgesia in mouse osteotomy: Tramadol and Buprenorphine applied via the drinking water

Department of Rheumatology and Clinical Immunology, Charité-Universitätsmedizin Berlin, Germany[1], Division of Surgical Research, University Zurich, Switzerland[2], Julius Wolff Institute and Centre for Musculoskeletal Surgery, Charité-Universitätsmedizin Berlin, Germany[3]

Introduction:
Managing pain in rodents is crucial for animal welfare and experimental quality. Some injectable analgesics need to be administered within short intervals; this comes with increased stress for the animals due to handling and restraining. Applying medication with the drinking water can be a method for refining the pain management. However, recommendations on dosages for medication in the drinking water vary strongly or lack completely. Additionally a reliable voluntary drug intake after painful procedures is controversially discussed.

Methods:
This refinement project was integrated into a basic research study on bone healing. Three commonly used analgesia protocols (Tramadol (0.1 mg/ml vs. 1 mg/ml) and buprenorphine (0.009 mg/ml)) were administered via drinking water in the mouse osteotomy model. The drinking behaviour was assessed. The analgesic efficiency was evaluated with clinical and behavioural parameters as well as model specific pain parameters to assess reduced general wellbeing and pain. Short and long-term stress was assessed with faecal corticosterone metabolites and changes in the adrenal glands. The impact on bone healing was evaluated with µCT and histology.

Results:
Mice show more drinking events during the night than the day with reduced events in animals treated with the high tramadol dosage. Anaesthesia itself strongly influences the clinical and behavioural parameters. The high dosage of tramadol leads to a reduced general wellbeing and to higher scores in the pain detecting parameters. Short-term stress occurs in all groups on the first day while there is no visible long-term stress. There are no differences in bone healing with the three different analgesics.

Conclusion:
The integration of a refinement study into a basic research project proved to be useful to evaluate different pain management protocols. A reduction of the animal number is possible. Pain related parameters suggest tramadol in the low dosage and buprenorphine administered via the drinking water are efficient. Tramadol in the high dosage has a negative impact on the animal's wellbeing without providing a better pain relief. Though bone healing is not influenced by the different pain management protocols in this study, the effects of a changed pain management protocol should always be evaluated in the particular animal model. With this study, an evidence-based recommendation on the pain management in the mouse osteotomy model can be given.

3934

H. Mbunkah[1], A. Marzel[1], S. Schmutz[2], Y. Kok[1], O. Zagordi[2], M. Shilaih[1], N. Nsanwe[3], E. Mbu[3], L. Besong[5], B. Sama[4], E. Orock[6], R. Kouyos[1], H. Günthard[1], K. Metzner[1]

Low Prevalence of Transmitted HIV-1 Drug Resistance Detected By a Dried Blood Spot Based NGS Method in Newly Diagnosed Individuals in Cameroon in the Years 2015/16

Infectious Diseases and Hospital Epidemiology, University Hospital Zurich, Zurich[1], Institute of Medical Virology, University of Zurich[2], HIV Treatment Centre, Regional Hospital Bamenda, Cameroon[3], HIV Treatment Centre, District Hospital Ndop, Cameroon[4], HIV Treatment Centre, District Hospital Kumba, Cameroon[5], HIV Treatment Centre, Regional Hospital Ngaoundere, Cameroon[6]

Introduction:
The use of combinations of antiretroviral drugs has proven remarkably effective in controlling the progression of HIV-1 and prolonging survival, but these benefits can be hampered by the development of drug resistance. In resource-limited settings, many individuals receiving first-line drugs develop virological failure and may transmit drug resistant viruses. In order to determine the most recent prevalence, risk factors and transmission patterns of drug resistance mutations (DRMs), we monitored HIV-1 drug resistance using a novel next-generation sequencing assay applicable to dried blood spot (DBS) samples.

Methods:
DBS samples and questionnaires were collected from 360 newly HIV-1 diagnosed individuals in four hospitals in urban areas in Cameroon in the years 2015-16. We developed an HIV-1 protease and reverse transcriptase drug resistance genotyping assay applicable to DBS and all HIV-1 subtypes of at least group M, called DBS-NGS-GRT. The World Health Organization (WHO) 2009 list of mutations for transmitted drug resistant HIV-1 strains was used to analyze DRMs.

Results:
Applying our DBS-NGS-GRT assay, baseline HIV-1 drug resistance data were obtained from 298/360 (82.8%) newly diagnosed individuals. Of those, 63% were females and the median CD4 count was 303 cells/µl blood. Most patients were between the primary stage and stage 2 of the infection following the WHO clinical staging. Patients had a median age of 36 years, with no viral load records but a median cDNA copy number of 4.4 Log_{10} copies/ml. Samples that failed amplification were significantly lower in cDNA copy number than those which were successfully amplified ($p<0.0001$). The predominant HIV-1 subtype was CRF02_AG (63.4%) (Figure 1a). At frequencies >15%, DRMs to nucleoside reverse transcriptase inhibitors (NRTI) were observed in 3.0% (9/298), to non-NRTIs in 4.0% (12/298), and to protease inhibitors in 1.3% (3/240). The NNRTI-mutation K103N was the most commonly detected (2.7%). Expanding the analysis to low abundant DRMs, i.e. 3-15%, 12 additional individuals (4.0%) were found (Figure 1c). Scoring the DRMs with the Stanford system, high-level drug resistance profiles to any antiretroviral drug were found in 10/298 (3.4%) patients while 6.7% (20/298) of patients had DRMs that caused low-level resistance. Questionnaire data revealed that having unprotected sex with a known HIV-1 positive person (adjusted odds ratio 9.6 (95% C.I. 1.79 - 51.3, p=0.008)) was significantly associated with the transmission of DRMs ($p = 0.018$).

Conclusion:
Transmitted HIV-1 drug resistance is currently low in the study sites in Cameroon. Evidence of some risky sexual behaviors depicts a public health problem with possible implications on the prevention of new HIV-1 infections in the country.

3935

P. Kamat[1], B. Kollar[1], R. Schweizer[1], J. Plock[1]

Assessment of the vascular glycocalyx and the endothelium during graft vasculopathy following vascularized composite allotransplantation

Department of Plastic Surgery and Hand Surgery, University Hospital Zurich, Zurich[1]

Introduction:
Vascularized composite allotransplantation (VCA) is a promising treatment for composite tissue defects. A major challenge in this procedure is graft vasculopathy (GV), characterized by vascular endothelial cell damage and vascular inflammation, resulting in graft rejection. Early identification and understanding the mechanisms of GV could help to curate potential therapeutic interventions in preventing graft rejection. The vascular glycocalyx contributes extensively towards endothelial cell activation and inflammation. However little is known about the glycocalyx as extracellular matrix of the vasculature with regards to transplantation. We therefore analyzed the vascular glycocalyx and the endothelium to identify potential biomarkers for GV.

Methods:
A rat model of hind limb transplantation from Brown Norway to Lewis was used to simulate VCA. Post transplantation, all rats were treated with tacrolimus (TAC) for 1week after which treatment was withdrawn until they developed grade II rejection. Thereafter, the rats followed different treatment conditions as described below and monitored for 8days or until grade III rejection. Group 1 received no treatment. Group 2 obtained TAC (0.5 mg/Kg BW/d) and dexamethasone (4 mg/Kg BW/d) to counteract rejection. In the remaining rats, immunosuppressive effects of adipose derived stem cells (ADSCs) were tested by administrating two doses of $5x10^6$ cells within 3days either systemically (group 3) or locally (group 4). Stainings were performed on 5µm thick sections of formalin fixed paraffin embedded samples from the proximal artery. The van gieson stain revealed intimal vessel wall thickness. The compositional change in the glycocalyx was determined by alcian blue staining. Immunostaining was performed for vWF as a marker for endothelial cell activation.

Results:
After withdrawal of TAC, group 1 showed grade III rejection within 4days. For group 2, all rats survived the 8days monitoring period. One rat from group 3 and 4 rejected the graft at day5 and two rats in group 4 rejected at day7. The intimal wall thickness and alcian blue staining showed no differences between the groups. The vWF staining showed significant decrease in groups 3&4 when compared to group 1 ($p=0.0197$) indicating endothelial cell protective nature of ADSCs. Similar decrease for group 3&4 was observed when compared to group 2 ($p=0.0342$) indicating endothelial cell damage despite the use of immunosuppressants.

Conclusion:
ADSCs improved survival of grafts in absence of immunosuppressants. Indifferences in Van gieson and alcian blue staining between the groups shows their inadequacy to identify acute GV. The significant increase of vWF for group 1 and 2 emphasizes endothelial damage as an initiator of GV and provides as an early marker. Further analysis of inflammatory markers to confirm GV in the control group is warranted. Assessment of other markers for endothelial damage and changes in the glycocalyx is ongoing.

3936

R. Reimann[1], A. Assunta[1], C. Caflisch[1], I. Irpinio[1], H. Hornemann[1], S. Schneider[2], A. Aguzzi[1]

The structural basis of prion-associated neurodegeneration

Neuropathology, Neuropathology, Zürich[1], Brain Mind Institute, Ecole Polytechnique Fédéral de Lausanne, Lausanne[2]

Introduction:
Expression of the cellular prion protein (PrP^C) is a prerequisite for neurodegeneration in fatal transmissible spongiform encephalopathy (TSE) *(1, 2)*. PrP^C is encoded by *Prnp* and structurally consists of a globular domain (GD) hinged to an amino-proximal tail (FT, amino-acids 23-125) (*3*). Neurotoxicity induced by antiprion antibodies triggers converging pathways as in bona fide TSE (*4*). By using this paradigm, we have identified the FT as the executive domain in prion mediated neurodegeneration (*5*). In order to identify well-defined therapeutic targets, we now address the relation between the known functional domains of the FT and its pathological function by AAV mediated simultaneous expression of NeonGreen and unaltered of mutated PrP^C in cerebellar organotypic slice cultures (COCS). The functional domains comprise the polybasic region, including the charged cluster 1 (CC1, amino-acids 23-27), the octarepeat (OR, amino-acids 50-90), the charged cluster 2 (CC2, amino-acids 95-110) and the hydrophobic core (HC, amino-acids 111-120) (*6*).

Methods:
COCS from PrP deficient mice ($Prnp^{ZH3/ZH3}$) are infected on day zero in culture with Adeno Associated Virus (AAV), resulting in a transient expression of a bicistronic construct. Different constructs under the synapsin promoter allows for the expression of the fluorescent reporter NeonGreen simultaneously with unaltered or mutated PrP^C (synthetic DNA). After two weeks in culture, neurotoxicity is induced with the Fab fragment of the antiprion antibody POM19 (FabPOM19, binding the GD). The read out is based on NeonGreen morphometry.

Results:
COCS of $Prnp^{ZH3/ZH3}$ infected with AAV expressing NeonGreen without murine wild type PrP^C are resistant against neurotoxicity induced by antiprion antibodies. In contrast, antiprion antibody mediated neurodegeneration is restored in neurons from $Prnp^{ZH3/ZH3}$ COCS after infection with AAV allowing for the PrP^C alongside with NeonGreen. In contrast, expression of prion protein depleted for the polybasic region ($PrP_{\Delta 23\text{-}31}$) does not restore neurotoxicity. Lysine residues of the CC1 are functionally essential, since mutations of these residues to alanine are sufficient for blocking antiprion antibody mediated neurodegeneration. Furthermore, expression of the deleting mutant $PrP_{\Delta 32\text{-}93,}$ with an intact polybasic region but a lack of larger part of the FT including the OR, does not restore FabPOM19 induced neurotoxicity. Additionally an entire flip of the OR (OR-mirror) blocks the pathological function of prion protein. However, neither the five tryptophan nor the four-histidine residues are essential for antiprion antibody mediated neurodegeneration. Additionally expression of a CC2 deletion mutant restores pathological function.

Conclusion:
We identified the polybasic region and the OR as key functional domains in antiprion antibody mediated neurodegeneration. In contrast, CC2 is not required for the pathological function of the prion protein. We further pinpointed the pathological domains of the polybasic region to its three-lysine residues. The physical properties of OR alone seem not to be sufficient for an intact functional FT in our paradigm nor is the OR a simple spacer between the two charged clusters, as demonstrated by the OR mirror construct. However, selective alterations of the copper binding site or the tryptophan residues of the OR does not interfere with antiprion mediated neurodegeneration.

1. S. Brandner et al., Nature 379, 339-343 (1996). / **2**. G. Mallucci et al., Science 302, 871-874 (2003). / **3**. R. Riek et al., FEBS Lett 413, 282-288 (1997). / **4**. U. Hermann et al., PLOS Pathogens (2015). / **5**. T. Sonati et al., Nature 501, 102-106 (2013). / **6**. A. Aguzzi et al., Annu Rev Neurosci 31, 439-477 (2008).

3937

W. Baumgartner[1], L. Otto[1], S. Hess[2], W. Stark[2], S. Märsmann[1], M. Calcagni[1], P. Cinelli[3], J. Buschmann[1]

Biomimetic Cartilage/ Bone Interface

Division of Plastic and Hand Surgery, University Hospital Zurich, Rämistrasse 100, CH-8091 Zurich, Switzerland[1], Institute for Chemical and Bioengineering, Department of Chemistry and Applied Biosciences, ETH Zurich, CH-8093 Zurich, Switzerland[2], Division of Trauma Surgery, University Hospital Zurich, Rämistrasse 100, CH-8091 Zurich, Switzerland[3]

Introduction:
The interface between cartilage and bone is characterized by a gradient of calcium phosphate phases that decline in content from bone towards cartilage. Adipose-derived stem cells are able to differentiate into chondrocytes and osteoblasts, offering the option to use one single cell source for tissue engineering of a cartilage/ bone interface.

Methods:
We used an electrospun poly-lactic-co-glycolic acid (PLGA) mesh with incorporated amorphous calcium phosphate nanoparticles in different weight percentages, having a gradient from 30%, 20%, 10% and 0% towards the cartilage mimicking side of the biomimetic interface. The materials were seeded with human adipose-derived stem cells (ASCs) and either cultivated under static conditions or under dynamic conditions in a perfusion bioreactor without any further supplementation of the culture medium. After a total of four weeks, quantitative RT-PCR was performed for eleven relevant genes, including typical marker genes for osteo- and chondrogenesis, but also for adipo- and angiogenesis.

Results:
Under static conditions, the presence of amorphous calcium phosphate nanoparticles did not have any impact on osteo- and chondrogenesis related genes – only CD31 (and endothelial marker gene) was upregulated in the presence of nanoparticles compared to pure PLGA. In contrast, under dynamic conditions, ASCs exhibited an increased expression of chondrogenic marker gene Sox9 towards the cartilage mimicking side. In addition, ASCs showed an increased expression of osteogenic marker gene osteocalcin towards the bone mimicking side.

Conclusion:
We conclude that amorphous calcium phosphate nanoparticles incorporated in electrospun PLGA meshes influence the differentiation behaviour of human ASCs. Electrospun meshes with gradients of nanoparticles may act as promising cartilage/bone interfaces when cultivated under perfusion in a bioreactor system.

3938

N. Cohrs[2], K. Schulz-Schönhagen[2], D. Mohn[3], W. Stark[2], P. Wolint[1], G. Meier Bürgisser[1], J. Buschmann[1]

Modification of silicone elastomers with Bioglass 45S5® increases in vivo tissue biointegration

Division of Plastic and Hand Surgery, University Hospital Zurich, Rämistrasse 100, CH-8091 Zurich, Switzerland[1], Institute for Chemical and Bioengineering, Department of Chemistry and Applied Biosciences, ETH Zurich, CH-8093 Zurich, Switzerland[2], Clinic of Preventive Dentistry, Periodontology and Cariology, University of Zürich, Center of Dental Medicine, Zürich, Switzerland[3]

Introduction:
Silicone is an important material for medical devices. Not only for breast implants, but also for the driveline of ventricular assist devices (VADs) in cardiovascular surgery. These drivelines have exit sites at the patient's abdomen where problems may occur in form of chronically wounded tissue most susceptible to infection.

Bioglass (BG) which is a mixture of several oxides is antibacterial and has been shown to activate and support wound healing. BG-silicone composites may therefore be a viable option for drivelines of VADs.

Methods:
We used Bioglass 45S5® which is a composition of 45 wt% SiO_2, 24.5 wt% Na_2O, 24.5 wt% CaO and 6 wt% P_2O_5. BG-silicone composites with microBG and nanoBG were manufactured and characterized *in vitro* (simulated body fluid) and *in vivo*. Smooth and porous composites were used and compared in terms of biointegration in the chorioallantoic membrane assay (CAM) of the chicken embryo.

Results:
Porous nano- and microcomposites were obtained with interconnected pores up to 1 mm in diameter. Formation of hydroxyapatite upon exposure to simulated body fluid was determined on the surfaces of the porous materials incorporating BG. Incorporation of BG nanoparticles resulted in a stiffer material compared to pure silicone, while microparticles' incorporation had similar stiffness like pure silicone. Tissue integration as assessed by the CAM assay increased in the following order:

Silicone << microBG < nanoBG.

Conclusion:
Porous and non-porous BG/silicone composites offer a viable option for medical devices. Compared to pure silicone, nanocomposites of silicone with Bioglass 45S5® exhibit a better biointegration and might be favorable by reducing infection.

3939

M. Schwarzfischer[1], M. Morsy[1], C. Stanzl[1], K. Atrott[1], S. Lang[1], G. Rogler[1], M. Scharl[1], M. Spalinger[1]

Heat shock protein GP96 is essential for self renewal of the intestinal epithelial barrier

Department of Gastroenterology and Hepatology, Universital Hospital Zurich, Zurich[1]

Introduction:
The intestinal epithelium constitutes an important barrier that separates the body from the external environment to prevent access of external pathogens or potential hostile agents. Defects in epithelial barrier function are a characteristic clinical feature of intestinal disorders, such as inflammatory bowel disease (IBD). Genome-wide association studies identified the gene locus encoding heat shock protein GP96 (also known as GRP94) as a risk factor to develop IBD, and recent in vivo data suggest a role for GP96 in maintaining intestinal barrier function and gut homeostasis.

Methods:
To induce an intestinal epithelial cell-specific deletion of GP96, mice with a loxP flanked GP96 gene were bred with VillinCre mice (constitutive deletion) or VillinCre-ERT2 mice (inducible deletion). To induce GP96 deletion in GP96-VillinCre-ERT2 mice (N=11), Tamoxifen was injected at five consecutive days (1mg/day).

Results:
Constitutive deletion of GP96 in the intestinal epithelium turned out to be embryonically lethal. Conditional GP96 deletion upon tamoxifen application resulted in the development of severe diarrhea and rapid weight loss after 5-6 days after treatment. Colonoscopy revealed macroscopic signs of inflammation, including increased granularity of the colonic mucosa, fibrin deposits, and strong vascularization of the colon. While the wall of the small intestine appeared transparent and fragile, the colon was thickened and significantly shortened. Histological analysis revealed severe lesions throughout the small intestine, characterized by a loss of goblet cells, decay of crypts and villi, as well as immune cell infiltration, culminating in complete eradiation of the intestinal epithelium and subversion of the mucosal architecture. Morphological changes in the proximal and the distal colon were also observed, but less prevalent. Surprisingly, staining for cleaved caspase 3 disclosed a comparable low number of apoptotic cells throughout the whole intestinal epithelial. However, staining for the proliferation marker Ki67 revealed the absence of proliferating cells in the bottom of the remaining crypts.

Conclusion:
Our results indicate that GP96 plays a crucial role in the maintenance of the intestinal epithelial architecture, self-renewal and regeneration of the mucosa, possibly via mediating proliferation and differentiation of intestinal stem cells. Strikingly, our hypothesis is in line with clinical studies, reporting elevated expression levels of GP96 in the intestinal epithelium of IBD patients, where recurring damage and inflammation of the intestinal surface require intense *regeneration* and constant epithelial restitution. Due to this important role of GP96 in mediating self-renewal capacities in intestinal epithelial cells, it may serve as a new target for therapy in IBD, offering the potential to induce mucosal healing.

3940

A. Özcan[1], D. Bunton[2], G. Macluskie[2], M. McAteer[3], T. Coulter[3], Y. Ding[3], U. Peral[3], O. Boyman[1], A. Kolios[1]

Topical MTX-GNPs reduce IMQ-induced inflammation in mice

Klinik für Immunologie, Universitätsspital Zürich[1], ReproCELL Europe Ltd, Weipers Centre, Glasgow, U.K.[2], Midatech Pharma, Milton Park, Abingdon, Oxfordshire, U.K.[3]

Introduction:
Methotrexate (MTX) is a widely used immunosuppressive agent for the treatment of several autoimmune and chronic-inflammatory conditions, such as rheumatoid arthritis (RA) and psoriasis. MTX is usually administered systemically, which can cause side effects, including liver damage and kidney failure. Due to its polarity and high molecular weight topical MTX penetrates very poorly through the skin barrier and therefore needs a targeted drug delivery systems (TDDS) to overcome biological barriers. Gold nanoparticles (GNP) have been used as TDDS in cancer therapy and have recently been shown to deliver MTX into the skin by topical application (Bessar H et al., 2016).

Methods:
Here, we explored the therapeutic potential of a novel topical MTX formulation in inflammatory skin disease. The skin permeability of MTX was increased via conjugation to GNP (MTX-GNP). Using the imiquimod (IMQ)-induced mouse model of psoriasis, where IMQ is applied on the ear of a mouse, we evaluated in vivo efficacy and functionality of MTX-GNPs.

Results:
Subcutaneous administration of MTX-GNPs ameliorated IMQ-induced inflammation in a dose-dependent manner, as measured by ear thickness, erythema and scaling. The effect of systemic MTX-GNP compared to systemic MTX alone demonstrated a superior anti-inflammatory action on IMQ-induced inflammation. At day 5, mean ear thickness (MET) of MTX-GNP treatment group was 286.25µm whereas the MET of MTX group was 335µm, the former being significantly lower and latter not, compared to the treatment group who received IMQ only (MET=351µm), p values being $p=0.0340$ and $p>0.999$, respectively. Additionally, MTX treatment displayed higher toxicity than MTX-GNP. Topical MTX-GNPs were formulated based on the systemic dose inducing the highest clinical efficacy but the least toxicity. Topical application of MTX-GNP gel significantly reduced IMQ-induced inflammation whereas a gel formulation of MTX, showed no improvement (MET of mice treated with IMQ only: 390µm; MET of MTX-GNP group: 288µm, MET of MTX group: 346.25µm. MTX-GNP vs. IMQ only: $p=0.0025$; MTX vs. IMQ only $p=0.3767$, all calculated on day 5).

Conclusion:
GNPs significantly improve delivery of MTX to the skin, thus allowing transdermal application of the drug. Topical MTX-GNPs reduced IMQ-induced inflammation in mice without significant toxicity. MTX-GNPs should be considered as a non-steroidal therapeutic option for inflammatory skin diseases.

3941

I. Zygoula[1], C. Schori[1], C. Grimm[1], D. Barthelmes[1]

Plasma levels of hypoxia-regulated factors in patients with age-related macular degeneration

Department of Ophthalmology, University Hospital Zurich[1]

Introduction:
Various hypoxia-related proteins are differentially expressed in the retina and secreted to the vitreous and/or aqueous humor of patients affected by dry or neovascular age-related macular degeneration (nAMD). To determine whether these conditions alter concentrations of cytokines also in the systemic circulation, we measured plasma levels of six hypoxia-related proteins.

Methods:
Plasma was prepared from EDTA blood that was collected from patients affected by dry AMD (n = 5), nAMD (n = 11), proliferative diabetic retinopathy (PDR; n = 9), and patients with an epiretinal membrane (ERM; n = 11). ERM samples served as negative controls, PDR samples as positive controls. Protein concentrations of vascular endothelial growth factor (VEGF), erythropoietin (EPO), angiopoietin-like 4 (ANGPTL4), placental growth factor (PlGF), tumor necrosis factor alpha (TNF-α), and pigment epithelium-derived factor (PEDF) were determined by enzyme-linked immunosorbent assay (ELISA).

Results:
The concentration of PlGF was significantly increased in plasma of patients affected by nAMD. Although no statistically significant differences were found for EPO, ANGPTL4, PlGF, TNF-α, and PEDF, the mean concentration of VEGF was lowest in the nAMD group. Plasma concentrations of the six factors did not correlate with gender or age of patients.

Conclusion:
nAMD may increase plasma concentrations of PlGF, making it a candidate as a biomarker for the neovascular form of AMD. Other factors, however, were not differentially regulated, suggesting that their systemic concentrations are not generally increased in hypoxia-related retinal diseases.

3942

M. Brüggen[1], V. Djamei[1], E. Contassot[1], K. Kabashima[2], P. Romanelli[3], S. Oro[4], P. Wolkenstein[4], L. French[1]

IRTEN - an international registry for toxic epidermal necrolysis

Department of Dermatology, University Hospital Zurich, Zurich[1], Department of Dermatology, University of Kyoto, Kyoto[2], Department of Dermatology, University of Miami Miller School of Medicine, Miami[3], Department of Dermatology, Henri-Mondor Hospital Paris, Paris[4]

Introduction:
Stevens-Johnson syndrome (SJS) and toxic epidermal necrolysis (TEN) are severe cutaneous adverse drug reactions associated with high rates of morbidity and mortality (25-30%). Our aim is to address some of the most relevant open questions regarding SJS/TEN. Clinically, these include I) the identification of risk factors (causative drugs, geographic variations) and the assessment/comparison of II) treatment strategies applied as well as III) the long-term outcome (incidence and impact of complications) in SJS/TEN patients. On a translational research level, our main scope is to identify biomarkers and gain a better understanding of the pathomechanisms underlying SJS/TEN.

Methods:
Given the rare occurrence of SJS/TEN, it is extremely challenging to conduct representative clinical studies and translational research with sufficient numbers of patients. To overcome this issue, we have established an international online Registry for SJS and TEN, shortly IRTEN. IRTEN provides an international platform for investigating important clinical and scientific issues in the field within an internationally representative prospective cohort of validated cases. It combines clinical data collection and optional biobanking with the knowledge of an expert network from three continents (Europe, Asia, America).

Results:
We have established an online electronic case report form (eCRF) based on the results of a Delphi exercise assembled by an international expert panel (National Institutes of Health SJS/TEN working group; Maverakis et al, 2017). The roll-out phase, during which we have optimized work flows and validated the eCRF, has been succesfully completed (11/2017). Patient inclusion will start in 01/2018. We have started expanding our network of participating centers.

Conclusion:
IRTEN aims to increase our understanding of the pathogenesis, risk factorsa and optimal clinical management of SJS/TEN by addressing these aspects in an internationally representative prospective cohort of validated SJS/TEN cases.

3943

C. Scheckel[1], M. Marigona[1], A. Adriano[1]

Systematic Profiling of Molecular Changes during Prion Disease Progression

Institute of Neuropathology, University Hospital Zürich, Switzerland[1]

Introduction:
Prion diseases are fatal neurodegenerative diseases and are caused by proteinaceous infectious particles termed prions. While the infectious agent of prion disease has been identified decades ago, the actual cellular processes that subsequently cause neurons to degenerate remain poorly understood. Importantly, different cell types show remarkable differences in their susceptibility to prion clearance, replication and toxicity, yet what determines these differences is entirely unknown. This highlights the importance of studying individual cell types rather than entire tissues. Of particular interest to prion disease are microglia and astrocytes, which are activated during prion disease progression, as well as neurons, which are especially vulnerable to prions.

Methods:
Using ribosome profiling, we will analyse translation rates in in a genome-wide and unbiased manner, specifically in prion disease-relevant cells. Mice will be injected intraperitoneally with either non-infectious brain homogenate or rodent-adapted scrapie prions, and analysed at 2, 4, 8, 16, and 24 weeks after inoculation and at the terminal stage of the disease (approximately 32 weeks post inoculation).

To quantitatively measure protein synthesis rates specifically in disease-relevant cells we will utilize a combination of two previously published techniques, ribosome profiling and TRAP (tandem ribosome affinity purification). Taking advantage of the binary Cre/lox system, GFP tagged ribosomes will be expressed in specific cell types in a Cre recombinase dependent manner. Ribosome protected fragments (RPF) will be recovered by partial nuclease digestion followed by the immunoprecipitation of tagged ribosomes. RPF libraries will be cloned and submitted for high-throughput sequencing.

Results:
We have generated mice that express GFP-tagged ribosomes specifically in either excitatory or inhibitory neurons, microglia, or astrocytes. These mice were subjected to prion injection, and, at the specified time points post prion infection, brain samples were frozen for cell-type specific ribosome profiling as well immunohistochemistry. We are currently applying cell-type specific ribosome profiling to assess protein synthesis rates in prion-infected mice, as well as immunohistochemistry to validate obtained genome-wide results.

Conclusion:
The outlined approach will identify a comprehensive list of genes that are differentially regulated during the progression of prion disease and that are important for different aspects of disease pathogenesis. The investigation of different cell types at multiple time points after prion infection, allows the dissection of the dynamics of disease progression and will shed light on the role and interplay of different cell types in pathophysiology. This project will not only yield novel and important insights into prion disease pathophysiology, but also will also contribute to our understanding of other neurodegenerative diseases and provide potential starting points for the development of targeted therapeutic interventions.

3944

I. Schneider[1], W. Baumgartner[1], O. Gröninger[2], W. Stark[2], S. Märsmann[1], M. Calcagni[1], P. Cinelli[3], P. Wolint[1], J. Buschmann[1]

Impact of cultivation condition and cell format of human adipose-derived stem cells: 3D-microtissues versus single cells seeded on an electrospun nanocomposite in a perfusion bioreactor or static cell culture

Division of Plastic and Hand Surgery, University Hospital Zurich, Rämistrasse 100, CH-8091 Zurich, Switzerland[1], Institute for Chemical and Bioengineering, Department of Chemistry and Applied Biosciences, ETH Zurich, CH-8093 Zurich, Switzerland[2], Division of Trauma Surgery, University Hospital Zurich, Rämistrasse 100, CH-8091 Zurich, Switzerland[3]

Introduction:
Working with stem cells requires cues for desired differentiations. For example, in bone tissue engineering, osteogenesis of stem cells is intended which is often achieved by supplementation of the culture medium in order to trigger this process. As an alternative option, different cultivation conditions – like dynamic culture under perfusion - may help to induce such a differentiation. Moreover, also the cell format may have an impact, as for example realized with 3D-microtissues.

Methods:
We used a bone-biomimetic nanocomposite material, poly lactic-co-glycolic acid and amorpous calcium phosphate nanoparticles (PLGA/aCaP) and seeded it with human adipose-derived stem cells (ASCs), either as single cells (SCs) or as 3D-microtissues (MTs). After a 2-week static cultivation, SC-seeded and MT-seeded constructs were either cultivated under dynamic conditions in a perfusion bioreactor or further under static cultivation. Quantitative RT-PCR was performed for CD73, CD90 and CD105 (minimal criteria stem cell markers), CD31 and CD34 (markers of endothelial cells), ALP and RUNX2 (early osteogenesis markers), for collagen 1 (medium osteogenesis marker) and osteocalcin (late osteogenesis marker), for PPAR-gamma-2 (adipogenesis marker) and Sox9 (chondrogenesis marker) expression.

Results:
Intended osteogenic differentiation was achieved best when ASCs were cultivated under static conditions as MTs, because the expression of typical osteogenic marker genes as well as genes relevant for angiogenesis was increased compared to the other conditions examined.

Conclusion:
We conclude that osteogenic differentiation of ASCs seeded on a bone-biomimetic nanocomposite is supported best when the cells are seeded as MTs and cultivated under static conditions.

3945

J. Gawinecka[1], H. Reiser[1], F. Schönrath[2], E. Arvaniti[3], C. Matter[4], V. Falk[2], M. Claassen[3], A. Von Eckardstein[1]

Comprehensive molecular profiling in acute aortic dissection: seeking diagnostic biomarkers

Institute for Clinical Chemistry, University Hospital Zurich[1], Department of Cardiothoracic and Vascular Surgery, German Heart Institute Berlin, Germany[2], Institute of Molecular Systems Biology, ETH, Zurich, Switzerland[3], Department of Cardiology and Cardiovascular Physiology, University Hospital Zurich, Switzerland[4]

Introduction:
Acute aortic dissection (AAD) is associated with extremely high lethality also because of a high rate of initial misdiagnosis. As yet, easily accessible and cost-effective blood tests only play a minor role in the diagnostics of patients with suspected AAD. Such biomarkers may also aid in the monitoring of patients at increased risk for AAD, for example patients with Marfan syndrome or with thoracic aneurysm. To discover biomarker candidates for the clinical management of AAD, we performed a comprehensive molecular profiling study as well as initial validation of biomarker candidates.

Methods:
First, we compared protein abundances in secretomes, which were produced by tissue culture of aortic samples from patients with AAD, aortic valve replacement (AVR), or thoracic aortic aneurysm (TAA). Second, we used RNA-Seq to quantify gene expression in aortic tissues themselves. Third, we measured 360 inflammation- or cardiovascular disease related proteins in plasma by using Proseek multiplex immunoassays.

Results:
Almost 1500 proteins were identified in aortic secretomes. First standard classification of proteins with fold change greater than two revealed 149 proteins differentiating AAD from AVR or TAA. Further computational analysis via regularized classification based on fold change identified platelet factor 4 (PF4), intelectin-1 and platelet basic protein as the best discriminators of AAD from either control group. In a first validation study, PF4 plasma levels were significantly decreased in AAD patients when compared to patients with AVR. The transcriptomic approach and Proseek immunoassays produced 20 and 8 top biomarker candidates, respectively. Among them plasminogen inhibitor type 1 (PAI1) proved itself as capable to discriminate better than D-Dimer, AAD patients from patients with either TAA, AVR or the two most relevant AAD differential diagnoses, namely pulmonary embolism and myocardial infarction.

Conclusion:
In a proof of principle study, we demonstrated the feasibility of discovering biomarkers for AAD by comprehensive molecular profiling of aortic tissues and plasmas and identified several promising candidates.

3946

A. Wyss[1], T. Raselli[1], G. Schmelczer[1], M. Spalinger[1], K. Atrott[1], I. Frey-Wagner[1], A. Sailer[2], M. Scharl[1], G. Rogler[1], B. Misselwitz[1]

Role of EBI2 and Oxysterols in the Development of Intestinal Lymphoid Structures and Colitis

Department of Gastroenterology and Hepatology, University Hospital Zurich, University of Zurich, Zurich[1], Chemical Biology & Therapeutics, Novartis Institutes for BioMedical Research, Basel[2]

Introduction:
Epstein Barr virus induced gene 2 (EBI2) is a G-protein coupled receptor expressed on immune cells. The EBI2 ligand 7α,25-Dihydroxycholesterol is produced by two enzymes, CH25H and CYP7B1. EBI2 and its oxysterol ligand were shown to mediate migration, positioning and differentiation of B cells within secondary lymphoid organs. The formation of gut lymphoid structures includes the interaction between a variety of chemotactic factors and their ligands. In the colon, there are two types of lymphoid structures, large colonic patches (CLP) and much smaller solitary intestinal lymphoid tissues (SILT). EBI2 is a risk gene for inflammatory bowel disease (IBD), however, neither SILTs nor EBI2 have been implicated in the pathogenesis of colitis.

Methods:
DSS colitis was induced by administration of 2-3% dextran sodium sulfate (DSS) for 7 days or 4 cycles of 7 days interspersed with 10 day recovery periods. To study the effect of EBI2 in the IL10 colitis model, $EBI2^{-/-}$ and $IL10^{-/-}$ mice were crossbred and examined after 200 days. Using a whole mount approach the colons of $EBI2^{-/-}$ mice and wildtype littermates were stained to determine the number of B cell follicles. We quantified lymphoid structures in HE stained colon “Swiss rolls” by analyzing 20 sections (~100µm apart) per colon.

Results:
In inflamed tissue of rectal biopsies from ulcerative colitis (UC) patients the oxysterol synthesizing enzymes CH25H and CYP7B1 and the oxysterol receptor EBI2 were significantly upregulated compared to non-inflamed tissue of UC patients or tissue of healthy controls. A similar upregulation was found in mouse colon tissue from acute and chronic DSS colitis, suggesting increased oxysterol production upon inflammation. However, loss of CH25H or EBI2 did not affect the severity of acute or chronic DSS colitis. In the IL10 colitis model, $EBI2^{-/-}/IL10^{-/-}$ mice showed less inflammation in histologically examined colon tissue compared to wildtype ($EBI2^{+/+}/IL10^{-/-}$) controls. Furthermore, $EBI2^{-/-}$ mice had significantly less B cell follicles and overall lymphoid structures within the colon than littermate wildtype controls. The difference was restricted to smaller lymphoid structures, pointing to a role of EBI2 in SILT generation or maturation. Wildtype mice with chronic colitis showed an increase of the number of colonic lymphoid structures, which was not observed in $EBI2^{-/-}$ mice.

Conclusion:
Oxysterol production is likely increased in the inflamed gut and knockout of the oxysterol receptor EBI2 affected the severity of colitis in experimental mouse models. We demonstrate a role of EBI2 in the development of intestinal lymphoid tissue during homeostasis and after immunological challenge. These findings establish a role for EBI2 and oxysterols in the maturation of the gut immune system and in the pathophysiology of inflammatory bowel diseases.

3947

B. Weder[1], C. Mamie[1], G. Rogler[1], S. Clarke[2], B. McRae[2], P. Ruiz[1], M. Hausmann[1]

BCL2 regulates differentiation of intestinal fibroblasts

Department of Gastroenterology and Hepatology, University Hospital Zurich, Zurich, Switzerland[1], AbbVie Bioresearch Center, AbbVie Worcester, MA, USA[2]

Introduction:
B-cell lymphoma (BCL)2 family members induce or abolish apoptosis. Activation and differentiation of fibroblasts is linked to the expression of the BCL2 family. As fibroblasts are activated during fibrosis, decreasing BCL2 might represent a potential treatment approach. Fibrosis as a common problem in patients with Crohn's disease (CD) is resulting from an imbalance towards excessive fibrous tissue formation driven by fibroblasts. We investigated the impact of BCL2 repression on fibrogenesis.

Methods:
Fibroblasts were stimulated with the BCL2 antagonist ABT-737 (AbbVie, USA, final concentration 0.01 – 100 nM). BCL2, BCLXL, α-SMA and COL1A1 were determined by qPCR, IF and WB. The impact of BCL2 antagonist treatment on TGFβ signaling pathways in primary human colonic fibroblasts was investigated using WB and IF. mRNA expression pattern in primary human colonic fibroblasts was determined by Next Generation Sequencing (NGS). For *in vivo* experiments, both the murine heterotopic transplantation model of intestinal fibrosis and the model of dextran sodium sulfate (DSS)-induced chronic colitis were used. Animals received BCL2 antagonist (50 mg/kg/day, intraperitoneally (i.p.)). Collagen layer thickness and hydroxyproline (HYP) content were determined.

Results:
BCL2 and BCLXL were significantly decreased in primary human colonic fibroblasts upon administration of 1nM and 10nM BCL2 antagonist treatment compared to vehicle in a dose-dependent manner (0.68 ± 0.12 and 0.49 ± 0.04 vs. 1.00 ± 0.00, respectively, * $p < 0.05$ for BCL2, 0.41±0.26 and 0.35±0.22 vs. 1.00 ± 0.00, respectively, * $p < 0.05$ for BCLXL). *COL1A1 and α-SMA* were decreased in both human and murine colonic fibroblasts upon BCL2 antagonist treatment compared to vehicle. WB analysis revealed a decrease of pERK1, pERK2 and SMAD3 from the TGFβ signaling pathways in primary human fibroblasts in a dose dependent manner upon BCL2 antagonist treatment compared to vehicle. NGS and qPCR revealed a link to the transcription factors GATA6 and SOX9 for mediating pro-fibrotic effects and for reprogramming fibroblasts. Collagen layer thickness was significantly decreased in the mouse model of fibrosis upon BCL2 antagonist administration compared to vehicle (* $p < 0.05$). Decreased HYP content upon BCL2 antagonist administration confirmed the preventive effects of the BCL2 antagonist on intestinal fibrosis *in vivo*.

Conclusion:
The BCL2 antagonist changed the expression profile of *BCL2* family members and prevented fibroblast differentiation into myofibroblasts. BCL2 antagonist administration partially prevented intestinal fibrogenesis in both the murine heterotopic transplantation model of intestinal fibrosis and the DSS-induced chronic colitis model and therefore may represent a potential treatment option against CD associated fibrosis.

3948

M. Spalinger[1], M. Schwarzfischer[1], A. Geirnaert[2], C. Gottier[1], S. Lang[1], C. Lacroix[2], G. Rogler[1], M. Scharl[1]

Loss of PTPN22 abrogates the beneficial effect of fecal microbiota transfer

Clinic for Gastroenterology and Hepatology, University Hospital Zurich, Zürich, Switzerland[1], Institute of Food, Nutrition and Health, ETH Zürich, Zürich, Switzerland[2]

Introduction:
In inflammatory bowel disease (IBD), shifts in microbiota composition and reduced microbial diversity have been described. There are attempts to transfer microbiota from healthy subjects to persons suffering from intestinal diseases. In *Clostridium difficile* infections, this approach is very efficient but the therapeutic value of fecal microbial transfer (FMT) in IBD remains controversial. Further, it remains elusive, how presence of genetic variants affects the outcome of FMT. In this study, we investigated whether FMT promotes recovery in a mouse model of colitis, and whether a variant in protein tyrosine phosphatase non-receptor type 22 (PTPN22), which is associated with reduced risk for Crohn's disease, affects the outcome of FMT.

Methods:
Acute colitis was induced in PTPN22 deficient (KO), PTPN22-variant (TG), or wild-type (WT) mice by administration of 2% DSS in the drinking water for 7 days. Mice with colitis were co-housed with healthy mice after removal of DSS. Due to coprophagy, this results in fast transfer of the microbiota between co-housed mice. Stool samples were collected every second day and sequenced for the V4 hyper-variable region in the bacterial 16S DNA.

Results:
As expected, DSS treatment resulted in weight loss, and even 7 days after withdraw of DSS (day 15), histology confirmed colitis. In line with previous reports, KO mice suffered from enhanced colitis, while TG animals were protected. In all genotypes, intestinal resulted in reduced microbial diversity (decreased Shannon index, $p<0.01$), and a marked shift in microbial composition, which normalized upon recovery (day 15). DSS-treated WT mice, which were co-housed with healthy WT or TG mice after colitis induction, showed faster recovery (earlier weight gain, reduced histological scores, less pronounced shortening of the colon, $p<0.01$ for all) and an earlier normalization of the microbiota. However, co-housing with healthy KO mice did neither promote recovery, nor normalization of the microbiota. Further, co-housing of KO mice with healthy WT mice did not result in faster recovery, and co-housing with healthy KO mice even promoted disease. In contrast, although presence of the variant resulted in reduced colitis severity upon DSS treatment, it did not affect the outcome of FMT.

Conclusion:
Our results indicate that in WT and PTPN22 TG mice, co-housing promotes normalization of the microbiota and recovery from colitis. However, loss of PTPN22 in the donor or recipient abrogated the beneficial effect of FMT. This indicates that the genetic make-up of both, donor and recipient affects the outcome of FMT, which might – at least in part – explain the controversial findings from FMT studies conducted in IBD patients.

3949

M. Spalinger[1], M. Schwarzfischer[1], L. Hering[1], A. Geirnaert[2], C. Gottier[1], S. Lang[1], C. Lacroix[2], G. Rogler[1], M. Scharl[1]

Presence of an autoimmunity-associated variant in PTPN22 promotes chronic colitis in a microbiota dependent manner

Clinic for Gastroenterology and Hepatology, University Hospital Zurich, Zürich, Switzerland[1], Institute of Food, Nutrition and Health, ETH Zürich, Zürich, Switzerland[2]

Introduction:
The gut microbiota is an important factor for intestinal health, and intestinal inflammation is accompanied with profound changes in intestinal microbiota composition. A variant in the gene locus encoding protein tyrosine phosphatase non-receptor type 22 (PTPN22) is associated with enhanced susceptibility for autoimmune diseases, but negatively associates with inflammatory bowel disease (IBD). In previous work, we demonstrated that PTPN22 affects molecular pathways involved in IBD pathogenesis, but the role of PTPN22 in shaping the intestinal microbiota has not been addressed so far.

Methods:
Acute and chronic DSS colitis was induced in mice expressing the autoimmunity-associated PTPN22 variant (TG), PTPN22 deficient (KO) mice, or wild-type (WT) littermates. Stool samples were collected at day 8 (acute colitis), day 18 (recovery from the first DSS cycle) and day 76 (chronic colitis) and sequenced for the V4 hyper-variable region in the bacterial 16S DNA.

Results:
During acute DSS treatment, TG mice were protected from colitis onset, while KO mice suffered from more severe disease. During induction of chronic colitis with four consecutive DSS cycles, however, enhanced colitis was observed in TG mice from the 2nd DSS cycle onwards whitch persisted until the end of the experiment. Of interest, at day 7, DSS-induced dysbiosis was milder in TG mice than in WT or KO counterparts. However, at day 18 the microbiota normalized in WT and KO mice, while DSS-induced dysbiosis was still present in TG mice. To address the role of persistent dysbiosis in subsequent disease progression, cecum content from TG or WT mice after recovery from the first DSS cycle (day 18) was collected and transferred it into treatment-naïve TG or WT mice. Of interest, transfer of cecum content from DSS-challenged TG mice promoted subsequent DSS-induced acute colitis, while transfer of cecum content from WT or naïve TG mice had no effect. Further, in TG mice, we observed an initially very high, but transient expression of the anti-microbial peptide Reg3g, which was drastically reduced upon recovery from the first DSS-cycle. On the other hand, KO mice showed delayed induction of anti-microbial peptides upon acute DSS treatment, but normal or even increased levels in following DSS cycles. Presence of beneficial bacteria such as *Roseburia* gradually decreased in TG mice, while it increased in WT and KO mice after the first DSS cycle. On the other hand, potential pathogenic bacteria, such as *Helicobacter ssp* increased in TG mice after recovery from the first cycle, while they decreased in KO mice.

Conclusion:
Taken together, our results indicate that presence of the PTPN22 variant affects intestinal inflammation via modulating the host's response to the intestinal microbiota.

3950

C. Greis[1], C. Zürcher[4], V. Djamei[1], A. Moser[3], S. Lautenschlager[2], A. Navarini[1]

Unmet digital Health Service Needs in Dermatology Patients

Dermatologische Klinik, Universitätsspital Zürich, Zürich[1], Dermatologisches Ambulatorium, Triemli Spital, Zürich[2], novaderm Praxis, Affoltern a.A.[3], Department für Physiotherapie/Ergotherapie, Universitätsspital Zürich, Zürich[4]

Introduction:
Digital health services are rapidly gaining acceptance in healthcare systems. Dermatology as an image-centric specialty is particularly well suited for telemedical services. However, dermatology patients' demands of electronic services remain largely unexplored.

Methods:
This study investigated patients' views in primary, secondary and tertiary referral centers. In August 2017, 841 questionnaires were filled in by dermatology patients.

Results:
76.34% expressed interest in using digital healthcare services as part of medical consultations. 84.41% of all patients would complete their initial registration form electronically. Fewer patients were comfortable with sending pictures of skin changes to their doctors using email (40.89%) or mobile health applications (40.61%). Specific interest was indicated for arranging appointments online (90.80%) and electronically-placed prescriptions (76.56%), rather than online learning videos (42.03%), and actual online consultations (34.53%). 65.37% of patients would pay for online consultations themselves.

Conclusion:
Taken together, interest in electronic health services is high in dermatology patients. Our data suggests that readily understandable electronic services such as online-arranged appointments and electronic prescriptions are of higher interest to patients than the current type of online consultations. Therefore, the full potential of teledermatology still remains to be tapped by newer, more attractive forms of services closely adapted to patients' demands.

3951

M. Mannil[1], J. Von Spiczak[1], R. Manka[1], H. Alkadhi[1]

Texture Analysis and Machine Learning for Detecting Myocardial Infarction in Non-Contrast Low Dose CT: Unveiling the Invisible

Institute of Diagnostic and Interventional Radiology at the University Hospital of Zurich, Switzerland[1]

Introduction:
Non-contrast enhanced cardiac CT (CCT) images are usually performed for quantifying the calcium load of coronary arteries (so called *calcium scoring*). These non-contrast CCT images are acquired using electrocardiography (ECG)-gating and at low radiation doses. Because of refraining from contrast media administration and applying low radiation doses, non-contrast enhanced CCT images usually do not allow to diagnose cardiac abnormalities other than calcifications, which also includes the diagnosis of MI.

Methods:
In this IRB-approved retrospective study, we included non-contrast enhanced electrocardiography-gated low radiation dose CCT image data (effective dose 0.5mSv) acquired for the purpose of calcium scoring of 27 patients with acute MI (9 female, mean age 60±12 years), 30 patients with chronic MI (8 female, mean age 68±13 years), and in 30 subjects (9 female, mean age 44±6 years) without cardiac abnormality, hereafter termed *controls*. TA of the left ventricle was performed using free-hand regions-of-interest and texture features were classified twice. Model I: controls vs. acute MI vs. chronic MI; Model II: controls vs. acute and chronic MI. For both classifications, six commonly used machine learning classifiers were used: decision tree C4.5 (J48), k-nearest neighbors (k-NN), locally weighted learning (LWL), RandomForest, sequential minimal optimization (SMO), and an artificial neural network employing deep learning. Additionally, two blinded, independent readers visually assessed non-contrast CCT images for the presence or absence of MI.

Results:
In model I, best classification results were obtained using the k-NN classifier (sensitivity 69%, specificity 85%, false-positive-rate (FPR) 0.15). In model II, best classification results were found with the LWL classification (sensitivity 86%, specificity 81%, FPR 0.19) with an area-under-the-curve from receiver operating characteristics analysis of 0.78. In comparison, both readers were not able to identify MI in any of the non-contrast, low radiation dose CCT images.

Conclusion:
This study indicates the ability of TA and machine learning for detecting MI on non-contrast low radiation dose CCT images being not visible for the radiologists' eye.

3952

M. Mannil[1], J. Von Spiczak[1], T. Hermanns[2], H. Alkadhi[1], C. Fankhauser[2]

Predicting the Success to Shock Wave Lithotripsy: Added Value of 3D Texture Analysis and Machine Learning on CT Images of Urinary Stones

Institute of Diagnostic and Interventional Radiology at the University Hospital of Zurich, Switzerland[1], Department of Urology, University Hospital Zurich, Zurich, Switzerland[2]

Introduction:
Urinary stone disease has a continuously increasing prevalence which currently ranges at around 10%. Treatment options for urinary stones include shock wave lithotripsy (SWL), flexible ureterorenoscopy (URS), percutaneous lithotripsy, and retrograde intrarenal surgery. The American Urological Association recommends either SWL or URS as first-line interventions for the treatment of symptomatic urinary stones below 20 mm in size.SWL is cost-effective and convenient for the patients since it can be performed in an outpatient setting without the use of general anaesthesia. However, insufficient stone disintegration may occur in up to 50% of patients undergoing SWL, which necessitates repeated SWL sessions or alternative, more invasive procedures such as URS. Invasive procedures are associated with higher morbidity, complication rates, and costs. Thus, accurate prediction of success to stone disintegration is desirable for identifying patients who benefit from primary SWL treatment.

Methods:
In this IRB-approved, retrospective multicentre study, 51 patients (mean age 55±15 years) with symptomatic urinary stone disease were included. All patients had non-enhanced abdominal CT before (median 31 days) and after (median 36 days) SWL. 3D TA including the entire urinary stone was performed on CT images acquired before SWL after postprocessing for pixel spacing and image normalization. Classification of successful SWL (defined as residual stone size < 2 mm) was performed based on CT images obtained after SWL. 3D TA features and the body mass index (BMI), initial stone size, and skin-to-stone distance (SSD) were analyzed with five commonly used machine learning models: (1) J48 decision tree (2) k-nearest neighbour (kNN), (3) artificial neural network (aNN) with backpropagation (Multilayer Perceptron), (4) Random Forest, and (5) sequential minimal optimization (SMO). To account for overfitting, the data set was split in a ratio of 2/3 for model derivation and 1/3 for validation. Machine learning-based predictions on the validation cohort were evaluated calculating the sensitivity, specificity, and the area-under-the-curve (AUC) from receiver operating characteristics (ROC) analysis.

Results:
Non-TA features BMI, initial stone size, and SSD each showed individually a weak correlation with SWL success. An added value was observed when combining these features with selected 3D TA features. ROC analysis consistently showed overall highest ROC AUC values (0.85) for 3D TA analysis (Histogram Kurtosis3D, and GLCM S(2,-2,0)SumEntrp, and S(0,3,0)DifEntrp) + SSD by use of a RandomForest classifier. When taking into account sensitivity and specificity two other RandomForest models showed comparable predictive ability on a previously unseen data set: a) 3D TA features + BMI, and b) 3D TA features + initial stone size, with comparable AUC values (0.8 and 0.81, respectively, P = 0.29).

Conclusion:
3D TA with machine learning of urinary stone CT image data provides added value for predicting the success to stone disintegration with SWL.

3953

A. Lakkaraju[1], R. Marpakwar[1], U. Hermann[1], P. Liberski[2], A. Ballabio[3], A. Aguzzi[1]

Identifying the determinants of spongiform phenotype in prion infections

Institute for Neuropathology, Universitätsspital Zürich, Zürich CH-8091[1], Medical University of Lodz, Lodz 92 216, Poland[2], Telethon Institute of Genetics and Medicine (TIGEM), Via Campi Flegrei 34, 80078 Pozzuoli, Naples, Italy[3]

Introduction:
Prion diseases are protein misfolding and aggregating disorders (PMA) implicated in Creutzfeldt-Jakob disease (CJD) and several transmissible spongiform encephalopathies of humans and animals. It is characterized by the accumulation and deposition of an abnormal conformer (PrP^{Sc}) of the endogenous prion protein (PrP^{C}). In addition to generic neuropathological changes (astrogliosis, neuronal loss, deposition of amyloid plaques), prion-infected brains feature a characteristic "spongiosis" which is caused by the accumulation of intraneuronal/intraneuritic vacuoles containing membrane fragments and, sometimes, degenerating organelles which are of uncertain biogenesis and content. Previous studies have documented the accumulation of PrP^{Sc} in multivesicular bodies after prion infection, suggesting impairment of the endo/lysosomal machinery. Depletion of PIKfyve and/or FIG4, which are involved in synthesis of phospholipid PI(3,5)P2 a key cog of endo/lysosomal machinery, induces vacuolation similar to spongiosis. We therefore decided to investigate whether the breakdown of the endolysosomal fusion machinery is the cause of spongiosis in prion infections.

Methods:
To address the mechanistic details of spongiosis, we use animal models (mice), organotypic slice cultures and cell lines. Techniques such as immunohiostochemistry, electron microscopy and *in vitro* biochemical assays will be utilized in all these model systems identify determinants of vacuolation. Rescue experiments will be performed using osmotic minipumps to deliver a water-soluble version of PI(3,5)P2 to the brains of prion-infected mice and we will monitor the survival and evaluate the neuropathology of brain.

Results:
We monitored the protein levels of PIKfyve and FIG4 in the brains of prion-infected *tga20* mice (overexpressing PrP^{C}) infected with the Rocky Mountain Laboratory strain 6 (RML6) of prions. PIKfyve was significantly depleted at 90 days post-infection and profoundly depleted in terminally sick mice. The mRNA levels of PIKfyve were unaltered, suggesting that posttranslational events led to destabilization. We found that PIKfyve was deacylated in prion infected brain lysates obtained from tga20 mice and deacylation led to the ubiquitination and degradation of PIKfyve, which further leads a plethora of effects on lysosomal biogenesis. ER stress plays an important role in the toxicity in prion infections and time course analyses in cells revealed PIKfyve depletion upon ER stress induction. Treatment with GSK2606414, which alleviates the ER stress induced via the PERK pathway, restored acylation and steady state PIKfyve levels. Restoration of PI(3,5)P2 levels in cells and culterd slices by treating them with a water soluble analog rescued vacuolation and lysosomal defects.

Conclusion:
Our data suggests that spongiform change may directly result from the suppression of the PIKfyve kinase, resulting in the impairment of endolysosomal machinery and formation of progressively larger vacuoles. In our study, activation of ER stress preceded the depletion of PIKfyve, which was rescued by ER stress inhibitors. We propose to dissect the events leading to PIKfyve downregulation and investigate their importance for prion toxicity in a variety of models. Furthermore, the possibility that PIKfyve-dependent events may play a causative role in additional neurodegenerative disorders exhibiting vacuolation will be investigated.

3954

A. Plate[1], A. Anagnostopoulos[1], J. Glanzmann[1], L. Stadler[1], L. Weigelt[2], R. Sutter[2], A. Zinkernagel[1], P. Zingg[2], Y. Achermann[1]

Synovial C-reactive protein for diagnosis of periprosthetic joint infection (PJI)

Division of Infectious Diseases and Hospital Epidemiology, University Hospital Zurich[1], University Hospital Balgrist, University of Zurich, Zurich[2]

Introduction:
Periprosthetic joint infections (PJIs) are rare but serious complications after joint arthroplasty. An early and correct diagnosis is crucial for a tailored surgical and antibiotic treatment. Synovial C-reactive protein (CRP) has recently described as a new biomarker in the preoperative diagnostic to identify PJIs. The aim of this study was to evaluate synovial CRP in a large cohort of patients with suspected PJIs and calculate the optimal cut-off to diagnose PJIs.

Methods:
Between September 2015 and June 2017, we included patients with a suspected PJI and with CRP as an additional preoperative diagnostic in joint aspiration. Cases with dry synovial aspiration were excluded. We analyzed sensitivity and specificity of synovial CRP using receiver operating characteristic (ROC) curves based on standard diagnostic criteria for PJI, published by the Consensus Meeting Guidelines in 2013. The optimal cut-off was subsequently determined using the Youden index.

Results:
We included 25 PJI (13.0%) and 168 non-PJI cases (median age 67 years; range 41 – 91) with a preoperative diagnostic joint aspiration of hip (n=81), knee (n=91), or shoulder (n=21). The following pathogens were cultured: Coagulase-negative staphylococci (n=9), *Staphylococcus aureus* (n=6), polymicrobial infections (n=4), *Streptococcus agalactiae* (n=1), *Propionibacterium* avidum (n=1), and *Candida tropicalis* (n=1). Three PJI were culture-negative. The synovial fluid CRP values combined for all joints were significantly higher in the PJI group compared to the non-PJI group (mean: 17.42 vs. 2.3; $p<0.001$). The optimal cut-off (Youden-Index: 0.70) for the PJI diagnosis combined for all joints was a synovial fluid CRP of 2.9mg/l with a sensitivity of 88.0% and specificity of 81.5% (AUC: 0.929, 95%CI: 0.884 - 0.974).

Conclusion:
Sensitivity and specificity of synovial CRP was lower than previously published with a cut-off of 2.5mg/l for chronic PJI (Omar M et. al. Bone and Joint J, 2015). We propose to use synovial CRP only as an additional tool together with serum (CRP, erythrocyte sedimentation rate) and synovial biomarkers (leucocytes, neutrophils, microbiological culture) for a reliable diagnosis of PJI.

3955

A. Plate[1], L. Stadler[1], R. Sutter[2], A. Anagnostopoulos[1], D. Frustaci[2], R. Zbinden[3], S. Fucentese[2], A. Zinkernagel[1], P. Zingg[2], Y. Achermann[1]

Inflammatory disorders mimicking periprosthetic joint infections may result in false positive α-defensin

Division of Infectious Diseases and Hospital Epidemiology, University Hospital Zurich[1], University Hospital Balgrist, University of Zurich, Zurich[2], Institute of Medical Microbiology, University of Zurich, Switzerland[3]

Introduction:
For the reliable diagnosis of periprosthetic joint infections (PJIs), the guidelines recommend the presence of two positive microbiological cultures growing the same pathogen. Preoperatively, PJIs are suspected when serum (CRP, ESR) and/or synovial parameters (leucocytes, neutrophils) are elevated and a single positive microbiological culture is found. The antimicrobial peptide α-defensin was recently introduced as potential "single" biomarker in the preoperative diagnostic of PJI. However so far, most studies assessing the benefits of the α-defensin assay excluded patients with inflammatory diseases.

Methods:
Between June 2016 and June 2017, we prospectively investigated the lateral flow test α-defensin (Synovasure®) for assessing the synovial fluid of patients with suspected PJIs and compared it to the diagnostic criteria for PJI published by the International Consensus Group in 2013 (adapted criteria of the Musculoskeletal Infection Society (MSIS)).

Results:
We included 109 cases (49 hips, 60 knees) in whom a preoperative α-defensin test had been performed. Among these, 20 PJI (16 hips, 4 knees) were diagnosed based on the MSIS criteria. Preoperative α-defensin tests were positive in 25 out of 109 cases (22.9%) with a test sensitivity and specificity of 90% and 92.1%, respectively, and a high negative predictive value of 97.6% allowing to exclude a PJI. False positive α-defensin test results were seen in seven cases, mainly in four patients with inflammatory diseases such as crystal deposition diseases, rheumatoid arthritis, and psoriasis arthropathy.

Conclusion:
Since α-defensin test can be false positive in patients with inflammatory diseases, we propose to include a rheumatological evaluation including crystals in synovial aspirate in routine diagnostic.

3956

A. Magalhaes[1], M. Emmenegger[1], A. Kerschenmeyer[1], A. Aguzzi[1], S. Hornemann[1]

Establishment of a high-throughput microELISA screen for naturally occurring human tau autoantibodies

Institute of Neuropathology, University of Zurich, University Hospital Zurich, Zurich[1]

Introduction:
Pathologically phosphorylated tau aggregates are a major component of neurofibrillary tangles in tauopathies including Alzheimer's disease. Currently, treatment strategies for tauopathies are scarce and there is a need for specific treatment options. Studies in mice expressing mutant tau protein that were vaccinated with phospho-tau peptides demonstrated the generation of anti-tau antibodies that were able to reduce tau pathology and to rescue behavior. This is in line with a new approach striving towards the development of novel disease-modifying strategies for neurodegenerative diseases that use naturally occurring monoclonal antibodies as therapy. To interrogate the human immune repertoire, a high-throughput screen for naturally occurring tau antibodies will be performed to explore the potential value of tau antibodies as diagnostic biomarkers and therapeutics.

Methods:
The Institute of Neuropathology has developed a high-throughput screening platform that allows for screening of 20'000 patients for naturally occurring antibodies against multiple antigens. Recombinant monomeric and aggregated tauK18 as well as full-length tau441 will be absorbed to 1536-well plates and residual heparin plasma samples from the Institute of Clinical Chemistry will be serially diluted using acoustic dispensing technology. Tau autoantibodies will be detected using an indirect microELISA that runs in a fully-automated robotic platform. IgG-depleted serum will be used as negative control and commercially available monoclonal tauK18 antibodies as positive controls.

Results:
Preliminary data from an initial 953-patient screen showed 16% of distinctly reactive patients (negative logarithmic EC50 >= 2) for tauK18 monomers (corresponding to the 4-repeat sequence of the aggregation domain of tau) and 11% of positive hits for tauK19 monomers (3-repeat sequence of the aggregation domain of tau). A competitive ELISA was performed using 3 positive patients samples for each of the targets in which the patient blood samples were successfully competed with soluble tau.

Conclusion:
The initial 953-patient screen served as proof-of-feasibility for the microELISA screen for naturally occurring human tau autoantibodies. We will complement our study with epitope mapping experiments. After this, we will screen 20,000 patients and perform an epidemiological study of tau autoantibodies correlating patient reactivity with clinical data (e.g. age, gender, ICD-10 codes). This will enable us to explore the potential of tau autoantibodies as diagnostic biomarkers of tauopathies and further elucidate on the current controversy about the occurrence of anti-tau autoantibodies in healthy vs. diseased subjects. In addition, B cells of reactive patients will be isolated by flow-cytometry sorting and single-cell sequenced, allowing the expression of the antibodies in appropriate expression models. Lastly, these antibodies will be characterized and tested *in vitro* and *in vivo*.

3957

F. Scholkmann[1], T. Karen[2], S. Kleiser[1], D. Ostojic[1], H. Isler[1], D. Bassler[2]

Brain oxygenation in preterm neonates measured with a novel NIRS oximeter: Preliminary findings of a new study

Biomedical Optics Research Laboratory, Department of Neonatology, University Hospital Zurich, CH-8091, Zurich, Switzerland.[1], Department of Neonatology, University Hospital Zurich, CH-8091, Zurich, Switzerland[2]

Introduction:
Brain oxygenation is a critical aspect that determine the short- and long-term well-being of preterm neonates. Aim: In our study, we aimed to analyse relationships between brain oxygenation with age, Apgar score, SpO_2, pulse rate and haematological parameters.

Methods:
In 35 preterm neonates (gestational age [GA]: 32.0 ± 3.4 weeks, chronological age [CA]: 23.0 ± 24.1 d), absolute values of cerebral tissue oxygenation (StO_2) were measured at the left frontotemporal lobe (FTL) (5 x repetitions, 1 min each) and the occipital lobe (OL) (5 min continuously) with a novel NIRS device (OxyPrem v.1.3; technical specifications: 2 light detectors, 4 light sources; 690, 760, 805 und 830 nm; source-detector separations: 13, 20, 30 and 35; spatially-resolved spectroscopy). 1 min median values of StO_2 were used for further analysis. Heart rate and SpO_2 were measured in parallel by pulse oximetry (Sensmart-X100, Nonin).

Results:
The following statistically significant ($p < 0.05$) correlations were found: Absolute StO_2 values (frontotemporal lobe: 61.75 +- 9.45 %, occipital lobe: 57.18 +- 12.94 %) were (i) positively correlated with SpO_2, (ii) positively correlated with Hb and Hct (measured with a blood-gas analyser), (iii) positively correlated with the GA, (iv) negatively correlated with the CA, and (v) positively correlated with all three Apgar scores. In addition, StO_2 at the FTL was statistical significantly higher than at the OL.

Conclusion:
Our analysis showed that (i) absolute values of StO_2 in preterm neonates depend on several factors, including SpO_2, age (CA and GA), Hb, Hct, and Apgar score. On the frontal part of the head, StO_2 values were higher compared to the occipital part. That the Apgar score is significantly determining StO_2 even weeks after birth is an interesting finding, indicating long-term effects on brain oxygenation in preterm born neoantes.

3958

L. Hering[1], C. Gottier[1], S. Lang[1], B. Becher[2], G. Rogler[1], M. Scharl[1], M. Spalinger[1]

Loss of PTPN2 in dendritic cells promotes T cell activation and expression of co-stimulatory molecules

Division of Gastroenterology and Hepatology, University Hospital of Zurich, Switzerland[1], Institute of Experimental Immunology, University of Zurich, Zurich, Switzerland[2]

Introduction:
Variants within the gene locus encoding protein tyrosine phosphatase non-receptor type 2 (PTPN2) are associated with the development of inflammatory disorders. The role of PTPN2 in T cells and intestinal epithelial cells has been investigated in depth, but its role in dendritic cells (DCs) remains unclear. Here, we addressed whether loss of PTPN2 in DCs affects the expression of the co-stimulatory molecules and subsequently activation of T cells.

Methods:
For this aim, we generated mice lacking PTPN2 specifically in DCs (PTPN2-CD11cCre mice). Using flow cytometry, we analysed spleen, mesenteric lymph nodes and lamina propria in PTPN2-CD11cCre and their wildtype littermate controls.

Results:
PTPN2-CD11cCre mice show symptoms of splenomegaly and dermatitis, as well as inflammatory infiltrations in the liver and lung in some mice. Severity of the inflammation varies between individuals, resulting in spontaneous death in some mice. PTPN2-CD11cCre mice do not differ in terms of DCs frequencies in spleen and mesenteric lymph nodes compared to their wildtype littermate controls, but we observed an increased expression of co-stimulatory molecules CD80 and CD86. In the lamina propria, however, DC frequencies were reduced, and the remaining DCs expressed reduced levels of CD80 and CD86. Of note, there was no difference regarding the expression of MHCII on CD11c+ cells between PTPN2-CD11cCre and their littermate controls. Consistent with increased expression of co-stimulatory molecules, we observed increased numbers of CD44+ effector/memory CD4+ and CD8+ T cells, as well as IFN-gamma+CD4+ T cells, indicating an enhanced T cell activation capacity of PTPN2-deficient DCs.

Conclusion:
In conclusion, our results show that PTPN2 has an important anti-inflammatory role in DCs. Loss of PTPN2 in DCs promotes T cell activation as well as increased expression of CD80 and CD86. Further, it increases the ratio between CD11b+ DC2 and CD24+DC1 in skin and lymph nodes.

3960

G. Traber[1], M. Kanku[1], S. Sele[2], G. Jaggi[1], U. Held[2], K. Landau[1]

Assessment of cyclotorsion using SLO fundus imaging in patients with and without forth nerve palsy

Department of Ophthalmology, University Hospital Zurich, Zurich, Switzerland[1], Epidemiology, Biostatistics and Prevention Institute, Department of Biostatistics, University of Zurich, Switzerland[2]

Introduction:
Scanning Laser Ophthalmoscopy (SLO) imaging is a new method of foveo-papillary angle (FPA) measurement for objective assessment of cyclotorsion. This case-control study assesses the SLO-based FPA in patients with forth nerve palsy and in healthy controls.

Methods:
25 patients with forth nerve palsy and 25 matched controls were recruited at the University Hospital Zürich. The FPA measurements in both eyes were performed on SLO fundus imaging using the integrated algorithm by Heidelberg Spectralis. In addition, the FPA was measured on conventional fundus photographs.

Results:
Using SLO imaging, the mean FPA in the patient group (18 congenital, 7 acquired; 11 men, 14 women; mean age 45.5, range 24 – 80 years) was -11.3° compared with -5.8° in the controls (mean age 46.9, range 25 – 79 years). There was a statistically significant difference between these two groups ($p < 0.0001$). The discrimination between patients and controls by the foveo-papillary angle is very good with an AUC=0.92 [95% CI ranging from 0.84 to 0.99].

The mean FPA measured manually on fundus photographs was – 11.4° in patients with forth nerve palsy and - 5.8° in healthy controls ($p < 0.0001$). Comparing the FPA on SLO imaging with the FPA on photographs, the differences showed limits of agreement of -6.02° and +6.58° in the Bland-Altman plot.

Conclusion:
Semi-automated measurement of the FPA with SLO imaging is a convenient and reliable method for objective assessment of cyclotorsion. The FPA obtained with this method showed very good discrimination between patients and controls. Patients with forth nerve palsy had significantly higher FPAs both on SLO imaging and on fundus photographs. The Bland-Altman plot did not show evidence for a systematic bias in the difference between SLO- and photograph-based FPAs. However, the limits of agreement were quite large.

3961

D. Vuong[1], M. Bogowicz[1], M. Huellner[2], P. Veit-Haibach[2], N. Andratschke[1], J. Unkelbach[1], M. Guckenberger[1], S. Tanadini-Lang[1]

Robustness study on radiomic features in [18F]-FDG PET/CT and [18F]-FDG PET/MR

Department of Radio-Oncology, University Hospital Zurich[1], Department of Nuclear Medicine, University Hospital Zurich [2]

Introduction:
Radiomics is a promising tool for identification of new prognostic biomarkers. However, image reconstruction settings and test-retest variability may influence the absolute values of radiomic features. Unstable radiomic features cannot be used as reliable biomarkers. PET/MR is becoming more available and often replaces PET/CT. The aim of this study was to quantify to what extend [18F]-FDG PET/CT radiomics models can be transferred to [18F]-FDG PET/MR.

Methods:
Nine patients with non-small cell lung cancer underwent first an [18F]-FDG PET/MR scan followed by an [18F]-FDG PET/CT scan (SIGNA PET/MR and Discovery PET/CT 690, GE Healthcare) with a delay time of 38 min +/- 5 min. Patients had one single FDG injection for both scans. The primary tumors were segmented independently on the PET dataset from PET/CT and PET/MR with two semi-automated methods (gradient-based and threshold-based). The resolution of the scans was 2.73 x 2.73 x 3.27 mm and 2.34 x 2.34 x 2.78 mm for PET/CT and PET/MR, respectively. Resampling was performed to 3.27 mm. In total, 1358 radiomic features were calculated, i.e. shape (n = 18), intensity (n = 17), texture (n = 136) and wavelets (n = 1186). The intra-class correlation coefficient (ICC(3,2)) was calculated to compare the radiomic features in both imaging modalities. An ICC larger than 0.9 was considered stable among both types of PET scans. An average linkage hierarchical clustering was performed to identify classes of stable and uncorrelated features with a cut-off value of 0.7.

Results:

Feature Type	Gradient [%]	Threshold [%]
Shape	83.3	83.3
Intensity	76.5	76.5
Texture	51.8	44.5
Wavelet	27.7	25.8
Overall	31.4	29.1

Table 1: Percentage of stable features shown for all four feature groups, i.e. shape, intensity, texture and wavelet, and the overall percentage of stable features. Results are shown for both segmentation methods gradient-based and threshold-based.

The median of the relative volume difference of the primary tumor segmented on PET/CT and PET/MR was 4.8% (range 0.4% to 39.9%) for the gradient-based method and 18.0% (range 0.7% to 71.2%) for the threshold-based method. The fraction of features stable between the scans is shown in Table 1. A larger number of radiomic features was stable when segmentation was performed using the gradient-based compared to the threshold-based method, which is in agreement with the improved reproducibility of tumor volume using gradient-based method. More than 75% of shape and intensity features yielded an ICC > 0.9 between the scans for both segmentation methods. However, only 51.8% of the texture and 27.7% of the wavelet features reached this criterion (for gradient-based method and even less in threshold-based method). In the wavelet features analysis, more features were robust in the smoothed images (low-pass filtering) in comparison to images with emphasized heterogeneity (high-pass filtering). Hierarchical clustering revealed 9 uncorrelated groups of stable features.

Conclusion:
Shape and intensity radiomic features were robust when comparing the two types of [18F]-FDG PET scans (PET/CT and PET/MR). In contrast, texture and wavelet features showed reduced stability, which needs to be considered for their use in prognostic modelling. This instability can be caused by different factors, such as the different attenuation correction methods or test-retest variability.

3962

A. Bicvic[1], N. Scherrer[1], J. Schneider[1], A. Luft[1], M. Katan[1]

Identification of a Novel Blood Biomarker Panel Index for Improved Mortality Prediction in Acute Ischemic Stroke

Neurology Department, University Hospital Zürich, Zürich[1]

Introduction:
We investigated a set of 92 blood biomarkers that have been implicated in the pathogenesis of cardiovascular diseases to predict post-stroke mortality. Based on the most promising markers, we aimed to create a novel biomarker panel index for risk stratification.

Methods:
In this prospective study, we simultaneously measured 92 biomarkers within 72 hours of symptom onset in 320 stroke patients by a novel proximity extension assay technique (Proseek Multiplex CVD III, Olink Proteomics, Uppsala, Sweden). The primary outcome measure was mortality within 90 days. We first estimated the association of each biomarker by using logistic regression models adjusting for multiple testing. The most significant 16 biomarkers were used to create a biomarker panel index where each biomarker was weighted according to their distance to the median. We fitted regression models to estimate odds-ratios and 95% confidence intervals (OR, 95% CI) for the association of the biomarker panel index with mortality. The discriminatory accuracy was assessed with the area under the receiver-operating-characteristic curve (AUC).

Results:
After adjustment for demographic and vascular risk factors, the biomarker panel index remained independently associated with mortality (OR 1.67, 1.29 – 2.17 95% CI) and improved the discriminatory accuracy to predict mortality (AUC of 0.89, 0.84 – 0.94 95% CI, to 0.93, 0.89 -0.96 95% CI), as compared to the clinical prediction model alone.

Mortality				
	Univariate Analysis		Multivariate Analysis	
Predictor	OR (95% CI)*	*p* value†	OR (95% CI)*	*p* value
Biomarker Panel Index	1.16 (1.08-1.24)	<0.001	1.67 (1.29-2.17)	<0.001
Age (increase per year)	1.09 (1.05-1.14)	<0.001	1.10 (1.05-1.15)	<0.001
NIHSS at admission (per point)	1.20 (1.14-1.25)	<0.001	1.18 (1.11-1.26)	<0.001
TACS	6.67 (3.19-13.96)	<0.001	1.31 (0.39-4.42)	0.664

Table 1. Univariate and Multivariate Logistic Regression Analysis for Mortality at 90 Days after Stroke

OR indicates odds ratio; CI, confidence interval; NIHSS, National Institutes for Health Stroke Scale; TACS, total anterior circulation syndrome.

* Note that the odds ratio corresponds to a unit increase in the explanatory variable; for the biomarker panel, this corresponds to an increase per unit of the index. †*p* value <0.001 was included in the multivariate analysis.

Conclusion:
We identified a novel blood biomarker panel index which improved risk stratification after ischemic stroke beyond established demographic and vascular risk factors. These results need to be validated in a larger independent cohort study.

3963

S. Isringhausen[1], U. Süssbier[1], N. Kräutler[2], L. Kovtonyuk[1], A. Gomariz-Carillo[1], P. Helbling[1], H. Wong[1], M. Manz[1], A. Oxenius[2], C. Nombela-Arrieta[1]

Chronic viral infections induce major disruption of bone marrow stromal cell networks and persistent loss of hematopoietic stem cell function

Department of Experimental Hematology, University Hospital Zurich, Zurich[1], Institute of Microbiology, ETH Zurich, Zurich[2]

Introduction:
Hematopoiesis as the primary function of the bone marrow (BM) is a highly dynamic and tightly regulated process sustained by a rare population of self-renewing, multipotent hematopoietic stem and progenitor cells (HSPCs) which reside in specialized nurturing microenvironments within BM cavities. The BM is extremely diverse, comprising all hematopoietic lineages as well as complex stromal cellular networks of mesenchymal, neural and vascular origin. Beyond providing a structural scaffold for hematopoietic cells, stromal cells are critically involved in the fine regulation of different stages of hematopoiesis. Whereas there is a basic understanding on the functional interplay of stromal components with hematopoietic cells during homeostasis, little is known about how inflammatory conditions may alter this relation. Viral infections act as major stressors to the hematopoietic system, inducing a massive and adaptive response in cellular output. Although the effects of viral infections on hematopoietic output have been characterized, it remains poorly defined to date how viral infections can alter BM stromal scaffolds. We herein investigated the structural and functional alterations imposed on the BM after chronic infection with Lymphocytic Choriomeningitis Virus (LCMV).

Methods:
For multidimensional analyses, we combine conventional *in vitro* and *in vivo* assays with cutting edge 3D confocal imaging technology.

Results:
Our results indicate that viral infections result in rapid vasodilation of BM sinusoids and a strong disruption of extracellular matrix networks throughout the BM cavity. Notably, chronic infections with LCMV strains induce a profound and sustained reduction in the number of phenotypic HSCs which correlates with a downsizing of the population of endothelial and mesenchymal stromal progenitor cells and a decrease in their capacity to produce HSPC-sustaining factors. On a functional level, competitive repopulation assays revealed a striking and persistent loss of HSC function after chronic LCMV infection. In line with this, functional assays on BM mesenchymal stromal cells indicate a strong loss of the HSC supportive function. Finally, preliminary results indicate that this mechanism is governed by CD8 T cells.

Conclusion:
We herein report that chronic LCMV infections lead to massive alterations in the hematopoietic and stromal compartments in the BM. Intriguingly, the functionality of HSCs as well as mesenchymal stromal cells stays impaired even at time points of immunological exhaustion long after the initial infection. Considering the long standing clinical observation of an increased transplant rejection within chronically CMV-infected patients, precisely delineating the mechanisms that govern loss of functionality and immune pathology might pave the way for clinical applications in the future.

3964

B. Pouymayou[1], O. Riesterer[1], M. Guckenberger[1], J. Unkelbach[1]

A Bayesian network model for personalized elective CTV definition in head & neck cancer

Klinik für Radio-Onkologie, Universitätsspital Zürich, Zürich[1]

Introduction:
Definition of the clinical target volume (CTV) is one of the largest source of uncertainties and inter-observer variability in radiotherapy. In the case of head & neck cancer, the CTV contains lymph node (LN) levels that are at risk of harboring microscopic metastases despite negative findings on imaging. Thereby, a large portion of the neck is irradiated prophylactically, adding to treatment-related toxicity. Currently, population-based guidelines are being used to determine the LN levels to be included in the CTV, which typically only incorporate the site of the primary tumor (PT) (e.g. oropharynx, hypopharynx or larynx) and N-stage. We present a statistical model to estimate the probability of microscopic involvement of LN levels based on the individual patient's state of lymphatic tumor progression.

Methods:
To estimate the probability of microscopic involvement of LN levels, patient specific characteristics (site of the PT and macroscopic LN metastases) have to be combined with population-based statistics on the lymphatic progression patterns. Bayesian networks (BN) are well suited to quantitatively describe this problem. A BN consists of nodes (which represent random variables) and edges (which represent probabilistic relationships). We developed a BN model in which each LN level is associated with two binary nodes. One corresponds to the detected macroscopic state (e.g. visible LN metastases on imaging) while the second corresponds to the microscopic involvement and cannot be observed. The edge linking the two nodes models the detection probabilities and is used to infer the microscopic state. PT sites are modeled by additional binary nodes. The edges connecting the LN levels and the PT nodes represent the probability for tumor cells to spread from one site to another. The graph structure and the model parameters are chosen based on current guidelines and to match the risks of microscopic involvement reported in the literature. To demonstrate the potential of the BN approach, we study a simple model including 2 PT sites (oropharynx and hypopharynx) and 4 LN levels (ipsilateral Ib, II, III and IV).

Results:
Once the BN is defined, it can be applied to personalize CTV definition for a newly diagnosed patient. To that end, an inference algorithm retrieves the probabilities of the microscopic state, given the observed macroscopic state. For instance, in a patient with an oropharyngeal cancer in whom levels II and III harbor LN metastases, the BN model predicts that level IV is microscopically involved with a probability of 11%. An advantage of the BN model is that it describes how the risk of microscopic involvement depends on the macroscopic progression (Table 1). For example, when level III has no observed metastases, the involvement probability of level IV drops to 5%.

	Macroscopically involved LN levels:			
Probability of microscopic involvement at level:	*none*	*II only*	*II and III*	*III only*
II	0.725	1	1	0.825
III	0.137	0.156	1	1
IV	0.045	0.046	0.107	0.107

Table 1: Probability of microscopic involvement at level II, III and IV given different combinations of macroscopically involved LN levels, assuming a primary tumor in the oropharyngeal region.

Conclusion:
Bayesian networks represent a statistical model to estimate the probability of microscopic LN involvement for cancers with lymphatic spread. It provides a framework for combining patient characteristics with population based patterns of lymphatic progression, and thereby provides a method to individualize CTV definition.

3965

A. Henzi[1], A. Senatore[1], A. Lakkaraju[1], S. Hornemann[1], R. Moos[1], K. Airich[1], A. Aguzzi[1]

A Novel Tool for the Treatment of Peripheral Demyelinating Neuropathies

Neuropathology, University Hospital of Zurich, Zurich[1]

Introduction:
Peripheral demyelinating diseases like Guillain-Barré Syndrome (GBS) or chronic inflammatory demyelinating polyneuropathy (CIDP) are diseases of the peripheral nervous system, in which the myelin sheath is the main site of damage. The treatment options for these diseases are currently unsatisfying, with a substantial number of patients showing no good recovery or remaining severely disabled. The adhesion-G-protein coupled receptor Gpr126 is essential for initiation and maintenance of the myelin sheath. A peptide derived from the N terminal flexible tail region (FT-peptide) of the normal cellular prion protein (PrP^C) was previously described as an activating ligand of Gpr126, increasing the expression of myelination related genes in Schwann cells in vitro and in vivo. A common strategy to prolong the half-life of peptides in the circulation is the fusion of a peptide to crystallisable fragment (Fc-γ) of antibodies. We aim to exploit the pro-myelinating properties of PrP^C by coupling the flexible tail of PrP^C to an Fc-γ antibody fragment, resulting in the $(FT)_2$Fc-fusion protein. This fusion protein might be applied to treat demyelinating diseases of the peripheral nervous system. In the present study, we have analysed the properties of the $(FT)_2$Fc-fusion protein expressed by HEK293 cells.

Methods:
HEK293T cells are transfected with plasmids coding for the $(FT)_2$Fc-fusion protein. By western blotting and ELISA, we are analysing the cell culture supernatant to detect the expression and secretion of $(FT)_2$Fc. The binding of $(FT)_2$Fc to Gpr126 is measured by Flow cytometry analysis using Gpr126 overexpressing HEK293T cells. The activation of Gpr126 is measured in the Schwann cell like SW10 cells, using a cAMP assay which measures a spike in cAMP upon activation of the receptor.

Results:
We have generated plasmids that express $(FT)_2$Fc. We show that HEK293T cells transfected with the plasmid using polyethylenimine secrete the protein into the cell culture supernatant. The presence of the protein in the cell culture supernatant is detected by western blotting using both an antibody recognizing mouse Fc and a Fab specific for PrP (Fab83), and in a specific sandwich ELISA. $(FT)_2$Fc is present as homodimer. Under reducing conditions, a shift to the monomeric state can be observed. $(FT)_2$Fc in the cell culture supernatant is binding to HEK cells overexpressing Gpr126, and elicits an increase in cAMP in SW10 cells expressing Gpr126, but not in SW10 cells devoid of Gpr126 suggesting that the generated $(FT)_2$Fc is functional and specifically activates Gpr126.

Conclusion:
The promyelinating property of PrP^C might be exploited to treat demyelinating diseases of the peripheral nervous system. We have developed a $(FT)_2$Fc-fusion protein which it is binding to and activating Gpr126 similarly to the FT-peptide. We aim to apply $(FT)_2$Fc in vivo by treating mice with the purified protein or by adeno-associated virus mediated expression. Our goal is to understand whether this protein can rescue the PrP^C-ablation related peripheral demyelination, and to test whether it can support the maintenance of the myelin sheath in demyelinating diseases like CIDP, GBS or Charcot Marie Tooth disease.

3966

A. Schneider[1], A. Rickenbacher[1], L. Frick[1], D. Cabalzar-Wondberg[1], S. Käser[1], P.-A. Clavien[1], M. Turina[1]

Insurance status influences the use of minimally invasive surgical techniques, but does not affect the rate of postoperative complications

Department of Surgery & Transplantation, University Hospital of Zurich, Zurich, Switzerland[1]

Introduction:
Controversy exists whether surgical treatment is influenced by insurance status. Previous studies in the USA have suggested higher morbidity and mortality in patients with colorectal cancer who were Medicare/Medicaid insured. It remains elusive, however, whether these findings apply to European countries with mandatory, government-driven insurance systems. We therefore aimed to analyze whether operative techniques, oncological quality of care and perioperative complication rates differ among patients suffering from colorectal cancer, who were covered either by basic general (GI) or additional private (PI) healthcare insurance.

Methods:
Based on the prospective database of the AQC (*Arbeitsgemeinschaft für Qualitätssicherung in der Chirurgie, Switzerland*), all patients undergoing elective resection for colorectal cancer between 2002 and 2016 were identified. A propensity score match for age, gender and ASA-score of eligible cases was performed and outcomes assessed. Wilcoxon-test was used to compare interval data and Fisher's Exact test for nominal/ordinal data respectively.

Results:
The propensity score match yielded 1530 patients with either general (n=765) or private insurance (n=765). Hierarchical status of the operating surgeon differed substantially between patients with GI and PI (p≤0.001). Residents and junior staff surgeons operated on >50% of patients with GI, whereas over 80% of patients with PI were operated senior and experienced surgeon. Minimally-invasive techniques were used more frequently in patients with PI (GI: 65.4% vs. PI: 77.9%, p≤0.001, OR: 1.83), and in addition patients with GI were converted more often to open resections (GI: 17.9% vs. PI: 13.5%, p=0.165, OR: 1.39). Length of surgery was longer (GI: 200 min [IQR: 150-264] vs. PI: 180 min [IQR:135-235], p≤0.001) and blood loss higher in GI compared to PI patients (GI: 150 ml [IQR: 20-300] vs. PI: 100 ml [IQR: 20-200], p=0.002). Anastomotic leaks were more frequent in patients with GI, although not reaching significance (GI: 2.16% vs. PI: 1.40%, p=0.296). Overall length of hospital stay was comparable in both groups (GI: 12 days [IQR: 9-16] vs. PI: 12 days [IQR: 9-15], p=0.361).

With respect to the oncologic quality of care, neither the rate of positive resection margins (GI: 3.79% vs. PI: 4.32%, p=0.795, OR: 0.87), the number of resected lymph nodes (GI: 19 [IQR: 15-27] vs. PI: 19 [IQR: 15-27], p=0.812) nor the number of positive lymph nodes (GI: 0 [IQR: 0-2] vs. PI: 0 [IQR: 0-3], p=0.085) differed among groups. Mortality (GI: 0.78% vs. PI: 1.43%, p=0.329, OR: 1.84) and overall complications occurred with similar frequencies (GI: 16.47% vs. PI: 15.03%, p=0.483, OR: 1.11). Furthermore, severity & rates of intraoperative and postoperative complications (p=0.811) were not different between groups.

Conclusion:
The use of minimally invasive techniques was favored in patients with private insurance, while differences in blood loss and duration of surgery likely reflect the higher levels of expertise of surgeons operating on patients with private insurance coverage.

The quality of the oncological resection was however not affected by insurance status and only non-significant differences in perioperative complications were observed.

3967

D. Kirschenbaum[1], F. Voigt[2], A. Gomariz Carillo[3], M. Smith[4], C. Nombela Arrieta[3], F. Helmchen[2], A. Aguzzi[1]

Reconstruction of the entire vascular web of the mouse brain by novel tissue clearing and imaging approaches

Institute of Neuropathology, University Hospital Zürich, Switzerland[1], Brain Research Institute, Universität Zürich, Zürich[2], Hematology, University Hospital Zurich, Zurich, Switzerland[3], Novartis Institutes for Biomedical Research, Cambridge, MA, USA[4]

Introduction:
Classical histology was based on thin mechanical sectioning of tissue in the past 150 years, until recently. Classical histology covers a series of technical steps during which tissue is fixed, processed, embedded, sliced and stained, followed by microscopic analysis. The two salient steps are slicing and staining. Slicing has such an importance because tissue is not transparent, that is, light cannot pass through it beyond a shallow depth - limiting accessibility by light microscopy. This problem is addressed by tissue clearing. Tissue clearing renders tissue transparent by homogenizing the refractive indices between cell membranes and water, which enables deep imaging without slicing. Recently, multiple tissue clearing approaches were published. Tissue clearing techniques can be characterized in the space of processing time, quenching of fluorescent genetic reporters, or implementation complexity.

Methods:
We developed a clearing technique of unprecedented rapidity and user-friendliness based on the CLARITY method, which we termed CRYSTAL (Clarification by RapidlY Substituting Tissue with Acrylamide devoid of Lipids). With CRYSTAL we were able to transparentize whole mouse brains within a matter of hours. We then imaged cleared whole brains with light-sheet microscopy within minutes.

Results:
Here we show the power of this method by rapidly clearing and imaging the brains of CLDN5-EGFP transgenic mice. These mice express the green fluorescent protein in endothelia throughout the brain. By clearing and imaging these brains we were able to visualize the entire vascular web. As a next challenge, we aimed to segment these datasets and extract variables which describe the vascular tree. For this, we deployed a custom designed convoluted neuronal network which segmented our highly complex datasets robustly.

Conclusion:
In summary, we present a combined methodology for high-throughput whole-mount tissue clearing, imaging, and analysis.

3968

D. Schoenenberg[1], G. Osterhoff[1]

CT-based evaluation of volumetric bone density in fragility fractures of the pelvis – a matched case-control-analysis

Klinik für Traumatologie, Universitätsspital Zürich[1]

Introduction:
The aim of this study is to compare the computed tomography-based regional bone density measured by Hounsfield units (HUs) in patients with and without fragility fractures of the sacrum.

Methods:
Patients aged ≥ 50 years with a fragility fracture of the sacrum were compared to patients of similar age and gender who had a fall from standing height without fracture (n = 46). A matched case-control analysis was conducted by retrospective chart review and assessment of areal bone mineral density by lumbar DXA and by volumetric regional HU measurements in uncalibrated computed tomography (CT) scans of the sacrum.

Results:
Patients with a sacral fracture (age 74 ± 11 years) showed a lower bone density in the body of S1 (HU 85 ± 22) when compared to the matched control group without fracture (age 73 ± 10 years, HU 125 ± 37, $p < 0.001$). The CT-based bone density of S1 did not correlate with the DXA values of the lumbar spine ($r = 0.223$, $p = 0.136$), and lumbar spine T-scores did not differ between the groups (- 2.0 ± 1.3 vs. - 1.9 ± 1.2, $p = 0.786$). All measurements are based on uncalibrated scans, and absolute HU values are restricted to scans made on Siemens SOMATOM Force or SOMATOM Edge scanners.

Conclusion:
Patients with fragility fractures of the sacrum demonstrated a lower regional volumetric bone density of the sacrum when compared to a cohort without a fracture. Local sacral volumetric bone density as measured by CT seems to be independent from the areal BMD as measured by DXA of the lumbar spine.

3969

C. Muller[1], C. Fenwick[2], G. Pantaleo[2], C. Münz[3], R. Speck[1]

In vivo control of HIV-1 infection by broadly neutralzing antibodies in humanized mice

Department of Infectious Diseases and Hospital Epidemiology, University Hospital Zurich, Zurich[1], Centre Hospitalier Universitaire Vaudois (CHUV), Division of Immunology and Allergy, Lausanne, Switzerland.[2], University of Zuerich, Institute of experimental immunology, Zuerich[3]

Introduction:
Combined anti-retroviral therapy (cART) is the cornerstone of HIV treatment resulting in a pronounced inhibition of viral replication leading to undetectable viremia in most patients, reduced morbidity and mortality. However, daily drug intake, side effects and the risk of emergence of resistance in patients with poor drug adherence make the development of new therapeutic strategies necessary. Over the last years, broadly neutralizing antibodies (bNAbs) targeting the HIV-envelope have become a promising new treatment approach.
We investigated the anti-HIV effects of bNAbs in HIV infected humanized NOD-*scid* $g_c^{-/-}$ (NSG) mice. The bNAbs we are exploring are VRC07, PG9 and 10-1074 targeting either the CD4 binding site, V1/V2 region or the glycan V3 region and a novel bNAb LN01, targeting the membrane proximal external region of gp41.

Methods:
Pharmacokinetics: The half-life of each HIV-Env bNAb was determined in NSG mice. A single dose of HIV-Env bNAbs was injected subcutaneously. Blood samples were collected prior to the injection (day 0) and on days 1,3,5 and 7 after the injection. HuIgG plasma concentration was analyzed by ELISA.
HIV-Env bNAb treatment: HIV-1 infected humanized NSG mice were treated every 2-4 days with a single HIV-Env bNAb or a mixture of 2-3 Abs. Treatment was started 5 weeks after infection. Mice receiving the single HIV-Env bNAb were treated for 5 weeks and mice receiving the Ab-mixtures for 12 weeks. Throughout the experiment blood samples were collected to determine viral loads by PCR, plasma concentrations of huIgGs by ELISA and to characterize human immune compartments by flow cytometry.
Characterization of escape mutants: In case of escape, viruses were isolated by co-culturing mice splenocytes and human peripheral blood mononuclear cells (PBMCs) and neutralization capacity of treatment Ab was analyzed by the TZM-bl neutralization assay.
Sequencing of escape mutants: cDNA was generated from isolated viral RNA and PCR amplified. PCR products were cloned using the TOPO-TA cloning kit. Sequencing reads were aligned to the YU-2 sequence (accession number M93258).

Results:
The half-life and serum concentration of the bNAbs ranged from 0.4-9.6 days and 19-141 µg/ml. Using a single bNAb resulted in a significant but transient reduction of HIV viremia 7 days after start of the therapy. We assume that viral rebound was due to the emergence of escape mutants. Delayed rebound occurred when using two bNAbs, whereas three bNAbs resulted in long-term suppression of viremia within 1-7 weeks and in reduced expression of activation markers on T cells when compared to the untreated control. The LN01 antibody was as efficient as the gp120 specific antibodies in the mixture of 3 antibodies.
Furthermore, bNAbs not only have the ability to neutralize free virus but also are capable of killing already infected cells via Fcγ receptor mediated mechanisms such as antibody-dependent cell mediated cytotoxicity or phagocytosis. Therefore, we are investigating the efficacy of the tested bNAbs to induce Fc-dependent clearance of infected cells *in vitro* and the contribution of this mechanism during bNAb therapy *in vivo*.

Conclusion:
We conclude that bNAbs are a very promising alternative to cART, since small molecule drugs lack the ability to induce Fcγ receptor mediated killing of HIV infected cells and since bNAbs may be modified for increasing their half-life and effector functions, permitting an extended dosing schedule and improved efficacy.

3970

A. Gomariz[1], P. Helbling[1], S. Isringhausen[1], U. Suessbier[1], A. Becker[3], A. Boss[3], G. Paul[2], G. Székely[2], S. Stoma[4], S. Nørrelykke[4], O. Goksel[2], M. Manz[1], C. Nombela-Arrieta[1]

Quantitative Characterization of Bone Marrow Stroma Using Deep Learning

Hematology, University Hospital Zurich, Zurich[1], Computer Vision Laboratory, ETH Zurich, Zurich[2], Department of Diagnostic and Interventional Radiology, University Hospital Zurich, Zurich[3], Scientific Center for Optical and Electron Microscopy ScopeM, ETH Zurich, Zurich[4]

Introduction:
Bone marrow (BM) cavities are the primary sites of blood cell production, which is sustained by a rare population of self-renewing and multipotent hematopoietic stem cells (HSC). Local cues deriving from non-hematopoietic BM stromal cells of vascular, mesenchymal or neural origin critically modulate hematopoiesis and HSC maintenance through cell-cell interactions. Among stromal components, perivascular mesenchymal CXCL12-abundant reticular cells (CARc) and endothelial cells lining sinusoidal BM microvessels (sinusoids) have been shown to fulfill prime roles in the orchestration of hematopoietic development. Thus, the study of spatial distributions of different BM components can reveal key information on cellular crosstalk and the molecular mechanisms underlying hematopoietic regulation.

Methods:
Understanding how cells interact with their microenvironment requires imaging the tridimensional spatial context surrounding them. For this, we have established advanced tissue processing and clearing protocols for the generation of 3D microscopy reconstructions of entire BM cavities with subcellular detail. To generate a high-throughput and unbiased analysis, we have developed a deep learning approach for automatic detection of the observed cellular components, which are then represented as segmented objects. We subsequently used robust spatial statistics to quantify how these segmented structures mutually constrain the available volume and interact with each other within the tissue boundaries.

Results:
Applied to our BM datasets, these methods are used to segment 3D sinusoidal microvascular networks with unprecedented speed and accuracy. The sinusoids are seen to occupy 20% of the total BM volume and leave little space for other cellular populations. We use classical segmentation methods to automatically detect the positions of CARc and to report their preferential location in perisinusoidal regions, with 64% of them being in direct contact with the abluminal side of endothelial cell walls.

Conclusion:
Deep learning methods are currently revolutionizing biomedical image analysis. However, their application to 3D microscopy data is still hindered by some technical difficulties. The pipeline we have designed overcomes these difficulties and allow us to include state-of-the-art methods for detection of cellular components in this type of datasets.
In the BM, the results suggest that the stromal components have been previously inaccurately characterized, and we have proposed rigorous descriptors of their spatial confinement and cell frequencies. Furthermore, this approach can be used for uncovering novel spatial phenotypes of immunostained cellular components in different organs.

3971

N. Keller[3], J. Woytschak[1], E. Marques-Maggio[2], O. Boyman[1], A. Norrby-Teglund[4], AS. Zinkernagel[3]

Streptococcal DNase interferes with migration and type I IFN secretion of plasmacytoid dendritic cell

Department of Immunology, University Hospital Zurich, University of Zurich[1], Department of Pathology and Molecular Pathology, University Zurich and University Hospital Zurich[2], Division of Infectious Disease and Hospital Epidemiology, University Hospital of Zurich, Zurich[3], Center for Infectious Medicine, Karolinska Institute, Karolinska University Hospital, Stockholm, Sweden[4]

Introduction:
In healthy skin, plasmacytoid dendritic cells (pDCs) are rare but increase under pathological conditions. Recognition of pathogens by pDCs occurs through the highly abundant intracellular localized Toll-like Receptors (TLR)-7 and 9. Due to the constitutive expression of IRF7 high amounts of interferon (IFN) are produced by pDCs, in particular IFN-alpha. We recently showed that IFN-alpha enhanced clearance of Group A Streptococcus (GAS) in human blood despite neutropenia and monocytopenia. GAS is a major human pathogen responsible for mild as well as severe, life-threatening infections. A hypervirulent clone carrying a prophage encoding for the streptococcal DNase Sda1, emerged over the last decade and is associated with severe invasive diseases. Sda1 is an important virulence factor that degrades neutrophil extracellular traps and reduces TLR-mediated recognition.

The high-mobility group box 1 (HMGB1) protein is a danger-associated molecular pattern secreted either actively through activated innate immune cells or passively through necrotic cells and tissue. HMGB1 is able to form complexes with DNA leading to an enhanced IFN response by pDC. Furthermore, levels of HMGB1 show a positive correlation to the severity of streptococcal soft tissue infections. We thus aimed to corroborate whether pDCs are involved in GAS skin and soft tissue infections and whether the DNase Sda1 has an influence on the DNA-HMGB1 mediated IFN response in patients and murine necrotizing fasciitis (NF).

Methods:
Tissue biopsies from patients with NF were analyzed by immunofluorescence for the presence of pDCs and compared to tissue biopsies from healthy individuals. With our established *in vivo* mouse model of NF, pDCs abundance, IFN response and the role of the bacterial virulence factor DNase Sda1 were further analyzed by FACS, ELISA and immunofluorescence. In a next step we investigated the involvement of the host molecule HMGB1 by using an *in vitro* 3D human skin tissue model to further explore pDCs pathophysiology.

Results:
Tissue from patients with GAS NF had a higher number of pDCs as compared to tissue from healthy individuals. Using loss-of-function in the mouse model we found increased pDC infiltration in mice infected with a sda1-deficient GAS mutant as compared to the GAS wild type strain. Corroborating these findings tissue from patients infected with a streptococcal strain naturally lacking the sda1 showed a higher number of pDCs compared to GAS infected tissue. *In vivo,* the enhanced infiltration was related to higher type I IFN levels and staining for HMGB1 revealed a close association with the bacterial cocci. The interaction was significantly more pronounced in the sda1-deficient GAS mutant.

Conclusion:
We found increased numbers of pDCs in invasive skin infections in mouse and man. The presence of the streptococcal DNase Sda1 reduced the number of pDCs at the infection site. Additionally, *in vitro* data propose a role of the DNase Sda1 interfering with the binding of HMGB1 to GAS.

3972

M. Gagesch[1], P. Chocano-Bedoya[2], J. Kanis[3], B. Vellas[4], R. Rizzoli[5], H. A. Bischoff-Ferrari[1]

Physical Frailty and Quality of Life – Baseline data from a large European Multi-Centre Trial (DO-HEALTH)

Department of Geriatrics, University Hospital Zurich, Zurich[1], Centre on Aging and Mobility, University of Zurich, Zurich[2], Centre for Metabolic Bone Diseases, University of Sheffield, United Kingdom[3], Gerontopole, University of Toulouse, France[4], University of Geneva, Geneva[5]

Introduction:
Physical Frailty influences the quality of life and self-rated health of seniors, and both have been associated with multiple negative health outcomes and increased mortality. However, there is limited data on the association of physical frailty and self-perceived health status in community-dwelling seniors and by different European countries. Our study aims (1) to investigate the baseline association of physical frailty/pre-frailty and quality of life among DO-HEALTH participants. (2) To investigate if the self-rated health component of our quality of life measure (EuroQoL EQ5D-3L) could rule out frailty/pre-frailty among community-dwelling seniors.

Methods:
DO-HEALTH is the largest European healthy aging trial testing the role of vitamin D and/or omega 3-fats and/or a simple home exercise program among 2'157 community-dwelling seniors age 70 and older. Participant recruitment was performed in seven trial centers (Basel, Geneva, Zurich, Berlin, Innsbruck, Toulouse and Coimbra) in five European countries. To address our 2 objectives we did a cross-sectional analysis of baseline data among all 2'157 DO-HEALTH participants, including an adapted Fried-Frailty phenotype for classification of frailty status (robust, pre-frail, frail), health-related quality of life with the EQ5D-3L, and self-rated overall health with the EQ5D-3L visual analogue scale component. For objective (1), we used linear models to present age- and center- adjusted mean self-rated health and stratified by gender and age groups (≤75 vs >75). For objective (2), we used ROC-curve analyses adjusted for age and center to establish optimal cut points.

Results:
There were significant differences in self-rated health between robust, pre-frail and frail seniors where robust seniors had higher scores than those who were pre-frail and frail (overall mean EQ5D-5L-VAS scores were 85, 78 and 64 respectively, $p<0.0001$ for all comparisons). We found the same pattern comparing gender, age group (≤75 years vs. >75 years) and faller status. In ROC analysis, self-rated health had high discriminative ability (AUC=0.91 for the adjusted model) to predict present frailty, with a suggested cut-off value of 75 points.

Conclusion:
With this analysis among a large sample of 2'157 relatively healthy community-dwelling European seniors, we were able to show in a first association between frailty and quality of life differs between the 5 DO-HEALTH countries, between men and women, and between younger and older seniors. Additionally, we will explore if and to what extend self-rated health could help rule out frailty/pre-frailty among community-dwelling European seniors.

3973

C. Maeyashiki[1], H. Melhem[1], K. Baebler[1], S. Lang[1], M. Scharl[1], G. Rogler[1], C. De Valliere[1]

Activation of pH-Sensing Receptor OGR1 (GPR68) Induces ER Stress and Autophagy in an Intestinal Epithelial Cell Model

Gastroenterology and Hepatology, University Hospital Zurich, Zurich[1]

Introduction:
OGR1 (also known as GPR68) is a pH-sensing G-protein coupled receptor previously identified to play an important role in physiological pH homeostasis. A local decrease in pH frequently occurs at sites of intestinal inflammation. A variety of stimuli, including acidosis, can induce endoplasmic reticulum (ER) stress. ER stress can activate autophagy, and both play important roles in gut homeostasis and contribute to the pathogenesis of IBD. To cope with stressful conditions and to ensure correct protein folding, eukaryotic cells have evolved the unfolded protein response (UPR). In a human intestinal epithelial cell (IEC) model, we investigate if the previously observed protective effect of GPR68 deficiency in experimental colitis are in part due to differences in UPR regulation, ER stress and autophagy.

Methods:
Caco-2 cells stably overexpressing OGR1 were subjected to an acidic pH shift for 24 h, compared to vector control cells and also to control pH. A novel small molecule OGR1 inhibitor and c-Jun N-terminal kinase (JNK) inhibitor (SP600125) were used to delineate the different signalling pathways. Expression of ER stress markers (binding immunoglobulin protein (*BiP*), inositol required 1-α (IRE-1α), phospho IRE-1α), apoptosis markers (caspase 3 and poly (ADP-ribose) polymerase (PARP)), and autophagy markers (microtubule-associated protein 1A/1B-light chain 3 (LC3)), were determined by RT-qPCR, immunoblotting and immunocytochemistry (ICC).

Results:
Proton-activated OGR1-mediated signalling led to a significant upregulation in the ER stress markers BiP and phospho-IRE-1α, after treatment for 24 h. The induction of ER stress was reversed in the presence of an OGR1 inhibitor and a JNK inhibitor. Furthermore, caspase 3 and PARP were not cleaved, indicating that apoptosis was not induced. In addition, LC3-II protein levels and LC3 fluorescent puncta, observed by immunoblotting and ICC respectively, increased significantly in our proton-activated OGR1 cell model, supporting our finding that autophagy is induced by OGR1-mediated signalling.

Conclusion:
As inhibition of JNK activity is usually associated with suppression of autophagy, our results imply that OGR1-mediated signalling pathways induce ER stress and autophagy. In an IEC model, a small molecule OGR1 antagonist reversed OGR1-mediated ER stress and autophagy suggesting that OGR1 inhibition might be a novel therapeutic approach for the treatment of IBD.

3974

Z. Gai[1], C. Hiller[1], I. Alecu[2], S. Youhanna[2], M. Lone[2], T. Hornemann[2], G. Kullak-Ublick[1]

FXR activation protects liver from nonalcoholic fatty liver disease through decreasing sphingolipid levels

Department of Clinical Pharmacology and Toxicology, University Hospital Zurich, Zurich[1], Department of Clinical Chemistry, University Hospital Zurich, Switzerland[2]

Introduction:
Increased sphingolipid level has a recognized role in non-alcoholic fatty liver disease (NAFLD) progression.

Methods:
In the present study, we analyzed the hepatic sphingolipids metabolism-related gene expression, and sphingolipid serum levels in both chow mice and HFD-induced obese mice. Finally we examined the regulatory effect of FXR agonist on liver sphingolipid metabolism.

Results:
HFD-induced increase of sphingolipid was significantly mitigated by the treatment with the farnesoid X receptor (FXR) agonist obeticholic acid (OCA). Liver from mice fed a HFD in treatment with OCA were characterized by a general reduction of sphingolipid metabolism genes which in turn results in a protective effect in the liver. In human Huh7 cells and in mouse primary cultured hepatocytes the regulatory effect of OCA on sphingolipid metabolism appeared to be dependent on sphingosine kinase 1. Free fatty acid (FFA)–induced sphingolipid levels were abolished by co-incubation with OCA. Furthermore, OCA was demonstrated to rescue hepatocytes from sphingolipid-induced apoptosis.

Conclusion:
Collectively, these findings suggest that increased sphingolipid levels are important biochemical features of NAFLD. Strategies that promote FXR activation in liver may offer therapeutic potential for hepatic steatosis in NAFLD and its downstream pathological consequences.

3975

M. Gruenbach[1], G. Schreiber[2], E. Schlaepfer[1], S. Bredl[1], B. Escher[3], M. Schlapschy[3], A. Skerra[3], R. Speck[1]

Do different IFN-α subtypes have distinct biological activities?

Department of Infectious Diseases, University Hospital of Zurich, University of Zurich, Switzerland[1], Department of Biomolecular Sciences, Weizmann Institute of Science, Rehovot, Israel[2], Chair of Biological Chemistry, Technical University of Munich, Germany[3]

Introduction:
The members of the IFN-α family are the most potent anti-viral cytokines. They are released subsequently to encounter with pathogens and orchestrate the immune response to fight the invaders. There are 13 IFN-α subtypes that all bind to the same interferon-α/β receptor (IFNAR) complex but with different affinity. Currently, a controversy exists whether the difference in biological activity of IFN-α subtypes is of quantitative or qualitative nature, *i.e.,* is it only a function of dose and affinity or activation of different signaling cascades altogether. In our *in vitro* experiments with human PBMCs, isolated $CD4^+$ T-cells and monocyte-derived macrophages, we found a dose-dependent anti-HIV activity of the various IFN-α subtypes. We did not see a qualitatively different response when judged by the transcriptomes of the treated cells. Here, we will further investigate distinct IFN-α subtypes in an *in vivo* humanized (hu) mouse model for their potencies and biological effects.

Methods:
We prepared PASylated IFN-α2, -α14 and a mutant YNS which has strongly enhanced affinity to IFNAR. PASylated IFNs have a much longer plasma half-life than the natural cytokines, which will be a major advantage when moving forward to their *in vivo* testing. To prove their efficacy in comparison with the wild-type IFNs, we used a reporter cell line bearing luciferase under the control of the IFN stimulated response element (ISRE). We treated cells with different concentrations of IFNs for 4h, then lysed the cells and measured the luciferase signal.
We further verified the efficacy of the different subtypes by examining the response of IFN stimulated genes (ISGs) at the highest concentration that was used in the ISRE stimulation experiment. Human PBMCs were treated for 2h, 6h, 10h and 24h, which was followed by measuring the expression of the ISGs IFIT1, MX1, OAS1 and PKR by means of quantitative real time PCR.

Results:
The luciferase expressing cell line treated with PASylated IFN or its unmodified counterpart showed exactly the same extent of induction when the treatment was done in an equimolar setting. Similarly, we observed the same rate of ISG induction in human PBMCs (n=3) in response to PASylated or non-PASylated IFNs.

Conclusion:
PASylation does not have any detrimental effect on the receptor-binding activity of IFNs, as was seen for the luciferase assay and ISG expression in human PBMCs, when the same molar concentration was used. Consequently, the biological activity *in vivo* of the PASylated IFNs should be much higher due to the longer circulation half-life. In the next step, we will determine the biological activity of the PASylated *vs*. wild-type IFNs in human PBMCs infected with HIV *ex vivo*. Subsequently, we will start with *in vivo* studies, first looking at dose-response curves and then moving forward to HIV experiments.

3976

S. Sorce*[1], M. Nuvolone[1], G. Russo[2], A. Chincisan[1], P. Schwarz[1], A. Aguzzi[1]

RNA sequencing of prion-infected mice uncovers early-onset, progressive derangement of transcription and splicing

Institute of Neuropathology, University Hospital Zürich, Switzerland[1], Functional Genomic Centre Zurich, Zurich[2]

Introduction:
Transmissible Spongiform Encephalopathies (TSEs) are a group of neurodegenerative diseases caused by the accumulation of infectious prion deposits and characterized by the presence of spongiform vacuoles in affected brain regions. Although some of the molecular mechanisms underlying prion neurotoxicity have been identified, so far it is not possible to definitively arrest the course of the disease. Treatment of TSEs remains therefore challenging; but clarifying all the components involved in prion neurotoxicity can be instrumental for novel possible therapeutic approaches.

Methods:
We injected RML prions, or non-infectious brain homogenate (NBH) for control, into wild-type C57BL/6J mice. In order to study the molecular alterations associated with the progression of the disease, we sacrificed RML- and NBH-injected mice at eight different time points during disease development: 4, 8, 12, 14, 16, 18 and 20 wpi, as well as at terminal stage. After intracardial perfusion and dissection, RNA was extracted from the hippocampus and subjected to next-generation RNA sequencing (RNAseq).

Results:
Altered gene expression and RNA processing between prion-inoculated and control mice are detectable as early as 4 weeks post inoculation and progressively exacerbate along the course of the disease. Transcripts known to be enriched in either neurons or glial cells appear differentially expressed or processed in the early phase of the disease. These changes precede the manifestation of neuropathological and clinical signs. We could also verify that early transcriptional perturbations depend from the expression of PrP^C in prion-infected mice, and similarly occur in the cerebellum.

Conclusion:
Our analysis of these results suggests that early disease-relevant alterations of RNA transcription and processing are already elicited in the presence of small trace amount of replicating prion seeds. Understanding these premature molecular changes occurring during the preclinical phase of the disease would therefore mean that novel targets of early diagnosis and intervention could be identified in order to prevent or delay neurodegeneration.

**equal contribution*

3977

S. Sorce[1], M. Nuvolone[1], P. Schwarz[1], P. Pelczar[2], EJ. Rushing[1], A. Aguzzi[1]

The role of the prion protein in the development of muscular pathology

Institute of Neuropathology, University Hospital Zürich, Switzerland[1], Institute of Laboratory Animal Science, University of Zurich, Zurich, Switzerland[2]

Introduction:
The prion protein (PrP^C, encoded by the *PRNP* gene) is best known for its involvement in the development of transmissible spongiform encephalopathies. However, it is also physiologically expressed in many tissues and organs, other than the nervous system, where its role remains unknown. Early transgenic studies in mice have indicated an association between high level of expression of the wild-type form of the prion protein and the occurrence of skeletal muscle diseases with aging. However, the involvement of PrP^C in muscular pathology has been generally overlooked.

Methods:
We have recently generated a new transgenic mouse line (termed CAG-CAT-PrP), which allows for conditional overexpression of PrP^C in specific cell types thanks to the cre-lox system. In order to study the effect of specific PrP^C overexpression in skeletal muscles we have crossed CAG-CAT-PrP mice with muscle specific cre lines: HAS-cre and tamoxifen-inducible ACTA1-creERt2. Both lines have the cre recombinase gene driven by the human alpha-skeletal actin (HSA or *ACTA1*) promoter.

Results:
In the derived mice (termed HSA-PrP and ACTA1creER-PrP) we have noticed that increased PrP^C expression in skeletal muscles is associated with the development of necrotizing myopathy. Histological analyses show signs of internalized nuclei and variation in myofiber diameter. These data are confirmed by biochemical analysis indicating a significant increase in creatine kinase, which is a marker of muscular damage. The clinical relevance of these data is suggested by early reports of enhanced PrP^C expression levels in samples of human muscular diseases, and confirmed by our re-analysis of published transcriptomic profiles of human muscle samples from several independent studies. From these data, it appears that *PRNP* expression is elevated in skeletal muscle upon aging and in pathological conditions, such as Duchenne muscular dystrophy.

Conclusion:
Our results are in line with an involvement of PrP^C in muscular pathology. Further analyses are ongoing to better investigate the mechanisms underlying the induction of myopathy following PrP^C overexpression. In light of the translational potential of these findings, it would be important to validate whether PrP^C, or related molecular mediators, could be used as novel alternative pharmacological targets for muscular diseases.

3978

R. Peterli[1], B. Wölnerhanssen[4], T. Peters[2], D. Vetter[6], D. Kröll[7], Y. Borbély[7], B. Schultes[9], C. Beglinger[3], J. Drewe[5], M. Schiesser[8], P. Nett[7], M. Bueter[6]

Effect of laparoscopic sleeve gastrectomy vs laparoscopic Roux-en-Y gastric bypass on weight loss in patients with morbid obesity: a randomized clinical trial

Department of Surgery, St. Claraspital, Basel, Switzerland[1], Department of Internal Medicine, St. Claraspital, Basel, Switzerland[2], Department of Clinical Research, St. Claraspital, Basel, Switzerland[3], Department of Biomedicine, University Hospital of Basel, Switzerland[4], Department of Pharmacology and Toxicology, University Hospital Basel, Switzerland [5], Department of Visceral and Transplantation Surgery, University Hospital Zürich, Switzerland [6], Department of Surgery, University Hospital Bern, Switzerland [7], Department of Surgery, Kantonsspital St. Gallen, Switzerland [8], eSwiss Medical and Surgical Center, St. Gallen, Switzerland[9]

Introduction:
Sleeve gastrectomy is increasingly used in the treatment of morbid obesity and is performed more often than the current gold standard Roux-en-Y Gastric Bypass (RYGB) despite lacking evidence of its superiority. It was the objective of this study to determine whether there is a difference between sleeve gastrectomy and RYGB in terms of weight loss, changes in comorbidities, increase in quality of life and adverse events.

Methods:
The Swiss Multicentre Bypass Or Sleeve Study (SM-BOSS), a two-group, randomized trial, was conducted from 1/2007 until 11/2011 (last follow-up: 3/2017). Of 3971 morbidly obese patients evaluated for bariatric surgery at four Swiss bariatric centers, 217 patients were enrolled and randomly assigned to sleeve gastrectomy or RYGB with a five-year follow-up period. Primary endpoint was weight loss expressed by percent excess BMI loss, exploratory endpoints were changes in comorbidities, and adverse events.

Results:
Among 217 patients randomly assigned to sleeve gastrectomy (n=107) or RYGB (n=110), mean age, 45.5 years; 72(%) women, mean BMI 43.9kg/m2, 205 (94.5%) completed the trial. Excess BMI loss was not significantly different at five years: sleeve gastrectomy 61.1% vs. RYGB 68.3%, (absolute difference: -7.18(95%CI -14.30 to -0.06), P=.22). Gastric reflux remission was observed more frequently after RYGB (60.4%) than following sleeve gastrectomy (25.0%). Gastric reflux worsened (more symptoms or increase of therapy) more often after sleeve gastrectomy (31.8%) than after RYGB (6.3%). The number of reoperations/interventions was 15.8% after sleeve gastrectomy and 22.1% after RYGB.

Conclusion:
Among patients with morbid obesity followed up for five years, there was no significant difference between sleeve gastrectomy and RYGB in excess BMI loss after adjustment for multiple comparisons. These findings do not support the current practice to perform sleeve gastrectomy more frequently than RYGB.

3979

D. Gero[1], R. Steinert[1], H. Hosa[1], D. Cummings[2], M. Bueter[1]

Appetite, Glycemia, and Entero-Insular Hormone Responses Differ Between Oral, Gastric-Remnant, and Duodenal Administration of a Mixed Meal Test After Roux-en-Y Gastric Bypass

Department of Visceral Surgery and Transplantation, University Hospital Zurich, Zurich, Switzerland[1], Department of Medicine, Division of Metabolism, Endocrinology & Nutrition, University of Washington, Seattle, WA, USA[2]

Introduction:
Human studies that investigated the effect of gastrointestinal re-routing after Roux-en-Y gastric bypass (RYGB) on glycemic control used meal tests (MT) administered by mouth and by gastrostomy. Significantly higher insulin response was observed after oral route, which can be attributed to the early exposure of intestinal L-cells to undigested food (hindgut theory) or to the lack of stimulation of an un-identified duodenal anti-incretin pathway (foregut theory). Given that the intestinal hormonal response to nutrients is caloric-rate dependent, we hypostatized that the meal administration by gastrostomy might be biased by the intact pyloric function regulating gastric emptying. Therefore, we examined the appetite and metabolic responses after RYGB by three feeding routes, with an additional duodenostomy.

Methods:
A standard liquid MT was administered orally, into the gastric remnant, or intraduodenally 6 months after RYGB in 1 patient, 2-times per each route. Changes in plasma glucose, insulin, GLP-1, GIP, PYY, and appetite were measured pre- and up to 120 minutes postprandially.

Results:
Postprandial GLP-1 (26,523 pmol/l/min *vs* 28,801 pmol/l/min) and PYY (62,871 pg/ml/min *vs.* 73,276 pg/ml/min) responses were similar, whereas glucose, insulin, and GIP levels differed markedly after oral *vs*. intraduodenal feeding. Intraduodenal feeding prompted an intermediate appetite response (i.e., between oral and intragastric). For postprandial glucose, insulin, and GIP levels, the intraduodenal route was more similar to the intragastric than oral route (30min insulinema: gastric ≈60 pmol/l, duodenal ≈250 pmol/l, and oral ≈1615 pmol/l). Intragastric administration did not evoke changes in appetite, glucose, or insulin; however, it slightly increased GLP-1 and PYY, and moderately increased GIP.

Conclusion:
This study is the first to compare metabolic responses to MT administered by three different routes after RYGB. Findings indicate that appetite and metabolic responses depend on the route by which nutrients enter the gastrointestinal tract and that the remnant gastric emptying rate interferes with outcomes. Hence, intraduodenal meal administration should be used in future studies to circumvent this bias.

3980

C. Zhu[1], P. Schwarz[1], A. Aguzzi[1]

Deficiency of Progranulin (PGRN) results in accelerated prion diseases

Institute of Neuropathology, University Hospital of Zurich, CH-8091 Zurich, Switzerland[1]

Introduction:
Progranulin (PGRN) is a secreted glycoprotein expressed mainly by microglia and neurons in in the central nervous system. Mutations in PGRN encoding gene GRN that result in haploinsufficiency lead to frontotemporal lobar degeneration and Alzheimer's diseases. However, the underlying molecular mechanisms remain largely unknown. To determine whether PGRN is involved in a broad spectrum of neurodegenerative conditions including prion disease, we aimed to delineate the role of PGRN in prion pathogenesis.

Methods:
We intracerebrally infected $GRN^{-/-}$ mice and their $GRN^{+/-}$ and wild type littermates with RML6 prions. Survival curves determined by the time lapse between the prion inoculation and end stage of disease were compared between the three genotypes. Vacuolation, lesion pattern, PrP^{Sc} deposition, astrogliosis and microglial activation in RML6-infected $GRN^{-/-}$ mice and their $GRN^{+/-}$ and wild type littermates were characterized by histology and biochemistry.

Results:
We found that $GRN^{-/-}$ mice showed accelerated prion progression in comparison to $GRN^{+/-}$ and wild type littermates. Histology revealed that $GRN^{-/-}$ microglia were aberrantly activated, resulting in amoeboid morphology and altered cytokine profiles. Biochemical analysis demonstrated that at 120 days post prion inoculation, $GRN^{-/-}$ microglia were more activated and competent to clear prions, resulted in decreased prion deposition. Whereas at 150dpi, over-activation of $GRN^{-/-}$ microglia led to excessive complement activation and insufficiency of prion clearance, resulting in similar level of PrP^{Sc} to that of $GRN^{+/-}$ and wild type littermates. These results suggest that Progranulin modulates prion-induced microglial activation and protects prion diseases by suppressing excessive activation of complement cascade.

Conclusion:
Microglial activation by prion infection is a stepwise process. Progranulin is an important negative regulator of prion-induced microglial activation. Depletion of PGRN resulted in aberrant microglial activation and accelerated prion disease, suggesting that Progranulin could be a potential target for prion therapeutics.

3981

D. Gero[1], B. File[2], J. Justiz[3], AC. Spector[4], M. Bueter[1]

A drinkometer to analyze microstructure of drinking in humans: a proof of concept study in healthy adults

Department of Visceral Surgery and Transplantation, University Hospital Zurich, Zurich, Switzerland[1], MTA Research Centre for Natural Sciences, Institute of Cognitive Neuroscience and Psychology, Budapest, Hungary[2], Human-Centered Engineering Institute of Applied Sciences, Biel, Switzerland[3], Department of Psychology and Program in Neuroscience, Florida State University, Tallahassee, FL, USA [4]

Introduction:
There are three dimensions of motivational state that can influence ingestive behavior: (1) the metabolic (e.g. hunger, thirst), (2) the oro-sensory (e.g. taste, texture) and (3) the post-ingestive (e.g. glycemic excursions, satiation) dimension. Understanding how these three dimensions interact in the control of food intake remains a primary objective for investigating ingestive behavior. Microstructural parameters are analytical reductions of eating and drinking. These are valuable in understanding the underlying processes that govern such behavior, including motivation and reward, neuro-hormonal interfaces, as well as learning and memory. To date, most studies on microstructural aspects of feeding have been performed in animal models. Our aim was to develop a device that is able to detect microstructural differences with high definition in human drinking behavior.

Methods:
The device ("drinkometer") records the drinking speed at 10 Hz and identifies individual sucks and bursts with their respective volumes, durations and rates. For validation purposes, we performed an experimental study on 12 healthy adults in 16 drinking sessions with 8 concentrations of sucrose (0 – 280mM) served in a blinded and random fashion, in fasted and non-fasted states.

Results:
Two-way RM-ANOVA revealed that total kcal intake during a drinking session depended on sucrose concentration and fasting state ($P < 0.001$ and $= 0.009$). Further, total drinking time ($P < 0.001$), total consumed volume ($P = 0.003$), number of sucks in total ($P < 0.001$) and number of sucks per burst ($P = 0.04$), mean burst duration ($P = 0.03$) and mean burst speed ($P = 0.02$) depended on the fasting state. In contrast, volume per suck ($P = 0.002$), average suck speed ($P < 0.001$), and maximal speed per suck ($P < 0.001$) depended on sucrose concentration. Average speed of drinking ($P = 0.006$) and volume per burst ($P < 0.001$) decreased significantly during meal progress when comparing the first half with the second half of all bursts during one drinking session.

Conclusion:
We conclude that the drinkometer is able to detect differences in microstructural parameters of human drinking behavior dependent on different motivational states. Therefore, the drinkometer might represent an experimental tool to directly measure human ingestive behavior.

3982

J. Schaffenrath[1], M. Neidert[1], L. Regli[1], A. Keller[1]

Determining the protein atlas of normal human blood-brain barrier and glioblastoma blood-brain barrier – towards understanding glioblastoma biology and improved therapies

Division of Neurosurgery, University Hospital Zurich, University of Zurich, Zurich CH8091, Switzerland[1]

Introduction:
Glioblastoma multiforme (GBM) is the most common primary brain tumor with high severity and low therapeutic success. Currently available therapies are not effective and the life expectancy is in average 12-15 month after diagnosis. One important aspect in successful treatment of GBM is to achieve entrance of cancer drugs into the tumor. It is well known that GBM vasculature is leaky to plasma. However, despite this, the drug delivery into the GBM is not successful. Thus, permeability to plasma proteins does not necessarily mean a better drug delivery. Most of prescribed drugs are small lipid soluble molecules, which are effectively removed from the brain endothelial cells via ABC transporters (e.g. P-glycoprotein). Until now, the development and homeostatic regulation of human blood-brain barrier (BBB) is poorly understood. The BBB is a multicomponent system and extending the knowledge about the molecular composition of the GBM BBB will hopefully bring insights into biology of GBM vasculature, and help to design better treatment strategies.

Methods:
In this study, we aim to characterize the transcriptome and proteome of the human BBB in health and GBM. Human endothelial cells (EC) are isolated from GBM and normal human brain tissue. As a control, we use autopsy material with a maximum PMI of 20 hours. For both tissues, normal and GBM, the isolation of EC includes tissue homogenization using collagenases, and a first step of negative selection with anti-CD15 and anti-CD45 antibodies coupled to magnetic beads to exclude leukocytes and circulating progenitor cells. ECs are isolated using anti-human CD31 antibody conjugated to magnetic beads. Isolated cell fractions are lysed for RNA and protein isolation. In addition to the characterization of RNA and protein profile of the EC fraction, we will perform RNA sequencing and proteome analysis on tumor tissue depleted for EC, in order to molecularly profile GBM and to identify neo-epitopes expressed by GBM.

Results:
We have obtained RNA sequencing data from ECs isolated from three GBM cases and three control cases. An unsupervised clustering analysis showed clustering of the sample groups according to their origin - GBM or control tissue. Our preliminary analysis shows deregulation of ECs SLC transporters in GBM ECs compared to control tissue. Interestingly, the expression of several ABC transporters is not altered in GBM vasculature, which highlights that the delivery of lipid soluble drugs is indeed an obstacle in GBM treatment. Our more detailed analysis of differences in transcriptome will be focused on BBB-specific EC genes. We want to understand which BBB characteristics (i.e. closed cell-cell junctions, expression of SLC and ABC transporters, low rate of transcytosis) are specifically altered in GBM ECs and whether we will find GBM specific changes that can be exploited for drug delivery (e.g. upregulation of a specific SLC transporter). In addition, our RNA sequencing data indicates that GBM vasculature has a very different composition of vascular cells (e.g. smooth muscle cells, pericytes, fibroblasts) in the vessel wall compared to the normal tissue. This as well may have consequences on the function of GBM endothelium and might be a therapeutic target.

Conclusion:
Preliminary analysis suggests a deregulation of several transporters (e.g. SLC2A1) in GBM ECs, which may occur due to a loss of some BBB-specific EC genes in GBM samples. For future, we aim to extend our analysis by RNA sequencing of single endothelial cells isolated from GBM regions showing differences in vessel permeability.

3983

V. Dengler Haunreiter[1], N. Leimer[1], D. Wipfli[1], C. Rachmühl[1], Y. Achermann[1], S. Benussi[2], R. Zbinden[3], A. Zinkernagel[1]

In vivo evolution of Staphylococcus epidermidis in a patient with pacemaker-associated endocarditis

Division of Infectious Diseases and Hospital Epidemiology, University Hospital Zurich, University of Zurich, Zurich, Switzerland [1], Department of Cardiology, University Heart Center, University Hospital Zurich, Zurich, Switzerland[2], Institute of Medical Microbiology, University of Zurich, Zurich, Switzerland[3]

Introduction:
Staphylococcus epidermidis is a frequent cause of foreign body associated biofilm infections. *S. epidermidis* adhere to implanted biomedical devices such as prosthetic joints or pacemakers and form a biofilm. The bacteria embedded in the extracellular biofilm matrix are protected from antibiotics to a certain extend making treatment inefficient. Thus, these infections usually require surgical removal of the implant in order to cure the infection.

Methods:
Here, we describe the case of a patient diagnosed with a *S. epidermidis* pacemaker-associated endocarditis. The patient developed a bacteremia despite being under antibiotic therapy with rifampicin and ciprofloxacin. We characterize the *S. epidermidis* isolates recovered during the persisting infection course to find the reasons that explain treatment failure.

Results:
The isolates differed in their morphological phenotypes but all showed a similar PFGE pattern and belonged to the same multi-locus sequence type. This confirms an *in vivo* evolution and rules out a reinfection with another strain. Later isolates from the pacemaker exposed to rifampicin developed rifampicin resistance but were susceptible to all other antibiotics of the treatment regime. The initial isolates from the pacemaker pocket and the bloodstream showed decreased biofilm forming capacity compared to later isolates recovered from the pacemaker as quantified in *in vitro* assays. Moreover, later isolates show slower growth and less hemolytic activity compared to isolates from the recovered at first admission to the hospital.

Conclusion:
Altogether, the case highlights the ability of *S. epidermidis* to adapt and persist under antibiotic treatment.

3984

V. Strouvelle[1], V. Vongrad[1], H. Günthard[1], K. Metzner[1]

48 hours in the life cycle of patient-derived HIV-1 isolates in primary CD4+ T cells

Infectious Diseases, University Hospital Zurich[1]

Introduction:
The HIV-1 life cycle is very difficult to investigate *in vivo*. Experimental models have been invented to better understand the dynamics and single steps in the HIV-1 life cycle; however, they were carried out using laboratory-adapted HIV-1 strains and/or cell lines. To further investigate the HIV-1 life cycle in a model closer to the *in vivo* conditions, we conducted a series of 48-hour long time course experiments using patient-derived HIV-1 isolates and primary CD4+ T cells from separate HIV-1 negative donors as inter-donor variability has been previously noted.

Methods:
Two HIV-1 isolates were selected according to their profound difference in viral fitness as measured by p24 ELISA. After infection with HIV-1, cell samples were collected at the time of infection (T0); six hours post infection (T6), and every 2 hours subsequently until 48 hours post infection. HIV-1 p24 antigen was measured to confirm infection, cellular HIV-1 DNA and RNA was isolated, and q(RT-)PCR assays carried out for various HIV-1 DNA and RNA forms associated with different steps of the HIV-1 life cycle.

Results:
Total HIV-1 DNA is detectable at hour 6 post infection followed by the appearance of 2-LTR DNA circles at hour 8 post infection. Early gene expression explored by multiple spliced HIV-1 RNA forms is first detected at hour 14 post infection, followed by late gene expression, i.e.,unspliced HIV-1 RNA, starting at hour 24 post infection.

Conclusion:
Our preliminary results reveal that the HIV-1 life cycle in primary CD4+ T cells infected with patient-derived HIV-1 isolates takes longer than observed in cell lines infected with laboratory-adapted HIV-1 strains. Furthermore, our model might be applicable to study differences in replication competence of distinct HIV-1 isolates in more detail.

3985

A. Leblond[1], R. Casanova[1], M. Rechsteiner[1], P. Wild[1], A. Jones[2], D. Heintze[2], A. Ciftlik[2], A. Soltermann[1]

Assessment of predictive biomarkers in cancer tissues using micro-immunohistochemistry followed by DNA sequencing

Department of Pathology and Molecular Pathology, University Hospital, Zurich, Switzerland[1], Lunaphore Technologies SA, EPFL Innovation Park, Lausanne, Switzerland[2]

Introduction:
Limited access to cancer tissues strikes the need to combine on the same clinical specimen immunohistochemistry (IHC) and molecular profiling. Micro-IHC using the Microfluidic Tissue Processor (MTP) allows a fast and reliable staining that could be used for diagnostic evaluation on formalin-fixed paraffin-embedded (FFPE) sections of cancer tissues. This study aims at combining on a unique FFPE tissue section MTP-based micro-IHC and molecular analysis.

Methods:
FFPE tissue sections from BRAF V600E mutated cancers were immunohistochemically stained for pan-cytokeratin and BRAF V600E mutation using MTP at room temperature. Positively stained cells were scored, dissected, processed for DNA extraction and next generation sequencing (NGS).

Results:
MTP-based micro-IHC was comparable to automated platform-based IHC. MTP-stained area displayed precise borders confining positive cells in a 17x17mm^2 zone and gradient of positive- towards negative-stained area across 38.5±8 micrometers. Titration curve experiments by MTP indicated that H score evolution fitted to an exponential model and strong immunoreactivity required 4-minute incubation time with primary antibody. Sufficient amounts of DNA (from 4.34±1ng /cell block to 152±27ng /surgical specimen) allowed to detect BRAF V600E mutation by NGS.

Conclusion:
MTP-based micro-IHC is a relevant approach to combine on a unique FFPE tissue section minute range IHC and NGS.

3986

N. Russkamp[2], R. Myburgh[2], J. Kiefer[1], A. Müller[2], M. Van Den Broek[3], B. Becher[3], D. Neri[1], M. Manz[2]

Generation of mouse CAR T-cells for the depletion of cKIT-positive hematopoietic cells

Insititute of Pharmaceutical Sciences, Department of Chemistry and Applied Biosciences, ETH Zurich[1], Department of Hematology, University Hospital Zurich[2], Institute of Experimental Immunology, University of Zurich[3]

Introduction:
Allogeneic stem cell transplantation (ASCT) is an effective treatment for hematologic diseases such as acute myeloid leukemia (AML). However, the relevant risk of transplant related mortality (TRM) and graft-versus-host-disease (GVHD) limit the application of ASCT to high-risk or relapsed patients. A large proportion of transplant-related side effects are thought to derive from the conditioning regiment containing highly cytotoxic chemotherapeutic agents and in some cases irradiation therapy. An alternative approach of conditioning might be the selective elimination of host hematopoietic stem and progenitor cells by immunological means. We hypothesize to use chimeric-antigen receptor (CAR) T-cells to enable engraftment of the donor-derived stem cells with potentially reduced toxicity. To this end, we focus on the stem cell marker CD117 (cKIT) as target antigen. To assess safety and applicability of this approach, testing in immunocompetent wildtype animals is essential.

Methods:
Primary mouse splenocytes were isolated from C57Bl/6 mice and stimulated with Concanavalin A in vitro. The following day, splenocytes were transduced with the primary mouse γ-retrovirus pMSCV containing the transcript for the anti-CD117 CAR under control of a PGK promotor. The CAR construct comprises an extracellular scFv antigen binding domain linked to an intracellular CD3 signaling and a 4-1BB costimulatory domain via a stalk and transmembrane domain derived from CD8. Murine sequences were used for all parts of the CAR construct. The scFv was generated using a phage display (ETH2-Gold) and demonstrates high and specific binding to the distal part of the extracellular domain of the target antigen. To allow for reproducible detection and purification of successfully transduced cells, a RQR8 domain was included in the construct. The primary mouse AML cell line TIB-49 was stably transduced with truncated mouse CD117 and subjected to *in vitro* killing assays. Incubation times from 4 hours to 4 days and effector-to-target ratios (E:T) from 2:1 to 1:12.5 were used. CAR T-cells activation status and phenotype were assessed by FACS.

Results:
When stimulated with Concanavalin A, mouse T-cells expanded logarithmically *in vitro*. After cultivation for 7 days, the percentage of CD3+ T-cells was >95%. The γ-retrovirus pMSCV exhibited a high transduction efficacy in primary mouse T-cells. Cells transduced with the CAR-construct stained positive for the surrogate marker RQR8. After in vitro expansion, CAR T-cells exhibited a predominantly T-naïve phenotype and a CD4:CD8 ratio of 2:3. In co-culture experiments, lysis of CD117-positive cells derived from a murine leukemia cell line was achieved in presence of CAR T-cells, but not in presence of control T-cells. Conversely, indiscriminate killing of CD-117 negative cells was not observed.

Conclusion:
The generation and cultivation of anti-CD117 CAR T-cells from primary mouse splenocytes is feasible. In analogy to the human system (conducted in a parallel project in the laboratory), mouse CAR T-cells exhibit high in vitro killing activity against CD117+ cells. In subsequent studies, the efficacy of mouse anti-CD117 CAR T-cells will be evaluated in a syngeneic environment *in vivo*. We expect these studies to produce highly relevant data on the potential toxicity profile of anti CD117 CAR T-cells as well as insights into the immunological mechanisms behind CAR T-cell mediated cell killing.

3987

D. Heinzer[1], M. Avar[1], M. Pfammatter[1], L. Irpinio[1], R. Moos[1], B. Kuhn[2], S. Mauerhofer[2], U. Rosenberg[2], A. Aguzzi[1], S. Hornemann[1]

A screen for prion decontaminants to enhance safety of surgical instrument reprocessing

Institute of Neuropathology, University Hospital Zürich, Switzerland[1], Borer Chemie AG, Gewerbestrasse 13, CH-4528 Zuchwil, Switzerland[2]

Introduction:
Prions, the infectious agents causing prion diseases such as the Creutzfeldt-Jakob disease, show extreme robustness to common decontamination procedures. Therefore, there is a risk of iatrogenic transmission of these lethal diseases by inefficiently decontaminated medical instruments. So far, improvement of effective decontaminating agents applicable to routine sterilization procedures has not been feasible as the traditional assays for measuring prion infectivity are time-consuming and constrained by a limited throughput. The development of the real-time quaking induced conversion (RT-QuIC) assay, a fast and ultra-sensitive method based on the self-propagation of proteinaceous agents in misfolding diseases, provides a new approach for the detection of infectious prions. The adaption of this assay to a carrier mimicking surgical steel allows evaluating the efficiency of novel potential decontaminants in a fast and proficient way. In addition, with the emergence of evidence of a-synucleinopathies exhibiting prion-like infectious properties, this method was further adapted and applied to assess inactivation procedures for potentially hazardous α-synuclein fibrils.

Methods:
316L steel type metal beads were treated with either brain homogenates from prion-infected mice or with preformed α-synuclein fibrils (PFFs). Beads were then treated with a series of different decontamination formulations and procedures to assess their decontamination efficiency in the RT-QuIC assays.

Results:
We demonstrated that the prion RT-QuIC assay is suitable to detect propagating prions adsorbed to metal beads, and that the treatment with the standard prion decontamination procedure (1 M NaOH for 2 h) completely abolished a positive signal in the assay. Around 120 different formulations were tested for their efficiency to inactivate or remove prions from the steel beads. We identified one potential candidate formulation with good material compatibility that strongly and reliably reduced a positive signal in the RT-QuIC assay. The candidate formulation will be further validated in a cell assay to confirm its decontamination properties. In addition, we developed an a-synuclein RT-QuIC assay that we used to test the inactivation efficiencies of known prion decontaminants on a-synuclein fibrils.

Conclusion:
We showed that the RT-QuIC can be applied as sensitive and fast method for the detection of propagons on metal surfaces. So far, we identified one suitable formulation that will be challenged further by orthogonal prion infectivity assays. Interestingly, some of the commonly used prion decontamination procedures were less effective to deactivate the propagation efficiency of α-synuclein fibrils. This implies that the resistance of a-synuclein fibrils might differ or even exceed the one of bona fide prions, and that other decontamination procedures need to be applied for the effective deactivation of a-synuclein fibrils.

3988

K. Baebler[1], C. Maeyashiki[1], P. Busenhart[1], M. Schwarzfischer[1], K. Atrott[1], S. Lang[1], M. Spalinger[1], M. Scharl[1], G. Rogler[1], C. De Vallière[1]

A novel OGR1 (GPR68) inhibitor attenuates inflammation in a murine model of acute colitis

Gastroenterology and Hepatology, University Hospital Zurich, University of Zurich[1]

Introduction:
Inflammatory bowel diseases (IBD) are characterized by local acidification of inflamed tissue. The proton-sensing G protein-coupled receptor OGR1, also known as GPR68, was previously identified to play an important role in pH homeostasis. Recently we demonstrated that OGR1 expression is increased in intestinal inflammation in IBD patients and that OGR1 deficiency protects from intestinal inflammation in a murine colitis model. We observed that ectopic overexpression of OGR1, in an intestinal epithelial cell model, inhibited cell migration and proliferation during *in vitro* wound healing. In the current study, we investigated the effects of a novel OGR1 antagonist in a murine colitis model.

Methods:
Acute colitis was induced in wild type (C57BL/6) mice by the addition of 1.5% dextran sulfate sodium salt (DSS) in the drinking water for 7 consecutive days. The small molecule OGR1 antagonist was administered by oral gavage in vehicle solution (methylcellulose 0.5%), twice daily (interval of 12 h). Doses used were per kilogram bodyweight per day: 25 mg, 50 mg, 100 mg (n=10 mice per group). Water or DSS control groups were gavaged with vehicle solution without inhibitor (n=10 mice per group). On day 8, mice were sacrificed and inflammatory parameters were evaluated.

Results:
An amelioration of murine DSS-induced colitis in the OGR1-inhibitor treated group compared to DSS-treated control animals was observed. The effect was detected by colonoscopic MEICS score, histology score and colon length. Macroscopically, the colon tissue of the inhibitor treated mice showed no thickening, vascularity was similar to control mice and no fibrin was detected. However, the inhibitor treated mice showed an elevated score in stool consistency. Microscopically, H&E staining revealed that inhibitor treated mice exhibited less infiltration and epithelial damage compared to DSS treated mice. However, a difference in body weight or health score could not be demonstrated among the groups treated with the inhibitor compared to controls.

Conclusion:
The inhibition of OGR1 (GPR68) reduces inflammation in the DSS-mouse model of colitis. Our data suggests that targeting proton-sensing OGR1, by a specific small molecule antagonist may be a novel therapeutic approach for the treatment of IBD.

3989

Y. Chang[1], M. Ziegler[1], D. Ignatova[1], P. Ivanov[2], R. Profanter[2], K. Kerl[1], J. Hafner[1], R. Clark[3], R. Dummer[1], E. Contassot[1], L. French[1], S. Misailovic[4], A. Cozzio[6], M. Vechev[2], W. Hoetzenecker[5], E. Guenova[1]

HLA I shield tumor skin T lymphocytes from NK-cell-mediated elimination

Department of Dermatology, University Hospital of Zürich, Switzerland[1], Department of Computer Science, ETH Zürich, Switzerland[2], Department of Dermatology, Brigham and Women's Hospital and Harvard Medical School, Boston, USA [3], Computer Science Department, University of Illinois at Urbana-Champaign, USA[4], Department of Dermatology, University Hospital Linz, Austria[5], Department of Dermatology, Kantonspital St. Gallen, Switzerland[6]

Introduction:
Targeted therapies and immune modulators are currently changing our understanding for the treatment of solid tumors, and promise to open a new perspective in the management of cutaneous T-cell lymphoma (CTCL) as well. The mechanisms of action of therapeutic antibodies in vivo is not fully elucidated in all cases, antibody-dependent cellular cytotoxicity (ADCC) mediated by natural killer (NK) cells often being presumed to be a key mode of action. However, since progressive impairment of cellular immunity is a hallmark of CTCL, we questioned the fact that patients with late stage CTCL will still be in a possession of fully functional ADCC.

Methods:
To investigate the mechanism of ADDC in CTCL patients. NK cells were isolated from patients with MF stage I-IV, Sézary Syndrom (SS) patients and healthy individuals. An aCella-TOX GAPDH assay was used to detect the amount of endogenous glyceraldehyde-3-phosphate dehydrogenase (GAPDH) and the level of ADCC in each individual patient.

Results:
In vitro ADCC in patients with MF stage I was comparable to that of healthy individuals, but severely abrogated in all MF Stage IV and SS patients included in the study. The percentage of NK cells in the blood of CTCL patients was within normal limits. Trogocytosis, a mechanism of cellular communication that can hamper ADCC by cleaving the surface of the tumor cells from the targeted molecule, seemed not to play an essential role in CTCL. However, overexpression of MHC I on the malignant tumor cells in CTCL was important factor in helping tumor cells escape NK-cell activity and MHC I blockade could restore impaired ADCC.

Conclusion:
Impaired ADCC may pose some problems when choosing a targeted drug therapy for the treatment of late stage CTCL. Understanding of the immunological mechanisms behind it will help improve NK cell activity in CTCL patients and overcome resistance to treatment.

3991

O. Török[1], B. Schreiner[2], A. Keller[1]

The role of brain pericytes in the regulation of leukocyte trafficking under homeostatic and pathological conditions

Department of Neurosurgery, University Hospital Zurich, Zurich[1], Institute of Experimental Immunology, University of Zurich, Zurich[2]

Introduction:
Under homeostasis lymphocyte trafficking into the central nervous system (CNS) is tightly controlled by the blood–brain barrier (BBB). In multiple sclerosis (MS) autoreactive leukocytes enter the CNS and cause demyelinating pathology. Although vast effort is made to understand the pathophysiology of autoimmunity in MS, knowledge about pathological changes of the CNS vasculature that permit the extravasation of autoimmune leukocytes is still limited. Although it was demonstrated that pericytes play an important role in the development of the BBB, further studies are needed to better define the role of pericytes in regulating immune cell trafficking in the CNS.

Methods:
In our studies we use genetically modified, pericyte-deficient (*Pdgfb ret/ret*) mice. These animals show approximately 85% reduction of pericyte coverage in the CNS vasculature. We use an animal model of MS (experimental autoimmune encephalomyelitis (EAE)) to investigate the role of pericytes in neuroinflammation. In this model, active immunization with myelin oligodendrocyte glycoprotein (MOG 35-55) peptide or an adoptive transfer with MOG 35-55 activated T-cell blasts is performed. To investigate if the permissive BBB for leukocyte entry observed in pericyte-deficient animals is accelerating spontaneous activation of self-reactive T-cells, we have crossed *Pdgfb ret/ret* mice with 2D2 transgene mice, which have myelin oligodendrocyte glycoprotein (MOG 35-55) specific T cell receptors (TCR). The following techniques are used: immunohistochemistry, histochemistry, confocal microscopy and flow cytometry.

Results:
The analysis of brains of naïve *Pdgfb ret/ret* mice has shown increased extravasation of leukocytes into the CNS. Leukocyte infiltrates are found mainly in the corpus callosum and in periventricular regions. Flow cytometry analysis demonstrated that, the number of $CD45^{high}CD11b^{+}$ myeloid cells was increased in the CNS of pericyte-deficient mice compared to control mice. Immunization of *Pdgfb ret/ret* mice with MOG peptide leads to an early, atypical EAE phenotype. An increased number of $CD45^{hi}$ leukocytes can be detected in the brain parenchyma in pericyte-deficient mice compared to controls, with an increasing tendency in $CD4^{+}$ and $CD8^{+}$ T-cells and a significant increase in the $CD11b^{+}$ and $Ly6C^{hi}$ populations. In the spinal cord of *Pdgfb ret/ret* mice show a decreased number of $CD45^{hi}$ leukocytes compared to the control animals. This is in accordance with the observed clinical phenotype (atypical EAE) and histological findings (leukocyte infiltrates in cerebrum) of *Pdgfb ret/ret* mice. We also demonstrate that permissive BBB for leukocyte entry into the CNS accelerates spontaneous activation of self-reactive T-cells. *Pdgfb ret/ret; 2D2* mice present an early onset of atypical EAE symptoms compared to control mice and show an infiltration of T-cells into the brain parenchyma.

Conclusion:
Our data suggest that pericytes restrict leukocyte extravasation into the CNS by contributing to the non-permissive properties of the endothelium during homeostasis. Pericyte-deficiency changes the clinical phenotype in EAE and is accompanied by an increased leukocyte infiltration into the brain compared to spinal cord. Pericyte deficiency promotes the development of clinical symptoms in MOG-specific TCR transgene mice. Our further studies will be directed towards understanding the molecular pathways regulated by pericytes in immune cell trafficking in the CNS.

3992

D. Ignatova[1], Y. Chang[1], A. Cozzio[3], R. Dummer[1], L. French[1], W. Hoetzenecker[2], E. Guenova[1]

Malignant T cells inhibit anti-cancer immunity in cutaneous T cell lymphoma

Department of Dermatology, University Hospital of Zürich, Switzerland[1], Department of Dermatology, University Hospital Linz, Austria[2], Department of Dermatology, Kantonspital St. Gallen, Switzerland[3]

Introduction:
In cutaneous T cell lymphoma (CTCL), the malignant T cells are a source of suppressive Th2 cytokines, such as IL-4, and progressive impairment of cellular immunity is a hallmark of the disease. IL-4 is known for its capacity to sustain Th2 cell differentiation, when acting directly on T cells, but can also initiate an IL-12 dependent negative regulatory feedback loop and initiate protective Th1 immune response when present during the initial activation of dendritic cells (DC)

Methods:

Results:
Interestingly, we found an association of increased IL-4 production and, at the same time decreased IL-12 levels, with advanced stage CTCL. Neutralization of IL-4 restored Th1 but not Th17 immune responses in CTCL, and DC activation was directly suppressed through co-inhibitory T cell surface molecules.

Conclusion:
This points out towards an abrogated DC-T cell regulatory loop in patients with CTCL and suggests an immune escape mechanism that allows cancer cells to evade recognition from the innate immune system, and subsequently abrogate the differentiation of a protective non-malignant effector $CD4^+$ T cell population.

3993

Y. Chang[1], D. Ignatova[1], D. Kollmann[3], T. Schweiger[3], S. Schwarz[3], G. Lewik[3], S. Schoppmann[3], W. Hoetzenecker[2], W. Klepetk[3], K. Hoetzenecker[3], E. Guenova[1]

PD1-positive tumor-infiltrating lymphocytes are associated with poor clinical outcome after pulmonary metastasectomy for colorectal cancer

Department of Dermatology, University Hospital of Zürich, Switzerland[1], Department of Dermatology, University Hospital Linz, Austria[2], Department of Surgery and Department of Thoracic Surgery, Medical University of Vienna, Vienna, Austria.[3]

Introduction:
Pulmonary metastasectomy (PM) is performed in colorectal cancer (CRC) patients with oligometastatic spreading to the lungs. Patients with an aggressive tumor phenotype should be excluded from PM, since its benefit is outweighed by early tumor recurrence and impaired prognosis. Expression of PD-1 and its ligands are prognostic factors in a variety of primary tumors. However, their impact on patients' outcome in the setting of PM for CRC has not been evaluated before.

Methods:
53 CRC patients with pulmonary metastases receiving PM with curative intent were included in this study. Tissue samples of resected pulmonary metastases and available corresponding primary tumors were collected and assessed for PD-1, PD-L1 and PD-L2 expression by tumor-infiltrating lymphocytes (TILs) and tumor cells. Expression patterns were correlated with clinical outcome parameters.

Results:
PD-1 and PD-L1 expression was commonly found in TILs and tumor cells. Expression levels significantly differed between metastases and primary tumors. High PD-1 expression by TILs was associated with impaired overall survival (low vs high expression (mean, 95% CI): 78 mo (60-96) vs 35 mo (25-44); p = 0.011). Additionally, the subgroup of patients, who experienced an upgrading in their TILs/PD1 status between primary and metastasis had a worse survival outcome compared with patients with the same grade or a downgrading (34 mo (26-42) vs 96 mo (72-120); p = 0.004).

Conclusion:
Thus, PD-1 expression by TILs is a strong prognostic marker in CRC patients with pulmonary spreading treated by PM. Moreover, this study provides a rationale for a therapeutic PD-1 pathway blockade in the treatment of CRC lung metastases.

3994

M. Kirschner[1], B. Vrugt[2], M. Friess[1], M. Meerang[1], P. Wild[2], N. Van Zandwijk[3], G. Reid[3], W. Weder[1], I. Opitz[1]

A combined microRNA-clinical Score as prognostic factor for malignant pleural mesothelioma

Department of Thoracic Surgery, University Hospital of Zurich, Zurich, Switzerland[1], Institute of Surgical Pathology, University Hospital Zurich, Zurich, Switzerland[2], Asbestos Diseases Research Institute, Sydney, Australia[3]

Introduction:
Prognosis for malignant pleural mesothelioma (MPM) is poor, and predicting the outcome of treatment is particularly difficult. In 2015, a 6-microRNA signature (miR-Score) was demonstrated to show high prognostic accuracy in a series of surgical specimens (with and without induction chemotherapy) from patients with MPM. In-depth analysis of matching pre- and post-chemotherapy tissue specimens has recently shown that a refined 2-miR-Score appears more suitable for use in diagnostic chemo-naïve specimens. Here, in addition to continued validation, we also aimed to further improve the prognostic accuracy by combining the 2-miR-Score with known clinical prognostic factors.

Methods:
Analyses were performed in two sets of matching pairs of chemo-naïve (diagnostic biopsy) and chemo-treated (extrapleural pneumonectomy, EPP) specimens. The training set consisted of samples from 34 patients, and was previously used to identify the refined 2-miR-Score. The test set consisted of an additional 33 pairs of chemo-naïve and chemo-treated specimens. In all samples, microRNA analysis was carried out by microRNA-specific RT-qPCR. On the training set, binary logistic regression modelling was applied to build a combined score consisting of the 2-miR-Score and the clinical prognostic factors age (<60 years vs >60 years at diagnosis), gender and histological subtype (epithelioid vs non-epithelioid). In both sets, accuracy of the investigated scores (2-miR-Score and combined microRNA-clinical score) in predicting a good prognosis (>20 months survival post-surgery) was evaluated by receiver operating characteristic (ROC) curve analysis, and evaluation of the area under the ROC curve (AUC with 95% confidence intervals (CI)).

Results:
Combining the refined 2-miR-Score with the clinical prognostic factors histological subtype and age at diagnosis, increased the overall accuracy of the 2-miR-Score in both chemo-naïve diagnostic (AUC=0.80; 95% CI: 0.65-0.95) and post-chemotherapy (AUC=0.86; 95% CI: 0.73-0.98) specimens. Addition of gender as clinical prognostic factor, did not result in further increases, hence this factor was not included in the combined score.
Investigation of an additional set of 33 matched pairs of chemo-naïve and post-chemotherapy tissue samples, confirmed the improved prognostic accuracy of the combined score, with AUCs of 0.76 (95% CI: 0.59-0.92) and 0.79 (95% CI: 0.64-0.95) for chemo-naïve and post-Chemotherapy specimens, respectively. Furthermore, addition of the clinical factors resulted in an increase in specificity of the prognostic score from previously 55-65% to now 65-75%, while keeping sensitivities at the previous levels of 75-85%.
Importantly, the combined microRNA-clinical Score did not only outperform the 2-miR-Score, but also the clinical factors alone.

Conclusion:
This validation has confirmed the prognostic potential of the novel 2-miR-Score. Furthermore, addition of known clinical prognostic factors was shown to result in a combined Score with increased prognostic accuracy.

In addition to continued validation, in currently ongoing analyses we are also investigating combining the 2-miR-Score with our previously proposed multimodality prognostic score (MMPS).

3995

O. Lauk[1], K. Brüstle[1], M. Friess[1], T. Nguyen[2], T. Frauenfelder[2], R. Stahel[3], W. Weder[1], I. Opitz[1]

Preoperative addition of anti-angiogenic bevacizumab to standard inductioncisplatin/ pemetrexed does not increase the risk of acute postoperative bleeding after surgery for malignant mesothelioma

Thoracic Surgery, University Hospital Zürich[1], Department of Radiology, University hospital Zurich, Switzerland[2], Department of Oncology, University Hospital Zurich, Switzerland[3]

Introduction:
Adding anti-angiogenic Vascular Endothelial Growth Factor (VEGF) inhibitor bevacizumab to doublet cisplatin/pemetrexed (cis/pem) in 2nd line treatment for malignant pleural mesothelioma was reported to have a significant improvement on overall survival. In the present analysis, we report for the first time on surgical mortality and morbidity when bevacizumab (avastin) was used as induction therapy before pleurectomy/decortication (P/D) for mesothelioma.

Methods:
15 patients were treated with 3 to 6 cycles of induction chemotherapy with cis/ pem and bevacizumab whereas the last cycle prior to surgery was conducted without bevacizumab. The period between last cycles of chemotherapy and surgery has been 4-6 weeks and 10 weeks for the last dose of bevacizumab in all patients. The use of erythrocytes until postoperative day (POD) 14 was analyzed. Standardized, tumor response to induction chemotherapy was assessed by modified response criteria in solid tumors (mRECIST) in a restaging CT scan as shown in Figure 1.
The present patient cohort was compared with a historical cohort undergoing doublet induction chemotherapy with cis/pem alone.

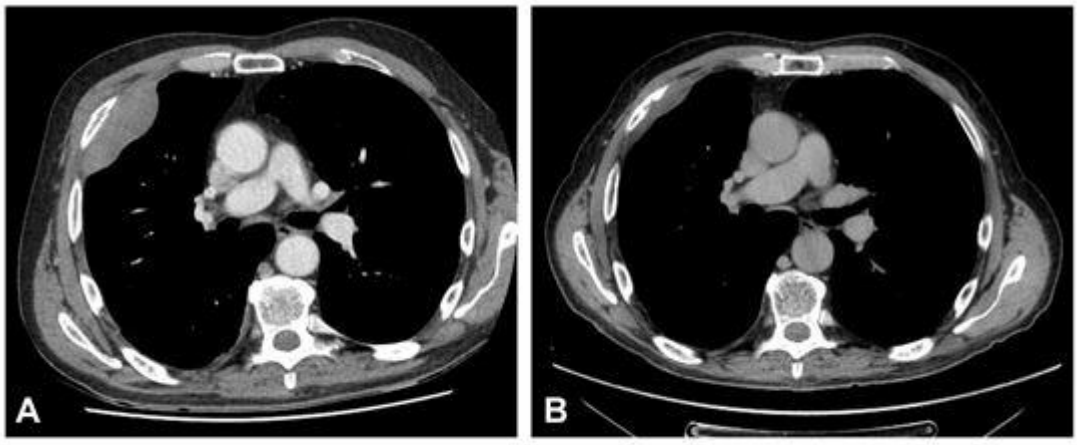

Figure 1: CT pre (A) and post (B) chemotherapy

Results:
According to mRECIST criteria, all patients, except four with partial remission (PR), showed a stable disease (SD) after triplet chemotherapy and no significant difference was seen between both groups (p=0.3). None of the patients showed intraoperative or postoperative bleeding complications. 90-day mortality was zero. The median intraoperative blood loss in the bevacizumab group was 650ml and in the historical group 750ml without necessity of blood transfusion in both groups. The use of erythrocyte concentrates was not higher during the first 2 weeks compared to our historical control.

Conclusion:
These initial data demonstrate that P/D can be performed safely if appropriate time frames are respected between last cycle of chemotherapy and surgery. Response rates were were not different when adding bevacizumab, but overall survival (OS) of this triplet induction chemotherapy has to be further evaluated.

3996

D. Ignatova[1], D. Kollmann[4], J. Jedamzik[4], Y. Chang[1], G. Jomrich[4], A. Baierl[4], D. Kazakov[5], M. Michal[5], W. Hoetzenecker[3], T. Schatton[2], L. French[1], R. Asari[4], M. Preusser[4], M. Gnant[4], S. Schoppmann[4], E. Guenova[1]

PD-L1 expression is an independent predictor of favorable outcome in patients with localized esophageal adenocarcinoma

Department of Dermatology, University Hospital of Zürich, Switzerland[1], Department of Dermatology, Brigham and Women's Hospital and Harvard Medical School, Boston, USA [2], Department of Dermatology, University Hospital Linz, Austria[3], Department of Surgery and Department of Thoracic Surgery, Medical University of Vienna, Vienna, Austria.[4], Department of Pathology, Charles University Hospital Plzen, Czech Republic[5]

Introduction:
The prognosis of adenocarcinoma of the esophagogastric junction (AEG) is bad. The programmed cell death protein-1 (PD-1), a co-inhibitory receptor primarily expressed by T-cells, represents a potential therapeutic target. PD-1, PD-1 ligand 1 (PD-L1), and PD-L2 expression is a prognostic factors in some cancers; however their expression in AEG is unknown.

Methods:
We analyzed PD-L1, PD-L2 and PD-1 expression by tumor-infiltrating lymphocytes (TILs) and cancer cells in tumor specimens of 168 esophagectomy patients and correlated it with disease free survival (DFS) and long-term overall survival (OS).

Results:
We found PD-L1 expression by cancer cells (cancer cell-PD-L1$^+$) in 43.5% of patients whereas we observed PD-L1 expression by TILs (TILs-PD-L1$^+$) in 69%. We found PD-L2 expression by cancer cells and TILs in only 3.5% and 1.8%. 77.4% of tumors contained PD-1$^+$ cancer cells and 81% PD-1$^+$ TILs. Patients with increased expression of PD-1 by cancer cells and TILs showed significantly reduced OS and DFS, as determined by univariate, but not multivariate analysis. We found that expression of PD-L1 by cancer cells is an independent predictor for improved DFS (p=0.038) and OS (p=0.042) in multivariate analysis.

Conclusion:
Taken together, our data demonstrate that expression of PD-L1 cancer cells and TILs is an independent predictor of favorable outcome in AEG, whereas PD-1 expression is associated with worse outcome and advanced tumor stage.

3997

C. Li[1], Y. Li[1], C. Hiller[2], G. Kullak-Ublick[2], Z. Gai[2]

Protective effect of obeticholic acid on obesity-induced cardiomyopathy

Shandong University of Traditional Chinese Medicine, Ji-nan[1], Department of Clinical Pharmacology and Toxicology, University Hospital of Zurich, Zurich, [2]

Introduction:
Obesity is a major contributor to myocardial cell apoptosis, fibrosis and ventricle hypertrophy, and associated with the increased risk of hypertrophic cardiomyopathy. Obeticholic acid (OCA), a farnesoid X receptor agonist, is a key regulator of lipid metabolism, inflammatory, fibrosis and metabolic pathways. This study was performed to investigate the effect and mechanism of OCA on myocardial cell injury induced by palmitic acid (PA).

Methods:
C57Bl/6 mice were fed with a 45% high fat diet (HFD) or a standard diet. Biochemical parameters and myocardial pathological changes were examined. In vitro, 3D cell culture, seahorse and mitochondria damage of C2C12 cells cultured with PA in the absence or presence of OCA were tested.

Results:
The body weight of HFD C57Bl/6 mice has increased by 22.7% compared with mice fed with normal diet. In addition, HFD-induced obese mice developed cardiac hypertrophy, fibrosis, inflammation, apoptosis, oxidative injury, which was rescued by OCA treatment. There was also a remarkably mitochondria damage in the obese mice and OCA prevented against the mitochondria damage. In vitro, PA increased the apoptosis rate of C2C12 cells and induced mitochondrial damage identified by the Tom20 level and ATP assay. Oxygen consumption rete (OCR) indicates that OCA promoted the metabolism of PA to protect cells against PA-induced mitochondrial damage.

Conclusion:
The present data suggested that OCA reduced the myocardial cell apoptosis, fibrosis and inflammation in the HFD-induced obese C57Bl/6 mice. OCA also protected the cardionmyocytes against PA-induced mitochondria injury through promoting the PA metabolism. Our findings provide evidence for the protective role of OCA in myocardial cell.

3998

V. Lysenko[1], N. Wildner[1], K. Zimmermann[1], P. Schürch[1], C. Fritz[2], L. Calabresi[3], A. Vannucchi[3], R. Flavell[4], P. Wild[2], M. Manz[1], A. Theocharides[1]

Enhanced support of myelofibrosis stem cells in next generation humanized mice

Division of Hematology, University and University Hospital Zurich, Zurich, Switzerland[1], Institute of Pathology and Molecular Pathology, University Hospital Zurich, Zurich, Switzerland[2], Center for Research and Innovation of Myeloproliferative Neoplasms, Azienda Ospedaliero Universitaria Careggi, University of Florence, Florence, Italy[3], Department of Immunobiology, Yale University, New Haven, Connecticut, USA[4]

Introduction:
Pre-clinical patient-derived xenograft (PDX) mouse models have emerged as powerful tools for investigating normal and leukemic stem cells (HSCs and LSCs), as well as HSC and LSC heterogeneity. A growing number of models have been developed for aggressive malignancies, such as acute leukemias (AML). However, engraftment of less aggressive malignancies, like myelofibrosis (MF), is often limited. MF is a HSC disorder characterized by bone marrow fibrosis that has the potential to transform into acute myeloid leukemia depending on the clonal evolution of MF stem cells (MF SCs). We hypothesized that the constitutive expression of human cytokines and growth factors in “next-generation” humanized mice could provide a supportive microenvironment for MF SC development and maintenance and could faithfully recapitulate disease phenotype and genetic heterogeneity allowing the development of a pre-clinical MF PDX model.

Methods:
Purified peripheral blood (PB) stem and progenitor (CD34+) cells were collected from MF patients and transplanted intra-hepatically into sublethally irradiated newborn MISTRG mice that express human MCSF, IL-3, GM-CSF, TPO, and SIRPα and into standard NSG mice as a control. Mice were sacrificed and characterized by flow cytometery, immunohistochemistry, and mutational profiling using a TruSight Myeloid Sequencing Panel 5-16 weeks after transplantation.

Results:
Engraftment of PB-purified CD34+ cells from six DIPSS intermediate-2 or high-risk patients was compared between NSG and MISTRG mice. All transplanted MISTRG mice and 50% of NSG mice had more than 1% human CD45+ cells in the bone marrow (BM). The total median engraftment in the BM of MISTRG mice was 29.3%, which is significantly higher than 1.6% in NSG mice ($p<0.0001$). Both NSG and MISTRG mice supported substantial myeloid engraftment. Also, higher overall median human engraftment was observed in the PB (34.3% vs. 0.5%, $p<0.0001$) and in the spleen (2.87% vs. 0.48%, $p<0.05$) in MISTRG vs. NSG mice. MISTRG mice also supported engraftment of PB-purified CD34+ cells from 2/2 DIPSS intermediate-1 risk patients. Furthermore, immunohistochemistry revealed development of human megakaryocytes, but no increase in reticulin fibers (Gömöri). In addition, preliminary data comparing the mutational profile of primary samples to their corresponding engrafted xenografts showed maintenance of the original clonal composition Finally, engraftment of purified human MF cells from primary mice into secondary recipients was observed.

Conclusion:
Overall, these results show that MISTRG mice support robust engraftment of MF SCs from all DIPSS risk categories investigated and are able to maintain stemness and the genetic heterogeneity found in patients. The MF PDX model will further be used to understand the disease pathogenesis and assess established and novel therapeutic agents in order to expedite their transition into clinical trials. Longterm experiments with co-transplantation of mesenchymal stromal cells and intra-bone injection of MF SCs to enhance the likelihood of fibrosis development are ongoing and available data will be presented at the meeting.

3999

Y. Zarb[2], D. Kirschenbaum[1], D. Kindler[3], J. Klohs[3], A. Aguzzi[1], A. Keller[2]

Ossifying environment accompanies brain capillary calcification in the mouse model of primary familial brain calcification

Institute of Neuropathology, University Hospital of Zurich, Zurich, Switzerland[1], Department of Neurosurgery, University Hospital Zurich, Switzerland [2], Institute of Biomedical Engineering, ETH Zurich, Zurich[3]

Introduction:
Primary familial brain calcification (PFBC) is a neurodegenerative disease, which exhibits an autosomal dominant inheritance. Clinical manifestations are variable (e.g. parkinsonism, dementia, psychosis), however, all patients present with bilateral brain calcifications in the basal ganglia. The pathogenic mechanism of PFBC is unknown, but several autopsy studies point to microvascular insufficiency. Although PFBC is a rare disease, brain calcifications are a common CT finding, and vascular dysfunction is the second cause of dementia after Alzheimer's disease. Thus insights into PFBC will aid in better understanding vessel-associated calcification in the brain. Loss of function of platelet-derived growth factor-B (PDGFB) and its receptor, PDGFRB, are associated with PFBC, nonetheless the pathomechanism of vessel calcification due to their haploinsufficiency is not known. Mouse PDGFB hypomorphs (*Pdgfb ret/ret*) develop brain calcifications similar to PFBC patients and possess a strong pericyte-deficiency in the brain, as PDGFB/PDGFRB signaling pathway is crucial for pericyte recruitment to developing vessels. In this study, we have investigated the pathomechanism of cerebral microvascular calcification using *Pdgfb ret/ret* mice. We show that ectopic mineralization of brain tissue in this mouse model is accompanied by an ossifying environment and the presence of a bone cells.

Methods:
In this study, we performed immunohistochemistry to investigate the presence of bone cell markers and to determine the osteoid consistency of brain calcification in *Pdgfb ret/ret* animals and a human case of PFBC. We performed MRI and whole brain clearing followed by Selective Plane Illumination Microscopy to monitor and quantify brain calcifications.

Results:
We detected the presence of bone forming and absorbing cell markers around calcifications in *Pdgfb ret/ret* animals and characterized the environment surrounding calcifications using immunohistological detection of markers for bone proteins. Supporting this data, we also found ossification evidence in a human PFBC case. Additionally, we present different approaches to monitor and quantify brain calcifications *in vivo* and *ex viv*o using MRI and whole brain clearing, respectively.

Conclusion:
We find evidence that the microvascular mineralization in *Pdgfb ret/ret* mice is a result of osteogenic calcification. In addition, we have developed different methodologies to quantify calcifications in the brain. Altogether, these results indicate that the pathogenesis of brain calcifications shares several aspects with other soft tissue calcification diseases (e.g. atherosclerosis, generalized arterial calcification of infancy, Hutchinson-Gilford progeria syndrome) and therapeuting approaches targeting the ossification could reduce the calcification load also in PFBC similarly to other soft tissue calcification diseases.

4000

M. Raeber[1], R. Rosalia[1], D. Schmid[1], O. Boyman[1]

IL-2-driven activation and expansion of dendritic cells

Department of Immunology, University Hospital Zurich and University of Zurich, CH-8091 Zurich, Switzerland[1]

Introduction:
Interleukin-2 (IL-2) belongs to the group of common γ chain (γ_c) cytokines, induces effector T cell expansion during immune activation and is crucial for regulatory T cell development and survival. Together with specific anti-IL-2 monoclonal antibodies, IL-2 forms so-called IL-2 complexes with enhanced *in vivo* activity. We recently discovered, that application of IL-2 complexes expands dendritic cell (DC) populations *in vivo*. This is rather surprising, as DCs do not express the IL-2 receptor β subunit (also termed CD122) and thus do not have a functional IL-2 receptor. Furthermore, incubation of DCs with IL-2 does not induce signalling downstream of the IL-2 receptor which is measured by phosphorylation of signal transducer and activator of transcription 5 (STAT5). This strongly suggests a secondary effect mediated by an IL-2 responsive cell.

Methods:
To assess the activation state and antigen-presenting functionality of DCs expanded by IL-2 complex treatment we analyse surface antigen expression with flow cytometry, use *in vitro* antigen-uptake and processing assays as well as investigate *in vivo* activation of antigen-specific T cells after adoptive transfer of antigen-loaded DCs.
Different mouse models allow us to narrow down possible IL-2 responsive cells inducing DC activation and expansion. These models include bone marrow chimeras and knock-out mice, such as T cell receptor (TCR)$\beta\delta^{-/-}$ and recombination activating gene (RAG)$^{-/-}$ mice. In addition, we more specifically deplete candidate immune cells by injecting monoclonal antibodies. To validate the results obtained from these knock-out mice we add back fluorescence-activated cell sorting (FACS)-purified immune cells or precursors to $\gamma_c^{-/-}$ mice.

Results:
Surface marker analysis shows upregulation of proteins involved in antigen-presentation and co-stimulatory molecules on DCs after *in vivo* IL-2 complex treatment, suggesting expansion of fully functional DCs. *In vitro* and *in vivo* assays investigating antigen uptake, processing, presentation and activation of $CD8^+$ T cells indeed confirmed that these DCs are mature and fully functional.
Bone marrow chimeras of $\gamma_c^{-/-}$ and wild type (WT) mice show that DC expansion is mediated by immune cells rather than non-immune cells. Depletion of T and B cells in sequential experiments was not sufficient to abrogate IL-2 complex mediated DC expansion, although total DC counts were reduced compared to controls.

Conclusion:
DCs proliferate and expand upon *in vivo* administration of IL-2 complexes, although they do not express a functional IL-2 receptor. These preliminary results suggest a novel mechanism of DC expansion by a yet to be defined immune cell subtype and cytokine. Moreover, IL-2 complexes not only expand T cells directly, as described by us and others, but likely also enhance DC mediated antigen-presentation and activation of T cells.

4001

E. Fioretta[1], A. Ksiazek[1], M. Putti[2], A. Fallahi[3], T. Mes[4], A. Bosman[4], C. Cesarovic[5], E. Caliskan[5], H. Rodriguez[5], P. Dankers[2], C. Bouten[2], S. Hoerstrup[1], M. Emmert[1]

Developing a Biodegradable Polymer-based Transcatheter Aortic Valve for the Young: a Proof-of-concept Study in Sheep

Institute for Regenerative Medicine, University of Zurich, Zurich, Switzerland[1], Eindhoven University of Technology[2], Medicut Stent Technology[3], Suprapolyx B.V.[4], University Hospital Zurich, Cardiovascular Center[5]

Introduction:
Transcatheter aortic valve implantation (TAVI) techniques have revolutionized the therapy options for valvular heart disease. Initially developed for elderly high-risk patients, TAVI is being extended to younger patients and may become a first-line treatment in the near future. However, the available bioprostheses for TAVI are prone to degeneration, and patients may thus require multiple re-interventions, significantly affecting their life quality. Therefore, next generation heart valve substitutes with self-repair capacity that stay for life are needed. In this context, novel bioresorbable polymer-based heart valves (PHVs) have shown encouraging results as pulmonary valve replacement in the preclinical setting. Here we describe the in vivo proof of concept of a novel PHV developed for aortic valve replacement and compatible with transcatheter techniques.

Methods:
Bioresorbable PHVs were manufactured using a ureidopyrimidone (UPy)-based supramolecular polymer processed via electrospinning. The highly porous scaffold has been sutured onto a crimpable nitinol stent suitable for TAVI techniques. Transcatheter implantation procedure was initially validated in the pulmonary (n=2) and thereafter in aortic (n=15) position using a transapical delivery route in an adult sheep model. Feasibility and safety of valve delivery, positioning and acute performance was assessed using fluoroscopy and echocardiography. At sacrifice, valve positioning and integrity were evaluated. Histological evaluation of leaflet samples was performed to assess early blood-material interaction.

Results:
The positioning and deployment of the PHV were first achieved in pulmonary position, with sufficient functionality of the prosthesis, good pressure gradient, and absence of stenosis. For the translation to the aortic position, multiple valve and stent designs have been tested to optimize the implantation procedure and ensure valve functionality. Thanks to this developmental process, we finally achieved a valve design that could be successfully implanted as aortic valve replacement (n=4). The prosthesis was functional in an acute fashion for up to six hours, with good leaflet mobility and only mild central insufficiency and mild paravalvular leakage. At explant, all the valves proved to be intact, with pliable leaflets and no signs of tears or ruptures. Histological evaluation showed time-dependent fibrin deposition, with the presence of nucleated cells both in the fibrin clot and in the scaffold material.

Conclusion:
In this proof-of-concept study we present the developmental process of a novel bioresorbable PHV as aortic valve replacement in a preclinical sheep model. Chronic studies are underway to assess the integration and regeneration potential of such prostheses. With long-term safety and efficacy proven, such PHVs may represent a next-generation heart valve concept, particularly beneficial for the young.

4002

Y. Liu[1], A. Aguzzi[1]

Lymphocyte activation gene 3 (Lag3) is upregulated after prion infection without significant contribution to prion disease pathogenesis

Institute of Neuropathology, University Hospital of Zurich, Zurich, Switzerland[1]

Introduction:
Prion diseases (PrDs) are fatal neurodegenerative disorders and share common features with other neurological conditions like Alzheimer's disease and Parkinson's disease. The replication, transmission and aggregation of pathological prion protein, PrP^{Sc}, play central roles in PrD pathogenesis. However, the molecular mechanisms underlying the cell-to-cell spreading of prions are still largely unknown. Previous study indicates that lymphocyte activation gene 3 (Lag3), a member of the immunoglobulin superfamily of receptors, is an receptor for pathologic α-synuclein, which binds to α-synuclein fibrils, triggers their endocytosis into neurons and facilitates the spreading of α-synuclein pathology in the parkinsonian brain. Here, we examined the possible role of Lag3 in the spreading of prion aggregates and pathogenesis of PrDs by using Lag3 knockout (KO) mice.

Methods:
The expression-level changes of Lag3 during PrD progression were examined by quantitative realtime PCR (qPCR) in a Rocky Mountain Laboratory strain, passage 6 (RML6) prion induced mouse model of PrD. Adult Lag3 KO and Wildtype (WT) littermate control mice were injected introcerebrally with RML6 prion brain homogenates or normal brain homogenates (NBH). The incubation time of PrD was measured and neuropathological examinations were performed to assess the effects of Lag3 depletion on PrD development.

Results:
We found that the expression levels of Lag3 in the adult mouse brain is very low, however, its expression levels were significantly upregulated after prion infection. We found only marginal differences regarding the incubation time of prion infection between the Lag3 KO mice and their littermate controls. Neuropathological examinations showed similar levels of neurodegeneration and glial reaction in RML6 prion infected Lag3 KO and WT mice.

Conclusion:
Our results indicate that Lag3 expression levels are significantly upregulated in the mouse brain infected with RML6 prion. However, loss of Lag3 has no significant influence on PrD pathogenesis. Since Lag3 is also an immune checkpoint molecule expressed on major immune cells, our results suggest that immune checkpoint blockade might not be an effective way to halt the progression of PrD.

4003

T. Kazimova[1], M. Pruschy[1]

Identification of Biologically Active Factors in Ionizing Radiation Regulated Secretome

Department of Radiation Oncology, University Hospital, Zurich[1]

Introduction:
Ionizing radiation (IR) leads to DNA damage and genome instability. In addition, IR also leads to stress responses in tumor cells by activating signal transduction pathways and inducing secretion of numerous auto- and paracrine factors. As part of an exhaustive IR-dependent secretome analysis, which was previously performed in our laboratory, placental growth factor (PlGF) was identified to be secreted in response to IR. It is a homodimeric protein, belongs to vascular endothelial growth factor (VEGF)-family and binds to VEGFR1. PlGF expression is low to undetectable in most tissues in healthy subjects, but becomes significantly upregulated in disease.

Methods:
PlGF expression and secretion were analyzed across multiple cancer cell lines and at different time points after irradiation with increasing doses of IR (0, 5 and 10Gy) by qRT-PCR and ELISA, respectively. Two medulloblastoma cell lines (p53 wildtype vs. p53-mutated) were chosen for further experiments with siRNA and the HIF1-alpha inhibitor BAY 87-2243 under normoxic and hypoxic (1% O_2) conditions. Samples were subjected to ELISA and Western blot analysis to investigate the downstream targets of BAY 87-2243.

Results:
PlGF expression and secretion was already upregulated at 4h and 24h, respectively, in p53 wild-type cancer cells. Interestingly, only minimal or delayed PLGF expression could be detected in p53-mutated cell lines. PlGF is also upregulated under hypoxic condition. Therefore, cells were treated with the HIF1-alpha inhibitor BAY 87-2243 under normoxic and hypoxic condition (1% O_2). Interestingly, BAY 87-2243 attenuated PlGF-secretion only in p53-mutated cells. These results suggest that PlGF is differentially regulated by either p53 or HIF1-alpha. To corroborate our hypothesis, parallel experiments were performed with p21, which is a known downstream target of p53 and HIF1-alpha in response to different stress conditions. Similar to PlGF, p21-expression was only affected by BAY 87-2243 under hypoxia and in p53-mutated cells.
In order to investigate the paracrine effect of PlGF, we are currently developing PlGF knock out cells using a CRISPR-Cas9 approach. These cells will be used for *in vitro* and *in vivo* experiments to study the paracrine effect of IR-induced PlGF secretion on tumor and endothelial cells and for tumor radiosensitivity.

Conclusion:
In conclusion, PlGF which has so far not been investigated in response to IR, might play a relevant role for the radiation response on the level of tumor angiogenesis.

4004

D. Canepa[1], E. Casanova[1], V. Tosevski[2], B. Eggerschwiler[1], E. Arvaniti[3], M. Claassen[3], HC. Pape[1], P. Cinelli[1]

Dissecting the Mesenchymal Stem Cells Heterogeneity for Clinical Applications

Division of Trauma Surgery, University Hospital Zurich, Switzerland; [1], Mass Cytometry Facility Zurich, Switzerland;[2], Institute of Molecular Systems Biology ETH Zurich, Switzerland[3]

Introduction:
Fractures with a critical size bone defect represent a serious issue in orthopaedic surgery because are associated with high rates of delayed- and non-union. The standard treatment involve autogenous bone grafts combined with allogenic materials, but this procedure implies different drawbacks. Tissue engineering with mesenchymal stem cells (MSCs), more precisely with adipose derived stem cells (ASCs), represents an interesting alternative to improve the clinical outcomes. MSC *per definition* must (1) adhere to plastic, (2) express CD73, CD90, CD105 and lack the expression of most of the hematopoietic stem cells markers and (3) differentiate toward adipocytes, chondrocytes, and osteocytes. However, MSCs/ASCs consist of a heterogeneous, not yet well-characterized population of different stem/progenitor cells. Understanding the heterogeneous composition of human ASCs is essential not only for understanding the biological properties of MSCs but also in the context of their potential outcomes in cell therapy.

Methods:
To dissect the heterogeneity of 18 human ASC lines we used the novel single cells real-time analysis Cytometry by Time-of-Flight (CyTOF**)**. CyTOF combines both flow cytometry and mass spectrometry and requires individual cells to be labelled with stable heavy metal isotopes. We generated a panel of 31 markers, which includes classical positive and negative MSC markers, epithelial and neural markers, several osteogenic, adipogenic, and chondrogenic markers.

Results:
For assessing the osteogenic differentiation potential of 18 human ASCs the cells were cultivated over a period of 21 days in osteogenic medium and at different time points real-time quantitative PCR and alizarin red staining were performed. Based on the results, we divided the ASCs in good, intermediate, and bad differentiating cells. In a second step, CyTOF was performed on the first 4 days of differentiation and, by using the T-Stochastic Neighbour Embedding (t-SNE) algorithm; we confirmed the phenotypic heterogeneous composition within the ASC lines. Moreover, the analyses given by the CellCNN (convolutional neural network) revealed distinct cell subpopulations between the good and bad differentiating cells, which also behave differently upon induction of osteogenic differentiation.

Conclusion:
The data showed fundamental differences between the patient-specific ASC lines and suggest that the heterogeneity observed *in vitro* mirrors the heterogeneity observed in the clinic. Thus, identifying populations with enhanced osteogenic differentiation potential would serve as a diagnostic tool to predict clinical outcomes of fractures and would improve therapeutic approaches.

4005

A. Okonska[1], S. Bühler[1], V. Rao[1], M. Ronner[1], M. Blijlevens[2], I. Van der Meulen-Muileman[2], R. De Menezes[3], E. Smit[4], W. Weder[5], R. Stahel[6], L. Penengo[7], V. Van Beusechem[2], E. Felley-Bosco[1]

Whole-genome RNAi Screen Reveals a Potential Therapy Depending on BAP1 Status in Malignant Pleural Mesothelioma

Laboratory of Molecular Oncology, Dept. of Thoracic Surgery, University Hospital Zürich, Zürich, Switzerland[1], Department of Medical Oncology, VU University Medical Center, Amsterdam, The Netherlands[2], Department of Epidemiology and Biostatistics, VU University Medical Center, Amsterdam, The Netherlands[3], NKI, Amsterdam, The Netherlands[4], Division of Thoracic Surgery, University Hospital Zürich, Zürich, Switzerland[5], Cancer Center Zurich, University Hospital Zürich, Zürich 8091, Switzerland [6], Institute of Molecular Cancer Research, University of Zürich, Zürich, Switzerland[7]

Introduction:
BRCA1 associated protein 1 (BAP1) is one of the most commonly mutated genes in malignant pleural mesothelioma (MPM). Recent studies on BAP1 function demonstrate its broad role in many cellular processes such as chromatin modification via H2A deubiquitination, transcriptional regulation, and DNA repair. Understanding the molecular function of BAP1 in MPM would contribute to targeted therapy.

Methods:
A genetically engineered model was established expressing either functional or non-functional BAP1 in the same genetic background. Whole-genome siRNA screens were performed assessing impaired survival comparing the BAP1-proficient *vs.* BAP1-deficient MPM cells. Hits were validated by survival assay after silencing with distinct siRNA reagents and verification of knockdown via Western blotting.

Results:
Functional BAP1 expressing cells in the genetically engineered cells was verified by histone 2A deubiquitination and resistance to olaparib compared to non-functional BAP1 expressing cells. The whole-genome siRNA screen revealed 11 hits with $p<0.05$ and FDR<0.05. Unexpectedly, actionable targets were revealed and validated by drug treatment in BAP1-proficient cells.

Conclusion:
These observations reveal a novel aspect of therapeutic potential in MPM depending on BAP1 status, where MPM patients could be stratified depending on BAP status of a tumor and treated with an already in use drug.

4006

U. Blache[1], Q. Vallmajo-Martin[1], V. Milleret[1], M. Ehrbar[1]

3D cell biology meets synthetic materials: Microvascular network formation by endothelial cells in ECM-free hydrogels

Klinik für Geburtshilfe, UniversitätsSpital Zürich [1]

Introduction:
The extra cellular matrix (ECM) is the physiological material surrounding cells in tissues. Components derived from the natural ECM such as fibrinogen, collagen type 1 or collagen type 4 (matrigel) are widely used as 3D hydrogel scaffolds in cell biology. However, such natural ECM components show batch-to-batch variability, are difficult to modify towards customized requirements and trigger by itself cellular responses. These limitations can be overcome by using synthetic materials that mimic the natural ECM and are formed under fully controlled conditions.

Methods:
Here, we introduce synthetic poly(ethylene glycol) (PEG) hydrogels as 3D cell culture platforms to study angiogenesis and micro-capillary network formation. Various human endothelial cells and human mesenchymal stem cells (MSCs) are 3D encapsulated in PEG hydrogels and the resulting co-cultures are analyzed by different microscopy techniques, gene silencing and transcriptome profiling.

Results:
We show that in synthetic environments MSCs and the endogenously deposited ECM enable endothelial cells to form stable, lumenized and 3D-aligned micro-capillary tubes that are surrounded by supporting cells and a dense ECM layer. Moreover, transcriptome analysis of MSCs, when isolated from micro-capillaries, showed perivascular lineage differentiation including Notch signaling. Functionalization of PEG-hydrogels with a Notch-activating ligand could partially phenocopy the switch of MSCs in absence of endothelial cells.

Conclusion:
We envision synthetic hydrogels to become powerful tools in cell biology to e.g. address the role of the endogenous ECM in cell biological processes such as but not limited to the formation of the microvasculature. Furthermore, this work shows how biomaterials can reveal novel biological insight, providing immediate feedback for the design of functional, cell-instructive biomaterials.

4007

R. Higgins[1], A. Jensen[6], C. Has[3], L. Bruckner-Tuderman[3], R. Spiegel[4], H. Traber[4], J. Achermann[4], M. Schaller[5], B. Fehrenbacher[5], M. Röcken[5], D. Ignatova[1], Y. Chang[1], L. French[1], W. Hoetzenecker[6], R. Hornung[2], A. Malzacher[2], A. Cozzio[6], A. Navarini[1], E. Guenova[6]

Uniparental inheritance of junctional epidermolysis bullosa through a novel mutation of the ITGA6 gene and trisomic rescue.

Department of Dermatology, University Hospital Zurich, Switzerland[1], Department of Dermatology and Department of Gynecology, Cantonal Hospital St. Gallen, Switzerland[2], Department of Dermatology, University Medical Center Freiburg, Germany[3], Human Genetics Laboratory Genetica, Zurich, Switzerland[4], Department of Dermatology, Eberhard Karls University, Tubingen, Deutschland[5], Department of Dermatology and Allergology, Cantonal Hospital St. Gallen, St. Gallen, Switzerland[6]

Introduction:
Junctional epidermolysis bullosa (JEB) is a rare genetic blistering disorder due to damaging mutations in genes encoding for laminin subunits, integrins or collagen XVIIa. Blistering can be triggered by mild trauma to the area but can also arise spontaneously. Any organ with a mucous membrane is at risk for involvement. There is as of yet no cure. Treatment of the blisters, prevention of infection and correction of extracutaneous complications is the only clinical treatment for patients. JEB is autosomal recessive. In very rare cases, germline mosaicism and uniparental isodisomy have been reported. Here we investigate the genetic cause in a female newborn with skin aplasia, progressive junctional epidermolysis bullosa with pyloric atresia. An amniocentesis was conducted due to developmental abnormalities in the embryo, which detected low-level fetal mosaic trisomy of chromosome 2.

Methods:
Prenatal amniocentesis, immunofluorescence mapping, transmission electron microscopy and genetic analysis were used for diagnostic evaluation.

Results:
Immunofluorescence mapping showed a junctional split and absence of immunoreactivity for integrin α6. Sequence analysis of the *ITGA6* gene on chromosome 2 revealed a homozygous frame-shift insertion, leading to a premature termination codon. This mutation was found in a heterozygous state in the mother, but not in the father. Segregation analysis with chromosome 2-specific short tandem repeat (STR) markers exhibited exclusive maternal inheritance of chromosome 2, thus demonstrating evidence for uniparental disomy (UPD2) due to trisomic rescue. Whole exome sequencing was used to confirm the *ITGA6* mutation and investigate any additional damaging homozygous mutations in chromosome 2 as a result of the UPD2. Interestingly, a damaging *COL4A4* mutation was identified, which is however not a gene previously described in epidermolysis bullosa.

Conclusion:
Full trisomy as well as high-level mosaicism would lead to spontaneous miscarriages or severe fetal malformations. Due to a very rare event of trisomy rescue, a uniparental disomy can lead to the manifestation of a recessive condition in case of mutation transmission by only one parent. This case demonstrates uniparental isodisomy caused a severe form of fatal junctional epidermolysis bullosa.

4008

R. Brun[1], E. Spoerri[2], L. Schäffer[3], R. Zimmermann[1], C. Haslinger[1]

Induction of labor and postpartum blood loss

Department of Obstetrics, University Hospital Zurich, Zurich[1], University of Zurich, Zurich[2], Department of Obstetrics, Kantonsspital Baden, Baden[3]

Introduction:
The risk for postpartum hemorrhage (PPH) following induction of labor (IOL) has been published with partially conflicting results, even though a majority of the studies suggested an association of IOL with PPH.The aim ou our study was to analyze blood loss after delivery in women with induction of labor compared to women with spontaneous onset of labor (SOL).

Methods:
In a prospective cohort study, 965 deliveries were analyzed including 380 women with IOL (39%) between 2015 and 2016. Primary outcome parameters were incidence of postpartum hemorrhage (PPH), estimated blood loss (EBL) and Δ hemoglobin (ΔHb, difference between prepartum and postpartum Hb). A multivariate linear regression analysis was performed for common risk factors for PPH.

Results:
Incidence of PPH and EBL were not significantly different in women with IOL compared to women with SOL (24.7% vs. 21.2%, p=0.20; and 400 (300-600) ml vs 400 (300-500) ml, p=0.03). Women with IOL had a significantly lower drop in hemoglobin after delivery (ΔHb 13 (5-21) g/l vs. 16 (9-24) g/l, p<0.01). Clinical relevant loss of hemoglobin defined as ΔHb ≥30 g/l did not differ between groups (12.9% vs. 13.8%, p=0.67). In the multivariate linear regression analysis, induction of labor remained associated with decreased loss of hemoglobin after delivery (ΔHb -3.9 g/l (CI 95 % -4.98 to -1.79 g/l), p<0.01).

Conclusion:
Induction of labor is not associated with postpartum hemorrhage. In fact, women with IOL show a statistically significant, however clinically not relevant lower loss of hemoglobin after delivery as compared to women with SOL.

4009

J. Hutmacher[1], S. Brandt[2], N. Samartzis[1], I. Ihnenfeld[1], A. Noske[2], D. Fink[1], P. Imesch[1], E. Samartzis[1]

ARID1A expression is ubiquitously retained in adenomyosis in contrast to endometriosis

Gynecology, University Hospital of Zurich, Zurich[1], Pathology, University Hospital Zurich, Zurich[2]

Introduction:
Adenomyosis is a benign gynecological disease affecting 5-70% of female patients. Symptoms include bleeding disorders, dysmenorrhea, dyspareunia and infertility. In comparison, endometriosis has similar symptoms and shares certain similarities. The pathogenic mechanism of disease development of both, adenomyosis and endometriosis, remain partly unknown. Yet emerging data provide evidence that they are diseases caused and regulated by epigenetic changes.
ARID1A encodes BAF2501, a DNA-binding protein and a subunit of human SWI/SNF-related complexes, which play a crucial, epigenetic role in proper cell differentiation, development and tumor suppression. ARID1A mutations, resulting in loss of protein expression, are frequent in gynecological cancers as ovarian clear cell, endometrioid and endometrial cancer as well as in lymphoma, gastric cancer or cholangiocarcinoma. In benign diseases, however, the loss of ARID1A expression has, so far only been observed in a subset of ovarian and deep-infiltrating endometriosis. The aim of the study was to examine the expression pattern of ARID1A in adenomyosis as a possible factor in the pathogenesis of the disease as well as in infertility.

Methods:
Preparation of two tissue micro arrays (TMAs) including 148 tissue samples of adenomyosis and eutopic endometrial tissue, 56 in the proliferative phase, 42 in the secretory phase and 50 samples in postmenopause. For a control TMA, 96 samples of normal endometrium were obtained from patients without adenomyosis. After, immunohistochemistry was performed and TMA slides were incubated with a polyclonal anti-ARID1A antibody and nuclear expression was scored. Stromal cells served as positive control.

Results:
Immunohistochemical staining of ARID1A was assessable in at least one of two punches in 90,5% of the study cases and in 100% of the control cases. All adenomyosis samples showed positive nuclear ARID1A expression. No complete or partial loss of expression was detected in any of the patients either in adenomyosis or in the eutopic endometrium of adenomyotic uteri.

Conclusion:
In conclusion, the present data show that ARID1A expression was fully retained in the ectopic as well as in the eutopic endometrium of all patients with adenomyosis examined in the TMA. These results present a contrast to endometriosis. Therefore, dysregulation of ARID1A expression does not seem to play a crucial role in the pathogenesis of adenomyosis. This also supports the theory that compared to endometriosis adenomyosis is a distinct disease and has its own pathomechanism.

4010

A. Senatore[1], M. Hermann[2], M. Nuvolone[1], P. Schwartz[1], J. Guo[1], S. Sahl[3], P. Pelczar[2], A. Aguzzi[1]

Therapeutic approach against genetic prion diseases linked to insertion mutation in the octapeptide repeat region of PrP

Institute for Neuropathology, Universitatsspital Zurich[1], Institute of Laboratory Animal Sciences, University of Zurich, Zurich[2], Department of NanoBiophotonics, Max Planck Institute for biophysical Chemistry[3]

Introduction:
Familial prion diseases account for approximately 10-15% of human prion diseases and are caused by dominantly inherited germ line mutations in the prion protein gene, PRNP. Insertions occurs solely in the octapeptide-repeat (OR) region which is located in its flexible N-terminal tail and normally contains one ninepeptide followed by four PHGGGWGQ octapeptide segments. OPRI mutation in PRNP gene is sufficient to cause the disease likely due to gain of toxicity of misfolded and aggregated mutant PrP with expanded OR and/or the generation of toxic signals ultimately leading to neuronal death. Approaches for therapy could either aim at blocking the toxic signal triggered by OPRI mutation in PrP or at promoting proper PrP folding and/or disassembling of mutant PrP aggregates. Antibodies directed against the OR of PrP could fulfill these needs. By directly binding to the extra OR in OPRI PrP, they could prevent the activation of toxic signaling. As an alternative "chaperone-like" mode of action, OR-binding antibodies could behave as "immunological chaperones" which either counteract OPRI PrP misfolding or package OPRI PrP in not toxic complex. In both cases, they could rescue OPRI-associated pathology.

Methods:
To model OPRI-PrP-linked genetic prion diseases, we created mouse/human PrP chimeras harboring the 9- or the 12-OPRI human mutation, flanked by the N- and C-Terminus of murine PrP, under control of CAG promoter. To characterize biochemical properties and cellular metabolism of OPRI PrP mutants, and WT-OR PrP as a control, we expressed the constructs in Prnp-/- hippocampal Hpl 3-4 cells and Prnp-/- CAD5 cell line obtained by CRISPR/Cas9 mediated Prnp gene ablation. Moreover, WT-OR, 9 and 12OPRI PrP conditional transgenic mouse lines were generated by inserting a floxed chloramphenicol acetyl transferase (CAT) stop cassette upstream the PrP open reading frame to have conditional expression of the PrP constructs by the Cre- lox system. The mice have pure C57B16/J background and, upon breeding to co-isogenic Prnp-/- (prnpZH3/ZH3) mice, only express transgenic PrP and not the endogenous one.

Results:
In transfected cells, both OPRI PrP mutants display PrPSc-like partial PK resistance and aggregation. Immunocytochemical experiments followed by confocal analysis confirmed OPRI PrP intracellular accumulation and super-resolution fluorescence microscopy (STED), showed ring-like structures of aggregated OPRI PrP an the cell membranes. By breeding to Syn-cre mice, we generated transgenic lines where WT-OR and OPRI PrP expression is driven selectively in neurons. Assessment of motor function of the OPRI mice by the accelerated rotarod test detected a deficit of the OPRI PrP mice starting from 24 weeks of age. In parallel, histological examination showed granular deposition of PK-resistant OPRI PrP in the brain of the mutants. Antibodies targeting the octarepeats, the anti-PrP mouse monoclonal POM2 holo- antibody or the phage derived human Fab100, will be tested in cells to rescue OPRI PrP mutant aggregation and in vivo to arrest motor dysfunction of OPRI mice and abnormal PrP deposition in their brain.

Conclusion:
The generation of these conditional transgenic mice expressing supernumerary OR PrP mutants will provide an invaluable model to dissect the pathogenic mechanisms of the OPRI PrP mutants. Finally, these mice will used be to test in vivo the therapeutic potential of octapeptide ligands as a rational approach for curing patients carrying OPRI PrP mutations.

4011

T. Maeyashiki[1], S. Arni[1], I. Iskender[1], W. Weder[1], I. Inci[1]

The impact of perfusion temperature during ex vivo lung perfusion in donation after circulatory death donors

Division of Thoracic Surgery, University Hospital Zurich, Zurich, Switzerland[1]

Introduction:
Normothermic ex-vivo lung perfusion (EVLP) has now been adopted in clinical practice to assess the quality of marginal donor lungs. However, the current protocols require advancement for longer perfusions. Different perfusate temperatures have been used to perfuse liver and kidney in ex-vivo settings. The purpose of this study was to investigate the impact of perfusate temperatures in a donation after circulatory death EVLP setting.

Methods:
Male outbred Sprague Dawley rats were euthanized and left at room temperature for two hours. Donor lungs were retrieved and perfused for 3 hours at severe hypothermic (21C°), moderate hypothermic (28C°) and normothermic (37C°) temperatures in a rat EVLP system (n = 3, each). EVLP physiology and perfusate biochemistry were monitored throughout perfusions. The lung weight was measured before and after EVLP.

Results:
Pulmonary vascular resistance (Fig A) and dynamic lung compliance (Fig B) were significantly better in moderate and normothermic groups than the severe hypothermia throughout perfusions ($p < 0.05$). Potassium ion concentrations were markedly increased in the normothermic group than the others (Fig C; $p < 0.05$). The lung weight gain was significantly higher in the severe hypothermia group than the normothermic group at the end of EVLP (Fig D).

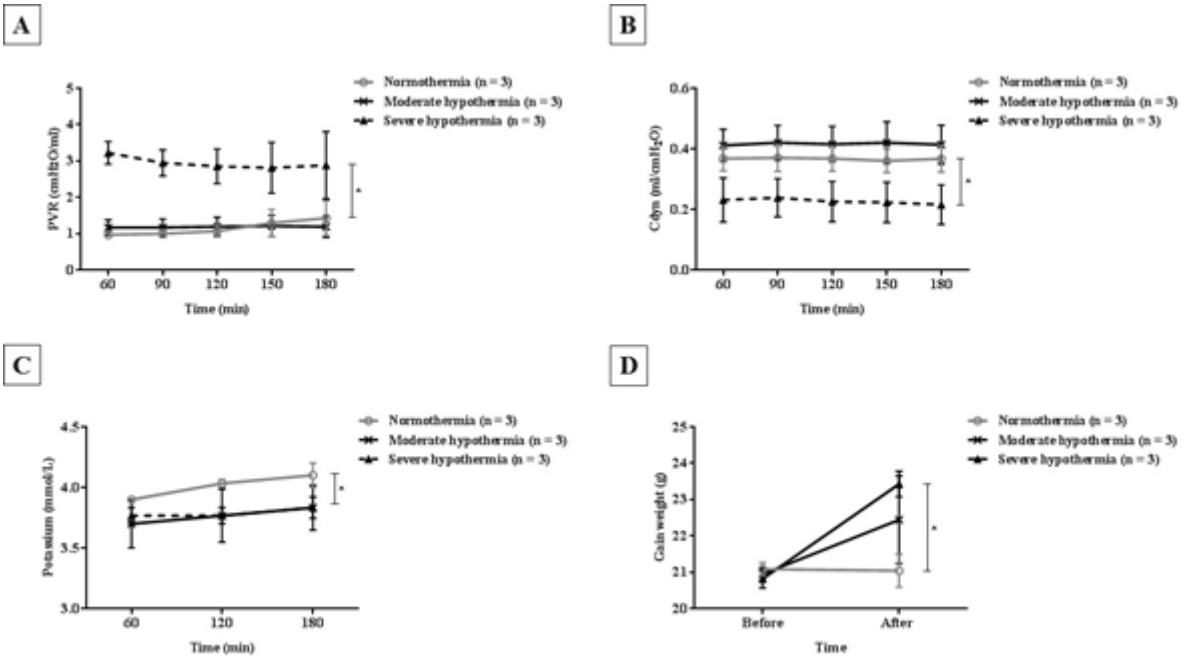

Conclusion:
Severe hypothermic perfusate temperatures showed significantly worse EVLP physiology and the lung weight gain as compared to moderate hypothermic and normothermic conditions in this setting.
Further experiments are warranted to understand the optimum perfusate temperatures during EVLP.

4012

P. Busenhart[1], L. Hering[1], K. Atrott[1], E. Patsenker[1], F. Stickel[1], K. Bäbler[1], B. Weder[1], A. Wyss[1], G. Rogler[1], M. Spalinger[1], M. Scharl[1]

Pharmacologic inhibition of integrin αvβ6 causes tumor shrinkage in the DSS/AOM mouse colon tumor model

Department of Gastroenterology and Hepatology, Universital Hospital Zurich, and University of Zurich, Zurich[1]

Introduction:
Integrins form structural and functional connections between cells and the extracellular matrix. They are involved in many critical cellular processes such as adhesion, migration, proliferation, differentiation and cell death. The β6-integrin subunit is merely detectable in normal epithelial tissues, whereas it is highly induced in epithelial cells during embryogenesis, wound repair as well as during tumorigenesis of many epithelial tumors such as colorectal cancer (CRC). In CRC, elevated β6-integrin levels are associated with reduced survival. Treatment of human CRC cell lines with immunoliposomes carrying siRNAs against β6-integrin reduced their migratory and invasive potential, induced apoptosis and reduced tumor growth of these cells. Since the exclusive expression of β6-integrin in epithelial tumors makes it an excellent drug target, we studied the efficacy of the αvβ6 inhibitor EMD527040 on tumor growth in mice with DSS/AOM induced colon tumors.

Methods:
Colitis-associated colon tumors were induced in C57BL/6 mice by repetitive administration of 1.5 % DSS in drinking water and intraperitoneal AOM (10 mg/kg) injections. After 4 cycles of DSS/AOM treatment, colonoscopy was performed to demonstrate tumor development in each mouse. Mice without endoscopically detectable tumors were excluded from further study. The remaining mice were randomized to the different treatment groups according to their tumor load to obtain comparable groups at the beginning of the further treatment. Mice were then treated with vehicle, 20mg/kg/d or 40mg/kg/d EMD527040 for 24 days. Colonoscopy was performed to detect tumor development during the treatment course and to evaluate tumor load over time.

Results:
Overall, treatment with EMD527040 was safe and we did not detect severe side effects of the tumor therapy. Mice that received vehicle or the low dose of EMD527040 showed either disease progression or no change in tumor load. No decrease in the number of colon tumors was observed in those two groups. However, in the group treated with the high dose of EMD527040 (40mg/kg/d), only 1 mouse had disease progression and in 2 mice, which started treatment with a high tumor load, no progression or regression was observable. Of note however, in the remaining 3 mice which started with a moderate to low tumor load, a complete loss of tumors was observed upon high dose αvβ6 inhibitor treatment for 24 days.

Conclusion:
In early stage CRC (small tumors), treatment with αvβ6 inhibitor showed a strong anti-tumorigenic effect. Therefore, αvβ6 inhibition might be a potent strategy for treatment of CRC. However, the exact molecular mechanisms conferring this anti-tumorigenic effect, and whether other treatment schedules or doses could improve the effect in subjects with a high tumor load remains to be elucidated.

4013

M. Hashimoto[1], O. Lauk[1], M. Friess[1], W. Weder[1], I. Schmitt-Opitz[1]

Poor nutritional status is a poor prognostic factor in a patient candidate for multimodal treatment for malignant pleural mesothelioma

Department of Thoracic Surgery, University Hospital of Zurich, Zurich, Switzerland[1]

Introduction:
Nutritional status has been reported as a prognostic factor in various malignancies. Herein we retrospectively assessed the prognostic impact of the nutritional status in patients with malignant pleural mesothelioma (MPM).

Methods:
We enrolled 87 patients with histologically proven MPM, intended to be treated within a multimodality treatment concept between September 1999 and April 2017 in this retrospective cohort study. We used the prognostic nutritional index (PNI) to evaluate the nutritional status (Buzby GP et al. Am J Surg 1980;139:160–167). The PNI was calculated as serum albumin (g/l) + 5×lymphocyte (G/L) in peripheral blood. Survival correlation between PNI and overall survival (OS) were assessed in univariate and multivariate analyses.

Results:
As of the last follow-up, of 87 patients, 70 patients (80.5%) had died. Median OS in all patients - including those who were not resected - was 16.2 months. Median pretreatment PNI was 45.1 (range: 24.5–58.8). We divided this cohort into Low-PNI group (PNI < 45, n=42) and High-PNI group (PNI >= 45, n=45). Low-PNI group had significantly (p=0.004) shorter median OS (12.0 months) than High-PNI group (21.3 months). In univariate analysis of OS, Low-PNI group (p=0.004), male (p=0.011) and non-epithelioid type (p=0.044) were significantly associated with shorter OS, respectively. In multivariate analysis using Cox regression model, which showed PNI and gender as an independent prognostic factor in MPM patients who intended to be treated within a multimodality treatment concept. Low-PNI group had elevated risk of death compared with High-PNI group (HR: 1.969; 95% CI, 1.208-3.209; p=0.007). Male had also elevated risk of death compared with female (HR 2.829; 95% CI, 1.199-6.672; p=0.018).

Conclusion:
Pretreatment PNI is a novel prognostic factor in MPM patients who intended to be treated within a multimodality treatment concept, which needs to be further confirmed in more uniform and prospective cohorts.

4014

D. Franke[1], J. Zepf[2], T. Burkhardt[1], P. Stein[3], R. Zimmermann[1], C. Haslinger[1]

Impact of the etiology behind retained placenta on postpartum blood loss

Division of Obstetrics, University Hospital of Zurich, Zurich[1], University of Zurich, Zurich[2], Institute of Anaesthesiology, University and University Hospital Zurich, Zurich[3]

Introduction:
Postpartum hemorrhage (PPH) is the major cause of maternal deaths worldwide and retained placenta - defined as a third stage exceeding 30 minutes - is responsible for nearly 20% of all severe PPH cases. The prevalence of retained placenta differs across settings and is higher in high- (2.7%) than in low-income countries (1.5%). Substantial differences between 14 European countries are observed: Northern European countries wait with manual removal of the placenta for 60 minutes or longer, whereas Central and Southern European countries intervene in the first 30 minutes postpartum. The aim of this study was to investigate the clinical course of women with retained placenta in a Swiss obstetrical cohort. Moreover, the influence of the time factor and the etiology of retained placenta on the dynamics of postpartum hemorrhage were analyzed. In contrast to most of the other studies and in order to avoid dilution of data by physiologic deliveries, our cohort consisted solely of women with retained placenta. We assumed that, besides the time factor, the etiology behind retained placenta is also crucial for the dynamics of PPH. We supposed that in women with retained or only partially detached placenta due to uterine atony, blood loss was increased immediately after delivery, whereas in women with retained placenta but without uterine atony (e.g. due to morbidly adherent placenta) the patterns of blood loss are entirely different.

Methods:
This retrospective monocentric cohort study investigated 296 women diagnosed with retained placenta after vaginal delivery at the University hospital Zurich. The third stage of labor was actively managed in all cases. Blood loss was estimated by weighing soaked drapes and using calibrated surgical drapes with a scaled blood-collecting pouch. PPH was defined as blood loss ≥500ml in 24 hours. Antepartum and one day postpartum hemoglobin levels were measured to obtain postpartum drop of hemoglobin (g/l). Descriptive statistics and stratification by length of the third stage of labor (<60 minutes, ≥60 minutes) as well as subgroup analysis of women with or without uterine atony was performed. A Spearman Rank correlation was conducted to analyze the association between third stage duration of labor with blood loss parameters in the overall population and within subgroups.

Results:
Postpartum hemorrhage was seen in 96.6% of all cases. The median blood loss was 1300ml (IQR 900-1900ml) and median drop of hemoglobin was 39g/l (IQR 26-54g/l). In patients with third stage of labor <60 minutes, uterine atony (p=0.001), blood transfusion (p=0.006) and multiple pregnancies (p=0.03) were significantly more common compared to women with third stage of labor >60 minutes. In women with uterine atony (27.4%), a significantly larger drop of hemoglobin (55g/l vs. 35g/l, p<0.001), higher blood loss (2000ml vs. 1100ml, p<0.001), more cases of PPH (100% vs. 95.4%, p=0.048), higher risk of blood transfusion (13.6% vs. 0.9%, p=0.002), general anesthesia (32% vs. 20%, p<0.001) and admission to the ICU postpartum (6.2% vs. 0.5%, p=0.002) was detected. Overall, we did not find a gradual increase in blood loss or drop in hemoglobin levels over time in the third stage of labor.

Conclusion:
Our data suggests that there is neither a safe time window in the management of retained placenta nor a clinically reasonable cutoff point, when a manual removal of the placenta has to be performed. In fact, increased blood loss depends on the etiology of the retained placenta and is not associated with the duration of the third stage of labor. Uterine atony leading to retained placenta causes heavy postpartum hemorrhage immediately after delivery, therefore early detection is required followed by instant manual removal of the placenta.

4015

N. Binder[1], M. El Amki[1], R. Steffen[1], H. Schneider[1], R. Luft[1], M. Weller[1], B. Imthurn[2], G. Merki-Feld[2], S. Wegener[1]

Contraceptive drugs against stroke? Mechanisms of progestin-induced neuroprotection in an Oxygen Glucose Deprivation/Reperfusion (OGD/R) Model

Department of Neurology, University Hospital and University of Zurich, Switzerland[1], Department of Reproductive Endocrinology, University Hospital Zurich, Switzerland[2]

Introduction:
Effective stroke treatments beyond reperfusion remain scant. The natural steroid hormone progesterone has shown protective effects in experimental models of brain injury. However, unfavorable bioavailability limits its clinical use. Desogestrel and drospirenone are new generation progestins with progesterone-like properties, developed as oral contraceptives with excellent bioavailability and overall safety profile. Previously, we have shown that these progestins protected mice from stroke-induced damage and functional impairment. Since progesterone interacts with $GABA_A$ receptors ($GABA_AR$), a similar mechanism could underlie the progestin-induced effect as well. In an oxygen glucose deprivation/reperfusion (OGD/R) model we tested if $GABA_AR$ mediated signaling is required for the neuroprotective effect of desogestrel and drospirenone and if this effect is dose-dependent. Furthermore, we analyzed changes in $GABA_AR$ subtype composition.

Methods:
Primary mouse neural cortex cells were purchased from Lonza (Basel, Switzerland) and exposed to either desogestrel, drospirenone or vehicle in increasing concentrations before OGD/R. Cells were cultured in poly-D-lysine-coated 96-well plates at 37 °C in a humidified atmosphere. After 13 days in culture, the cells were initially exposed to an OGD medium (glucose-free Dulbecco's Modified Eagle Medium), containing either desogestrel (0.01, 0.1, 1, 10µM), drospirenone (0.01, 0.1, 1, 10µM) or vehicle (DMSO, 0.1%). Immediately after, cells were placed in an anaerobic chamber with 95% N_2 and 5% CO_2 for 120 min at 37 °C. OGD was than terminated by replacing the OGD-medium with a glucose containing medium and the cell cultures were placed in the regular CO_2 incubator at 37 °C for 24 h. Control cells were incubated in a glucose-containing medium at 37 °C in a regular incubator. Twenty-four hours after OGD, cell viability was quantified by reduction of 3-[4,5-dimethylthiazol-2-yl]-2,5-diphenyltetrazolium bromide (MTT).
To address if neuroprotection requires $GABA_AR$ signaling we added picrotoxin (100µM), which interacts as an antagonist at the $GABA_A$ receptor channel, to each treatment.

Results:
Pretreatment of the cultured cells with desogestrel and drospirenone resulted in improved cell viability after OGD/R (47.6% and 54.5% compared to 21%). The best effects were achieved with 10µM of desogestrel and 0.01µM of drospirenone. Picrotoxin abolished the protection elicited by both desogestrel and drospirenone. Furthermore, both progestins increased the expression of α4 and δ subunits of the $GABA_A$ receptor, while the α5 subunit was not affected.

Conclusion:
This is the first study demonstrating neuroprotective properties of desogestrel and drospirenone, in stroke using an *in vitro* model. Furthermore, our data provide evidence that the progestin-induced neuroprotection after OGD/R injury requires signaling at the $GABA_AR$. Together with our *in vivo* data, these findings highlight the translational potential of desogestrel and drospirenone, both clinically approved and save drugs, for stroke treatment.

4016

C. Corrò[1], M. Healy[1], S. Engler[2], P. Schraml[1], B. Bodenmiller[2], A. Weber[1], I. Frew[3], M. Rechsteiner[1], H. Moch[1]

Renal cancer stem cells are characterized by IL8 and CXCR1 expression.

Department of Pathology and Molecular Pathology, University Zurich and University Hospital Zurich, Zurich, Switzerland[1], Institute of Molecular Life Sciences, University of Zurich, Switzerland[2], Clinic of Internal Medicine I, University Medical Center Freiburg, Germany[3]

Introduction:
Clear cell renal cell carcinoma (ccRCC) is a very heterogeneous tumor characterized by asymptomatic manifestation in early stage and poor response to radiotherapy and chemotherapy. Growing evidence suggests that ccRCCs as other solid tumors possess a rare population of cancer stem cells (CSCs) contributing to metastasis and resistance to therapy. Therefore, identifying CSCs and understanding the mechanisms underlying self-renewal properties in ccRCC is essential for dissecting tumor heterogeneity and drug treatment efficiency.

Methods:
In this study, we successfully isolate CSC populations from both human derived ccRCC cell lines as well as primary tissues by sphere formation assay. We evaluated CSC properties using state of the art *in vitro* and *in vivo* techniques such as sphere formation assay, clonogenic assay, cyTOF, gene expression arrays, flow cytometry, and xenografts. Finally, we propose a novel CSC biomarker for ccRCC.

Results:
CcRCC-derived CSCs exhibited potent self-renewal capabilities compared to parental cell lines and were characterized by upregulation of mesenchymal and stemness markers as well as genes involved in developmental pathways. Interestingly, ccRCC cell lines as well as primary cultures derived from metastatic tumors showed enhanced sphere formation capability compared to primary tumor-derived cultures suggesting an increased CSC fraction in metastatic sites compared to primary tumors. Interestingly, ccRCC-derived CSCs displayed high levels of the drug transporter ABCB5, the chemokine IL-8 and its receptor CXCR1 but not CXCR2 on both RNA and protein level. While the addition of recombinant IL-8 to culture media significantly increased CSC number and properties, CXCR1 inhibition (anti-CXCR1ab or repertaxin) significantly reduced cell proliferation, migration, invasion, sphere formation and self-renewal capabilities of ccRCC-derived cell lines. When injected into NSG mice ccRCC-derived CSCs not only formed tumors locally at the site of administration but were also capable of metastasizing to the lung and liver of these mice. Interestingly, xenograft tumors displayed high levels of IL-8 and CXCR1 *ex vivo*. Further, IL-8 expression correlated strongly with intratumoral lymphocytic infiltration, poor prognosis and decreased overall survival in ccRCC patients.

Conclusion:
Taken together, these results suggest that the IL-8/CXCR1 axis is associated with cancer stem cell-like properties in renal cancer and may represent a novel therapeutic target for ccRCC patients.

4017

T. Wildschut[1], P. Schürch[1], M. Van Oostrum[2], E. Milani[2], B. Wollscheid[2], A. Theocharides[1]

The Consequence of CALR Mutations on Proteostasis in Myeloproliferative Neoplasms

Experimental Hematology Division, University Hospital Zürich, Zürich[1], Institute of Molecular Systems Biology, ETH Zürich, Zürich[2]

Introduction:
Myeloproliferative neoplasms (MPN) are characterized genetically by a high prevalence of disease-driving mutations in the JAK2, MPL, and Calreticulin (CALR) genes. Although CALR mutations are prevalent in MPN patients, they are restricted to MPN and related myeloid diseases and sufficient for MPN development in mice. The multiple molecular mechanisms by which various CALR mutants result in different clinical phenotypes need to be elucidated.
CALR is a mostly endoplasmic reticulum (ER)-resident protein best known as a chaperone involved in folding of N-linked glycosylated proteins. Since CALR possesses many client glycoproteins and other interactors, mutations will result in a comprehensively affected cellular homeostasis. Homozygous CALR mutations lead to incorrect folding and subsequent deficiency of the glycoprotein myeloperoxidase (MPO) in patients, indicating a potential loss of CALR chaperone function. Furthermore, mutations in CALR can lead to gain of pathological interactions and activation of specific pathways.

Methods:
For investigation of unknown effects of CALR mutations, unbiased approaches are required. By applying proteomics, an exploratory overview of cellular responses can be determined. Glycoproteomics enriches N-linked glycosylated proteins to yield high coverage of potential glycoprotein CALR chaperone clients. Interactomics using BioID enables elucidation of changes in interactors of CALR upon mutations. RNAseq enables a comparison of mRNA with protein levels.
By comparing CALR knockouts and various mutants among each other, loss of function and gain of function effects can be discriminated and linked to clinical outcome. By combining unbiased proteomics techniques, effects of CALR mutations on the protein function itself, its chaperone clients, and various directly and indirectly affected interactors and pathways can be elucidated together with their relevance for the related clinical pathologies and potential for therapy development.

Results:
Significant differences are present in both the proteomes of a CALR mutant and knockout cell line compared to their respective parental wildtypes. Interestingly, among the upregulated proteins in both situations many interacting proteins can be related to ER stress. Presence of ER stress would indicate that similarly to the CALR knockout, the CALR mutant would possess impeded chaperone functioning. Functional experiments validated upregulation of ER stress proteins on both an mRNA and protein level. Furthermore, the mutant CALR cell line seems to be more resistant to increases in ER stress.

Conclusion:
Proteomics, glycoproteomics, and interactomics provide possibilities to detect affected CALR chaperone clients. CRISPR is and will be applied to investigate CALR knockouts and mutations in different cell type backgrounds. By these unbiased approaches, potential therapeutic vulnerabilities of CALR mutants can be discovered. Validation and targeted inhibition experiments can subsequently be performed in available cell lines, patient samples, and humanized mouse models.

Currently mainly receptor and kinase inhibitors have clinical effectivity for MPN, including JAK2 inhibitors. Targeting malfunctioning chaperones therefor presents new possibilities that can improve the current treatment standard for patients suffering from MPN or related diseases, especially for those patients that do not respond or become resistant to current treatments.

4018

R. Higgins[1], M. Theiler[1], A. Smith[1], R. Wälchli[1], L. Weibel[1]

Genetic Architecture of Linear Localized Scleroderma

Department of Dermatology, University Hospital Zurich, Switzerland[1]

Introduction:
Linear localized scleroderma (LLS) is a rare connective tissue disorder (2.7/100'000 per year) characterised by chronic inflammation and massive accumulation of collagen. This results in hardening and thickening of the lesion leading to the affected areas to cave in from atrophy. The sharply delimited and linear lesions, can affect patients throughout the body and more rarely the face in the clinical subtypes *en coup de sabre* and Parry-Romberg syndrome. This leads to terrible disfigurement. The disease affects mostly children and is limited in treatment options, which are most often unsatisfactory. Very little is understood about the condition in terms of genetic and clinical aetiology. There is evidence that LLS might be based on genetic alterations in affected tissues. Blaschko's lines are the patterns of cell migration and proliferation during embryological development. Multiple skin conditions have been shown to follow Blaschko's lines including LLS. Several of these diseases have been demonstrated to be caused by genetic factors such as a *de novo* somatic mutation causing a cutaneous mosaicism. Here we test the hypothesis that LLS is caused by a somatic genetic mutation.

Methods:
Blood and affected skin taken from 19 confirmed LLS patients was Whole Exome Sequenced (WES). Library preparation and hybridization was performed using the SureSelectXT Reagent kits (Agilent Technologies). Sequence analysis was performed as per GATKv3.5.

Results:
Somatic mutations were called using 3 somatic callers. All SNPs and indels were analysed and no rare and damaging mutation was found in common. A gene-based analysis did not reveal any gene burdened with a high number of somatic mutations in common between the patients. Furthermore a pathway-based analysis did not reveal any pathway that could be implicated in LLS.
An analysis of the 3 somatic callers revealed that an increase in read depth (DP) allowed for a more sensitive detection of mutations at low allelic fraction. To this end 4 patients with similar lesions were chosen for deep sequencing (DP of >300). However, somatic analysis of these samples revealed no suitable causative mutation. CGH was performed on 6 patients to find large scale chromosomal aberrations too large to be detected by WES. Samples were compared with 3000 control karyotypes. No rare aberrations were found in common between patients. CNV analysis did not reveal a common CNV event within the cohort.

Conclusion:
Taken together, our analysis revealed the absence of genetic mosaicism in LLS.

4020

E. Avilla Royo[1], M. Ehrbar[1]

Healing-triggering biomaterials for the minimal-invasive treatment of iPPROM

Obstetrics, Universitätsspital Zürich, Zürich[1]

Introduction:
The advance of fetal diagnosis is triggering the development and increase of fetal interventions. However, the progress of intrauterine prenatal surgery is hindered by the risk of miscarriage due to fetal membrane rupture (Iatrogenic Preterm Prelabor Rupture of Fetal Membranes, iPPROM), which remains the main complication after invasive interventions in the intrauterine cavity (such as fetoscopy), and has been associated with serious consequences for the newborn such as deafness, blindness and cerebral palsy.
Due to the poor vascularization of the fetal membranes (FM), they lack the classical wound healing response observed in the skin and other organs in the human body. However, recent *in vitro* and *in vivo* studies have shown that, under the appropriate stimuli, FM cells can be recruited to the wound site and participate in healing. Hence we hypothesize that fetal membranes do have the capacity to heal, as long as the appropriate guiding matrix and chemical cues are provided. To confirm this hypothesis, we will engineer growth factor-presenting cell-instructive biomaterials that sequentially promote cell migration, proliferation and ECM deposition. We will test their stability in amniotic fluid and FM defect models in *ex vivo*, and finally test them in a preclinical sheep model.

Methods:
Using a previously developed three-dimensional hydrogel as the cell culture platform, we will assess the effect of growth factor stimulation in human bone marrow-derived mesenchymal stem cells (bmMSCs) and in human amnion-derived mesenchymal stem cells (hAMSCs). We will evaluate the growth factor capacity to stimulate proliferation, migration and ECM deposition via DNA quantification, migrated distance in the hydrogel, and proteomics, respectively. In a further step, the chemical and physical stability of our biomaterial will be determined. Once an optimal material has been found, its performance will be confirmed in vivo by its implantation in ewes operated at the mid-gestation period, and examined post delivery.

Results:
Preliminary results obtained in the first year of the project are:

1. Successful isolation and expansion of mesenchymal and epithelial amnion-derived cells. Both mesenchymal (hAMSCs) and epithelial (hAECs) cells have been successfully isolated from FM of patients undergoing caesarean section at the University Hospital Zürich and expanded in vitro.

2. Characterization of hAMSCs and hAECs. The success of isolation and separation of the two cell types has been evaluated via immunostainings for specific markers and characterization of the surface markers via FACS.

3. Migration of bmMSCs and hAMSCs under GF stimulation. The effect of PDGF stimulation in the proliferation and migration of bmMSCs and hAMSCs has been quantified, and the optimal growth factor concentration found.

4. Modification of growth factors and stimulatory capacity evaluation. The modification of FGF2, PDGF and EGF to different degrees has been successfully achieved (proven by MS/MS), and it has been as well proven that they retain their stimulatory capacity.

Conclusion:
Engineering a platform that restores membrane integrity after intervention is essential for the advance of the field of intrauterine interventions. The initial results of this and previous projects show promising results, and the efforts of the research group will continue towards solving an unmet clinical need.

4021

Q. Vallmajo-Martin[2], M. Lütolf[1], M. Ehrbar[2]

Deciphering hematopoietic stem cell niche factors in bioengineered human bone marrow models in vivo

Laboratory of Stem Cell Bioengineering, Institute of Bioengineering, École Polytechnique Fédérale de Lausanne, CH[1], Ehrbar Lab, Department of Obstetrics, UniversitätsSpital Zürich, CH[2]

Introduction:
Sufficient numbers of hematopoietic stem cells (HSCs) needed for bone marrow transplantations remains a major challenge in medicine today. HSCs expanded *in vitro* rapidly lose their regenerative capacity likely due to the lack of niche-derived signals comprising molecular and cellular components. Identification of critical hematopoietic niche components necessitates both the generation of more tractable *in vivo* models and, in parallel, novel approaches for heightened throughput in screening such systems *in vivo*. We have previously reported on a blank biomaterial that can be decorated with different growth factors and cell types known to be present in the niche *in vivo*. Here, we present a minimalist human bone marrow model based on a synthetic material, and have applied it for use in discovery of critical HSC niche factors.

Methods:
Functionalized biomimetic polyethylene glycol (PEG) hydrogels were laden with human mesenchymal stem cells (hMSCs) and supplemented with or without bone morphogenetic protein-2 (BMP-2). These PEG gels were polymerized directly in the individual wells of novel multiplexing polydimethylsiloxane (PDMS) devices. Next, the screening devices containing PEG hydrogels were subcutaneously implanted in immunocompromised mice. At 8 weeks, the devices were explanted and analysed for bone and bone marrow formation by microCT, histology and FACS. Moreover, human cells were retrieved from the gels and further examined by quantitative RT-PCR.

Results:
Screening devices featuring 2mm diameter wells were shown to be the minimal size for niche formation allowing 8 conditions to be screened per implantable site (32 unique conditions per mouse). MicroCT analysis revealed mineralization in all wells containing gels with hMSCs, with or without BMP-2. Histological analysis corroborated these findings. Hydrogels containing hMSCs and BMP-2 developed into bone marrow-like constructs including a typical bone shell filled with marrow and trabecular bone structures. Ultimately, long-term HSC enrichment in the constructs containing cells and BMP-2 compared to only BMP-2 gels was confirmed by FACS analysis on the recruited murine cell population. Intriguingly, qPCR of retrieved hMSCs revealed heightened expression of osteogenic markers in all samples irrespective of BMP-2 addition. These results indicate the formation of a functional ectopic niche in cell-laden and fully synthetic hydrogels.

Conclusion:
An implantable screening device was developed to optimize hydrogel conditions, cell type, and soluble factors to support bone marrow niche formation *in vivo*. Up to 32 unique conditions could be tested per mouse. Results indicated a direct participation of hMSCs in both bone formation and murine HSCs recruitment. This device represents a powerful new tool for heightened *in vivo* screening of tissue engineering constructs with a broad range of applications.

4022

L. Kovtonyuk[1], H. Takizawa[2], M. Manz[1]

Intrinsic and Extrinsic Determinants of Hematopoietic Stem Cells Aging

Department of Hematology, Universitätsspital, Zürich[1], Kumamoto University, Kumamoto, Japan [2]

Introduction:
Lifelong continuous blood production is sustained through a stepwise differentiation program by a very limited number of self-renewing hematopoietic stem cells (HSCs) in bone marrow (BM). Hematopoietic cell development is tightly controlled by both cell intrinsic and extrinsic factors and its dysregulation can lead to aplasia or neoplasia. Upon aging, HSCs increase in number, reduce self-renewal capacity on a per cell basis, skew towards myeloid differentiation, and show less efficient bone marrow (BM)–homing ability. We here tested how extrinsic and intrinsic factors determine HSC behaviour during aging.

Methods:
CFSE-labeled young (8-12 week old), aged (>2 year old) and experimentally aged (e.g. serially transplanted) hematopoietic stem and progenitor cells (HSPCs) were transferred into non-irradiated young or aged recipients, respectively. To test biological function of HSCs with distinct divisional histories, quiescent (0-divided at 8 weeks) or cycling (>5-divided at 8 weeks) cells were isolated and transplanted into lethally irradiated mice. These were monthly bled to follow long-term donor engraftment and lineage repopulation. To dissect aging-associated extrinsic factors, we performed antibody based protein arrays and transcriptome analysis with total BM of young versus aged animals. The effect of identified candidates on HSC behavior was further tested in vivo by employing an in vivo HSPC divisional tracking assay (CFSE-dilution).

Results:
BM analysis at 8 weeks after tracking showed that young HSPCs proliferated faster than old HSPCs, independently of their environment. In addition, both young and old HSPCs were relatively more dormant in an old versus a young environment. This indicates increased intrinsic and extrinsic drive towards quiescence during ageing. To test HSCs function based on divisional histories, we isolated quiescent and various cycling HSPC fractions and transplanted them into lethally irradiated mice. Quiescent aged HSCs, irrespective of the environment exposed to, favoured myelopoiesis. In contrast, aged HSCs that were cycling in a young environment, showed balanced lineage repopulation, similar to young HSCs that were cycling within a young or an aged environment. Interestingly, experimentally aged HSCs behaved similar as aged HSCs in comparable experimental conditions. To test extrinsic factors that determine biology of ageing HSCs, we performed antibody based protein arrays and transcriptome analysis with total BM of young and aged animals. Differential analysis demonstrated that RANTES, MIP-2, IL-1α and IL-1β are upregulated in aged BM. Further analysis revealed that both, IL-1α and IL-1β drive young HSC towards proliferation, while this effect is mitigated in aged HSCs. Moreover, analysis of aged IL1RI KO mice revealed a reduced aging-associated HSCs phenotype.

Conclusion:
Our data demonstrate that proliferative history imprints a cell-intrinsic dormancy program on HSCs, which is associated with myeloid-biased differentiation and, at least in natural ageing, with increased IL-1 signaling. Interestingly, this HSC program can in part be “rejuvenated” upon cycling, but not upon dormancy, in young steady-state environments.

4023

D. Pease[1]

Identifying Novel Roles of MicroRNAs in PrPc Biosynthetic Regulation via miRNA Screening

Institute of Neuropathology, University Hospital of Zurich, Zurich, Switzerland[1]

Introduction:
Prion diseases are lethal transmissible neurodegenerative diseases afflicting a wide variety of species. Characterized by misfolding and aggregation of the cellular prion protein (PrP^{c}) into its pathogenic conformer, PrP^{Sc}, these infectious diseases have become the archetypal model for proteopathies. Despite advances in elucidating the mechanisms underlying neurotoxicity, the cellular machinery controlling PrP^{c} biosynthesis and the means by which host PrP^{C} is converted into PrP^{Sc} remains poorly understood. The current project seeks to assess whether, and to what extent, the microRNAome may post-transcriptionally modify PrP^{c} through direct or indirect pathways. To do so, we have developed a cell-based high-throughput human miRNA screen, exploiting a genome-wide library encompassing 2019 mimics and 2019 corresponding antagonists. While this exploratory approach was bound to yield novel potentially therapeutic hits, their validity is contingent upon reproducibility of our results and to what extent the cells recapitulate a biological system.

Methods:
In order to assess potential effects of human miRNA on PrP^{C} levels, we utilized a reverse-transfection approach on a robotic screening platform in which miRNA mimics and antagonists were initially printed into 384-well plates in a randomized layout using an acoustic dispenser. Lipofectamine and cell suspensions are added using robotic micro-dispensers in subsequent steps. Plates were then incubated for 72 hours, prior to content lysis and PrP^{C} quantification via TR-FRET. A combined screening of U-251 MG and CHP-212 cell lines as well as SH-SY5Y cells overexpressing mouse Prnp, but lacking the 3'UTR, was applied. Convergent hits were selected for subsequent characterization. Following a secondary screening validation run, promising hits were characterized via genetic and biochemical tools to define the miRNA interaction modes.

Results:
Screening of U-251 MG and CHP-212 cells yielded 11 miRNA mimic hits that met the cutoff criteria. All hits eliciting PrP^{C} downregulation, except for miR-4686, were found to not reduce cell viability, while all mimics inducing PrP-upregulation concomitantly incurred enhanced cell growth. In congruence with the top 5 pooled *in-silico* miRNA target prediction algorithms, all members of the miR-148/152 family were among these hits, while the majority of the other miRNA hits, many of which bear no mention in the scientific literature, were not predicted as targeting PRNP transcripts, thus potentially indicating secondary interaction pathways.

Conclusion:
A highly robust cell-based high-throughput platform has been established allowing arrayed screening for effects of miRNAs on PrP^{c} levels. This platform thereby sets the groundwork for establishing functional guidelines for infectivity screening, which addresses the much more pertinent potential effects of miRNAs on PrP^{Sc} transmissibility. Discovery of a miRNA inducing decreased PrP^{Sc} propagation levels independent of altering endogenous PrP^{c} would by its very nature act through a secondary non-*PRNP* directed interaction pathway that could only be exposed by this manner of exploratory screening. Such a finding would undoubtedly represent a major breakthrough in the prion field but may also have ramifications for other multigenic diseases involving complex pathways. In conclusion, results gained from these experiments will not only help infer miRNA regulatory roles in PrP^{c} homeostasis, but may also ordain miRNAs as potent therapeutic targets for various transmissible spongiform encephalopathies.

4024

L. Reissner[1], G. Fischer[2], P. Giovanoli[1], M. Calcagni[1]

Kinematic analysis of the hand during opening a jar and yoghurt

University Hospital Zurich, Department of Plastic Surgery and Hand Surgery[1], University Hospital Zurich, Biomechanics ETH[2]

Introduction:
The great relevance of the upper extremities in activities of daily living has made researchers and clinicians gaining increased interest in the assessment of human hand movements. However, the measurement of the small hand joints remains challenging. The aim of the study was to prove feasibility to measure complex manual tasks with a 3D motion capture system, to quantify the repeatability and to analyse the angular motion patterns of two functional tasks in healthy volunteers.

Methods:
Twenty healthy volunteers were recorded during the performance of a set of basic motion tasks as well as during two functional activities: opening a jar and yoghurt. To analyse the test-retest repeatability, each subject was assessed twice on two different measurement days. The kinematic data was collected with a motion analysis system consisting of 11 infrared cameras. A marker set with 46 skin markers was used to record the kinematics of the hand, thumb and fingers simultaneously.

Results:
The kinematics of the functional tasks confirmed to be measurable with the chosen marker set and specific angular motion pattern of the two ADL were reported. Overall, the markers were visible during 97% of the time. The mean active range of motion (AROM) for the individual joints ranges from 17° to 77° and between 19-68.5% of the maximum range of motion was exploited during the daily activities.
The repeatability of the mean AROM during the functional tasks, expressed as the standard error of measurement (SEM), was within a range of 2°-13° for the individual joints. The mean SEM over all joints during the yoghurt- and jar-opening task was 5.7° and 6.8°, respectively. The coefficients of multiple correlations tended to show a better repeatability of the angular motion pattern within (0.66-0.92) the individuals than between (0.16-0.85) the subjects for both ADL and for all joints.

Conclusion:
Thus, the simultaneous motion analysis of the entire hand and fingers during functional tasks is feasible and the joint kinematics could be partially shown to be reproducible during the two analysed activities of daily living. The implementation of the kinematic analysis of the hand within daily activities has provided a first impression of angular motion patterns of two activities of daily living and therefore implies a first step towards the goal to quantitatively measure hand function.

4025

L. Reissner[1], G. Fischer[2], P. Giovanoli[1], M. Calcagni[1]

Wrist and Finger motion: A comparison of goniometric and 3D motion capture technique

University Hospital Zurich, Department of Plastic Surgery and Hand Surgery[1], University Hospital Zurich, Biomechanics ETH[2]

Introduction:
The objective measurement of finger and wrist range of motion (ROM) is of great importance to clinicians when assessing the outcomes of therapeutic interventions and surgical procedures. The aim of the study was to test the reproducibility of active range of motion (ROM) of all fingers and wrist joint angles measured with a 3D motion capture system and to compare it with manual goniometry.

Methods:
Active finger and wrist joints motion of 20 healthy volunteers without any previous hand and wrist pathologies were assessed with the 3D motion capture system and measured with a manual goniometer by a trained hand surgeon. Active maximum joint angles of all fingers and wrist were registered twice on two different days to evaluate the test-retest reliability. The mean absolute difference (MAD), standard deviation of the difference (SD) and standard error of measurement (SEM) between measurements were calculated for both measurement systems and compared within the same task.

Results:
SEM values for the motion capture method lie between 1.9-4.5° except for the MCP5, IP and MCP1 (5.1-8.5°). For the goniometric measurements, SEM was between 5-11° in all joints except for PIP2-5 and DIP5 (4.2-4.9°). Overall, all agreement parameters reveal smaller individual inter-session differences with the motion capture system. Mean MAD and SD of differences for maximal finger and wrist joint angle measurements were 4.5° and 5.8° for the motion capture system, compared to the goniometry with 7.4° and 9.0° respectively.

Conclusion:
Joint angles derived from 3D motion analysis showed smaller mean of absolute difference, suggesting overall a better reliability for this technique. Furthermore, the advantage of 3D motion analysis is the dynamic evaluation of the wrist and all finger joints simultaneously. Main advantage of the goniometric method are, that it is cheap, fast and does not require data post-processing or any knowledge about joint angle calculations.

4026

L. Reissner[1], G. Fischer[2], P. Giovanoli[1], M. Calcagni[1]

Gender difference in kinematic analysis of hand movements during opening a yoghurt

University Hospital Zurich, Department of Plastic Surgery and Hand Surgery[1], University Hospital Zurich, Biomechanics ETH[2]

Introduction:
The great relevance of the upper extremities in activities of daily living has made researchers and clinicians gaining increased interest in the assessment of human hand movements. The aim of the study was to analyse the motion patterns of opening a yoghurt in healthy volunteers.

Methods:
Twenty healthy volunteers (10 male, 10 female) mean age 28 (SD 4.7) years were performing a set of basic motion tasks and yoghurt-opening. The active range of motion (ROM) of the MCP joint of the small finger and of the wrist were calculated.

Results:
In 9 of 10 cases the functional task was performed with the MCP joint of the small finger in flexion in the male group, while only five persons in the female group had the MCP joint of the small finger in flexion during the task. All the other female volunteers had the small finger in extension. The group with the small finger in extension had significant less supination in the wrist, than the group with the small finger in flexion.

Conclusion:
Women performed the task opening a yoghurt in 50 % with the small finger in extension, while man preferring to flex the small finger. This gender difference has to be respect, when determining the necessaire needed ROM for this activity of daily living.

4027

S. Halvachizadeh[1], HP. Pape[1], V. Neuhaus[1]

Does the time of the day of surgery influence perioperative complications – a nationwide database analysis in 31'692 patients

Traumatology, University Hospital Zurich, Zurich[1]

Introduction:
Emergency and surgery for acute injuries is often required to avoid excessive bleeding and prevent from infections in open fractures. However, it has previously been discussed, that surgeon related factors (e.g. experience of the surgeon, teaching vs. non-teaching hospital) might play a role in adverse outcomes for these surgeries. We evaluated whether the time of day for emergent surgery is associated with complications.

Methods:
A prospective database (AQC, nationwide Swiss quality assurance project) was used to evaluate all trauma surgeries within 11 years in more than 70 Swiss surgical units. Inclusion criteria: All trauma coded diagnosis that were surgically treated in Swiss hospitals. Exclusion criteria: missing data for time of surgery. The daytime of surgery was stratified into morning (7AM - noon), afternoon (1PM – 6PM), evening (7PM – 11PM) and night (Midnight – 6AM). The primary outcomes were intraoperative (e.g., nerve, tendon, or vascular damage, iatrogenic fractures), postoperative (e.g., bleeding, infection, impaired wound healing, incorrect axial, rotational or length reduction) and general complications (pulmonary, cardiovascular, gastrointestinal, renal, or neurological) and mortality. Co-factors included age, gender, ASA classification, type of surgery, experience of the surgeon, length of surgery and length of stay)

Statistics: Mean and standard deviation expressed continuous data, frequencies and percentage expressed dichotomous data. For statistical analyses, we performed unpaired t-tests and Pearson's chi-squared tests or Fisher's exact test if minimum expected cell frequency was less than five. Significant or nearly significant variables ($p<0.10$) were sought in multivariate analysis (binary logistic regression analysis). A p-value of < 0.05 was considered statistically significant.

Results:
Of 31'692 patients, 44% were operated in the morning, 40% in the afternoon, 14% in the evening and 1.7% at night. The in-hospital mortality rate was significantly higher after nightly (2.4%) as well as afternoon surgery (1.7%). The time of surgery had no significant influence on intra- (0.5%) or postoperative complication rates (3.4%) in multivariable analysis, but a significant influence on general complications (7.9%). Afternoon- and night-surgery were significant predictors for general complications. Age, gender, higher ASA classification, and emergency procedures were typical risk factors for mortality and complications in this cohort.

Conclusion:
Emergency procedures performed at night and in the afternoon appears to be associated with an increased incidence of adverse outcomes. Further studies should evaluate whether this is relevant for certain diagnoses and/or procedures.

4028

O. Politikou[1], T. Giesen[1], R. Guggenberger[2], S. Wirth[3], P. Giovanoli[1], M. Calcagni[1]

Free vascularised corticoperiosteal medial femoral condyle flap for ankle and midfoot reconstruction; efficiency and donor site morbidity.

Plastic, Reconstructive and Hand Surgery Department, University Hospital Zurich, Zurich[1], Institut für Diagnostische Radiologie, Universitätsspital, Zürich[2], Orthopädie Universitätsspital Basel[3]

Introduction:
We used the vascularized corticoperiosteal medial femoral condyle (MFC) flap for distal tibia, ankle and midfoot reconstruction in cases of recalcitrant nonunion. Aim of this study is to evaluate the efficiency and the safety of this technique and to assess clinically and radiologically the donor site morbidity. Our hypothesis is that the use of MFC flap is a safe and efficient option with low donor site morbidity

Methods:
This is a 7 years retrospective study. We collected data from thirteen patients. The most common indication was failed ankle or subtalar arthrodesis after multiple reconstruction attempts. Ten patients were included to the radiological follow-up. We assessed the union rate, time to union and possible complications. We also conducted a radiological assessment of the donor knee through computed tomography and MRI examination in search for soft tissue impairment and early osteoarthritis signs.

Results:
The mean follow up was 2.4 years**.** Union was achieved in ten out of thirteen cases. Complete union was achieved in a mean time of 9.2 months. All the patients reported an important pain relief. The most common complication concerned numbness in the medial knee area. The MRI examination of the donor site showed no osteoarthritis signs, no injury of the medial collateral ligament of the knee and no fracture.

Conclusion:
The use of MFC flap for ankle and midfoot reconstruction is a reliable and safe option in cases of ankle or midfoot recalcitrant nonunion, after failure of other conventional techniques. The donor site morbidity is low.

4029

O. Politikou[1], T. Giesen[1], C. Erling[1], M. Calcagni[1]

Arthroscopic mid-carpal partial wrist arthrodesis. Early experience on eleven cases.

Plastic, Reconstructive and Hand Surgery Department, University Hospital Zurich, Zurich[1]

Introduction:
The technique of arthroscopic partial wrist arthrodesis has already been described in the literature, but a very limited number of studies are published. We present our experience of mid-carpal arthroscopic arthrodesis.

Methods:
From January 2015 to October 2017, the senior author performed 11 cases of arthroscopic mid-carpal wrist fusion, including 7 cases of 3-corner fusion and 4 cases of lunocapitate fusion. The indication was mid-carpal arthritis related to post-traumatic carpal instability with SNAC or SLAC wrist Grade II-III or to degenerative systemic diseases such as scleroderma or calcium pyrophosphate deposition disease. In 6 patients at least one operation to the affected wrist was already performed. Pre- and postoperative wrist assessments concerning range of motion, grip and strength, VAS evaluation, DASH and PRWE score were systematically recorded through our hand therapy department.

Results:
The mean operation time was 122 minutes (range 95-189). In all the cases the scaphoid was excised through a small palmar approach. The triquetrum was left in situ. Cancellous bone was harvested from the excised scaphoid and was inserted arthroscopically to the arthrodesis site before placing the K-wires. In all the cases we used cannulated headless screws to fix the bones.
The mean follow-up was 5.5 months (range 1.5-10). The first signs of union were recorded in 1.6 month (1-2.5). The wrist total range of motion was reduced about 27% and the strength about 22%.
We observed two complication concerning the distal migration of one screw in the carpometacarpal joint; we removed the screw 8 weeks and 12 weeks after fusion. In one case, a total wrist fusion was necessary because of rapidly progressed arthritis in the lunate fossa. All the patients reported important pain relief in active motion (post-op range VAS 0-3, pre-op 7-9) after surgery and all but one returned to work and usual daily activity in a mean time of 4,5 months (1,5-7).

Conclusion:
Dry arthroscopic mid-carpal partial arthrodesis seems to be an efficient surgical option in cases of mid-carpal arthritis.
The technique is reliable and in our study with an operative time comparable to the open technique. Moreover, the arthroscopic technique potentially reduces the risk of infections as well the surgical scars. The use of endomedullary compression screws reduces the complications related to the hardware. Long-term follow-up and bigger series are needed in order to draw a safe conclusion through quantitative research results.

4030

M. Müller[1], A. Rickenbacher[1], M. Schneider[1], D. Cabalzar-Wondberg[1], S. Käser[1], M. Turina[1]

Young patients with colorectal cancer present with more advanced tumors and lymph node metastases

Department of Surgery and Transplantation, University Hospital Zürich, CH-8091 Zürich, Switzerland[1]

Introduction:
In recent years, a decrease in the incidence and mortality of colorectal cancers has been observed, presumable through screening efforts. On the other hand, an increase in incidence in young patients below the age of 50 years has been noted. The goal of the present study was to evaluate tumor characteristics of young vs. older patients.

Methods:
All patients with a colorectal cancer were prospectively recorded in our database and patient records from January 2013 to July 2017 were analyzed. Patients were divided into two groups (age ≥50 und <50 years). Clinical as well as histopathological tumor characteristics were compared.

Results:
304 patients with colorectal cancer were treated at our institution between January 2013 and July 2017. 52 (17.1%) of our patients were younger than 50 years (33% female), whereas 253 patients (82.9%) were ≥50 years of age (37% female) at time of diagnosis. In the younger population 42% had a rectal and 58% a colon cancer which was not significantly different to the older population, in which 37% had a rectal and 63 a colon cancer (p=0.45). In addition, there were no significant differences regarding the distribution of left and right sided colon cancers. T4 cancer was diagnosed more often in young patients (32% vs 17%, p=0.03), so were lymph node metastases (57% vs. 39%, p=0.01). Distant metastases were not different between groups (35% vs 26%, p=0.24). Vascular invasion (V1) was present in 35% of young and 37% of older patients (p=0.9), while lymphatic invasion (L1) was more frequently in the young (75% vs. 46%, p=0.02). Tumor differentiation was not significantly different. Signet cell cancer was, however, more frequent in young patients (9% vs. 2%, p=0.002), whereas no differences were found with respect to mutational status (KRAS, NRAS, BRAF, microsatellite instability).

Conclusion:
Colorectal cancer appears to have a more aggressive phenotype in younger patients below the age of 50. They present with locally advanced tumors, lymphatic invasion and with more frequent lymphatic metastasis. These results suggest a worse disease specific survival and highlight the need for early detection of colorectal cancer in this age group.

4031

R. Schweizer[1], H. Klein[1], N. Fuchs[1], M. Waldner[1], B. Kollar[1], P. Kamat[1], F. Lehner[1], A. Taddeo[3], S. Salemi[2], D. Eberli[2], P. Giovanoli[1], J. Plock[1]

Adipose-derived Stromal Cells attenuate Acute Rejection and Graft Vasculopathy in Rodent Vascularized Composite Allotransplantation

Plastic Surgery and Hand Surgery, University Hospital Zurich, Zurich, Switzerland[1], Urology, University Hospital Zurich[2], Department of Clinical Research, University of Berne, Berne[3]

Introduction:
Vascularized composite allotransplantation (VCA) is successfully used for reconstruction of major defects of the upper extremity and face. Both rejection and graft vasculopathy (GV) seriously endanger long-term outcomes, eventually leading to graft failure. GV remains widely unexplored in VCA, and so does the role of adipose-derived stromal cells (ASCs) in acute rejection.

Methods:
ASCs were isolated from donors, characterized and their immunomodulatory capacity investigated. Systemic (SASC) versus local intragraft (LASC) ASC administration was evaluated for therapy of acute rejection and GV in fully mismatched rat hind-limb transplants after discontinuation of immunosuppression (FK-506). Tissues (skin/muscle/vessels) and blood samples were taken prior and after therapy for histopathology (H&E; Elastin van Gieson; von Willebrand factor [vWF]) and cytokine analysis (Multiplex).

Results:
ASCs (CD45- CD29+CD90+) suppressed alloresponse in vitro and reduced pro-inflammatory cytokine levels in mixed lymphocyte reactions (IL-α, IL-β, IL-2, GM-CSF). In vivo, ASC administration at grade II rejection significantly delayed progression to grade III (7.57±1.13 days SASC, 7.29±1.11 days LASC vs 2.75±0.7 days Controls; n=23 animals). Significant GV was detected during acute rejection in controls, whereas ASC administration reduced intima/media ratio (IMR) in arterioles of allograft skin and muscle. However, GV did not affect the greater (femoral) vessels. vWF analysis revealed increased expression in femoral vessels of controls, compared to significantly reduced expression after both local and systemic cell therapy, similar to naïve vessels.

Conclusion:
Systemic or local ASC therapy significantly reduces progression of onset acute rejection in VCA through attenuation of alloresponse and suppression of pro-inflammatory cytokines. GV was observed during acute rejection in small arterioles, but not in femoral vessels, and was significantly reduced after cytotherapy. vWF was increased in femoral vessels, despite no manifest GV, suggesting early endothelial damage. If vWF is a potential early marker for GV development in VCA needs to be investigated.

4032

R. Schweizer[1], M. Waldner[1], H. Klein[1], N. Fuchs[1], F. Lehner[1], S. Salemi[2], D. Eberli[2], A. Taddeo[3], P. Giovanoli[1], J. Plock[1]

Evaluation of a Novel Conditioning Regimen including Belatacept, Cylophosphamid and Adipose-derived Stromal Cells in Rodent Vascularized Composite Allotransplantation

Plastic Surgery and Hand Surgery, University Hospital Zurich, Zurich, Switzerland[1], Urology, University Hospital Zurich[2], Department of Clinical Research, University of Berne, Berne[3]

Introduction:
Vascularized composite allotransplantation (VCA) is successful in reconstruction of major defects of the upper extremity and face in patients where conventional therapeutic options come to their limit. The hurdle of chronic drug immunosuppression and its associated complications might be overcome or attenuated by using novel conditioning regimens. Here we investigate a novel, clinically translatable protocol including CTLA4-Ig, Cylophosphamid and Adipose-derived Stromal Cells (ASCs).

Methods:
Donor ASCs were characterized and their immunomodulatory capacity investigated in vitro. Full-mismatched rat hind-limb transplant recipients received 14 days of immunosuppression with FK506 (0.5mg/Kg BW). Controls received no conditioning, whereas one group received CTLA4-Ig (2.5mg/rat s.c. day 2, 4, 7) and ASCs (1x10^6 i.v. day 2, 4, 7, 15, 28) (CTLA4-Ig+ASC). A third group received the latter regimen in addition to Cylophosphamid (50mg/Kg BW day 3) (CTLA-4- Ig+ASC+Cyp). Flow cytometry for regulatory T cells (Treg) and donor-specific chimerism (RT1Ac) was performed on day 21 and tissue samples harvested at endpoint (rejection grade III).

Results:
ASCs were CD45- CD29+CD73+CD90+, suppressed alloresponse after addition into mixed lymphocyte reaction assays and reduced pro-inflammatory cytokine levels in supernatants (IL-α, IL-β, IL-2, IFN-y, GM-CSF). The mean allograft survival was 34.2±1.6 days in the CTLA4-Ig+ASC group (n=5), 27±1.7 days in the CTLA4-Ig+ASC+Cyp group (n=3), versus 29.0±1.8 days in the control group (n=5). Peripheral blood Treg levels were significantly increased in CTLA4-Ig+ASC at day 21 compared to controls ($p<0.01$), whereas in CTLA4-Ig+ASC+Cyp there was only a slight increase ($p>0.05$). Similarly, multi lineage donor-specific chimerism was significantly increased in CTLA4-Ig+ASC ($p<0.01$) and not significantly increased in CTLA4-Ig+ASC+Cyp at 21 days postop. H&E stained skin samples confirmed clinical gross appearance at endpoint according to BANFF classification.

Conclusion:
Our preliminary data show that transplant conditioning with co-stimulatory blockade with CTLA4-Ig and repeated ASCs administration, combined to 14 day-immunosuppression with FK-506, was able to significantly increase peripheral Treg levels and donor-specific multi lineage chimerism at 3 weeks posttransplant. This lead to slightly prolonged allograft survival compared to controls. Addition of Cyclophosphamid to the regimen worsened both Treg levels and chimerism compared to CTLA4-Ig+ASC, and resulted in graft survival time similar to controls. This probably is due to a deleterious toxic effect of Cyclophosphamid which kills donor-specific cells instead of promoting their engraftment into recipient lymphatic organs. In conclusion, CTLA4-Ig and ASC administration, along with 2 weeks of FK-506, is promising in increasing Treg and donor-specific chimerism in VCA, which correlates to slight prolonged graft survival but failed to induce tolerance.

4033

M. Kahr[1], R. Brun[1], R. Zimmermann[1], C. Haslinger[1]

Validation of a quantitative System for real-time Measurement of postpartum Blood Loss: A prospective Cohort Study in the daily Obstetric Setting

Obstetrics, Universitätsspital Zürich, Zürich[1]

Introduction:
Postpartum haemorrhage (PPH) is one of the major obstetric complications. Reliable real-time estimation of blood loss is crucial for the prompt management of PPH.Our study aims at the validation of measured blood loss (MBL) with a quantitative real-time measurement system during 1) vaginal delivery and 2) caesarean section by comparison with a haemoglobin based formula (*Brecher`s* formula) for blood loss as an objective control. 921 patients were prospectively enrolled into this study (vaginal delivery: n= 461, caesarean delivery: n=460) at a tertiary care hospital in Switzerland.

Methods:
Blood loss was measured by quantitative fluid collection bags. “Calculated blood loss” (CBL) was determined by *Brecher`s* formula based on the drop of haemoglobin after delivery. MBL based on our measurement system was compared to CBL by correlation analysis and was stratified by the mode of delivery.

Results:
During vaginal delivery, MBL was determined by our quantitative measurement system and highly correlated with CBL (p<0.001, r=0.683). This was also true for patients with caesarean deliveries (p<0.001, r=0.402), however in a less linear amount. In women with caesarean deliveries, objectively low blood loss tended to be rather overestimated while the condition in patients with high blood loss showed a contrary trend.

Conclusion:
The technique of real-time measurement of postpartum blood loss after vaginal delivery as presented in this study is practicable, reliable and strongly correlating with the actual blood loss and therefore poses an actual improvement in the management of PPH.

4034

M. Kahr[1], D. Franke[1], R. Brun[1], J. Wisser[1], R. Zimmermann[1], C. Haslinger[1]

Blood Group 0: A novel Risk Factor for increased Postpartum Blood Loss?

Obstetrics, Universitätsspital Zürich, Zürich[1]

Introduction:
Blood group 0 is known to be associated with lower levels of active von Willebrand factor (VWF) and with increased incidence of bleeding complications. The influence of maternal blood group 0 on postpartum blood loss was assessed by a few studies, however without adjustment for important obstetric risk factors for postpartum blood loss.
Aim of this study was to investigate whether women with blood group 0 exhibit increased blood loss after delivery in consideration of established risk factors for postpartum bleeding.

Methods:
1487 patients were prospectively included into this cohort study. Blood loss was assessed by estimated blood loss (in ml) and drop of hemoglobin (Δ hemoglobin) was calculated. Association of blood loss with risk factors (such as blood group 0, cervical tears, morbidly adherent placenta, placenta praevia and uterine atony amongst others) was assessed with Pearson correlation or t-test as appropriate. Significant variables were entered into a stepwise multivariate regression analysis.

Results:
Women with blood group 0 showed a significantly higher blood loss when compared to women with blood group non-0 (529.2ml ± 380.4ml and 490.5ml ± 276.4ml respectively, p=0.024)). The increased blood loss in women with blood group 0 remained significant after multivariate regression analysis (difference 47 ml, p=0.019).

Conclusion:
This is the first study reporting significantly increased blood loss following delivery in women with blood group 0 after adjustment for major risk factors for postpartum blood loss. Albeit having a statistically significant, but clinically minor effect on absolute blood loss, blood group 0 carriers may suffer from aggravated bleeding in the presence of additional obstetric bleeding pathologies.

4035

A. Vent[1], C. Surber[1], N. Graf[1], J. Jürg[1]

Painless local anesthesia with bicarbonate admixture in a ratio of 3:1: A phase II, monocentric, double blind, randomized, placebo controlled trial

University Hospital, Zurich, Dermatology[1]

Introduction:
Every day uncountable surgical interventions are performed under local anesthesia.
Our primary objective was to show that higher bicarbonate admixture to lidocaine at ratio 3:1 (meaning 3 units of lidocaine and one unit of bicarbonate) causes less burning sensation during injection than ratio 9:1 (meaning 9 units of lidocaine and one unit of bicarbonate). Secondary outcomes were to compare unbuffered lidocaine and placebo (saline), assess clinical relevance for the subject, and to assess anesthetic effect and duration of local anesthesia.

Methods:
48 volunteers were included. Inclusion criteria were age 18-75, no sensitization or allergy to lidocaine, no anticoagulant medication, no pregnancy and intact skin of both volar forearms.
Subjecs were divided into 2 groups. Group 1 received four subcutaneous injections: lidocaine 1% with epinephrine 1:100,000 buffered with bicarbonate 8.4% at ratio 3:1 (IMP1) versus lidocaine 1% with epinephrine 1:100,000 buffered at ratio 9:1 (IMP2) versus unbuffered lidocaine with epinephrine 1:100,000 (IMP3) versus sodium chloride 0.9% (IMP4) as control. Group 2 received the two buffered solutions at ratio 3:1 and 9:1 respectively. Pregnancy was excluded by a urine Beta-hCG-test the same day of injection. Injection pain was assessed using a Numerical Rating Scale (NRS) from 0 to 10 and in view of clinical relevance rated as “desirable”, “acceptable”, “less acceptable” or “almost/totally unacceptable”. Anesthetic effect was assessed with a needle stitch.

Results:
27 women and 21 men were included. Lidocaine 1% with epinephrine 1:100,000 buffered with bicarbonate 8.4% at ratio 3:1 versus lidocaine 1% with epinephrine 1:100,000 buffered at ratio 9:1 causes less burning sensation since burning sensation of the solution at ratio 9:1 (IMP2) was rated significantly higher than the one with ratio 3:1 (IMP1) ($p=0.044$). The secondary outcome comparing the painfulness between IMP1 and IMP3 showed that IMP3 was rated significantly higher than IMP1 ($p<0.001$). Placebo was rated significantly higher than IMP1 ($p<0.001$). IMP3 was rated significantly higher than IMP2 ($p=0.033$). Placebo was rated significantly higher than IMP2 ($p<0.001$).

Conclusion:
The present study demonstrates that a bicarbonate admixture in a ratio of 3:1 causes even less discomfort. Of an important note, the higher buffer admixture does not affect the anesthetic effect, which starts almost immediately after injection and lasts for a mean of 6.85 hours. The discomfort versus the comfort during injection was relevant for the majority of participants. There were no severe adverse events.

4036

E. Kapfhammer[1], T. Pfammatter[2], D. Balsyte[1], R. Zimmermann[1], C. Haslinger[1]

Success rate and long-term effects of embolization of pelvic arteries for the treatment of postpartum hemorrhage

Division of Obstetrics, University Hospital of Zürich, Frauenklinikstrasse 10, 8006 Zürich, Switzerland[1], Institute of Diagnostic and Interventional Radiology, University Hospital of Zürich, Raemistrasse 100, 8091 Zürich, Switzerland[2]

Introduction:
Postpartum hemorrhage (PPH) is the leading cause of peripartum maternal mortality and accounts for 25% of all maternal deaths worldwide. The most common reasons of PPH are uterine atony, retained placenta or morbidly adherent placenta. Treatment of PPH depends on the etiology and includes administration of uterotonic drugs and curettage if retained placental tissue is suspected. In severe refractory PPH, hysterectomy has been the ultima ratio for many decades. In recent years the interventional embolization of the pelvic arteries (PAE) has become a popular alternative. Besides being a highly effective minimal-invasive method, PAE avoid hysterectomy with consecutively reduces morbidity and mortality. However, data on the long-term effects of PAE on fertility and menstrual cycle is scarce.

Methods:
We performed a monocentric study, which consists of retro- and prospective parts and includes all women who had undergone a PEA between January 2012 and 2016 in the University Hospital of Zürich. Descriptive characteristic of patients, clinical course during PPH and effectiveness of PAE defined as cessation of bleeding was analyzed retrospectively. In the prospective part all the patients were contacted and asked to complete a questionnaire to obtain a long-term follow up regarding pattern of menstruation and fertility after embolization.

Results:
Twenty patients with PAE were evaluated. Our data showed a success rate of PAE in 95% of patients with PPH, only one patient needed a second PAE. No patient needed a hysterectomy or any other surgical intervention. The reason for PPH differed according to the mode of delivery. After spontaneous delivery, the main reason of PPH was retained placenta (83%), while after cesarean section, uterine atony was identified in most cases (66%). Regarding menstruation after embolization, most patients reported a regular pattern with a shorter duration (72%) and lower or similar intensity (62%). Dysmenorrhea decreased in 90% of patients. Four patients planned another pregnancy, of whom only one had become pregnant without assisted reproductive technology in the pregnancy before PAE. This patient became pregnant spontaneously as well after the delivery with PAE with a subsequent miscarriage.

Conclusion:
Our study confirms the effectiveness of PAE in PPH. This additional method obviates severe surgical interventions and thus reduces morbidity. The success of PAE does not depend on the primary cause of PPH. Furthermore, PAE might increase patient's quality of life due to short convalescence and no side effects on menstrual pattern in the long-term follow up. Our results may encourage the promptly decision to perform PAE in the management of severe PPH.

4037

I. Iskender[1], T. Maeyashiki[1], S. Arni[1], M. Lipiski[2], S. Fehlings[3], T. Frauenfelder[4], M.P. Krafft[5], D.R. Spahn[6], W. Weder[1], I. Inci[1]

Treatment of donor lungs with perfluorocarbon based oxygen carrier during ex vivo lung perfusion in uncontrolled donation after cardiac death

Department of Thoracic Surgery, Univeristy Hospital of Zurich, Zurich[1], Department of Surgical Research, University Hospital Zurich, Zurich[2], Department of Cardiac and Vascular Surgery, University Hospital Zurich, Zurich, Switzerland[3], Department of Radiology, University Hospital Zurich, Zurich[4], Institute Charles Sadron, University of Strasbourg, Strasbourg[5], Department of Anesthesiology, University Hospital Zurich, Zurich[6]

Introduction:
Ex vivo lung perfusion (EVLP) has proven its efficacy in assessing marginal donor lungs prior to transplantation. However, the use of EVLP for treatment of injured donor lungs remains limited. Oxygen (O_2) carriers mimic blood O_2 transport properties and may be used as a therapeutic agent by preserving microvascular and organ function during EVLP. Our objective was to test the efficacy of systemic administration of a perfluorocarbon based O_2 carrier (PFCOC) in an uncontrolled donation after cardiac death (DCD) model.

Methods:
Domestic female pigs were subjected to a cardiac death with administration of potassium chloride and left in supine (Group 1; n=2) or prone (Group 2; n=4) positions at room temperature. At the end of 2 hours of warm ischemic period, the lungs were flushed with Perfadex and retrieved followed by 6 hours of EVLP according to the Toronto protocol. One lung in Group 1 and two lungs in Group 2 were treated with PFCOC at a dose of 1.1 g/100mL of STEEN. EVLP physiology and biochemistry were monitored hourly. A lung X-ray was performed at the end of EVLP.

Results:
Lactate levels were significantly lower throughout EVLP in the treated lungs ($p<0.05$). When we look at the effect of donor positioning, STEEN consumption was significantly higher in group 1 (960±210 mL) than in group 2 (363±55 mL; $p<0.05$). Delta PaO_2 was significantly higher in the prone group throughout perfusion ($p<0.05$). Radiologic lung injury scoring was also higher in the supine group (Group 1: 6.5±0.5 vs. Group 2: 3.8±0.5).

Conclusion:
Lactate production, a marker of donor quality during EVLP was significantly better in the PFCOC treated lungs regardless of donor positioning. Supine versus prone positioning affects the quality of donor lungs in this uncontrolled DCD model. Further experiments are currently performed to understand the efficacy of PFCOC treatment during EVLP.

4038

I. Iskender[1], M. Schuurmans[2], S. Hillinger[1], I. Opitz[1], D. Schneiter[1], C. Benden[2], W. Weder[1], I. Inci[1]

Survival after lung retransplantation: A single-center experience over 25 years

Department of Thoracic Surgery, Univeristy Hospital of Zurich, Zurich[1], Department of Pulmonology, University Hospital Zurich, Zurich[2]

Introduction:
Lung retransplantation (ReLTx) is a treatment option carried out at experienced lung transplant (LTx) programs. In this study, we aim to analyze our experience with ReLTx from the initiation of our LTx Program.

Methods:
We reviewed our prospectively recorded database for patients with end-stage lung disease undergoing LTx between 1992 and 2016 and the subgroup of LTx recipients receiving ReLTx. The short-term and long-term outcomes of ReLTx were summarized. The Kaplan-Meier test was used for survival analysis and compared with the log-rank test.

Results:
A total of 489 LTx were performed during the study period, among those 22 (4.5%, 12 male, median age 46 [16 - 67] years) underwent ReLTx. In-hospital mortality was 32% (n = 7). The median survival for patients who underwent ReLTx due to chronic lung allograft dysfunction (CLAD, n = 19) and early graft dysfunction (n = 3) was 43 [95% confidence interval (CI) 0 - 85] and 1 (95% CI 0 - 3) months, respectively ($p < 0.05$). The median survival, conditional to discharge from hospital was 51 [95% CI 37 - 66] months in the CLAD Group. Recipient age, procedure type (unilateral versus bilateral ReLTx), downsizing of donor lungs, initial diagnosis at the time of LTx, CLAD type (bronchiolitis obliterans syndrome versus restrictive allograft syndrome), time to ReLTx, and era did not significantly impact on survival for patients undergoing ReLTx due to CLAD.

Conclusion:
Although our numbers of patients undergoing ReLTx were limited, ReLTx for early graft dysfunction seems unfavorable and troublesome as donor shortage continues to limit LTx. For patients with CLAD, ReLTx provides survival benefit.

4039

I. Inci[1], M. Schuurmans[2], I. Iskender[1], S. Hillinger[1], I. Opitz[1], D. Schneiter[1], C. Caviezel[1], C. Benden[2], W. Weder[1]

The incidence of chronic lung allograft dysfunction after cadaveric lobar lung transplantation is comparable to conventional lung transplantation

Department of Thoracic Surgery, Univeristy Hospital of Zurich, Zurich[1], Department of Pulmonology, University Hospital Zurich, Zurich[2]

Introduction:
Cadaveric lobar lung transplantation (L-LTx) is developed to overcome donor-recipient size mismatching. Controversial short and long-term outcomes following L-LTx has been reported compared to conventional lung transplantation (C-LTx). However, there is a lack of data regarding the development of chronic lung allograft dysfunction (CLAD) following L-LTx. The aim of this study was to compare the incidence of CLAD between L-LTx and C-LTx.

Methods:
We reviewed our database for patients undergoing LTx between 2000 and 2016 with a minimum 12-months follow-up. Heart-lung, unilateral and re-transplantations were excluded. The decision to perform L-LTx was made based on height discrepancy and visual assessment of the donor lungs. Survival was calculated by the Kaplan–Meier method and compared with the log-rank test. Cox regression was used to assess risk factors for mortality. Primary outcome was CLAD-free and overall survival.

Results:
A total of 371 bilateral LTx were performed during the study period, among those 250 (67%) underwent C-LTx and 121 (33%) underwent L-LTx. ICU-stay was significantly longer after L-LTx ($p = 0.01$). One- and 5-year survival rates were 83% vs. 90% and 50% vs. 63% for L-LTx and C-LTx, respectively ($p = 0.02$). However, survival conditional to 90-day mortality was comparable between groups ($p = 0.08$). CLAD-free survival at 5-year was 63% in L-LTx and 70% in C-LTx recipients ($p = 0.2$). Multivariate analysis showed that age, procedure, intraoperative ECMO use, and postoperative renal replacement therapy were significant prognostic factors for survival.

Conclusion:
CLAD-free survival was comparable between C-LTx and L-LTx. Overall survival following L-LTx was inferior compared to C-LTx. This discrepancy disappeared after implementing 90-day conditional survival into the cohort. Given the ongoing donor organ shortage, cadaveric L-LTx is still a viable option, especially for small and urgently listed patients.

4041

A. Papachristodoulou[1], R. Signorell[2], B. Werner[3], D. Brambilla[2], M. Rudin[4], J. Grandjean[2], E. Martin[3], M. Weller[1], JC. Leroux[2], P. Roth[1]

Overcoming temozolomide resistance in experimental gliomas: MRI-guided focused ultrasound-mediated blood-brain barrier opening facilitates the local delivery of liposome encapsulated MGMT inhibitors

University Hospital Zurich, Department of Neurology, Zurich[1], ETH Zurich, Institute of Pharmaceutical Sciences[2], Children's University Hospital, Center for MR research[3], ETH Zurich, Institute for Biomedical Engineering[4]

Introduction:
The standard of care for patients with newly diagnosed glioblastoma comprises surgical resection followed by radiation therapy and chemotherapy with the alkylating agent, temozolomide (TMZ). Still, the median overall survival of glioblastoma patients is only approximately 16 months in clinical trial populations. Importantly, the survival benefit derived from the addition of TMZ is almost exclusively restriced to the rather small subgroup of patients with tumors harboring a methylation of the O^6-methylguanine-DNA methyltransferase (MGMT) gene promoter.

Methods:
The clinical development of drugs that inhibit MGMT in order to sensitzes tumors to TMZ was largely unsuccessful because of systemic toxicity. We applied magnetic resonance image-guided focused ultrasound (MRIgFUS) to transiently open the blood brain barrier (BBB) in mice bearing MGMT-expressing experimental gliomas. We generated a novel MGMT inhibitor that was encapsulated in liposomes and subsequently evaluated in appropriate in vitro and in vivo models.

Results:
We demonstrate that a novel liposomal *O^6-(4-bromothenyl)guanine (O^6BTG)* derivative can efficiently target MGMT, thereby sensitizing murine and human glioma cells to temozolomide *in vitro.* Furthermore, we report that MRIgFUS mediates the delivery of the long-circulating liposomal MGMT inactivator in the tumor region resulting in potent MGMT depletion *in vivo*. Treatment with the liposomal MGMT inactivator facilitated by MRIgFUS-mediated blood-brain barrier opening reduced tumor growth and significantly prolonged survival of glioma-bearing mice, when combined with temozolomide chemotherapy.

Conclusion:
Our dataset demonstrates that MRIgFUS allows for transient and circumscribed BBB opening in the tumor region which can be used for targeted MGMT downregulation. Overcoming MGMT-mediated alkylator resistance sensitizes gliomas in vivo to TMZ, ultimately resulting in a survival benefit. Based on these data, a clinical assessment of this approach in human patients is warranted.

4042

P. Lanz[1], K. Fischer[2], H. Bischoff-Ferrari[1]

Association of cognitive function and mental health with quality of life in seniors with severe knee osteoarthritis undergoing total knee replacement surgery

Klinik für Geriatrie, Universitätsspital Zürich, Zürich[1], Zentrum für Alter und Mobilität, Universtiätsspital Zürich, Zürich[2]

Introduction:
Osteoarthritis (OA) is the most common musculoskeletal disorder in seniors and a leading cause of disability in later age. Total knee replacement (TKR) surgery has been shown to reduce pain, disability, and increase health-related quality of life (HRQL) in knee OA patients. A decline in cognitive function (CF) and/or impaired mental health (MH) also lead to disability in seniors and may affect HRQL. In the context of TKR, good CF and MH contribute to the individual's capacity to meet the challenges of this disabling condition and consequently have an impact on postoperative HRQL.
The aim of this study was to prospectively investigate the association of CF and MH with HRQL in seniors with severe knee OA undergoing TKR surgery.

Methods:
In this ancillary study to the Zurich Multiple Endpoint Vitamin D Trial in Knee OA study, we analyzed 273 seniors age 60 years and older (mean age 70.3 years, 53.5% women) undergoing unilateral TKR due to severe knee OA. Baseline (8 to 10 weeks after surgery) CF was assessed using the mini-mental state examination (MMSE). Baseline global MH was assessed using the MH subscale of the SF-36, and the 15-item Geriatric Depression Scale (GDS-15) was used to assess the degree of depression. HRQL was repeatedly assessed using the EuroQol EQ-5D-3L index score (preoperative, baseline, 2, 6, 12, 18, and 24 months). The association between baseline median group scores of the MMSE , MH SF-36, and GDS-15 and the EQ-5D-3L index score was analyzed using multivariable repeated-measures linear regression models adjusted for age, gender, body mass index, Charlson comorbidity index, preoperative functional impairment of the operated knee, presence of OA at the contra-lateral knee, and recruitment center. Subgroup analysis was performed by gender, age (<70 vs. ≥70 years), and baseline serum 25-hydroxyvitamin D (25(OH)D) status (<20 vs. ≥20 ng/mL).

Results:
Among all participants, EuroQol EQ-5D-3L index score improved significantly over the 24-month duration of the study (time main effect $P < 0.0001$). Moreover, over 24 months, seniors with baseline SF-36 MH scores ≥ 84 had overall higher SF-36 MH scores than seniors with baseline SF-36 MH scores < 84 ($P_{overall} < 0.0001$). In subgroup analysis, this association was only significant among seniors with 25(OH)D status <20 ng/mL, but not among seniors with 25(OH)D status ≥20 ng/mL or in subgroups of age or gender. Over 24 months, there were also no significant prospective associations between baseline median group scores of the MMSE and GDS-15, or in the respective subgroups of age, gender, and 25(OH)D status, and the EuroQol EQ-5D-3L index score.

Conclusion:
Our prospective study suggests that independent of age, gender, body mass index, Charlson comorbidity index, preoperative functional impairment of the operated knee, and presence of OA at the contra-lateral knee, overall, over 24 months after TKR, HRQL improved more among senior knee OA patients with better baseline global MH, but was not associated with baseline CF or baseline depression.

4043

G. Spaltro[1], L. Kovtonyuk[1], M. Manz[1]

Dissecting Mechanisms that Drive Hematopoietic Stem Cells to Quiescence

Department of Hematology, University Hospital Zurich and University Zurich[1]

Introduction:
Hematopoietic Stem Cells (HSC) are heterogeneous, multipotent cells that sustain lifelong blood production. As in all organs, aging leads to functional alterations also of the hematopoietic system, most notably expansion of stem cells number and increased myeloid differentiation bias. The cycling state of HSC is highly diverse, with most HSCs being quiescent (>90% in steady state) and a small fraction of HSC actively dividing. Notably, aged HSC are more quiescent than young ones, suggesting the existence of an intrinsic mechanism that acts to prevent replicative stress due to accumulating divisions. These changes seem to be caused by altered epigenetic patterns associated with self-renewal and cell differentiation. We hypothesize that increased proliferative history activates an intrinsic program that drives HSC towards quiescence. In this “dynamic repetition model” cells can re-enter the dormant state upon accumulating divisions to ensure a homogeneous divisional history of the HSC pool at the end of life. This in turn would prevent old and damaged stem cells to proliferate in steady state.

Methods:
We used a combination of CFSE labelling and in vivo tracking and Ki-67 proliferation assay to assess HSC cell cycle status after each division (i.e. from 0- to >5-divided cells). Briefly, we isolated HSC from young and old donor mice by FACS sorting, labelled them ex vivo with CFSE and transplanted them into young, non-irradiated recipients. After 3-8 weeks we harvested the bone marrow from recipient mice and analysed HSC proliferative history and cell cycle status by FACS.

Results:
Our data show that after each cell division, a small subset of HSC re-enters dormancy while the rest immediately re-enter cell cycle. The mechanisms driving these decisions are still unknown. Interestingly, aged HSC are more prone to return to quiescence after each cycle, compared to young ones. In addition, cells that return to quiescence seem to be hardwired to remain in G0 phase, since most HSC do not re-enter cell cycle even after 2 months, in our experimental, steady-state setting. External stimuli that mimic viral infections, such as PolyI:C treatment, completely abolish this phenotype, suggesting that the intrinsic drive to quiescence can be suppressed/overcome upon external stimulation in case of need.

Conclusion:
Our results seem to confirm our initial hypothesis that increased proliferative history with aging or inflammation drive HSC towards quiescence to ensure a balanced turnover at the end of life. This would prevent HSC exhaustion and minimize the risk to develop malignancies. Dysregulation of this drive to quiescence might lead to accumulation of genetic alterations and clonal expansion. To mechanistically analyse our findings and identify molecular targets of this process, we will in a next step perform RNA sequencing on non-divided, quiescent HSC from young and aged mice.

4044

M. Wulf[1], J. Guo[1], K. Frontzek[1], A. Aguzzi[1]

Electrophysiological Alterations in Hippocampal Neurons induced by Anti-PrPc antibodies

Institute of Neuropathology, University Hospital Zürich, Switzerland[1]

Introduction:
Prion diseases are fatal transmissible neurodegenerative diseases caused by misfolding of cellular prion protein (PrP^C) into a protease-resistant isoform (PrP^{res}). We have previously shown that antibodies targeting the globular domain of PrP^C (POM1) elicit neurotoxicity in cerebellar organotypic slice cultures (COCS) via similar signaling pathways as *bona fide* prions, but without induction of misfolded PrP^{res}. We therefore utilized these antibodies as a model system in order to investigate cellular electrophysiological changes in hippocampal neurons in prion neurotoxicity.

Methods:
Acute horizontal slices from the hippocampus of adult wild-type Bl6/J mice were incubated for 1 h with POM1 [500nM] at RT before being transferred to the recording chamber. Visually guided whole-cell patch clamp recordings were then performed from single pyramidal neurons in the CA1 region of the hippocampus. Basal cellular parameters (input resistance, cell capacitance), action potential parameters, medium and slow afterhyperpolarization as well as spontaneous excitatory postsynaptic currents (EPSCs) and mini EPSCs were assessed.
COCS were prepared from 9-12 days old pups from PrP^C -overexpressing Tga20 mice. After 10DIV, they were treated with POM1 (134nM) for 4 days, before fixation and NeuN staining. Neurotoxicity was quantified as the loss of NeuN staining. Differences between groups were analyzed using student‘s t-test and one-way ANOVA where appropriate and p values lower that 0.05 were considered significant.

Results:
Incubation of acute hippocampal slices with prion mimetic POM1 antibody induced a significant increase in the frequency of spontaneous EPSCs (control: 0.4481 ± 0.06554 Hz vs. POM1: 1.141 ± 0.1525 Hz, $p = 0.0002$) while the frequency of mini EPSCs after application of Tetrodotoxin (TTX, 1uM) to block voltage-gated sodium channels was unaltered (control: 0.2214 ± 0.05865 Hz vs POM1: 0.2311 ± 0.05833 Hz, $p = 0.9182$). There was no significant difference in the other parameters. Moreover, application of TTX (10nM) protected cerebellar organotypic slice cultures from POM1-induced neuronal cell death.

Conclusion:
Using toxic anti-PrP^C antibodies as a model system for prion toxicity, we found that after only 1h of incubation, spontaneous excitatory synaptic currents were significantly increased in frequency. This observation seems to be dependent on neuronal action potential firing, as application of TTX abolished the difference. This increase in synaptic transmission might be linked to neurodegeneration, as TTX was neuroprotective in an organotypic slice culture model of prion toxicity. However, the underlying molecular mechanisms remain elusive. Whether this neuroprotective effect can be translated into *bona fide* prion infections remains to be investigated.

4045

L. Roth[1], E. Breuer[1], R. Graf[1], A. Gupta[1], PA. Clavien[1], K. Lehmann[1]

The impact of HIPEC (chemotherapy plus hyperthermia) treatment on the immunogenicity of cancer cells

Department of Surgery & Transplantation, University Hospital of Zurich, Zurich, Switzerland[1]

Introduction:
The outcome of peritoneal carcinomatosis, originating from appendix or colorectal cancer, has dramatically improved with the combination of cytoreductive surgery (CRS) and hyperthermic (43^0C) intraperitoneal chemotherapy (HIPEC). Nevertheless, recurrence of the disease presumably due to remnant cancer cells after the treatment limits survival of the patients. To remove microscopic cancer cells efficiently, we need to improve the HIPEC treatment. The current HIPEC treatment consists of either, Oxaliplatin alone or the combination of Doxorubicin/Mitomycin. Since chemotherapies can induce immunogenic changes in cancer cells; we examined effects of Oxaliplatin and Doxorubicin/Mitomycin on immunogenic cancer testis antigens (CTA) in colorectal tumor cells after HIPEC treatment.

Methods:
Different colorectal cell-lines were treated with either Oxaliplatin alone or Doxorubicin/Mitomycin for 90 minutes with and without hyperthermia (43^0C). After the treatment, CTA expression was analyzed using qPCR and western blotting.

Results:
We noticed that three different CTA, namely SPAG 9, Cyclin A1 and SSX-4, were upregulated after HIPEC treatment. Both drugs led to the expression of Cyclin A1 and SSX-4 in HIPEC conditions. However, the expression of SPAG9 was variable. Oxaliplatin enhanced expression of SPAG9 without hyperthermia. Whereas Doxorubicin/Mitomycin enhanced SAPG9 expression only in HIPEC conditions.

Conclusion:
These data show that both chemotherapeutics can induce expression of CT-antigens in the combination with hyperthermia. However, heterogenic pattern of CTA expression in different cell lines upon HIPEC treatment suggests that a prescreening of the patients may help in selecting best patients that would benefit from these HIPEC treatments.

4046

S. Steiner[1], G. Wanner- Seleznik[1], T. Reding[1], A. Gupta[1], D. Lenggenhager[2], K. Endhardt[2], R. Graf[1]

Identification of Gastrokine, a gastric tumor suppressor, in pancreatic carcinogenesis

Department of Surgery and Transplantation, University Hospital Zurich, Zurich, Switzerland [1], Department of Pathology and Molecular Pathology, University Hospital Zurich, Zurich, Switzerland [2]

Introduction:
Pancreatic ductal adenocarcinoma (PDAC) has one of the most dismal prognoses of all cancers. Diagnostic techniques for early detection are limited, which shows a need to better understand the patho-mechanism leading to PDAC and identify biomarkers for early detection. Gastrokine 1 & 2 (GKN1 & GKN2) are secreted proteins derived from gastric epithelium, where they are involved in homeostasis and tumor suppression. Recently, we noticed GKN1 & GKN2 upregulation in the pancreas of mice with premalignant cancer lesions. We aimed to further investigate gastrokine expression and function during pancreatic carcinogenesis.

Methods:
GKN1 & GKN2 expression was confirmed by qPCR in human and mouse pancreas samples. The presence of GKN1 was verified by western blot and immunohistochemistry (IHC) in mouse pancreas. Mouse pancreatic juice and serum were analyzed by proteomic analysis. To investigate the role of GKNs in pancreatic carcinogenesis in vivo, we established mouse models by intercrossing KC mice with Gkn1-/- and Gkn2-/- mice respectively.

Results:
GKNs were upregulated during early stages of pancreatic carcinogenesis in mouse and peri-tumoral human pancreas. GKNs were absent in healthy pancreas and tumor tissue. IHC showed specific GKN1 and GKN2 expression in premalignant PanIN lesions. Proteomic analysis in mice confirmed the secretion of GKNs into pancreatic juice. Preliminary results from the first time point of analysis showed accelerated tumor development in GKN1-/- KC mice.

Conclusion:
We identified for the first time specific gastrokine expression in pre-neoplastic lesions in human and mouse pancreatic tissue. The secretion into pancreatic juice during carcinogenesis could make gastrokine a potential biomarker for the detection of early pancreatic premalignant lesions. With our mouse models we aim to provide in vivo evidence on the role of GKNs as potential tumor suppressors in the pancreas.

4047

A. Krättli[1], R. Uka[1], M. Levesque[2], R. Dummer[2], O. Shakhova[1]

The role of SOX10 in melanoma resistance

Oncology, University Hospital, Zurich[1], Dermatology, University Hospital, Zurich[2]

Introduction:
Melanoma is the most aggressive skin cancer and its incidence is steadily rising. When detected early, melanoma can be cured by surgery; however, the prognosis for patients having metastatic melanoma is poor. In the recent years treatment for patients was revolutionized by usage of targeted kinase inhibitors as e.g. vemurafenib, dabrafenib or trametinib. These small molecule inhibitors target specifically kinases from the RAS/RAF/MEK/ERK (MAPK) pathway. Most patients, however, develop resistance against these therapies and succumb to the disease eventually. Sox10 (sex-determining factor 10) is a transcription factor playing a crucial role in the self-renewal of neural crest stem cells as well as in the maintenance of giant congenital nevi and melanoma.

Methods:
To investigate the role of SOX10 in resistance acquisition we cultured several sensitive patient-derived cell lines in presence of the drug (either vemurafenib or binimetinib). Our goal was to mimic *in vitro* the patients' situation in which treatment shows an effect rapidly, unfortunately, however, also resistance develops fast. Moreover, we made use of sensitive patient-derived cell lines that harbor an inducible lentiviral SOX10 overexpression construct in order to test the effect on constitutive high expression of SOX10 on the cells potential to gain resistance.
In parallel, we are investigating the role of Sox10 in resistance acquisition also *in vivo*. To this end, we injected a panel of different melanoma patient-derived cell lines into immunocompromised mice. Moreover, we make use of the *Tyr::CreER^{T2} Braf^{V600E} Pten$^{fl/fl}$* mouse model combined with either floxed or wildtype Sox10. By this, we will be able to study the role of Sox10 in resistance acquisition *in vivo*. After induced melanoma formation, the mice are treated with food containing BRAF and MEK inhibitors.

Results:
Our preliminary *in vitro* data reveal that sensitive melanoma cell lines upregulate the expression of SOX10 protein upon the treatment with vemurafenib or binimetinib in order to cope with the drug. These results were supported by the fact that stably overexpressing SOX10 in sensitive melanoma patient-derived cell lines, using a lentiviral construct, rendered the cells faster resistant towards the targeted inhibitors.
Unfortunately, there was no correlation found between tumor growth in the immunocompromised mice and *in vitro* SOX10 expression levels of the patient-derived cell lines or their resistance towards BRAF or MEK inhibitors. Mice from the *Tyr::CreER^{T2} Braf^{V600E} Pten$^{fl/fl}$* model receiving control food had to be sacrificed shortly after tumor onset, whereas the tumor regressed completely in mice provided with treatment containing food already few days after treatment start. Currently we are waiting for resistance development in order to investigate the role of SOX10 in this step *in vivo*.

Conclusion:
Taken together, our preliminary data show that SOX10 seems to play an important role in resistance acquisition towards targeted inhibitors *in vitro*. However, more experiments need to be done in order to see if this effect is functionally relevant.

4048

R. Myburgh[1], J. Kiefer[4], S. Pfister[1], M. Wilk[1], N. Russkamp[1], C. Magnani[1], S. Alexander[1], A. Müller[1], M. Van den Broek[2], B. Becher[3], D. Neri[4], MG. Manz[1]

Treatment of AML with immunotherapies

Hematology, University Hospital Zürich[1], Experimantal Oncology, Institute of Experimental Immunology, University of Zurich, Zurich [2], Neuro and Tumor Immunobiology, Institute of Experimental Immunology, University of Zurich, Zurich[3], Department of Chemistry and Applied Biosciences, ETH Zürich, Switzerland[4]

Introduction:
Immunotherapies hold promise and have made major progress in the treatment of hematological malignancies in recent years. One particularly effective approach is the use of chimeric antigen receptor (CAR) T cells, consisting of high affinity single-chain monoclonal antibodies or single-chain variable fragments (scFv), linked to the signaling machinery of the T-cell receptor and costimulatory molecules. Recently, ground-breaking clinical responses to CAR T- cell therapy in CD19+ B-cell malignancies have been reported. Acute Myeloid Leukemia is a clonal disorder of the hematopoietic stem cell (HSC) and contains a subpopulation of leukemia-initiating cells (LIC) that can self-renew and give rise to the hierarchy of maturing blasts. While the proliferating mature blast pool is highly sensitive to chemotherapy, the more quiescent LICs are relatively resistant and can be a source of relapse. We postulate that the only way to lasting success in poor-risk disease is to radically eliminate LICs and accept collateral damage to HSCs that, subsequently, can be replaced by transplantation. We aim to create a platform for the generation of human CAR T-cells directed against leukemic and HSC antigens, the first of which will be c-Kit (CD117).

Methods:
We used humanized mouse models as well as human xenograft models of AML cell lines and primary human leukemia to evaluate safety and efficacy of Chimeric Antigen Receptor (CAR) T-cell, Bispecific T-cell engaging (BiTEs) antibodies and monoclonal depleting antibodies. The capacity to eliminate LICs as well as bystander effects on healthy hematopoiesis will be assessed.

Results:
An anti-human cKit scFv engineered to form part of a CAR T cell gene, a BiTE antibody, and monoclonal depleting antibody. Binding of cKit by the BiTe and monoclonal antibody was confirmed by flow cytometry. The human CAR T cell consists of an extracellular CD8α sequence linking the anti-cKit scFv to the intracellular 4-1BB co-stimulatory and CD3zeta stimulatory domains including a dual purpose positive/negative selection gene called RQR8 allowing for magnetic selection of CAR T cells using an anti-human CD34 antibody prior to administration of the cells. RQR8 also acts as a safety gene since it binds the B cell depleting antibody Rituximab. Administration of Rituximab will allow for the in vivo depletion of CAR T cells. Targeting of cKit+ cells in human AML cell lines as well as primary AML and healthy HSPCs was assessed in vitro. The human CAR T cells were able to eliminate >95% of target cells within 24hours and even at low effector : target ratios, >95% killing of target cells was achieved during long-term (5 days) in vitro killing assays. We also show the CAR T cells are exquisitely sensitive target cell surface antigen density and antigen density has a dramatic effect on killing capacity. We show that cKit+ cells can be targeted and killed in humanized mice and xenograft models of human AML cell lines in vivo.

Conclusion:
The human CAR T cells targeting human cKit efficiently identify and eliminate target cells in vitro and in vivo. We aim to further development of the BiTe and monoclonal antibodies against cKit in order to assess side by side the effect and toxicities of the different immunotherapies.

4049

R. Senn[1], A. Luft[1], M. Christ-Crain[2], M. Katan[1]

Prognostic value of copeptin dynamics over 5 days after onset of ischemic stroke

Universitiy Hospital of Zurich, Department of Neurology, Zurich , Switzerland[1], University Hospital of Basel, Department of Endocrinology, Basel, Switzerland[2]

Introduction:
In acute ischemic stroke (aIS), baseline copeptin (BC) measured within 72 hours from symptom onset, is a validated prognostic blood biomarker. The release kinetics of copeptin after aIS are unknown. We hypothesize that copeptin-change (CC) over time may be an even more accurate predictor of outcome as compared to mere baseline levels.

Methods:
Copeptin was serially measured in 348 consecutive aIS patients. Outcome measures were unfavorable functional outcome (modified Rankin-Scale (mRS) >2 points) and mortality at 90 days. CC was evaluated by calculating the beta-coefficients for copeptin-change over time (admission, day 1, 3, 5). We fitted multivariate logistic regression models to estimate adjusted odds-ratios (OR, 95%CI) for the association of CC with functional outcome, and adjusted hazard ratios (HR, 95% CI) for the association with mortality. The discriminatory accuracy was determined by the area under the receiver-operating-characteristic (AUC) curve.

Results:
Out of 348 patients 140 had a mRS >2 and 33 died. CC was not significantly associated with functional outcome in contrast to BC (OR 2.57; 95%CI 1.27-5.17). However CC was an independent predictor for mortality (adjusted HR 1.83; 95%CI 1.27-2.65) comparable to BC levels (HR 3.94; 95%CI 1.63-9.53). Both CC (AUC 0.92, p=0.022) as well as BC (AUC 0.91, p=0.036) significantly added incremental value to known vascular risk factors and demographics (AUC 0.88, model without biomarkers served as reference) for mortality. The comparison of the model including CC as compared to the model including BC showed no incremental prognostic value (p=0.7).

Conclusion:
Copeptin-change over the first 5 days showed a strong association with 90-day mortality, but copeptin-change compared to baseline-copeptin provided no significant additional prognostic information; therefore no repeated measures are need for an accurate prognosis.

4050

H. Bolck[1], C. Corrò[1], A. Von Teichman[1], C. Pauli[1], P. Schraml[1], H. Moch[1]

A critical evaluation of in vitro renal cancer cell models for translational studies

Pathology, University Hospital, Zürich[1]

Introduction:
Recent advances in cancer research have uncovered the considerable diversity and complexity of renal cancers. This has fostered the development of patient-derived cell (PDC) models that are potentially capable of representing renal cancers much more accurately *in vitro.* However, a detailed understanding of their ability to mirror the primary tumor and their suitability for functional assays and drug profiling is lacking to date.

Methods:
We have established a cohort of patient-derived renal cancer cell models and employed targeted sequencing, fluorescence *in situ* hybridization, cytology and immunohistochemistry to validate their resemblance to the primary tumors. Representative two-dimensional PDC models were further characterized by next-generation sequencing to gain insights into genotypic changes associated with PDC culturing. Finally, we compared PDC monolayer cell cultures to state-of-the-art 3D cell models and explored their benefits in comparative drug screening.

Results:
We describe a biobank of renal PDC models that recapitulate histological and genetic features of their respective original tumors. We reveal that during serial passaging of PDC cultures, genetically distinct subclones of the primary tumor are retained but are subject to clonal selection. By comparing PDC monolayer cell cultures to state-of-the-art 3D cell models, we determined that monolayer cultures represent the most easily to implement, cost-effective yet relevant method to culture patient-derived renal cancer cells for translational cancer studies. To conclude our findings, we suggest a general workflow for living cell biobanking from renal cancer tissue.

Conclusion:
Establishing PDC models as a part of routine biospecimen collection will provide important resources for scientists aiming to utilize *in vitro* cell models that more closely resemble human renal cancers and are therefore suitable tools to advance pre-clinical drug development and precision medicine.

4051

D. Impellizzieri[1], Y. Yamada[2], Y. Yamada[3], T. Nguyen[1], J. Jang[2], U. Karakus[1], I. Inci[2], C. Benden[4], W. Weder[2], W. Jungraithmayr[2], O. Boyman[1]

Induction of tolerance by interleukin-2 complexes in experimental lung transplantation

Department of Immunology, University Hospital Zurich, University of Zurich[1], Department of Thoracic Surgery, Univeristy Hospital of Zurich, Zurich[2], Department of General Thoracic Surgery, Chiba University Graduate School of Medicine, Chiba, Japan[3], Department of Pulmonology, University Hospital Zurich, Zurich[4]

Introduction:
Background
Interleukin-2 (IL-2) is an important cytokine involved in homeostasis and development of T cells. IL-2 activity can be enhanced by combining IL-2 with a monoclonal antibody (mAb) JES6-1 to form IL-2/JES6-1 complexes (IL-2cx). Such IL-2cx have been shown expand to preferentially expand $CD4^+$ regulatory T cells (Treg) in vivo. Treg cells are crucial in immune homeostasis, suppressing inflammatory responses toward self-antigens, but they represent only 5-10% of the total $CD4^+$ T cells pool. The selective boosting of this T cell subset improves graft acceptance in fully major histocompatibility complex (MHC)-mismatched mouse models of pancreatic islet cell, liver and skin transplantation. Based on these observations, we tested IL-2cx in a model of experimental lung transplantation in a fully MHC-mismatched setting.

Methods:
Lung transplantation (Tx) on a fully MHC-mismatched background was performed by orthotopic transplantation of single lungs from BALB/c to C57BL/6 mice. PBS or IL-2cx were administered by intraperitoneal injection (ip) 5 days before Tx. Outcomes of transplantation were analyzed on days 5, 15, 30, and 60 by flow cytometry, histology, immunofluorescence and lung functionality tests. We also used transgenic Foxp3-DTR mice (on a C57BL/6 background) that express the human diphtheria toxin (DT) receptor under the control of the Foxp3 promoter to selectively deplete $Foxp3^+$ regulatory T cells.

Results:
IL-2cx induced vigorous Treg expansion in both secondary lymphoid and peripheral non-lymphoid organs. Short-term IL-2cx treatment before transplantation significantly reduced graft rejection. Use of DT in Foxp3-DTR mice confirmed the crucial role of Treg cells in inducing a tolerant immunological state in lung Tx and the importance of boosting this subset through IL-2cx administration.

Conclusion:
IL-2cx administration in lung transplantation leads to long-term acceptance of a highly vascularized and fully MHC-mismatched solid organ. The current findings are promising for further testing of this therapeutic approach with possible application to the clinical setting.

4052

C. Yang[1], M. Gualandi[1], N. Jauquier[2], J. Joseph[2], K. Balmas Bourloud[2], A. Mühlethaler-Mottet[2], O. Shakhova[1]

The Metastatic Role of SOX9 in Neuroblastoma

Department of Hematology and Oncology, USZ, Zurich[1], Pediatric Hematology-Oncology Research Lab, CHUV-UNIL, Lausanne[2]

Introduction:
Approximately 50% of neuroblastoma patients suffer from metastatic disease at diagnosis and require intensive treatment. Despite intensive therapy, the vast majority of patients still have a poor clinical outcome (5-year survival rate of 30% to 40%). Investigating the molecular basis of neuroblastoma metastasis is crucial to develop an effective therapy. The similarities between neural crest development and neuroblastoma progression have been recognized. Transcription factor SOX9 is involved in cell migration during neural crest delamination, and has also been implicated in formation and growth of various tumors. Currently, little is known about the role of SOX9 in neuroblastoma pathogenesis. We hypothesized that SOX9 plays a crucial role in neuroblastoma metastasis, and the goal is to investigate the function of SOX9.

Methods:
To understand whether SOX9 promotes metastasis in neuroblastoma, low and high SOX9 expressing neuroblastoma cell lines were chosen to generate overexpression and knockdown clones individually. Cell migration, invasion and colony formation assays were performed to determine metastatic and tumorigenesis abilities of SOX9 overexpressing and knockdown cells *in vitro*. Orthotopical implantation of SOX9 overexpressing and knockdown cells in mouse adrenal gland were used to evaluate tumorigenicity and metastasis ability *in vivo*, and growth of tumor was followed by echography. For further analysis of metastasis, immunohistochemistry were applied to detect metastatic cells in distant organs. To further discover how SOX9 promotes metastasis in neuroblastoma, RNA sequencing was used to profile gene expression and analyze SOX9 target genes.

Results:
Two low SOX9-expressing cell lines: IMR-5 and SK-N-BE(2), and one intermediate SOX9-expressing cell: SH-SY5Y were chosen to overexpress SOX9. High SOX9 expressing cell: SK-N-AS was used to knock down SOX9. Overexpression of SOX9 significantly enhanced cell migration, invasion, and colony formation in IMR-5 and SH-SY5Y cells. On the other side, knockdown of SOX9 reduced these abilities in SK-N-AS. In *in vivo* model, it showed that tumor growth remarkably increased in IMR-5 SOX9 overexpressing compared to IMR-5 vector control, while it signifcantly decreased in SK-N-AS SOX9 knockdown compared to SK-N-AS control. No metastasis was found in IMR-5 control and SOX9 overexpressing; however, micrometastasis was detected in lung sections in 3 of 6 SK-N-AS control mice, while none of 11 SOX9 knockdown mice was found metastasis. By comparing gene expression profile of IMR-5 versus SK-N-AS and SK-N-AS control versus SOX9 knockdown, 1394 genes were identified as SOX9-activated genes and 739 genes were identified as SOX9-repressed genes. Analysis of gene ontology and KEGG pathway revealed that SOX9-activated genes were highly related to extracellular matrix organization, cell adhesion, and cell migration, which was compatible with our *in vivo* and *in vitro* results. On the other side, SOX9-repressed genes were mainly involved in neuron development and differentiation. This result gave a hint that SOX9 serves tumor cells to remain undifferentiated and aggressive phenotype.

Conclusion:
Taken together, these results clearly indicate that SOX9 enhances in cell motility and invasive ability of neuroblastoma cells *in vitro*, and promotes tumorigenesis and metastasis in *in vivo* model. Analysis of RNA sequencing suggests that SOX9 potentially maintains neuroblastoma undifferentiated and aggressive phenotype, and leads to metastasis. Based on our study, we expect to figure out the molecular mechanism how SOX9 boosts metastasis, which will provides promising targets in prevention of metastasis.

4053

U. Süssbier[1], HC. Wong[1], A. Gomariz[1], S. Isringhausen[1], P. Helbling[1], T. Nagazawa[2], M. Manz[1], A. Müller[1], C. Nombela-Arrieta[1]

Functional and structural dynamics of the bone marrow stromal microenvironment after cytoreductive therapies

Experimental Hematology Division, University Hospital Zürich, Zürich[1], Institute for Frontier Medical Sciences, Kyoto University, Kyoto, Japan[2]

Introduction:
The bone marrow (BM) is the primary site for the continuous production of all blood cells throughout the entire adult lifespan. Hematopoiesis is sustained by a rare population of hematopoietic stem and progenitor cells (HSPCs). Signals, which tightly regulate the proliferation and differentiation of HSPCs to prevent their over-proliferation and exhaustion are provided by the BM stromal microenvironment, which comprises different non-hematopoietic cell types, including endothelial cells, adipocytes, osteoblasts and mesenchymal fibroblastic reticular cells. Chemotherapy is the primary therapeutic approach for multiple hematological and non hematological cancers. 5-fluorouracil (5-FU), which targets cycling cells, is employed in the treatment of colorectal cancers and has been extensively used to investigate the potent deleterious effects of chemotherapy on BM hematopoiesis, as well as the dynamics of hematopoietic recovery post-myeloablative stress. Although the action of 5-FU on hematopoietic progenitors has been precisely dissected, the kinetics of the structural alterations induced by 5-FU in the different components of the BM stromal infrastructure and the process of tissue regeneration have not been studied and visualized in detail to date.

Methods:
In our study we provide a comprehensive analysis of the changes in the BM upon 5-FU treatment through two complementary approaches. Advanced flow cytometric protocols were used to study quantitative changes of the hematopoietic stromal components, comprising mesenchymal and endothelial cell populations. To investigate effects on the murine BM microarchitecture, thick bone slices were analyzed using advanced 3D-quantitative imaging techniques developed in our laboratory.

Results:
Analysis by flow cytometry revealed not only a severe loss of HSPCs, but also of stromal cells including $CD45^{-}Ter119^{-}Sca1^{+}CD31^{+}$ endothelial cells and $CD45^{-}Ter119^{-}Sca1^{-}CD31^{-}CD140b^{+}$ fibroblastic reticular cells 7 days post 5-FU administration. A gradual reversal of these destructive effects were observed starting at day 14 days post treatment. Through 3D-imaging we observed that the initial signs of destruction of the vascular system manifested as a massive sinusoidal vasodilation followed by a complete disruption of the vessel walls. By day 14 post administration not only cell numbers were found to recover, but also the vascular network started to reorganize, eventually regenerating a normal microvascular network 28 days after treatment. In contrast to the analysis by flow cytometry, CXCL12 abundant reticular stromal cells were only slightly affected when quantified by 3D-imaging. The striking regenerative potential of the BM after severe tissue damage is remarkably robust. Indeed similar kinetics of recovery post 5-FU-induced stress were also observed in the BM microenvironment of aged mice (< 2 years), as well as after repeated challenge of the system through 3 consecutive treatments with 5-FU.

Conclusion:
Our observations demonstrate that mesenchymal stromal populations of the BM are highly resistant to myeloablative damage with 5-FU and most likely drive the complex process of rapid and complete regeneration of BM tissues after injury.

4054

S. Santos[1], S. Santos[2], C. Haslinger[1], M. Hamburger[2], M. Mennet[3], O. Potterat[2], M. Schnelle[3], U. Von Mandach[1], AP. Simões-Wüst[1]

In vitro effect on myometrial contractility of a combination of Bryophyllum pinnatum press juice and nifedipine

Department of Obstetrics, University Hospital Zurich, Zurich, Switzerland [1], Department of Pharmaceutical Sciences, University of Basel, Basel, Switzerland[2], Clinical Research, Weleda AG, Arlesheim, Switzerland[3]

Introduction:
Herbal preparations of *Bryophyllum pinnatum* have been used as tocolytic agent in anthroposophic medicine and, recently, in conventional settings as an add-on medication with tocolytic agents such as nifedipine. However, the influence of *B. pinnatum* on the effect of known tocolytics has not yet been investigated. Our aim was to investigate the effects of *B. pinnatum* leaf press juice and nifedipine, alone and in combination, on the spontaneous contractility of human myometrial tissue *in vitro*.

Methods:
Myometrial biopsies were collected during elective Caesarean section. Four myometrial strips were placed under tension into a myograph chamber, and spontaneous contractions were recorded. After a 30 min period of regular contractions, Krebs solution (control; two strips) or nifedipine (final concentration 9 nM; two strips) was added and contractility was recorded for 30 min. To measure the effects of *B. pinnatum* alone and of the combination, *B. pinnatum* press juice (final concentration 0.25% corresponding to 2.5 µg/mL) was then added to all chambers, and contractions were recorded for 30 min. After a washout period, vitality of strips was observed for additional 30 min. Area under the curve (AUC) and amplitude of contractions were determined as a measure of the strength of contractions. Results are expressed as percentage of initial value.

Results:
All test substances lowered the strength of myometrium contractility, i.e. they led to significantly lower AUC and to lower amplitude compared to control (in all cases $p<0.05$). Nifedipine lowered AUC to 71.9 ± 6.59%, and *B. pinnatum* decreased it to 78.7 ± 6.49%. The combination of *B. pinnatum* and nifedipine lowered the AUC to 36.5 ± 8.30%, which was significantly different from the effect of *B. pinnatum* or nifedipine alone. Nifedipine lowered the amplitude to 87.1 ± 8.63% of initial contraction, and *B. pinnatum* to 93.4 ± 6.36%. The combination of *B. pinnatum* and nifedipine lowered the amplitude to 63.0 ± 9.29%, which was significantly different from *B. pinnatum* or nifedipine alone.

Conclusion:
B. pinnatum and nifedipine, alone or combined, exert inhibitory effects on the strength of spontaneous myometrial contractions *in vitro*. At the concentrations tested, the effect of the combination was significantly stronger than the effects of the *B. pinnatum* alone and of nifedipine alone. A combination of both substances in the clinical practice thus appears promising.

4055

J. Friemel-Bauersfeld[1], I. Torres[2], E. Brauneis[2], A. Schäffer[2], M. Gertz[2], T. Ried[2], A. Weber[1], K. Heselmeyer-Haddad[2]

Single cell-based assessment of copy number changes in nonalcoholic fatty liver disease (NAFLD), nonalcoholic steatohepatitis (NASH) and NASH-induced hepatocellular carcinoma (HCC).

Pathology, University Hospital Zürich[1], National Cancer Institute, NIH, Bethesda MD, USA[2]

Introduction:
Nonalcoholic fatty liver disease (NAFLD) and nonalcoholic steatohepatitis (NASH)-induced hepatocellular carcinoma (HCC) are emerging entities. To characterize genomic aberrations in this subgroup of HCC and its preceeding conditions (NAFLD/NASH), multiplex single cell fluorescent in situ hybridization (FISH) was used. This approach allows to simultaneously analyze copy numbers of multiple genomic markers on a single cell level.

Methods:
Liver tissues of 11 patients with NAFLD/NASH (steatosis >5%; absence of chronic hepatitis; no alcohol abuse) and 11 NASH-HCC patients were included. Genomic markers comprised telomerase reverse transcriptase (*TERT*), the Myc oncogene (*MYC*), hepatocyte growth factor receptor tyrosine kinase (*MET*), tumor protein 53 (*TP53*), cyclin D1 (*CCND1*), human epidermal growth factor receptor 2 (*HER2*), the fragile histidine triad gene (*FHIT*) and the FRA16D oxidoreductase (*WWOX*), and centromeric control probes. The FISH tree 3.0 software was used to predict phylogenetic trees of single-cell data.

Results:
Frequently observed numerical aberrations in NASH-induced hepatocellular carcinoma were *MYC* (8q24.21) amplification, loss of *TP53* (17p13.1) and gain of *TERT* (5p15.33). Cases were characterized by multiclonality with up to 12 different FISH signal patterns per case indicating high genomic instability associated with tumor grade (p=0.03). Phylogenetic analysis of single cell data predicted order of events, with early genomic changes being *MYC* gain, *WWOX* loss, *TP53* loss. Preliminary results indicate that NAFLD/NASH samples do not harbor clonal copy number changes, but low frequent changes similar to the baseline in normal liver. Polyploidy was present in normal and malignant hepatocytes (average ploidy >2.5 in 60% of the cases), though in the setting of hepatocellular carcinoma, polyploid tumor clones were rooted in aberrant diploid cells.

Conclusion:
NASH-induced HCCs are characterized by chromosomal instability due to extensive multiclonality confirmed with single-cell analysis. Preliminary results for NAFLD/NASH specimens of patients without incident HCCs show very low frequent genomic imbalances and polyploidization.

4056

N. Sanchez Macedo[1], M. McLuckie[1], L. Gruenherz[1], R. Lorenzini[1], D. Rittirsch[1], S. Uyulmaz[1], P. Giovanoli[1], N. Lindenblatt[1]

Nanofat: novel tissue regeneration factors and molecular profiling

Division of Plastic and Hand Surgery, University Hospital Zurich, Zürich, Switzerland[1]

Introduction:
Autologous fat transplantation has become a very popular procedure in plastic and reconstructive surgery to correct physical defects requiring soft tissue augmentation such as scars, cancer, trauma, burns, and congenital defects. Liposuction aspirates are a rich source of adipose-derived stem cells (ADSCs), which can differentiate into several cell lineages, such as adipocytes, endothelial cells, pericytes, and a variety of dermal cells. Recently in the clinics, methods have been developed to break down the adipose in order to make it more easily injectable. Nanofat was therefore created to cover this need and is an ADSC-rich emulsion produced directly from liposuction through mechanical shuffling. Retrospective studies performed in our clinic showed that the use of nanofat yields dramatic results including a large reduction in fibrotic scars and skin rejuvenation.

Methods:
Micro and nanofat samples were collected during liposuction and fat grafting procedures (approx. 1 g/sample).
We extracted protein from microfat and nanofat samples and performed proteome profile arrays (R&D Systems) in order to screen the presence of cytokines, growth factors and other inflammatory proteins. Furthermore, immunostainings were performed on microfat and nanofat cryo-sections.

Results:
Nanofat proteome arrays revealed the presence of hormones potentially involved in tissue regeneration such as angiogenin, leptin and lipocalin-2. Also, cytokines with an emerging role in wound healing like IL-33 and CD-14 were detected in both microfat and nanofat samples. Furthermore, endothelial markers such as CD-31. VCAM-1 and TIM-3 suggest the presence of microvascular fragments in nanofat and microfat.

Conclusion:
No difference in cytokine levels between microfat and nanofat were detected in their profiles. This suggests that nanofat consists of the same beneficial components as fat, yet in a more injectable form without adding unnecessary volume.

4057

L. Peterer[1], K. Jensen[2], G. Osterhoff[2], L. Mica[2], HP. Simmen[2], HC. Pape[2], K. Sprengel[2]

Implementation of new standard operating procedures: What are the benefits for geriatric trauma patients with multiple injuries.

Cantonal Hospital Grisons, Department of Surgery, Chur[1], University Hospital Zurich, Department of Trauma, Zurich[2]

Introduction:
The demographic changes towards ageing of the populations in developed countries imposes a challenge to trauma centers, as geriatric trauma patients require specific diagnostic and therapeutic procedures. This study investigated whether the integration of new standard operating procedures (SOPs) for the resuscitation room (ER) has an impact on the clinical course in geriatric patients. The new SOPs were designed for severely injured adult trauma patients, based on the Advanced Trauma Life Support (ATLS) and imply early whole-body computed tomography, damage control surgery, and the use of goal-directed coagulation management. We investigated whether there were changes in the in-hospital mortality, infection rate, and rate of palliative care after the implementation of new SOPs.

Methods:
Single-center cohort study. We included all patients >= 65 years of age with an Injury Severity Score (ISS) >= 9 who were admitted to our hospital primarily via ER. A historic cohort was compared to a cohort after the implementation of the new SOPs. Person's chi-square, Fisher's exact and Mann–Whitney U test were used to compare the treatments. Binary logistic regression analysis was conducted to measure the strengths of associations and to identify possible risk factors.

Results:
We enrolled 311 patients who met the inclusion criteria between 2000–2006 (group PreSOP) and 2010–2012 (group SOP). In group SOP, the mortality rate was significant lower (64.1% vs. 44.4%; standardized mortality ratio 0.90 vs. 0.70, P = .001) whereas the rate of infections (21.4% vs. 21.9%) and palliative care (23.7% vs. 28.3%) was comparable and not significant different with group PreSOP. TBIs were the leading cause of death in both time periods (60.2% vs. 72.5%). However, the rate of exsanguinating patients decreased from 26.5% to 7.5%. This benefit was seen only for severely injured patients (ISS ≥ 16), but not for moderately injured patients (ISS 9–15).

Conclusion:
Our findings suggest that the implementation of new SOPs comprising early whole-body CT, damage control surgery, and the use of goal-directed coagulation management significantly reduced the mortality rate in severely injured geriatric trauma patients, whereas moderately injured patients seemed not obtain the same benefit and with no influence on the infection rate. Further research is needed to improve the outcomes for this fast-growing population.

4058

PW. Schreiber[1], V. Kufner[2], K. Hübel[3], O. Zagordi[2], S. Schmutz[2], C. Bayard[1], M. Greiner[1], A. Zbinden[2], R. Capaul[2], J. Böni[2], T. Müller[3], N. Mueller[1], A. Trkola[2], M. Huber[2]

Virus transmission during kidney transplantation assessed by virome analysis of living donor and recipient

Division of Infectious Disease and Hospital Epidemiology, University Hospital Zurich[1], Institute of Medical Virology, University of Zurich[2], Department of Nephrology, University Hospital Zurich[3]

Introduction:
Transplantation of solid organs can result in concomitant transmission of viruses from the donor to the recipient. Prior to living donor kidney transplantation, donors and recipients are therefore routinely screened for a number of active or latent viral infections using specific tests in order to minimize the risk of donor-derived infections. Little is known about other, untested, apathogenic viruses a donor might carry and likely will transmit. Here, we aimed to characterize the viral metagenome in clinical samples of both, the donor and the recipient, using an open metagenomic approach at time of transplantation as well as up to one year after.

Methods:
Recipients of kidney grafts and the corresponding donors were enrolled at the time of transplantation. Follow-up study visits for recipients were scheduled 4-6 weeks and 1 year thereafter. At each visit, plasma, urine and stool samples were collected and patients were evaluated for signs of infection or transplant-related complications.
For metagenomic analysis, blood and urine samples were enriched for viruses, amplified using an anchored random PCR system and sequenced using high-throughput metagenomic sequencing. Viruses detected by sequencing were confirmed using real-time PCR.

Results:
We analyzed a total of 30 living kidney donor/recipient pairs with a follow up of at least 1 year. Post transplant routine virus diagnostics mainly detected cytomegalovirus (CMV) and BK polyomavirus (BKPyV) replication in blood and respiratory viruses in throat swabs.
In addition to routine diagnostics, metagenomic sequencing detected JC polyomavirus (JCPyV) in urine of 7 recipients as well as all corresponding donors. Phylogenetic analysis confirmed that donor and recipient were infected with the same strain in 6 cases, suggesting a transmission from living transplant donor to recipient. Moreover, Torque teno virus (TTV) was found frequently in time points after transplantation, as expected in patients under immunosuppressive therapy.

Conclusion:
Using metagenomic sequencing, we detected transmission of JCPyV from infected kidney transplant donors to the recipients in several cases. The role of JCPyV infection after renal transplantation is still unclear. Future studies within larger cohorts may help to define the relevance of the donor's virome for the recipient, thereby enabling the prediction of relevant transplant outcomes, such as rejection, graft loss or death of the recipient.

4059

H. Rehrauer[1], L. Wu[2], W. Blum[3], L. Pecze[3], T. Henzi[3], V. Serre-Beinier[4], C. Aquino[1], B. Vrugt[6], M. De Perrot[2], B. Schwaller[3], E. Felley-Bosco[5]

How asbestos drives tumor development: YAP activation, macrophage and mesothelial precursor recruitment, RNA editing and somatic mutations

FGCZ, UZH/ETHZ, Zurich[1], Division of Thoracic Surgery, Toronto General Hospital, University Health Network, University of Toronto, Toronto[2], Department of Medicine, University of Fribourg, Fribourg[3], Department of Thoracic Surgery, University Hospitals of Geneva, Geneva[4], Lungen- und Thoraxonkologie Zentrum, University Hospital Zürich, Zürich[5], Institute of Surgical Pathology, University Hospital Zurich, Zurich[6]

Introduction:
Mesothelioma development is associated with asbestos exposure but early steps of carcinogenesis are unknown. Our aim was to assess the role of loss of homeostasis in the mesothelial environment during mesothelioma development.

Methods:
Nf2+/- mice were injected eight times with asbestos fibers every three weeks in the peritoneum and several parameters were assessed thirty-three weeks after the first exposure.

Results:
Chronic exposure to intraperitoneal asbestos triggered a marked response in the mesothelium well before tumor development. Macrophages, mesothelial precursor cells, cytokines and growth factors accumulated in the peritoneal lavage. Transcriptome profiling revealed YAP/TAZ activation in inflamed mesothelium with further activation in tumors, paralleled by increased levels of cells with nuclear YAP. *Arg1* was one of the highest upregulated genes in inflamed tissue and tumor. Inflamed tissue showed increased levels of single nucleotide variations, with an RNA-editing signature, which were even higher in the tumor samples. Subcutaneous injection of asbestos-treated, but tumor-free mice with syngeneic mesothelioma tumor cells resulted in a significantly higher incidence of tumor growth when compared to naïve mice supporting the role of the environment in tumor progression.

Conclusion:
In this study, we comprehensively describe alterations of tissue homeostasis prior to cancer development by analysis of the mesothelium and its environment at the histological and molecular level and we report for the first time A to G RNA-editing signature, YAP/TAZ activation and a pro-tumorigenic environment as early steps in pre-neoplastic lesions.

4061

M. Meerang[1], J. Kreienbühl[1], V. Orlowski[1], M. Kirschner[1], W. Weder[1], I. Opitz[1]

Role of Cullin4 Ubiquitin Ligase in Malignant Pleural Mesothelioma

Thoracic Surgery, University Hospital Zürich[1]

Introduction:
Malignant pleural mesothelioma (MPM) is an aggressive and difficult to treat thoracic malignancy commonly associated with asbestos exposure. Discovering the key pathway alterations that regulate MPM progression is critical for the development of effective treatment.
Cullin4 ubiquitin ligase regulates various pathways in cells such as DNA repair, epigenetic regulation. Two cullin4 paralogs, CUL4A and CUL4B, have been shown to facilitate the development and aggressiveness of some malignancies such as hepatocellular carcinoma. CUL4A overexpression due to gene amplification has been reported for MPM. Recent evidence showed that NF2, the tumor suppressor gene mutated/lost in 30-40% of MPM, prevents tumorigenesis by inhibiting the Cullin4 complex. In this study, we investigate the role and mechanisms of CUL4A and CUL4B in the regulation of MPM progression.

Methods:
RNA samples were isolated from MPM tumor tissues collected at surgery. Two different siRNAs targeting CUL4A and CUL4B were employed to silence gene expression in three MPM cell lines and one primary MPM cell line. mRNA and protein expression levels were assessed by quantitative real time PCR and western blot, respectively. Cell cycle analysis was performed by flow cytometry following BrdU incorporation and PI staining. Cell death and apoptosis was measured by Annexin V/ZombieNIR staining. Immunohistochemical staining of protein expression on tissue microarrays was quantified semi-quantitatively based on histo score.

Results:
Gene expression of CUL4A and CUL4B were significantly elevated in MPM tumors (n=43) compared to non-malignant pleural tissues (e.g. pleural plaques, inflammatory pleural tissues (n=18)); p=0.04 for CUL4A and p=0.002 for CUL4B. In MPM cells, CUL4A or CUL4B silencing lead to significantly reduced cell proliferation and colony formation capacity, increased apoptosis and cell death. The depletion of CUL4A or CUL4B resulted in down regulation of YAP1, a transcription coactivator, on mRNA and protein levels. Accordingly, expression of YAP1 target genes, BIRC5 (Survivin) and CTGF, was reduced in CUL4 and CUL4B depleted cells. In MPM tumor specimens, mRNA levels of CULA and CUL4B were positively correlated with YAP1 (CUL4A *vs* YAP1 (n=42) p=0.003, r=0.447; CUL4B *vs* YAP1 (n=43) p=0.017, r=0.363). We assessed protein expression of CUL4A, CUL4B and YAP1 on a tissue microarray comprised comprising of MPM tumor tissues collected from 111 patients at diagnosis. A positive correlation between CUL4A and YAP1 (p=0.01; r=0.240) was detected.

Conclusion:
Our results demonstrate that CUL4A and CUL4B maintain MPM cell growth and survival, suggesting their role in MPM progression. CUL4A and CUL4B may promote MPM progression by up-regulating YAP1 expression, thereby stimulating the expression of survival promoting genes. Targeting Cullin4/YAP1 may provide an option for a novel treatment.

4062

D. Cabalzar-Wondberg[1], D. Birrer[1], A. Rickenbacher[1], S. Käser[1], M. Schneider[1], M. Turina[1]

Rate of inapparent pathology in clinically inconspicuous specimens following routine hemorrhoidectomy

Universitätsspital Zürich, Department of Surgery, Division of Visceral and Transplant Surgery[1]

Introduction:
The aim of the present study was to analyse the rate of pathologic findings in patients who underwent routine haemorrhoidectomy.

Methods:
Data of 590 patients who underwent haemorrhoidectomy between 2001 and 2017 were collected retrospectively. Out of this patient group, 35 patients were operated using non-resective methods (ligation of the haemorrhoidal arteria (HAL), recto-anal-repair (RAR) or rubber band ligation). These patients were excluded from analysis, as were with the data of patients whose resected tissue was not sent to histological analysis.

Results:
The medical data and histological reports of 500 patients were reviewed. The majority of patients (62.4%) obtained a mucosectomy according to Longo (n=312). 34,6% (n=173) underwent a resection with the Ligasure device. The remainder of haemorrhoidectomies followed resection techniques according to Milligan-Morgan or Ferguson. In 22 patients (4.4%) a pathological finding was discovered in the analysed tissue. The median age of these patients was 54 years (range 32-82 years) and the gender ration 14 to 8 (male/female). The pathological findings were evenly spread among the different operation techniques. In 5 cases an isolated infection with the human papillomavirus (HPV) was found. Four patients already suffered from anal intraepithelial neoplasia (AIN) II and 6 patients even from AIN III. Four patients were diagnosed with AIN I, one patient with an “atypical squamous cells of undetermined significance“ (ASC-US) and one patient with a non-specified AIN. In one case a biopsy was conducted intraoperatively on a rectum tumor that qualified histologically as a carcinoma.

Conclusion:
The rate of 5% of inapparent pathologies in histologically analyzed tissue is surprisingly high. The most frequent pathological finding were HPV with intraepithelial dysplasia of different severity. Whilst knowing about such potential pathology is vital for the prophylaxis of the development of an invasive carcinoma, the results of the analysis underline the importance of routine histological analyses of all resected tissue.

4063

R. Uka[1], C. Britschgi[1], C. Matter[1], A. Kraettli[1], D. Mihic[2], M. Okoniewski[4], M. Levesque[3], R. Dummer[3], O. Shakhova[1]

WNT-dependent regulation of SOX10 expression in melanoma development

Oncology, University Hospital, Zurich[1], Surgical Pathology, University Hospital, Zurich[2], Dermatology, University Hospital, Zurich[3], Scientific IT Services, ETH, Zurich[4]

Introduction:
Melanoma is the most aggressive type of skin cancer, characterized by highly invasive and metastatic features. The high mortality rate is largely due to resistance of melanoma cells to conventional chemotherapy, and despite recent advances in melanoma treatment, including targeted therapies and immune checkpoint inhibitors, melanoma remains a deadly disease.The observation on striking parallels between cancer cells and normal stem cells might lead to fundamental changes in the future therapy against cancer. We have previously demonstrated that Sox10, a neural crest transcription factor, plays a crucial role in the development and maintenance of giant congenital melanocytic nevi and melanoma and we identified SOX10 as a novel promising candidate for melanoma treatment.

Methods:
We performed immunohistochemistry for SOX10 in a set of human melanoma samples. These samples derive from the same patients before and after the start of targeted therapy using vemurafenib, a BRAF inhibitor. We performed western blot analysis in several melanoma cultures derived from melanoma patients. We measured SOX10 expression in melanoma cultures carrying the $BRAF^{V600E}$ or $NRAS^{Q61K}$ mutation as well as double mutated $BRAF^{V600E}$ and $NRAS^{Q61K}$ cell lines. Moreover, we have included both MAPK inhibitor- sensitive and resistant cell lines in our analysis. To identify novel SOX10-interacting proteins, we took an unbiased approach performing a Mass Spectrometry. The Mass-Spectrometry was confirmed later by Co-IP. We performed immunohistochemical staining of a human tissue micro array containing samples from primary melanoma, metastases, brain metastases, and cell lines. Next, we used a pharmacological and a genetic approach to deplete SOX10 levels and we compared transcriptional changes in three human melanoma cells. Next, we examined whether our *in vitro* results could be recapitulated *in vivo*. To this end, we injected nude mice with a vemurafenib-resistant patient-derived melanoma cell line and moreover, because *Tyr::Nras^{Q61K} Ink4a$^{-/-}$* represents human melanoma, we also analyzed the effect of a GSK3α and β inhibitor in this murine melanoma model.

Results:
Interestingly, our data reveal that targeted therapies currently available for melanoma patients do not interfere with SOX10 expression neither *in vitro* nor *in vivo* in human patients. To gain further insight into SOX10-mediated melanoma progression, we have performed a mass spectrometry-based screen to identify proteins interacting with SOX10 in melanoma cells. We show here that SOX10 interacts with β-catenin, a key downstream effector of Wnt signalling pathway, and pharmacologic activation of Wnt signaling suppresses SOX10 in a β-catenin-dependent manner. The role of Wnt signaling and β-catenin pathway has been the subject of intensive research in the field of melanoma: in this study we demonstrate that inhibition of GSK3α and β results in ultimate downregulation of SOX10 protein in melanoma cell lines *in vitro* and consequently leads to the death of melanoma cells. Moreover, when Sox10 is suppressed via β-catenin stabilization, tumor formation is delayed and survival is extended in a genetic melanoma mouse model.

Conclusion:
Our study is the first to demonstrate the protein-mediated regulation of the SOX10-Wnt axis in melanoma biology, shedding light on the molecular mechanism of SOX10 regulation and untangling the controversy around the role of canonical Wnt signaling in melanoma.

4064

A . Batavia[1], M. Lukamowicz-Rajska[1], J. Kuipers[2], P. Schraml[1], N. Beerenwinkel[2], H. Moch[1]

Characterising renal cell cancer with wild type VHL clear cell renal cell cancers as a focal point.

Institute of Pathology and Molecular Pathology, University Hospital Zurich and University of Zurich, Zurich, Switzerland[1], Computaitonal Biology Group, D-BSSE, ETH Zurich[2]

Introduction:
The most prevalent form of kidney cancers are renal cell carcinomas (RCC), of which clear cell renal cell carcinomas (ccRCC) are by far the most common and largely characterised by the biallelic inactivation of the von Hippel-Lindau (VHL) tumour suppressor gene. However, up to 12% of patients have no inactivation in either allele of VHL but experience tumorigenesis. The molecular characteristics of tumours with wtVHL will be studied in detail in an attempt to implicate novel pathways for ccRCC development independent from VHL. In parallel, a multi-omics model will be developed in order to sub-classify all Kidney cancers in order to find novel therapeutic targets in light of precision medicine. Here we present preliminary data and the plan going forward.

Methods:
Inactivation of VHL can occur via direct mutation, chromosome 3p arm deletion and promotor methylation. Steps were taken to eliminate cases in which these have occurred in a stepwise manner. Sanger sequencing, which had previously been carried out for all our ccRCC cases, was used eliminate ccRCC with VHL mutations; from this data those with a wtVHL sequences were selected. Oncoscan analysis was carried out on the resulting 100 samples with 20 controls (with LOF VHL mutations) to determine their copy number aberrations and specifically their 3p arm status. Bisulfite sequencing will be carried out to determine the methylation status of the promotor regions of these samples (261 bp region of the promotor overlapping exon 1 of VHL). NGS will be carried out in the final cohort. The multi-omics model is being developed with the use of R 3.3.0 and RStudio. Clinical, CNV, expression, mutation and methylation data was obtained from TCGA for all Kidney subtypes for a broader look on the molecular profiles of RCCs.

Results:
Oncoscan identified an intact 3p arm in 12 of 100 ccRCCs. 4 of the 12 cases are potentially TCEB1 mutated RCC suggested via a deletion in the 8q region. Deletions are also observed in 1p, 6q, 8p, 9, 10q and 14q and 18 while amplifications are observed in 2, 5q, 7, 12, 16 and 20q. Additionally, cases with wtVHL sequence with their 3p arm intact were associated with amplifications in chromosome 9p and 13 along with deletions of 8q and small regions within chromosome 1p. Cases with 3p arm deletion were associated with amplifications in the 5q region and deletions in chromosome 14q. For the development of the multi-omics model, a pipeline has been developed for the analysis of expression data using the Chromophobe RCC dataset from TCGA (66 tumour samples). Non-negative Matrix Factorisation was found to be the most suitable for clustering which is able to successfully discriminate between normal and tumour samples and cluster the tumour into further subgroups from which a list of genes has been obtained defining each group, these are yet to be validated.

Conclusion:
Oncoscan identified the new tumour subtype in of TCEB1 mutated RCC in a significant number of ccRCCs without VHL mutation. Exome sequencing data and potentially RNA-seq data will bring valuable information to elucidate pathways for the formation of these tumours. Methylation analysis will demonstrate the prevalence of epigenetic VHL inactivation allowing also the clinic-pathological characterisation of “true” wtVHL ccRCC.

4065

A. Moncsek[3], M. Al-Suraih[1], C. Trussoni[1], S. O'Hara[1], P. Splinter[1], C. Zuber[3], E. Patsenker[3], A. Weber[2], J. Kirkland[4], G. Gores[1], B. Müllhaupt[3], N. LaRusso[1], J. Mertens[3]

Combined targeting of senescent cholangiocytes and activated stromal fibroblasts with a Bcl-xL inhibitor ameliorates liver fibrosis in Mdr2-/- mice

Division of Gastroenterology and Hepatology and Center for Cell Signaling in Gastroenterology, Mayo Clinic, Rochester MN, USA[1], Department of Pathology and Molecular Pathology, University Hospital Zürich, Zürich, Switzerland [2], Department of Gastroenterology and Hepatology, University Hospital Zürich, Zürich, Switzerland[3], Robert and Arlene Kogod Center on Aging, Mayo Clinic, Rochester, MN, USA[4]

Introduction:
Primary sclerosing cholangitis (PSC) is a chronic cholestatic disorder characterized by persistent biliary inflammation and fibrosis. PSC cholangiocytes exhibit a senescence-associated secretory phenotype. The persistent secretion of growth factors such as platelet-derived growth factor (PDGF) by senescent cholangiocytes leads to the activation of fibroblasts. Activated stromal fibroblasts (ASF) are the drivers of fibrosis development. The activated phenotype of ASF is characterized by an increased sensitivity to apoptotic stimuli. We have previously shown that the survival of ASF is Bcl-xL-dependent. Moreover, senescent cells maintain their viability by upregulation of anti-apoptotic Bcl-xL. Therefore, we hypothesized that inhibition of Bcl-xL leads to depletion of ASF and reduction of growth factor-induced fibroblast activation by senescent cholangiocytes and finally to a reduction of biliary fibrosis.

Methods:
To induce apoptosis *in vitro*, PDGF-activated fibroblasts and senescent-induced cholangiocytes were treated with Bcl-xL-specific siRNA or a BH3-mimetic specific for Bcl-xL (A-1331852). Induction of apoptosis was examined biochemically by caspase-3/7 activity and morphologically using DAPI staining for apoptotic nuclei. To investigate the potential of senescent cholangiocytes to promote fibroblasts activation co-culture experiments were employed. To study the depletion of activated fibroblasts and senescent cholangiocytes and finally the anti-fibrotic potential of Bcl-xL inhibition *in vivo*, $Mdr2^{-/-}$ mice were treated with A-1331852 for 14 days by daily oral gavage. Liver fibrosis was assessed by morphometric analysis of Sirius red staining and quantification of hydroxyproline. Cholangiocyte senescence was analyzed by *in situ* co-detection of p16 mRNA and cytokeratin 19. Gene expression of fibrosis-associated growth factors and αSMA was assessed by qPCR.

Results:
We identified Bcl-xL as a key survival factor in PDGF-activated fibroblasts. Inhibition of Bcl-xL by siRNA or A-1331852 significantly increased caspase-3/7 activity as well as the number of apoptotic nuclei in PDGF-activated fibroblasts but not in quiescent fibroblasts. Likewise, treatment of senescent cholangiocytes with A-1331852 specifically reduced their survival and increased apoptosis as compared to non-senescent cholangiocytes. Co-culture experiments demonstrated promotion of fibroblast activation by senescent cholangiocytes in a PDGF-dependent manner.
Treatment of $Mdr2^{-/-}$ mice with A-1331852 resulted in an 80% decrease in senescent cholangiocytes, a reduction of fibrosis-inducing growth factors and cytokines, a decrease of aSMA-positive ASF, and finally in a significant reduction of liver fibrosis.

Conclusion:
This study provides new mechanistic insights into the interaction of senescent cholangiocytes and stromal fibroblasts in PSC. Furthermore, combined targeting of both activated stromal fibroblasts and senescent cholangiocytes with specific Bcl-xL inhibition is an attractive therapeutic strategy in biliary fibrosis.

4066

K. Frauenknecht[1], M. Emmenegger[1], A. Chincisan[1], A. Aguzzi[1]

Detection of human antibodies against the TREM2 cleavage site

Institute of Neuropathology, University Hospital Zürich, Switzerland[1]

Introduction:
Triggering receptor expressed on myeloid cells (TREM) 2 promotes phagocytic activity, cell survival, migration and proliferation of brain resident microglia. There is evidence that TREM2 enables microglia to clear beta amyloid from the brain. TREM2 ectodomain is physiologically shedded by cleavage of the H157-S158 bond by ADAM10, leading to the release of soluble protein into the extracellular space and abolishing TREM2-mediated signaling. A rare Alzheimer's disease associated variant of TREM2 (H157Y) occurs at the cleavage site and effects the shedding of the protein as well as phagocytic function. Reduction of the TREM2 ectodomain shedding may lead to restoration and improvement of TREM2 function/signaling. Whereas protease inhibitors might have detrimental side effects, direct targeting of the cleavage side by antibodies would offer a therapeutic strategy in AD. Especially human antibodies against the TREM2 cleavage site could have less adverse immune-mediated effects compared to mouse-derived humanized antibodies. Additionally, antibodies could be used as biomarkers in disease risk stratification. Thus, the aim of the project is i) to identify patients with reactivity against the TREM2 cleavage site, ii) to identify specific clinical patterns and iii) to clone anti-TREM2 antibodies for subsequent functional tests.

Methods:
We use a high-throughput screening (HTS) platform allowing screens of several targets and around thousand patients per day at the microliter scale (in 1536-well plates). A fourty amino acid (aa) peptide, spanning positions 135 to 174 of the TREM2 ectodomain is used for detection of antibodies. Secondary screens will include competition assays against the TREM2 cleavage site. Further, antibody-expressing B-lymphocytes will be extracted, sorted by fluorescence activated cell sorting (FACS) and the antibody sequence can be determined by single-cell polymerase chain reactions (PCR). Mammalian cell expression systems will be used for the recombinant production of antibodies.

Results:
In a first attempt, proof-of-principle screens were established. Thus, we tested anonymized pooled control plasma and commercially available monoclonal TREM2 antibodies for reactivity. Next, the peptide was implemented into the routine screening. Preliminary analyses indicate a low prevalence of anti-TREM2$_{135\text{-}174}$-antibody-harbouring patients, ocuring at a frequency of around 0.1% in an unselected patient cohort.

Conclusion:
On the long run, we aim to screen > 50,000 plasma samples of USZ patients. This unbiased quantitative approach may potentially reveal novel disease associations that could not be identified using cohorts of smaller sizes. Lastly, cloning of human antibodies targeting the cleavage site of TREM2 may provide safe therapeutics to treat Alzheimer's disease.

4067

M. Emmenegger[1], A. Chincisan[1], G. Meisl[2], K. Frontzek[1], E. Schaper[1], R. Müller[1], A. Rosati[1], J. Domange[1], N. Wuillemin[4], T. Sonati[4], I. Xenarios[3], L. Saleh[5], A. Von Eckardstein[5], S. Hornemann[1], A. Aguzzi[1]

High-throughput immune profiling for diagnostic and therapeutic antibodies in an ultra-large unselected hospital cohort

Institute of Neuropathology, University Hospital Zürich, Switzerland[1], Department of Chemistry, University of Cambridge, Cambridge, United Kingdom[2], Vital-IT at Swiss Institute of Bioinformatics, Lausanne, Switzerland[3], Mabylon AG, Schlieren, Switzerland[4], Institute of Clinical Chemistry, University Hospital of Zurich, Zurich, Switzerland[5]

Introduction:
Personalized medicine seeks to account for individual traits of patients to ameliorate the therapeutic outcome. This "individuality" is thought to be identified in the patients' genome where genetic risk factors are determined. However, the susceptibility to disease, and their prevention or therapy, is a dynamic interplay between genetic, emotional and environmental factors. In our approach, we try to overcome the limitations of a purely genomic medicine by studying the immune profiles of thousands of patients. The immune repertoire contains the records of a patient's exposure to internal and external cues and poses an important aspect of an individual's health and disease. Using *surplus blood samples of patients from University Hospital of Zurich (USZ) who signed the general consent (GC), the antibody reactivity against select antigens is assayed in a miniaturized, fully-automated high-throughput (HT) robotic platform.* Antibodies to therapeutically relevant targets are cloned from memory B cells of high-titer patients, expressed *in vitro*, and their therapeutic potential is elucidated in preclinical disease models. In addition, a quantitative correlation of antibody reactivity and encrypted clinical and demographic data is applied to unravel pattern in the data. Amongst others, preliminary data from analytic methods suggests a much higher prevalence of anti-phosophorylated TDP-43 antibodies in HIV-positive patients, while HIV-positive patients generally display higher autoreactivity across the panel of antigens analysed.

Methods:
To measure autoantibodies quantitatively and to enable subsequent clinical correlations, we have developed a fully automated HT platform. This platform allows the investigation of the immune profile of hundred thousands of patients against a vast panel of heterogeneous antigens. The data collected in each experiment are processed with a custom algorithm to derive the EC_{50}. Since the HT immune profiling of several hundred patients and up to 24 antigens can be completed within less than 24 hours from drawing blood, viable memory B-lymphocytes can be isolated by FACS or microfluidics and antibodies from high reactive patients can be cloned. The large datasets including experimental, clinical, and demographic data are stored in custom-designed database management systems (DBMS) that serve as a basis for analytic approaches. Data is subjected to unsupervised and supervised learning to visualize and interpret multidimensional data.

Results:
The daily growing biobank currently harbors 37'973 patient samples with associated pseudonymized encrypted disease-relevant and demographical information. Among the endogenous antigens (currently more than 10 in the pipeline), we observe a very low prevalence for target-specific antibodies. In over 15'000 patients screened against the recombinant prion protein (PrP) and two phosphorylated fragments of TDP-43 (pTDP-43), between 0.03 and 0.09% of patients display marked reactivity. Within these reactive patients, HIV-positive patients are generally overrepresented for all targets but occur most frequently for the pTDP-43 fragments.

Conclusion:
Here, we present a first test case of what the proposed unbiased quantitative approach may potentially reveal. Next steps include machine learning and clustering on the data sets, which may point to subgroups of HIV-positive patients that are predisposed to present with antigen-specific antibodies. Overall, we believe to enrich the current landscape of precision medicine with novel insights on the level of the immune repertoire. In the future, novel antigen-specific disease associations will emerge and may highlight prognostic and diagnostic IgG antibody biomarkers that could not be identified using cohorts of smaller sizes. Lastly, the molecular cloning of human-derived antibodies may provide safe immunotherapy to treat so far incurable diseases.

4068

A. Figurek[1], V. Luyckx[1], T. Müller[1]

Renal functional reserve in living kidney donors: Do we know enough?

Department of Nephrology, University Hospital Zurich[1]

Introduction:
Kidneys obtained from living donors (LD) are important in overcoming the organ shortage in kidney transplantation. Known favorable short-term outcomes in LD have led to expansion of accepted donors. However, long-term consequences on renal hemodynamics are not yet well enough understood. The renal functional reserve (RFR) reflects the ability of a kidney to increase it's glomerular filtration rate (GFR) in the setting of a higher functional demand. The implications of RFR in kidney donation have not been fully elucidated.

Methods:
We performed a systematic literature review of physiology studies that assessed RFR in LD in the time period 1956-2017. Databases Web of science, PubMed and EBSCO were searched using the following terms: kidney function, glomerular filtration rate, renal functional reserve capacity, renal blood flow and kidney donor.

Results:
3071 studies matched our searched terms and 272 studies were related to living kidney donation. Of these, 47 analyzed physiological changes in LD by measuring GFR and/or effective renal blood flow (ERBF). Only 16 studies measured RFR, defined as the difference between baseline and stimulated GFR, and 6 studies were performed in 'borderline' donors. These studies showed that stimulus-induced increase in GFR pre-donation was 18±9.36 ml/min/1.73m^2, whereas the increase in the remaining kidney post-donation was 4.52±4.83 ml/min/1.73m^2. RFR was reduced by up to 88% in obese compared to non-obese donors (37%), whereas in older donors RFR decreased by 72% compared to younger donors (31%).

Conclusion:
Prediction of long-term safety for living kidney donors is not possible without clear understanding of the physiological i.e. hemodynamic process in the remaining kidney after donation. Currently, there are not enough prospective data on RFR in living kidney donors, especially in 'borderline' donors, and the implications for long-term kidney function. Further studies on RFR in LD are needed in order to ensure minimal consequences of the kidney donation.

4069

Y. Zhang[1], V. Orlowski[1], B. Vrugt[2], M. Friess[1], W. Weder[1], I. Opitz[1], M. Kirschner[1]

Identification of microRNAs as chemosensitivity-related biomarkers in MPM patients

Department of Thoracic Surgery, University Hospital of Zurich, Zurich, Switzerland[1], Institute of Surgical Pathology, University Hospital Zurich, Zurich, Switzerland[2]

Introduction:
Malignant pleural mesothelioma (MPM) is an asbestos-induced, highly aggressive neoplasm with poor prognosis. Platinum-based chemotherapy is one of the few treatment options for MPM patients, but the response rate is at best 40%. Currently, there is no biomarker that helps to predict the chemosensitivity of MPM in individual patients. Therefore, clinicians are faced with the dilemma of making a chemotherapy decision for MPM patients, especially in late stage or after operation, without knowing if the patient will respond to the treatment. In this study, we aimed to identify microRNAs as chemosensitivity-related biomarkers for MPM patients. In addition, we also plan to further investigate their potential as therapeutic targets in MPM treatment.

Methods:
A total of 95 patients were selected from our MPM database. All patients had been treated with induction chemotherapy (platinum-doublet with pemetrexed or gemcitabine). From all subjects response data and formalin-fixed paraffin embedded (FFPE) tumor tissue specimens obtained at diagnosis were available. Samples were enriched for tumor content by microdissection using the Millisect System (Roche), and deparaffinized using xylene. Subsequently RNA was isolated using the RNeasy FFPE Mini Kit (Qiagen). For initial profiling a discovery set of 5 patients with partial response (PR) and 5 with progressive disease (PD) - based on modified RECIST criteria - was selected. On this discovery set, miRNA profiling was performed on 300 ng of total RNA from each sample using the TLDA (Taqman Low Density Assay) cards on which 754 target miRNA genes are measured. Initial preliminary analysis focused on 19 microRNAs previously described as being associated with prognosis of MPM patients undergoing induction chemotherapy followed by surgical resection. For these candidates, Mann-Whitney U test was used to assess the difference in target miRNAs expression between PR and PD group.

Results:
Of the 19 prognostic microRNAs expression levels of miR-625-3p ($p=0.056$), miR-19b ($p=0.056$) and miR-24 ($p=0.008$) were increased in patients with PD compared to those with PR, suggesting that high expression of these microRNAs might be associated with resistance to the platinum-doublet chemotherapy. For the remaining 16 microRNAs investigated in preliminary analyses, there was no significant differences were observed between the two groups.

Conclusion:
The high expression of miR-625-3p, miR-19b and miR-24 in the PD group suggests their possible use as a chemosensitivity-related marker in MPM patients. In currently ongoing analyses, the full set of 754 microRNAs is being further evaluated, in order to identify more microRNAs, which might serve as indicators of chemosensitivity. Following validation of identified candidates in additional tissue samples, we will also perform functional analyses in vitro to investigate the effect of altered microRNA expression on mesothelioma cells.

4070

M. Yalcinkaya[1], M. Cardner[2], S. Goetze[3], M. Hunjadi[4], A. Ritsch[4], J. Hartung[5], U. Landmesser[5], G. Liebisch[6], B. Wollscheid[3], N. Beerenwinkel[2], L. Rohrer[1], A. Von Eckardstein[1]

A Systems Biological Approach to the Anti-Atherogenicity of High Density Lipoproteins

Universitätsspital Zürich[1], BSSE, ETHZ Basel[2], HEST, ETHZ Zürich[3], Department of Internal Medicine, University Medicine Innsbruck, Austria[4], Department of Cardiology, University Medicine Charité Berlin, Germany[5], Institute of Clinical Chemistry, University of Regensburg, Germany[6]

Introduction:
Low blood levels of HDL-cholesterol increase the risk of coronary heart disease (CHD). HDL particles are complex macromolecules containing hundreds of lipid species and dozens of proteins and exerting many potentially anti-atherogenic activities. Pathological conditions cause quantitative and qualitative molecular changes in HDL components and, thereby, dysfunction.

Methods:
To identify structure-function-disease relationships of HDL we isolated HDL particles from the plasma of 25 healthy subjects and 41 patients with CHD. We characterized their protein and lipid abundances by mass spectrometry as well as their biological functionality towards cells relevant for the pathogenesis of CHD, namely the ability to induce cholesterol efflux from macrophages, to inhibit the apoptosis of endothelial cells and to promote the phosphorylation of endothelial nitric oxide synthase.

Results:
The data on clinical and anthropometric features of the patients, the protein and lipid composition as well as functionality of HDL are integrated to identify components and functions which differentiate HDL of patients and controls.

Conclusion:
The best discriminators of disease status as well as function and dysfunction of HDL will be followed-up by targeted validation studies to unravel their clinical utility as biomarkers for the diagnosis and personalized management of individuals at increased risks of CHD.

4071

M. Healy[1], Y. Boege[1], M. Hodder[2], F. Boehm[1], A. Scherr[3], M. Malehmir[1], J. Muhic[1], C. Klose[4], A. Macpherson[5], B. Koehler[3], M. Heikenwalder[6], A. Weber[1]

MCL-1 is a tumor suppressor ensuring intestinal mucosal integrity and stem cell homeostasis independent of microbiota-driven inflammation

Department of Pathology and Molecular Pathology, University Hospital Zurich, Zurich[1], Cancer Research UK Beatson Institute, Glasgow[2], Medical Oncology, University of Heidelberg, Heidelberg[3], Microbiology and Immunology, Cornell University, New York[4], Universitätsklinik für Viszerale Chirurgie und Medizin Inselspital, University of Bern, Bern[5], Chronic Inflammation and Cancer, University of Heidelberg, Heidelberg[6]

Introduction:
The IEC compartment comprises different cell types including stem cells, proliferative progenitor cells as well as highly specialized absorptive (enterocytes) and secretory cells (goblet, Paneth and neuroendocrine cells). IEC display a high cell turnover, necessitating a tight, balanced regulation of proliferation and cell death to guarantee intestinal epithelial homeostasis. While IEC death constantly occurs, reflecting IEC turnover under steady state conditions, excessive IEC death is a well-known hallmark of inflammatory bowel diseases (IBD) and inflammation-driven colorectal carcinoma development. In recent years, there has been a great scientific interest in determining the roles played by cell death regulating molecules in maintaining tissue homeostasis and preventing tumor formation. Interference with particular IEC circuits of regulated cell death (RCD) have been shown to result in increased IEC death, epithelial defects, and IBD-like inflammation. In contrast, mice deficient for other RCD-molecules display surprisingly little pathology under steady state conditions. The previously reported crucial role of the pro-survival BCL-2 family member, myeloid cell leukemia-1 (MCL-1), in highly regenerative tissues, prompted us to study its function in the intestinal tract.

Methods:
To elucidate the role of MCL-1 in maintaining intestinal homeostasis, we generated IEC specific *Mcl-1* knockout mice (Mcl-1$^{\Delta IEC}$ mice). In order to idnetify the immediate molecular changes associated with IEC specific MCL-1 deletion, we also generated a tamoxifen-inducible model of MCL-1 deletion within IEC (i-Mcl-1$^{\Delta IEC}$ mice).

Results:
IEC-specific *Mcl-1* deletion spontaneously increased IEC apoptosis, induced crypt hyper-proliferative, intestinal epithelial barrier dysfunction and microbiota-driven chronic inflammation. Surprisingly, depletion of mature T- and B-cells (Mcl-1$^{\Delta IEC}$/RAG1 mice) exacerbates intestinal inflammation, whereas α-Thy-1.2 treatment in Mcl-1$^{\Delta IEC}$/RAG1 mice reduces it, suggesting that innate lymphoid type cells mediate inflammation. In addition to triggering repeated wounding and repair cycles, MCL-1-deficiency renders IEC tumor-prone by directly promoting a stem-cell-like state and blocking differentiation. MCL-1-deficient IEC gain a WNT signaling-driven growth-advantage and accumulate DNA damage and genetic aberrations. Subsequently, Mcl-1$^{\Delta IEC}$ mice spontaneously develop intestinal carcinomas, which morphologically and genetically recapitulate the human adenoma-carcinoma-sequence. Whereas germ free housing of Mcl-1$^{\Delta IEC}$ mice attenuates intestinal inflammation, the incidence of intestinal tumor development was not reduced.

Conclusion:
Collectively, these data illustrate how MCL-1 executes two distinct crucial functions in the same tissue. By its anti-apoptotic activity, MCL-1 maintains mucosal integrity protecting against microbiota-driven intestinal inflammation. Beyond its anti-apoptotic activity, MCL-1 keeps in check WNT signaling, thus securing proper IEC turn-over and differentiation, protecting against inflammation- and microbiota-independent carcinogenesis.

4072

L. Hapouja[1], A. Figurek[1], V. Luyckx[1], T. Müller[1]

The effect of donor-recipient weight mismatch on kidney graft function – demand defines supply

Department of Nephrology, University Hospital Zurich[1]

Introduction:
In kidney transplantation, graft function and survival is dependent on immunological and non-immunological factors. A metabolic mismatch between nephron supply and recipient demand may influence the degree of hemodynamic changes induced in the graft. Transplantation of a small kidney into a large recipient with a higher metabolic need might lead to compensatory hyperfiltration with possible accelerated loss in graft function over the very long-term. Based on the correlation between kidney size and body weight, we have analyzed the effect of recipient-to-donor body weight ratio on function of the transplanted organ in the recipient.

Methods:
Parameters determining kidney function pre- and post-transplantation were analyzed one year before and one year after transplantation in 68 living donors and 48 of their recipients. Predicted values of kidney function in both, donors and recipients, were assessed according to the formula published by our group (Al-Sehli et al, 2015). The importance of the recipient-to-donor body weight ratio on the predicted graft function was evaluated.

Results:
Donors' kidney function showed an adaptive increase of the remnant kidney of 33 ± 15% ($r=0.9$, $p<0.001$). Small kidneys transplanted into a large recipient showed an additional increase in filtration, whereas larger kidneys given to a small recipient filtered less than expected. The difference between the body weight of living donors and their recipients significantly influenced the prediction of the recipient's kidney function ($r=0.55$, $p<0.001$), as depicted in Figure 1. In a linear regression analysis, the correlation coefficient r was 0.6 ($p<0.5$).

Conclusion:
Transplanted kidneys adapt to the recipient's metabolic needs by increasing or decreasing the filtration rate, indicating that demand determines the supply. However, long-term studies in kidney recipients concerning the impact of recipient-to-donor body weight ratio differences need to be performed in order to confirm whether hyperfiltration is permanently maintained, and as such, might lead to a declining kidney function in metabolically mismatched kidney grafts in the very long-term.

4073

S. Bengs[1], I. Burger[1], C. Lohmann[1], M. Messerli[1], A. Becker[2], V. Treyer[1], M. Schwyzer[1], D. Benz[1], A. Giannopoulos[1], K. Kudura[1], C. Gräni[1], O. Gämperli[1], A. Pazhenkottil[1], R. Büchel[1], P. Kaufmann[1], C. Gebhard[1]

Age- and Sex-dependent Changes in Sympathetic Activity of the Left Ventricular Apex Assessed by 18F-DOPA PET Imaging

Department of Nuclear Medicine, University Hospital Zurich, Zurich, Switzerland[1], Department of Diagnostic and Interventional Radiology, University Hospital Zurich, University of Zurich, Zurich, Switzerland[2]

Introduction:
Sexual dimorphism in autonomic nervous control of the cardiovascular system is currently gaining increasing attention in the context of Takotsubo cardiomyopathy. Previous studies suggest that there are sex- and age-dependent differences in peripheral autonomic control, however, data on cardiac-specific sympathetic activation in elderly women and men are lacking.

Methods:
Regional quantitative analysis of cardiac fluorine-18 (^{18}F)-Dihydroxyphenylalanine (DOPA) uptake was retrospectively performed in 133 patients (69 females, mean age 52.4±17.7 years, range 1-84 years) referred for assessment of neuroendocrine tumours by Positron-Emission-Tomography.

Results:
Overall cardiac ^{18}F-DOPA uptake was significantly higher in women as compared to men (1.32±0.21 vs. 1.21±0.38, p=0.002). This sex-difference was most pronounced in the apical region of the left ventricle (LV, 1.28±0.27 in women vs. 1.13±0.27 in men, p=0.001) and in elderly individuals >55 years of age (1.39±0.25 in women vs. 1.12±0.29 in men, p=0.001). Women showed a prominent increase in myocardial ^{18}F-DOPA uptake with age (Pearson r=0.37, p=0.002) with the strongest increase seen in the LV apical region (r=0.41, p<0.001). Accordingly, sex and age were selected as significant predictors of LV apical ^{18}F-DOPA uptake in a stepwise linear regression model. No age-dependent changes of cardiac ^{18}F-DOPA uptake were observed in men (r=-0.01, p=0.9) or in the right ventricular (p=NS) region.

Conclusion:
Our study suggests that aging is related to sex-specific changes in regional cardiac sympathetic activity. The strong increase in LV apical ^{18}F-DOPA uptake with age in women may be related to mechanisms potentially accounting for the higher susceptibility of postmenopausal women to Takotsubo-cardiomyopathy.

4074

A. Figurek[1], K. Hübel[1], C. Oberkofler[2], O. De Rougemont[2], T. Müller[1]

The kidney donor profile index (KDPI) is associated with early kidney transplant function

Department of Nephrology, University Hospital Zurich[1], Clinic for Visceral and Transplant Surgery, University Hospital Zurich[2]

Introduction:
Transplant physicians increasingly face the dilemma of accepting or rejecting kidney offers that are less than optimal. Predictive scoring tools that maximize organ utilization without compromising outcomes are needed. For the US organ allocation system the kidney donor profile index (KDPI) has been developed to rank donor kidney quality in relation to long-term allograft survival. We have assessed the KDPI in relation to outcome markers of early kidney graft function.

Methods:
In a retrospective study the KDPI score was calculated using the following donors' characteristics: age, height, weight, ethnicity, history of hypertension, history of diabetes, cause of death, serum creatinine, HCV status and DCD criteria. All adult patients who received a deceased donor kidney in the year 2017 in our center were included. As outcome markers for early kidney function were analyzed: (a) need for dialysis, i.e. delayed vs. immediate graft function (DGF vs. IGF), (b) fall in creatinine from postoperative day 1 to day 2 (CRR2), (c) lowest observed serum creatinine during the first postoperative month (LoObsSCr_Mo1), and (d) difference between observed and expected serum creatinine (D obs vs. exp). Data were analyzed by descriptive statistics with p-values <0.05 considered as statistically significant.

Results:
Of the total of 74 adult kidney transplants 27% were DCD organs, 63% of all showed IGF and 37% DGF, requiring at least one postoperative dialysis treatment. (a) The mean KDPI was 51% for all deceased donor kidneys, 44% for kidneys transplanted to recipients with IGF and 63% for those with DGF, the difference being statistically significant ($p<0.01$). (b) KDPI did not correlate with the earliest creatinine fall (CRR2, $p=0.09$), however a trend towards a higher fall in organs with a low (<20%) vs. moderate (20 to 85%) vs. high KDPI (>85%) was seen. (c) The lowest KDPI organs showed the best creatinine values in the first month (LoObsSCr_Mo1, $r=0.6$, $p<0.001$). (d) In the patients who received the organs with the highest KDPI (>85%) the difference between observed and expected creatinine levels was significantly higher than in those with KDPI organs <85% (D obs vs. exp of 64 vs. 35 umol/l). In contrast to the KDPI scores donor demographic data alone did not differentiate the various early.

Conclusion:
The KDPI score is associated with early post-transplant kidney graft function and is useful to capture kidney organ quality, i.e. nephron mass and regenerative capacity.

4075

L. Isenegger[1], R. Zuber[1], P. Bode[2], T. Van Cann[3], C. Pauli[2], A. Wozniak[3], U. Camenisch[2], C. Matter[1], B. Bode[2], H. Moch[2], M. Manz[1], O. Shakhova[1], P. Schoeffski[3], C. Britschgi[1]

Therapeutic Targeting of Clear Cell Sarcoma

Department of Hematology and Oncology, University Hospital of Zürich, Zürich, Switzerland[1], Department of Pathology, University Hospital of Zürich, Zürich, Switzerland[2], Laboratory of Experimental Oncology, University of Leuven, Leuven, Belgium[3]

Introduction:
Clear cell sarcoma (CCS) is a rare aggressive soft tissue sarcoma. When localized it can be cured by surgery, however, local relapses and distant metastases develop frequently. CCS is notoriously unresponsive to chemotherapy, targeted therapy or immune checkpoint inhibition and there is consequently a highly unmet medical need for new therapies.
CCS is closely related to melanoma, both of which are neural crest derived malignancies. SOX10 is a therapeutic target in melanoma and we have recently shown that it binds to the WNT effector protein b-catenin and is suppressed by WNT activation in melanoma, which can be therapeutically exploited. The first aim of this project was therefore to establish, whether SOX10 serves as a therapeutic target in CCS, as well.
Second, we set out to perform an unbiased high-throughput drug screen using a candidate kinase modulator library to identify novel therapeutic options for CCS.

Methods:
SOX10 mRNA and protein expression in CCS cell lines were assessed by qPCR and Western Blotting, respectively. Primary patient biopsies were analyzed by IHC on the tissue micro-array (TMA) generated from the CCS samples of EORTC CREATE trial. To study the importance of SOX10 for cell survival, we performed shRNA-mediated knock-down experiments and assessed apoptosis (PI / Annexin-V co-staining). To assess the effect of WNT signaling activation, we treated CCS cell lines with CHIR-99021, an inhibitor of the negative regulator GSK3a/b.
The drug screen was performed in cooperation with NEXUS (ETH Zurich) using the ActiTarg-K library (960 candidate kinase modulators). Three different cell lines (two CCS, one control) were plated on 384-well plates, cultured for 24 hrs, followed by robot-assisted addition of the library compounds in two concentrations. Cells were then cultured for 72 hrs and cell survival was eventually assessed using a resazurin read-out.

Results:
Both SOX10 mRNA and protein are strongly expressed in CCS cell lines. Moreover, there is also strong expression in the majority of primary patient samples. CCS cell lines show reduced cell proliferation and apoptosis when SOX10 was knocked down by shRNA. However, as opposed to our findings in melanoma, pharmacologic activation of WNT using CHIR-99021 did not impact on survival of CCS cells *in vitro*.
We have successfully set up and performed the screen. Using 960 compounds at two concentrations, we screened six 384-well plates per cell line (18 plates overall). Positive (doxorubicin 10µM) and negative controls (DMSO) were included and the Z-score was calculated as a quality control measure. This was above 0.6 on all the plates indicating very good assay quality. We performed bioinformatic analyses to identify library compounds, which efficiently killed both of the CCS cell lines, but not the normal control cell line.

Conclusion:
We have shown that SOX10 is expressed in CCS, as well, and similar to melanoma it serves as a potential therapeutic target. However, activation of WNT signaling surprisingly does not reduce proliferation of CCS. We are currently investigating why this is case by performing further analyses of the WNT pathway in CCS. Eventually, a shRNA-dropout screen might be employed to identify genes that mediate resistance to WNT activation in CCS cells.Second, we have successfully performed the small molecule library screen and will next validate the compounds in vitro and in vivo. Moreover, we will aim at identifying the involved signaling pathways and hence biomarkers of response to the novel drug candidates.

4076

T. Fedele[1], J. Niediek[2], L. Stieglitz[1], P. Hilfiker[3], K. König[3], F. Mormann[2], J. Sarnthein[1]

Multi-unit activity underlies epileptic fast ripple EEG in the mesial temporal lobe

Neurosurgery Department, University Hospital Zurich, Switzerland[1], Department of Epileptology, University of Bonn, Germany[2], Swiss Epilepsy Centre, Zurich, Switzerland[3]

Introduction:
High frequency oscillations (HFO) in the pre-operative intracranial EEG are a promising biomarker of the epileptogenic zone. While HFO are detected in intracranial human recordings with macrocontacts, little is known about the concomitant neural activity at the microscale. To address this issue, we recorded from the human mesial temporal lobe of epilepsy patients implanted with depth electrodes and microwires.

Methods:
We correlated clinically relevant macro-HFO (m-HFO) and micro-HFO (µ-HFO) automatically detected in the ripple (80-250 Hz) and fast ripple (FR, 250-500 Hz) spectral range with the underlying neuronal spiking activity.

Results:
While µ-FR exhibited higher rate than m-FR, only a subset of µ-FR co-occurred with m-FR. Multiple scale dynamics revealed the presence of fast spiking units at the microscale that were highly synchronized with m-FR at the macroscale. Among the 213 isolated units (137 multi-unit, 70 putative principal cells, 6 interneurons), 92% exhibited a spike rate increase during m-FR. Firing occurred above 200 Hz and firing patters were locked to the phase of the m-FR.

Conclusion:
By bridging the gap across spatial scales in the high frequency interictal activity, we show the contribution of microscale neuronal action potentials to the generation of clinically relevant FR recorded in macroscale EEG.

4077

D. Sahin[1], N. Arenas-Ramirez[1], D. Zingg[2], L. Sommer[2], O. Boyman[1]

Mechanisms of adaptive resistance to cancer immunotherapy

Department of Immunology, University Hospital Zurich, University of Zurich, Zurich[1], Stem Cell Biology, Institute of Anatomy, University of Zurich, Zurich[2]

Introduction:
Cancer immunotherapy has demonstrated remarkable therapeutic efficacy in several metastatic diseases, proving the ability of the endogenous immune response to control tumor progression. Therapies targeting immune checkpoints, such as programmed cell death protein-1 (PD-1) , PD-ligand-1 and cytotoxic T lymphocyte associated protein-4 (CTLA-4), have shown a significant increase in anti-tumor T cell activities leading to cancer regression or even elimination. Nevertheless, tumor relapse is observed in many patients indicating an escape from immune-mediated control. The intense immune response leads to the dedifferentiation of tumor cells and decrease in immunogenicity, including the loss of expression of potent tumor antigens and downregulation of the antigen processing and presentation machinery. We recently described a role for the epigenetic modulator enhancer of zeste homolog-2 (Ezh2) in conferring resistance to immunotherapy. T cell accumulation and consequent tumor necrosis factor-a (TNF-a) production were shown to be the driving factors of Ezh2 upregulation. Previous studies on the effect of TNF-a in cancer progression and tumor immunology remain controversial. In the herein presented study we investigated the contribution of Ezh2 and TNF-a to the adaptive resistance of melanoma to immunotherapy.

Methods:
We used three different mouse models of melanoma, namely the transplantable B16-F10 and RIM-3 models and the spontaneous *Nras^{Q61K} Ink4a$^{-/-}$* transgenic mouse model. Mice were treated with anti-CTLA-4 or IL-2/NARA1 complexes (IL-2cx), and the mechanisms of immunotherapy-induced resistance were investigated. We assessed the plasticity of tumor cells upon Ezh2 inhibition and studied the synergy between immunotherapy strategies and Ezh2 blockade in tumor control. We then investigated the factors responsible for Ezh2 upregulation and explored interference with the strongest factor, TNF-a, in a combination strategy with immunotherapy.

Results:
Analysis of tumor cells post immunotherapy revealed that increased expression of the polycomb repressive complex-2 (PRC2) members, including Ezh2, strongly depended on the infiltration of leukocytes. The enhanced Ezh2 activity in tumor cells led to downregulation of several markers of melanocyte lineage together with genes involved in antigen processing and presentation. A screening of immune cell related soluble factors revealed TNF-a as a strong inducer of Ezh2 in melanoma cell lines. In vitro exposure of tumor cells to TNF-a led to dedifferentiation and silencing of the antigen presentation machinery in an Ezh2-dependent manner. This was in line with the increased TNF-a levels detected in the tumor microenvironment in mice receiving immunotherapy. Blockade of Ezh2 or TNF-a synergized with immunotherapy prolonging immune mediated tumor control.

Conclusion:
Our study demonstrates that intratumoral T cell accumulation and TNF-a production promotes Ezh2 upregulation in melanoma cells leading to immune resistance. Inhibition of Ezh2 or TNF-a remains therefore an attractive approach to combine with immunotherapy for the treatment of solid tumors.

4078

S. Angori[1], A. Kahraman[1], R. Ohashi[2], F. Prutek[1], S. Dettwiler[1], P. Schraml[1], H. Moch[1]

Chromosomal Profiling of papillary Renal Cell Carcinoma

Department of Pathology and Molecular Pathology, University Hospital Zurich, Zurich, Switzerland [1], Histopathology Core Facility, Niigata University Faculty of Medicine, Japan[2]

Introduction:
Renal cell carcinoma (RCC) refers to a heterogeneous group of cancers derived from renal tubular cells. Papillary renal cell carcinoma (pRCC) represents the second most common histologic subtype, accounting for about 15% of all renal cell cancers. pRCC is further subdivided into type 1 with single layered small cell and scanty cytoplasm and type 2 with large pseudostratified cells and eosinophilic cytoplasm. pRCC type II are more often associated with a higher tumor stage and grade, higher frequency of necrosis and sarcomatoid features with worse and more aggressive outcome. pRCC type 1 is characterized by chromosome 7 gains and mutations in the oncogene MET, while recent data indicated that pRCC type 2 consists of several subgroups characterized by genome stability (with only few chromosomal aberrations) and instability (with many chromosomal alterations, mainly deletions). Based on this molecular background, the aim of the project is a detailed molecular characterization of pRCC type 2 to uncover potential new molecular subgroups.

Methods:
Comprehensive molecular characterization of 60 formalin-fixed, paraffin-embedded tissue of pRCC type 2 tumor samples is performed using a copy number variations analysis with the OncoScan assay. In this analysis, thousands of probes map to a specific location on a genome, allowing to visualize copy number changes in each chromosome. A cohort of 13 pRCC type 1 patients is used as a control. pRCC samples have been selected according to a percentage of tumor cells higher than 45% using the Nexus Express Software for OncoScan .Whole Exome Sequencing (WES) will be used to detect gene mutations that point to tumor promoting pathways affected in pRCC type 2.
Comprehensive Tissue Microarray (TMA) data of RCC patients (collected from 1993 to 2013) are available to analyse the expression pattern of a defined protein set in all RCC subtypes and correlate the expression data with clinic-pathological parameters.

Results:
The copy number variation profiles of pRCC samples are defined by a multiple chromosomal gains. pRCC type 1 show more copy number gains in chromosome 7 (92%) and 17 (100%) than in pRCC type 2 (74% in both chromosomes). Chromosome 16 gain, however, is more predominant in pRCC type 2 (74%), than in pRCC type 1 (38%). A chromosome gain is also common in chromosome 3 (29% pRCC type 2, 15% pRCC type 1), in chromosome 12 (34% pRCC type 2, 15% pRCC type 1) and in chromosome 20 (43% pRCC type 2, 23% pRCC type 1). A copy number loss is identified only in chromosome X (62% of pRCC type 1 and 46% pRCC type 2).
TMA analyses showed higher HIF2α (Hypoxia-inducible Factor-2α), NEMO (NF-kappa-B essential modulator) and AREG (Amphiregulin) expression levels in pRCC type 2 than in clear cell RCC.

Conclusion:
Type 1 and type 2 pRCC are shown to have a similar CNV profile, including gains in chromosome 3, 7, 12, 16, 17 and 20 and a loss in chromosome X. Further investigation by WES and functional assay will be needed to further characterize subgroups among type 2 pRCCs and to explain their aggressive behaviour. It is conceivable that HIF upregulation is coordinated by NEMO in VHL non-affected pRCC type 2.

4079

T. Turk[1], N. Bachmann[1], C. Kadelka[1], J. Böni[2], S. Yerly[3], V. Aubert[4], T. Klimkait[5], M. Battegay[6], E. Bernasconi[7], A. Calmy[8], M. Cavassini[9], H. Furrer[10], M. Hoffmann[11], H. Günthard[1], R. Kouyos[1]

Assessing the danger of self-sustained HIV epidemics from phylogenetic cluster analysis

Division of Infectious Diseases and Hospital Epidemiology, University Hospital Zurich, Zurich; Institute of Medical Virology, University of Zurich, Zurich[1], Institute of Medical Virology, University of Zurich, Zurich[2], Laboratory of Virology, Geneva University Hospital, Geneva[3], Divisions of Immunology and Allergy, University Hospital Lausanne, Lausanne[4], Molecular Virology, Department Biomedicine - Petersplatz, University of Basel, Basel[5], Division of Infectious Diseases and Hospital Epidemiology, University Hospital Basel, Basel[6], Division of Infectious Diseases, Regional Hospital Lugano, Lugano[7], Division of Infectious Diseases, Geneva University Hospital, Geneva[8], Service of Infectious Diseases, Lausanne University Hospital, Lausanne[9], Department of Infectious Diseases, Bern University Hospital, University of Bern, Bern[10], Division of Infectious Diseases, Cantonal Hospital St. Gallen, St. Gallen[11]

Introduction:
Assessing the danger of transition of HIV transmission from a concentrated to a generalized epidemic is of major importance for public health. Although HIV transmission in Swiss heterosexuals has never led to a self-sustained epidemic, the unknown potential of imported infections either from abroad or from other transmission groups in Switzerland remains a large concern. We investigated how far from a self-sustained epidemic HIV transmission within Swiss heterosexuals is, and assessed its time trend and determinants.

Methods:
From a phylogenetic tree containing Swiss and background HIV sequences, we identified 3100 Swiss heterosexual transmission clusters (estimated infection dates between September 1980 and July 2014). The demographic characteristics of the individuals forming these clusters were extracted from the highly-representative Swiss HIV Cohort Study. To capture the incomplete sampling of HIV sequences, the delayed introduction of the imported infections to the Swiss heterosexuals network, and potential factors associated with higher basic reproductive number R_0, we extended the basic branching process model to infer transmission parameters.

Results:
Overall, the R_0 of HIV in Swiss heterosexuals was estimated to be 0.44 (95%-confidence interval 0.42 - 0.46). The model also showed that subtype B had lower R_0 (0.35) compared to non-B subtypes with the highest R_0 occurring for CRF02_AG (0.62), highlighting the heterogeneity between subtypes. When assessing the time trend, we found that R_0 was decreasing by 11% per 10 years (4% - 17%). The multivariate model revealed that non-B subtype, reported sex with occasional partners and longer time to diagnosis were significantly associated with larger R_0, while age and the earliest CD4 cell count did not exhibit significant effect.

Conclusion:
These findings indicate that there is no imminent danger of a self-sustained epidemic among Swiss heterosexuals, but rather diminishing HIV transmission far below the epidemic threshold. Generally, our approach allows to assess the danger of a self-sustained epidemic from any viral sequences.

4080

P. Helbling[1], S. Isringhausen[1], A. Gomariz-Carillo[1], U. Suessbier[1], T. Nagasawa[2], T. Yokomizo[3], M. Manz[1], C. Nombela-Arrieta[1]

Identification of key niche cell types supporting expansive extramedullary hematopoiesis in the fetal liver.

Hematology, University Hospital Zurich, Zurich[1], Kyoto University Hospital, Kyoto[2], Kumamoto University, Kumamoto[3]

Introduction:
Sustained production of mature blood cell types depends on the continuous self-renewal and differentiation of a rare subset of hematopoietic stem cells (HSCs). During adulthood HSCs are maintained in a specialized microenvironment within the bone marrow, called the stem cell niche. Specialized mesenchymal and endothelial cell types nurture and control HSCs partially by the local secretion of supportive cytokines. During early embryonic development, a small number of HSCs is generated from hemogenic endothelium. Subsequently, HSCs are massively expanded in the fetal liver and spleen to meet the growing demands of the developing embryo. The exposure to different anatomic microenvironments has been suggested to play a fundamental role in the regulation of HSCs and to adjust the extent of hematopoietic output. Our aim is to dissect the putative stromal cell subsets existing in the fetal and early postnatal liver and spleen, and determine their contribution to the hematopoietic microenvironment, HSC expansion and maintenance.

Methods:
We employed flow cytometry to analyze the identity and phenotypic characteristics of non-hematopoietic stromal components present in the fetal liver. To study the anatomical distribution of the different hematopoietic and non-hematopoietic cellular components, analyze the composition of HSC niches and quantify relevant cellular interactions we employed organ-wide 3D imaging technology of transgenic reporter mice. Finally, an extensive analysis of gene expression profiles of FACS sorted stromal cell populations was performed to infer mechanisms by which HSCs are extrinsically regulated.

Results:
The cytokine stem cell factor (SCF) and chemokine CXCL12 have both been implicated as regulators of blood stem cells. Using knock-in reporter mice, we determined the cellular subsets, which express these two factors in the fetal liver. SCF and CXCL12 are both contained in the stromal, non-hematopoietic compartment. Developing DLK1-positive hepatoblasts and CD140b-positive mesenchymal cells were characterized by a similarly strong expression of both factors, whereby a third stromal subset, endothelial cells, exhibited only low expression levels. Hepatoblasts showing a cuboidal morphology and the CD140b-positive mesenchymal cells displaying a fibroreticular morphology are uniformly scattered throughout the entire tissue without any obvious distribution bias. Of special interest gene expression analysis revealed that SCF gets strongly downregulated at late embryonic time points particularly in hepatoblasts, coinciding with a decline in extramedullary hematopoiesis in the liver.

Conclusion:
In summary, our preliminary results point towards a model, where a rapidly expanding hematopoietic system in the fetal liver is enabled by two putative niche populations, hepatoblasts and mesenchymal cells. A decrease in hepatoblast cell numbers, but also a declining expression of the essential cytokine Kitl accompanied by a rapidly differentiating epithelial tissue might induce a closing HSC niche, that forces hematopoiesis to move to the succeeding hematopoietic organs, the perinatal spleen and postnatal bone marrow.

4081

F. Meier-Abt*[1], S. Amon*[3], L. Gillet*[3], W. Wolski[4], S. Dimitrieva[4], A. Theocharides[2], M. Manz[2], R. Aebersold[3]

Transcriptome-Proteome Correlation in Human Hematopoietic Stem and Progenitor Cells

*these authors contributed equally; Division of Hematology, University and University Hospital Zurich, Zurich Switzerland[1], Division of Hematology, University and University Hospital Zurich, Zurich, Switzerland[2], Department of Biology, Institute of Molecular Systems Biology, ETH Zurich, Zurich, Switzerland[3], Functional Genomics Center Zurich (FGCZ), University of Zurich, ETH Zurich, Zurich, Switzerland[4]

Introduction:
Hematopoietic stem cells (HSCs) can self-renew and/or differentiate into various functionally divergent progenitor cell types, such as common myeloid progenitors (CMPs), megakaryocyte-erythrocyte progenitors (MEPs) or granulocyte-macrophage progenitors (GMPs). When the process of self-renewal and differentiation is altered, e.g. upon genetic or epigenetic changes in HSCs, abnormal (pre)leukemic stem cell subpopulations may form, eventually resulting in the onset of hematological malignancies. To gain insight into the physiology and subsequent patho-physiology of self-renewal and differentiation, highly refined analyses of HSCs and downstream progenitor cells are needed.

Methods:
We developed an ultra-sensitive mass spectrometric method for robust quantitative proteomic analysis of highly purified, FACS-sorted cell populations and applied this method to quantify the proteome of 25'000 human hematopoietic stem and progenitor cell subpopulations isolated from five healthy donors. The proteomic analyses were complemented by transcriptomic analyses.

Results:
A comparison of proteomic and transcriptomic profiles of the respective cell types indicated hematopoietic stem/multipotent progenitor cell-specific divergent regulation of biochemical processes essential for maintaining stemness at the proteome rather than transcriptome level. Specifically, several telomerase complex proteins and quiescence-inducing isocitrate dehydrogenase proteins, both assumed to be essential for long-lived stem cells, were found to be upregulated in HSCs on the protein but not on the mRNA level when compared to myeloid progenitor cell subpopulations (CMPs, MEPs, GMPs).

Conclusion:
The divergent mRNA/protein regulation of telomerase complex and quiescence-inducing isocitrate dehydrogenase proteins in HSCs illustrates the relevance of generating high quality proteomic data for well-defined cell subpopulations with the goal to identify biological processes that are insufficiently determined by genomic or transcriptomic analyses. The presented approach is expected to increase our understanding of the dynamics of cell type-specific networks and to complete our knowledge on differentiation processes in healthy and pathological cells. It opens the door for proteomic profiling of disease sample sub-fractions such as (pre)leukemic stem cells in chronic and acute leukemias as well as cancer stem cells from solid tumors and ultimately might allow to find therapeutic targets in (pre)leukemic/cancer stem cells.

4082

H. Honcharova-Biletska[1], M. Egger[1], F. Bohm[1], Y. Boege[1], M. Healy[1], J. Schmidt[1], S. Comtesse[1], R. Davis[2], M. Heikenwalder[3], A. Weber[1]

A role of JNK signaling for biliary tract formation

Pathology, University Hospital Zürich[1], Howard Hughes Medical Institute and Program in Molecular Medicine, University of Massachusets Medical School, Worcester, MA 01605, USA[2], Institute of Chronic Inflammation and Cancer, DKFZ, Heidelberg, Germany[3]

Introduction:
The purpose of the present study was to determine the role of JNK signaling in liver parenchymal cells (LPC). We hypothesized JNK signaling to be crucial not only in hepatocytes but also in cholangiocytes. Moreover, we hypothesized that lack of Jnk1/2 in LPC of $Mcl1^{Dhep}$ murine model of chronic liver injury and hepatocarcinogenesis reduces tumor incidence.

Methods:
Mice were generated with a simultaneous conditional knock out of Jnk1 and Jnk2 under the albumin promoter ($Jnk1/2^{Dhep}$ mice). $Jnk1/2^{Dhep}$ mice were intercrossed with $Mcl1^{Dhep}$ mice to generate $Mcl1^{Dhep}$ $Jnk1/2^{Dhep}$ mice. All mice were analyzed by liver histology, immunohistochemistry, RNA in situ hybridization and liver enzyme function (alanine aminotransferase, aspartate aminotransferase, alkaline phosphatase).

Results:
LPC-specific knock out of JNK1/2 leads to the formation of biliary cysts with surrounding fibrosis, resembling human liver cyst diseases of the ductal plate malformation complex. LPC-specific knock out of JNK1/2 in a hyper-apoptotic, hyper-regenerative background ($Mcl1^{\cdot hep}Jnk1/2^{\cdot hep}$ mice) results in more severe biliary cyst formation and pronounced fibrosis. In contrast, the incidence of hepatocellular carcinoma in $Mcl1^{\cdot hep}Jnk1/2^{\cdot hep}$ mice compared to $Mcl1^{\cdot hep}$ mice is significantly reduced by JNK1/2 deficiency.

Conclusion:
Our findings demonstrate that JNK1/2 signaling is important for regular biliary duct development, and plays a substantial role in modulating of hepatocarcinogenesis.

4083

V. Lintas[1], E. Fioretta[1], P. Dijkman[1], E. Caliskan[3], H. Rodriguez[4], N. Cesarovic[5], S. Hoerstrup[2], M. Emmert[4]

Human cell derived off-the-shelf Tissue Engineered Heart Valves for next generation Transcatheter Aortic Valve Replacement: a proof-of-concept study in adult sheep

Institute for Regenerative Medicine, University of Zurich, Zurich[1], Institute for Regenerative Medicine, University of Zurich, Zurich[2], Clinic for Cardiac Surgery, University Hospital Zurich, Switzerland[3], Herz- und Gefäßchirurgie, Universitätsspital Zürich (USZ), Zürich[4], Division of Surgical Research, University Hospital, Zurich[5]

Introduction:
In the past decade transcatheter valve replacement technologies have remarkably evolved and are in the process to be extended to intermediate and lower risk patients. Nonetheless, all current bioprostheses used for such approaches are predisposed to tissue deterioration and calcifi cation, hence limiting their durability. Transcatheter based tissue engineered heart valves (TEHVs) may overcome these limitations and may thus represent a next generation transcatheter aortic valve replacement (TAVR) concept facilitating lifelong valve substitutes. After the promising outcomes of such TEHVs in the pulmonary position, we here report the proof-of-concept of novel off-the-shelf transcatheter aortic TEHVs using a state-of-the- art, anatomically orienting delivery system.

Methods:
Off-the-shelf TEHVs derived from human fibroblasts were cultured in a bioreactor, decellularized and sewn onto anatomically orienting TAVR systems (JenaValve, Irvine, US). The valves were implanted transapically into sheep (n=3) and tested for acute functionality including angiography and transesophageal echocardiography. Thereafter they underwent macroscopy and histological assessment. 3D CT reconstruction of the TEHV positioning within the aortic root was performed post-mortem.

Results:
Valve delivery and deployment were successful in all animals. Upon implantation, angiography demonstrated correct positioning and good acute functionality. Echocardiographic examination displayed sufficient valve function with proper leaflet mobility, satisfactory coaptation with a mild-to-moderate insufficiency and negligible paravalvular leak. At explantation, the valves showed intact pliable leaflets without thrombi or crimping damages. Histology revealed a dense collagenous matrix with scaffold residuals.

Conclusion:
This proof-of-concept study showed good and encouraging initial performance of our novel off-the-shelf TEHVs as aortic valve replacements. Further in-vitro functionality tests and chronic animal studies are underway to validate these findings. Once proven its long-term efficacy, this technology could serve as a basis to provide next generation regenerative aortic valve substitutes for younger patient populations.

4084

P. Cheng[1], S. Freiberger[3], N. Pornputtapong[3], A. Irmisch[1], M. Khan[5], R. Halaban[4], R. Dummer[1], P. Wild[2], M. Krauthammer[3], M. Levesque[1]

Melarray - a new sequencing platform for detecting genomic mutations and copy number changes in melanoma

Dermatologische Klinik, Universitätsspital Zürich, Zürich[1], Pathologie, Universitätsspital Zürich[2], Department of Pathology, Yale University School of Medicine, CT, 06511 New Haven, USA[3], Department of Dermatology, Yale University School of Medicine, 06520 New Haven, USA[4], Department of Molecular Cellular and Developmental Biology, Yale University, New Haven, USA[5]

Introduction:
Novel immune checkpoint inhibitors and targeted therapies have remarkably improved progression-free and overall survival in patients with metastatic melanoma. For therapy stratification, detection of specific mutations is needed. Commercially available gene panels cover the most frequently mutated genes in melanoma (*BRAF*, *NRAS*, *KIT*, *GNAQ*, *GNA11*). However, additional genes can be useful to stratify patients for specific clinical trials, off-label or compassionate therapy, and as prognostic markers. Therefore, we designed a gene panel covering 190 genes that play a specific role in melanoma. Our target capture design ("MelArray") covers over 4000 exons and 28 introns and includes inter-genic probes covering heterozygous SNPs for accurate estimation of CNVs.

Methods:
We have established a complete protocol consisting of DNA capture of normal and tumor cells, Illumina sequencing and intensive bioinformatics post processing to detect somatic SNVs, copy number alternations and canonical fusion breakpoints in melanoma. Our pipeline further extrapolates the number of exome-wide mutations for estimation of total tumor mutation burden, a recognized marker of immunotherapy response.

Results:
In this paper, we discuss the deployment of the MelArray platform at two institutions (Yale University, University of Zurich) and the sequencing of 83 patient samples with additional 43 samples representing repeat biopsies within the same patient. We validated our results using (a) Sanger sequencing for melanoma hotspot mutations in BRAF and NRAS, (b) Foundation Medicine panel sequencing for pan-cancer driver mutations, (c) sequencing of low-abundance synthetic sequences for subclonal mutations, and (d) whole exome sequencing for exonic mutations and the prediction of total mutation burden.

Conclusion:
Our results demonstrate MelArrays's high accuracy across the tested mutation types, it's ability to determine key MAPK drivers in triple WT melanomas, and it's usefulness for mapping patients to available targeted therapies. As such, we envision that MelArray can be broadly used across institution as a diagnostic tool to stratify patients for specific therapies or clinical studies according to their mutational profile.

4085

M. Gualandi[1], A. Serra Roma[1], C. Yang[1], A. Baggiolini[2], L. Sommer[2], O. Shakhova[1]

Dissecting the cellular origin of neuroblastoma: Characterization of new progenitor cell populations in the sympathetic nervous system.

Deparment of Oncology, University of Zürich, Zürich[1], Institute of Anatomy, University of Zürich[2]

Introduction:
Neuroblastoma (NB) is a pediatric cancer of the sympathetic nervous system, which occurs almost exclusively in infancy and early childhood. It is widely assumed that oncogenic mutations occur in the cells of sympathoadrenal (SA) lineage during prenatal and postnatal life, however, the exact cell of origin has not been characterized yet. The targeted expression of *ALK^{F1174L}* and *MYCN* oncogenes driven by a *tyrosine hydroxylase* or a *dopamine beta-hydroxylase* promoter results in NB development. However, these mouse models fail to faithfully recapitulate human NB. Indeed, there is a lack of schwannian stroma, only minimal metastasis formation, failure of mimicking the spontaneous regression and the onset of disease does not correspond to the pediatric characteristic of this tumor. A possible explanation for these discrepancies might be the fact that the oncogene expression is induced in progenitor cells rather than in stem cell population. Taken together, these data suggest that there is a strong need to develop more accurate mouse models of NB development and therefore, a comprehensive analysis of the cellular hierarchy within SA lineage is a first step to understand the origin of NB.

Methods:
In order to identify the cellular origin of NB, we used several Cre mouse lines where Cre expression is driven by promoters of genes that are expressed at different timepoints of differentiation. Through recombination is allowed population-specific transcription of *rosa26/tdTomato* reporter, or oncogenes as *rosa26/MYCN* and rosa26/*ALK^{F1174L}*.

Results:
First, we used a lineage tracing approach to fate-map different SA and glial progenitors and to quantify their contribution to the different derivatives, such as chromaffin cells, sympathetic neurons, and glia. Our findings pointed out a fixed hierarchy in development of sympathetic neurons and chromaffin cells, which occurred in different stages of organ maturation from different multipotent progenitor populations. Furthermore, we fate–traced uniquely the Schwann progenitors cells (SPCs) in different organs of the sympathetic nervous system. We described that Schwann-derived gliogenesis differed in an organ-specific fashion in embryo and demonstrated that neurogenesis could occur in the Schwannian lineage, although with a minor contribution. Furthermore, we identified Lgr5 expression, among SA derivatives, as a new and unique marker of chromaffin cells. Finally, we proved that expression of *ALK^{F1174L}* or *MYCN* in neural crest stem cells and in SPCs did not result in NB formation.

Conclusion:
This comprehensive study significantly improved understanding of the cellular origin of NB, since it covered different controversial topics in developmental biology of the SA lineage and connected it with NB tumorigenesis. Contrasting what was suggested previously, we proved that migrating neural crest stem cells could not be the cellular origin of NB *in vivo*. Fate-tracing of the different progenitors pointed out two interesting multipotent populations that are present after neural crest migration at the beginning of SA differentiation, but not committed yet to such fate. Oncogenes expression in such cells will show if at this stage NB can arise.

4086

M. Baláz[3], E. Luca[6], M. Yalcinkaya[1], M. Cardner[2], S. Goetze[3], L. Rohrer[1], J. Hartung[4], U. Landmesser[4], G. Liebisch[5], B. Wollscheid[3], N. Beerenwinkel[2], J. Krützfeldt[6], C. Wolfrum[3], A. Von Eckardstein[1]

A Systems Biological Approach to the Anti-Diabetogenicity of High Density Lipoproteins

Universitätsspital Zürich[1], BSSE, ETHZ Basel[2], HEST, ETHZ Zürich[3], Department of Cardiology, University Medicine Charité Berlin, Germany[4], Institute of Clinical Chemistry, University of Regensburg, Germany[5], Department of Endocrinology and Diabetology; University and University Hospital of Zurich[6]

Introduction:
Low blood levels of HDL-cholesterol increase the risk of diabetes mellitus type 2 (T2DM). HDL particles exert several potentially anti-diabetic activities but neither their relative importance nor their mediators are known. Understanding of these structure-function-disease relationships is essential to exploit HDL for prevention and treatment of T2DM.

Methods:
We isolated HDL particles from the plasma of 25 healthy subjects and 47 patients with T2DM to characterize their protein and lipid abundances by mass spectrometry as well as their functionality towards cells relevant for the pathogenesis of T2DM. We recorded the ability of HDL to inhibit the apoptosis of pancreatic beta cells, to modulate mitochondrial respiration in brown adipocytes and to regulate mitochondrial potential as well as phosphorylation of Akt and Acetyl-CoA carboxylase in myocytes.

Results:
The data on clinical and anthropometric features of the patients, the protein and lipid composition as well as functionality of HDL are integrated to identify components and functions, which differentiate HDL of patients and controls.

Conclusion:
Structural components of HDL that best discriminate patients and controls as well as function and dysfunction of HDL will be followed-up by experimental and clinical studies to unravel their mechanism and clinical utility as biomarkers, respectively.

4087

I. Grgic[1], N. Borgeaud[2], A. Gupta[2], PA. Clavien[2], M. Guckenberger[1], R. Graf[2], M. Pruschy[1]

Tumor reoxygenation and image-guided SBRT for the treatment of hypoxic tumors

Department of Radiation Oncology, University Hospital, Zurich[1], Department of Visceral and Transplant Surgery,Swiss HPB (Hepato-Pancreatico-Biliary) Center, University Hospital Zurich[2]

Introduction:
Reactive oxygen species are generated in response to ionizing radiation (IR) and produce amongst others irreversible DNA double-strand breaks. This IR-induced cytotoxic effect is less abundant under hypoxia and thus hypoxic cells are more resistant to IR. Hence, reoxygenation of the hypoxic tumor fraction by a combined treatment modality with a pharmaceutical agent is of high interest to reduce the required dose of IR and thereby to further minimize normal tissue toxicity. Here we investigated the combined treatment modality of the novel anti-hypoxia compound myo-inositol trispyrophosphate (ITPP) in combination with IR for the treatment of murine colorectal liver metastases.

Methods:
ITPP was developed as an effector of hemoglobin lowering the oxygen/hemoglobin affinity thereby resulting in an enhanced release of oxygen e.g. in hypoxic tumors. ITPP's capability for tumor reoxygenation was serially probed by a non-invasive hypoxia-directed ODD-luciferase-based bioimaging approach and by immunohistochemistry. Tumor growth delay was determined on treatment with ITPP and a single high dose fraction of IR in subcutaneous tumor models (FaDu, A549, MC38) and an orthotopic colorectal liver metastases tumor model. Tumor volumes were probed by caliper measurements (subcutaneous tumors) and by serial MRI (orthotopic tumors). Tumor detection and irradiation were performed by contrast-enhanced CT and a small animal radiotherapy platform, respectively.

Results:
Using our *in vivo* bioimaging approach, we confirmed increased pO_2 starting 2 hours after ITPP application. Dose-titration studies indicated that administration of ITPP at a maximal tolerable dose of 3g/kg on two consecutive days followed by immediate irradiation 2 hours after the second application of ITPP was optimal for maximal tumor response. Interestingly, ITPP alone did not affect the growth of tumor xenografts but significantly sensitized the tumor to IR in all tested tumor models. Immunohistochemical analysis of γH2AX foci demonstrated increased IR-induced DNA damage within hypoxic tumor regions after combined treatment with ITPP as compared to IR alone. Furthermore, IR-induced tumor hypoxia observed at 4 days after IR was associated with a decrease in tumor vascular density and pericyte coverage, which was prevented by combined treatment with ITPP. With IR-dose-titration experiments to orthotopic colorectal liver metastases, limiting single-doses of IR with tolerable toxicities could be defined, which are currently combined with ITPP as part of efficacy-oriented experiments using CT-based-image-guided radiotherapy.

Conclusion:
Here we demonstrated that the combined treatment modality of ITPP and IR results in a supra-additive tumor growth delay in multiple tumor models, which is most probably linked to neoadjuvant tumor reoxygenation and subsequently increased IR-induced DNA-damage and cell killing. Overall, our results support the strong rationale to combine ITPP with hypofractionated radiotherapy for hypoxic tumors.

4088

S. Ehrbar[1], A. Jöhl[2], M. Kühni[2], M. Meboldt[2], E. Ozkan Elsen[3], O. Goksel[3], Ch. Tanner[3], S. Klöck[1], J. Unkelbach[1], M. Guckenberger[1], S. Tanadini-Lang[1]

DELPHI: Dynamically deformable liver phantom for real-time adaptive radiotherapy treatments

Department of Radiation Oncology, University Hospital Zurich and University of Zurich, Zurich[1], Product Development Group Zurich, Department of Mechanical and Process Engineering, ETH Zurich, Zurich[2], Computer Vision Laboratory, Department of Information Technology and Electrical Engineering, ETH Zurich, Zurich[3]

Introduction:
Real-time adaptive radiotherapy of intrahepatic tumors needs to account for motion and deformations of the liver and therefore changes of the target location within the host organ. Phantoms representative of anatomical deformations are required to investigate and improve dynamic treatments.

Methods:
An artificial liver with vascular structures was casted from soft silicone mixtures with radiographic and ultrasonic contrast. An actuator was used for compressing the liver in inferior direction according to a prescribed respiratory motion trace. Electromagnetic (EM) transponders integrated in our dynamically deformable liver phantom help provide ground truth motion traces. They were used to quantify the motion reproducibility of the phantom and to validate motion tracking based on ultrasound imaging. Ultrasound motion tracking was based on following the vascular structures in the ultrasound image plane. A two-dimensional ultrasound probe was mounted on the phantom surface and the position of one vessel was followed with a template-matching algorithm. To quantify the accuracy of ultrasound motion tracking, the vessel position was compared to the EM transponder position by calculating the root-mean square error (RMSE).
The phantom was also used to investigate the dose deposition of dynamic treatment deliveries. Two dosimetry systems, radio-chromic film and plastic scintillation dosimeters (PSD), were integrated in the phantom. The PSD allow for time-resolved measurement of the delivered dose, which can be compared to a time-resolved dose of the treatment planning system. Both, film and PSD, were used to investigate dose delivery to the deforming phantom without motion compensation and with treatment-couch tracking for motion compensation.

Results:
The phantom showed a high reproducibility with a submillimeter RMSE. The motion of the vasculature detected with ultrasound agreed with the EM transponder position with a RMSE below 1 mm. The agreement of the planned and measured PSD dose decreased with increasing motion amplitude. The RMSE for a motion amplitude of 8, 16 and 24 mm was 1.2, 2.1 and 2.7 cGy/s, respectively. With couch tracking as active motion compensation, these values decreased to 1.1,1.4 and 1.4 cGy/s. This is closer to the static situation, with a RMSE of 0.7 cGy/s. In film measurements, the mean dose to the target was reduced by 41% for an internal motion amplitude of 24 mm compared to a static situation. Couch tracking was able to compensate for this motion. In the motion-compensated case, the mean dose was within 5% of the static situation.

Conclusion:
The developed liver phantom features multi-modality image contrast, realistic breathing-induced motion and deformation, and includes a time-resolved dosimetry system. The presented phantom was therefore suitable for quality assurance of real-time adaptive radiotherapy.

4089

H. Wirsching[1], J. Richter[2], F. Sahm[5], C. Morel[1], N. Krayenbühl[3], E. Rushing[4], A. Von Deimling[5], A. Valavanis[2], M. Weller[1]

Preoperative embolization of meningioma: inferior neurological outcome, increased risk of cardiovascular complications and shorter time to recurrence?

Department of Neurology and Brain Tumor Center, University Hospital Zurich and University of Zurich, Zurich[1], Department of Neuroradiology, University Hospital Zurich, Zurich[2], Department of Neurosurgery, University Hospital Zurich, Zurich[3], Department of Neuropathology, University Hospital Zurich, Zurich [4], University Hospital Heidelberg and Clinical Cooperation Unit Neuropathology, German Consortium for Translational Cancer Research (DKTK), German Cancer Research Center (DKFZ), Heidelberg[5]

Introduction:
Clinical outcomes of meningioma resection with respect to pre-operative embolization have not been studied in detail.

Methods:
All patients undergoing resection of an intracranial meningioma at the University Hospital Zurich 2000-2013 (N=741) were reviewed for the inclusion of pre-operative embolization in the management strategy. Annotations included demographics, radiographic, surgical, histological and hematological parameters, cardiovascular risk factors, pre- and postoperative neurological function and gene methylation-based classification. Binary regression and Cox proportional hazards models were applied to determine factors associated with outcome.

Results:
Pre-operative embolization was performed in 337 patients (42%). The decision for embolization was associated with larger tumor size and peritumoral edema. On multivariate analyses controlling for these and other established prognostic factors, pre-operative embolization was associated with inferior post-operative neurological outcome (odds ratio [OR] 1.85, 95% confidence interval [CI] 1.30-2.63), whereas gross total resection was associated with better neurological outcome (OR 0.59, 95% CI 0.39-0.87). Cardiovascular events after surgery comprised mostly deep vein thrombosis (N=39) and pulmonary embolisms (N=64). There were also associations with embolization (OR 2.38, 95% CI 1.37-4.00), and with female gender (OR 2.18, 95% CI 1.17-4.08). Recurrence-free survival (RFS) of embolized patients was less favorable among patients with WHO grade II or grade III meningiomas (median RFS: 4.3 versus 7.0 years, p=0.029) or in patients with intermediate or malignant gene methylation subtype meningiomas (median RFS: 2.0 versus 8.2 years, p=0.005).

Conclusion:
Pre-operative meningioma embolization may cause adverse surgical outcomes. Randomized trials to determine benefit-risk ratios are warranted to clarify the role of pre-operative embolization for meningioma surgery.

4090

E. Krajnc[1], Z. Gai[1], M. Visentin[1], GA. Kullak-Ublick[1]

Nefazodone effects on aerobic and anaerobic ATP production in liver cells

Department of Clinical Pharmacology and Toxicology, University Hospital Zürich and University of Zurich, Rämistrasse 100, 8091 Zurich, Switzerland[1]

Introduction:
Nefazodone is very effective antidepressant drug by inhibiting serotonin and norepinephrine reuptake. The originator Bristol Mayer Squib withdrew this drug from USA market in 2004, because of serious liver side effects and the end of patent time. Nefazodone-induced hepatotoxicity is considered to be, at least in part, due to inhibition of oxidative phosphorylation (complex I and IV) (Dykens et al. 2008). Other pathways might be affected by nefazodone exposure and contribute to the toxicity.
The aim is to elucidate the mechanism of nefazodone-induced hepatotoxicity and investigate possible protective strategies.

Methods:
All experiments were performed after two hours treatment with nefazodone. ATP content and cell viability were assessed in human liver carcinoma cell line Huh7 and in human primary cultured hepatocytes by CelltiterGlo and alamarBlue, respectively. Metabolites were measured by liquid chromatography/ mass spectrometry (LC-MS). Oxygen consumption rate and extracellular acidification rate were monitored with Seahorse instrument.

Results:
Untargeted global metabolomics assay with LC-MS showed significant changes in energy metabolism (e.g. citric acid cycle, glycolysis, gluconeogenesis and branched chain amino acid pathway). ATP production in Huh7 cells was mainly dependent on anaerobic glycolysis (~70-80%) and only partially on oxidative phosphorylation (~20-30%). Nefazodone exposure did not affect cell viability, but it fully depleted ATP intracellular content in a dose-dependent manner (IC_{50}= 57.8µM, 95% CI= 50.4 to 66.4), indicating that nefazodone could block both anaerobic glycolysis and oxidative phosphorylation. When Huh7 cells were cultured in absence of glucose, the ATP production was exclusively dependent on oxidative phosphorylation. In this experimental setting (no glucose) Huh7 cells were more sensitive to nefazodone, than in regular growth medium conditions (D-glucose 2g/l) (IC_{50}= 9.2µM, 95% CI=8.6-9.9), suggesting that nefazodone targeted oxidative phosphorylation at a lower concentration, and anaerobic glycolysis at a higher concentration. Similarly, primary cultured human hepatocytes, which rely on oxidative phosphorylation to produce ATP, were more sensitive than Huh7 cells to nefazodone (IC_{50}=3.5µM, 95% CI=3.0-4.1). Oxygen consumption rate (OCR) and extracellular acidification rate (ECAR) can be considered reliable readout of oxidative phosphorylation and anaerobic glycolysis, respectively. Huh7 cells exposed to low concentrations of nefazodone (10-50µM) showed reduced OCR and no changes in ECAR. At higher concentrations of nefazodone (100-400µM), a drop in ECAR was also observed. The activation of the Farnesoid X Receptor (FXR), a major regulator of liver metabolism, could protect Huh7 cells from nefazodone-induced ATP depletion only in glucose containing medium (four fold), suggesting the protective effect was at the anaerobic glycolysis level.

Conclusion:
To conclude, nefazodone depleted ATP production by blocking oxidative phosphorylation and anaerobic glycolysis. Such dual inhibition might contribute to liver toxicity *in vivo*. FXR activation to protect from nefazodone-induced hepatotoxicity might be further studied *in vivo*.

4091

K. Airich[1], K. Luk[1], D. Pease[1], M. Emmenegger[1], A. Aguzzi[1], S. Hornemann[1]

High-throughput small RNA screens to identify modifiers of alpha-synuclein aggregation

Neuropathology, University Hospital of Zurich, Zurich[1]

Introduction:
Synucleinopathies, including Parkinson Disease and Lewy body dementia, belong to the family of neurodegenerative diseases and are hallmarked by the intracellular accumulation of aSyn amyloid fibrils. The molecular mechanisms and pathways underlying aSyn aggregation and aggregate spreading between cells are still poorly understood. Aggregate formation can however be induced in cellular model systems. Cells are transduced with exogenously produced pre-formed fibrils (PFF), which serve as a template for triggering the intracellular aggregation of endogenous aSyn into pathological hyperphosphorylated species. With the aim identifying genes involved in αSyn aggregation and pathology, we combined the cell-based model that best recapitulates human synucleinopathies with the latest methodology in automation to perform unbiased high-throughput RNA interference (siRNA) and microRNA (miRNA) screens.

Methods:
We first established a cell-based aggregation assay based on PFF induced transduction that results in hyperphosphorylated aSyn aggregates. We then transferred the protocol of the assay to a robotic platform for automation and optimized all steps for the high-content siRNA and microRNA screens. The assay is performed in 384 multiwell plates and its workflow comprises the following four main steps: (i) Precoating of the plates; (ii) printing of the small RNA libraries; (iii) Lipofectamine mediated reverse transfection of the RNAs into aSyn overexpressing cells followed by PFF transduction; and (iv) single cell detection and quantification of hyperphosphorylated αSyn aggregates using automated, quantitative immunofluorescence microscopy.

Results:
Our final protocol revealed uniform seeding across all wells, allowing reliable detection of de novo formed hyperphosphorylated αSyn aggregates. In this set-up simultaneously scanned 348-well plates showed uniformly distributed immunofluorescence across cells positive for hyperphosphorylated αSyn aggregates and allowed a direct comparison to previously validated controls (e.g. knock-down of αSyn by siRNAs). This automated image-based quantification of phosphorylated αSyn aggregates revealed an intense signal and a very high signal to noise ratio, which are prerequisites for accurate high content image analysis. We successfully tested our platform in a pilot screen with the aim to identify new miRNA targeting aSyn as well as confirming miRNAs involved in regulating PD relevant proteins, thereby serving as a first proof of concept for our siRNA screen. Identified hits from the miRNA screen will be compared with the results obtained from the genome-wide siRNA screen in which mediated changes in aggregate formation might directly be picked up.

Conclusion:
The effective adaptation of the cell-based model of αSyn pathology towards an automated protocol is applicable for high-throughput screenings and is convenient for high quality data acquisition in an unbiased manner. The successful development of this platform will now allow performing genome-wide RNA screens to discover new modifiers and pathways that control the molecular mechanism of αSyn aggregation as well as to identify novel molecular targets with therapeutic potential.

4092

P. Beeler[1], M. Cheetham[1], E. Battegay[1]

Depression is independently associated with an increased length of stay in hospitalized patients

Klinik und Polyklinik für Innere Medizin, UniversitätsSpital Zürich[1]

Introduction:
Depression as a comorbidity reduces therapeutic success and impairs clinical outcomes, e.g. in patients with chronic obstructive pulmonary disease (doi:10.1183/16000617.0026-2017). We investigated whether depression is associated with a longer length of stay (LOS) among a broad range of hospitalized patients with various conditions.

Methods:
We analyzed 287,255 inpatient stays (aged 18-105, discharged August 1, 2009-August 31, 2017) from all clinical units of the University Hospital Zurich. We used multivariable linear regression modelling to analyze a possible association between depression and increased LOS. The model was adjusted for age, gender, marital status, in-hospital mortality, and the total number of diagnoses; depression and potential confounders (Atrial fibrillation, cancer [including metastatic, non-metastatic cancer and lymphoma], chronic heart failure, chronic kidney disease, diabetes) were identified using the validated ICD-10 code definitions by Tonelli et al. (doi:10.1186/s12911-015-0155-5).

Results:
The 287,255 stays featured a median of 5 coded diagnoses (IQR 3-8), of these stays 14,409 (5.0%) featured a depression diagnosis. Overall, the median inpatient age was 56 (IQR 37-70), the median LOS was 5 days (IQR 3-9), 50.6% of stays concerned females, and 53.6% of patients were married or had a partner. Over the course of the hospitalization died 2.4% of patients.
The unadjusted linear regression model showed a LOS increased by 6.07 days (95% CI: 5.90 to 6.24) due to depression. However, the adjusted model (Table 1) showed that depression was independently associated with a 2.26-day (95% CI: 2.11 to 2.41) increase of LOS ($p<0.0001$), and the number of diagnoses was the strongest confounding factor ($p<0.0001$). In that model, cancer was a further condition associated with a substantially increased LOS ($p<0.0001$).

Table 1. Multivariable linear regression to investigate the association of depression with longer LOS.

Variable	Estimate (number of days)	95% CI
Depression	2.26	(2.11 to 2.41)
Number of diagnoses, per additional diagnosis	1.22	(1.21 to 1.23)
Patient died in hospital	-1.97	(-2.18 to -1.76)
Age, per additional year	-0.02	(-0.02 to -0.02)
Female gender	0.19	(0.12 to 0.25)
Marital status		
Married/partnered	ref	
Other/unknown	-0.3	(-0.5 to -0.1)
Single	0.11	(0.02 to 0.19)
Widowed/divorced/separated	-0.04	(-0.12 to 0.05)
Atrial fibrillation	-1.27	(-1.48 to -1.06)
Cancer	0.68	(0.58 to 0.78)
Chronic heart failure	-1.61	(-1.75 to -1.47)
Chronic kidney disease	-1.08	(-1.19 to -0.98)
Diabetes	-1.99	(-2.1 to -1.89)

Conclusion:
We found that depression was independently associated with an increased LOS among a broad range of hospitalized patients with various conditions. This has important clinical and health economic implications. Firstly, our results suggest that screening for and firm treatment of depression may be crucial for all hospitalized patients, since this may significantly improve well-being and accelerate recovery of patients. Secondly, increased duration of hospital stays induce additional costs. And finally, this study further highlights the importance of multimorbidity expertise and research.

4093

E. Boran[1], T. Fedele[1], L. Stieglitz[1], P. Hilfiker[2], T. Grunwald[2], J. Sarnthein[1]

Persistently active neurons in human hippocampus support verbal working memory network.

USZ Neurochirurgie[1], Epi-Klinik[2]

Introduction:
Sustained neural activity has been proposed as a mechanism for verbal working memory maintenance. Maintenance relies on a widespread network of brain areas, but the areas and their roles remain unclear.

Methods:
While subjects maintained sets of letters in memory, we recorded single neurons and local field potentials in the human medial temporal lobe, and EEG from the scalp.

Results:
In the hippocampus, neural activity was specific for workload and task condition. Trial-by-trial variability in neuronal firing predicted the accuracy of memory recall. The task modulated the theta/alpha synchronization between hippocampus and cortical areas.

Conclusion:
This manifests the involvement of hippocampal firing in the verbal working memory network mediated by synchronized EEG oscillations.

4094

V. Eckhardt[1], B. Li[1], E. Schaper[2], J. Jérôme[2], P. Goloubinoff[3], A. Aguzzi[1]

Elucidating the role of chaperones in prion biosynthesis and replication by siRNA mediated high-throughput screening

Institute of Neuropathology, University Hospital Zürich, Switzerland[1], Swiss Institute of Bioinformatics[2], Department of Plant Molecular Biology, University of Lausanne[3]

Introduction:
Prion diseases fatally affect humans and animals. The central event in prion pathogenesis is the conformational conversion of physiologically expressed prion protein (PrP^{C}) into PrP^{Sc}, an insoluble and partially protease-resistant isoform. PrP^{Sc} propagates itself by converting PrP^{C} molecules into the aggregation-prone and disease associated conformation. The molecular mechanisms underlying the conformational alterations from PrP^{C} to PrP^{Sc} are still unknown. Chaperones assist proper folding of proteins, specifically prevent aggregation of aggregation-prone proteins, disaggregate the latter and convert them into harmless native proteins or degraded peptides. Up to date over 20 different chaperones have been found to act neuroprotective in cell or animal models of various neurodegenerative diseases. We propose to identify chaperone genes that are involved in PrP^{C} biosynthesis, unfolding and disaggregation of PrP^{Sc} in murine and human cells.

Methods:
In an unbiased approach, we are using small interfering RNAs (siRNAs) targeting the entire mammalian chaperome (241 genes) in murine neuroblastoma and human glioblastoma cell lines. This bears the potential to detect unexpected hits and novel pathways. Since chaperones collaborate with co-chaperones, we plan to simultaneously knock down two or three chaperones. PrP^{C} and PrP^{Sc} levels serve as readout. Cells are transfected with siRNAs in 384 well plates with a robotic acoustic dispensing platform, and are incubated for 72 hours. At the assay day, cell viability is assessed and cells are lysed. PrP^{C} signals are measured by homogeneous phase fluorescence resonance energy transfer (HPFRET). Experimental data and numerical and graphical quality controls are automatically compiled in RMarkdown documents by a customized software.
After accomplishing PrP^{C} and PrP^{Sc} screens in CAD5 cells, the findings are validated in other cell types and different siRNAs than used in the screen and by CRISPR-Cas9 genome editing.

Results:
The PrP^{C} single knockdown screen in CAD5 neuroblastoma cells was successfully completed and resulted in 21 hits. Hit validation by Western and qPCR that we established on the robotic platform is ongoing. A PrP^{C} double and triple knockdown screen will be performed soon. In order to gain mechanistic insight to PrP^{Sc} replication, we generated a new murine cell line with high PrP^{Sc} levels by stable transfection and chronical infection, elaborated suitable conditions for the murine PrP^{Sc} screen and established the protocol to measure PrP^{Sc} levels by Enzyme-linked Immunosorbent Assay (ELISA).

Conclusion:
The results of the PrP^{C} single knockdown screen give evidence that our RNAi HTS system provides an unbiased approach to identify chaperone genes involved in prion biosynthesis because Hspa5 (BIP), which is known to downregulate PrP^{C} and PrP^{Sc} levels is ranked as hit. A detailed understanding of the molecular basis of chaperone interactions with PrP could contribute to the general understanding of other protein misfolding diseases such as AD or PD.

4095

P. Schürch[1], T. Wildschut[1], E. Milani[2], B. Wollscheid[2], A. Theocharides[1]

Functional differences between CALR mutations in the pathogenesis of Myeloproliferative Neoplasms

Department of Hematology and Oncology, University Hospital of Zurich, Zurich, Switzerland[1], Department of Health Sciences and Technology, ETHZ, Zurich, Switzerland[2]

Introduction:

Myeloproliferative neoplasms (MPN) are a group of pre-leukemic hematopoietic disorders consisting of polycythemia vera (PV), essential thrombocythemia (ET) and myelofibrosis (MF). Roughly, a quarter of patients with ET or MF carry a mutation in Calreticulin (CALR). The most frequent variants of CALR are a 52-bp deletion (type-1) and a 5-bp insertion (type-2 mutation). CALR is a chaperone that resides in the endoplasmic reticulum (ER) that folds N-linked glycoproteins (GP), such as the thrombopoietin receptor (TpoR), myeloperoxidase (MPO) or major histocompatibility complex class I (MHC-I). Several observations lead us to believe that CALR mutations alter the interactome of mutant CALR. First, mutant CALR was shown to interact in a pathological fashion with the TpoR leading to the constitutive activation of the JAK/STAT signaling pathway, thereby acting as the main driver of the disease. Second, our group has shown that MPN patients with homozygous CALR mutations develop a maturation defect in MPO. In addition, there are phenotypic differences between the mutant variants since type-1 mutations are associated predominantly with the MF phenotype and type-2 mutations with ET, respectively. Based on these findings, we hypothesize that the interactome of mutant CALR is altered and that subtle changes in the interactome may explain the observed clinical differences between type-1 and type-2 mutations.

Methods:

An unbiased analysis of the interactome of CALR will be conducted via a proximity-dependent biotinylation assay (BioID), which allows a promiscuous biotin ligase (BirA*) fused to CALR to biotinylate all interacting proteins. A pulldown of biotinylated proteins coupled with a subsequent proteome analysis will allow a qualitative and quantitative assessment of the interactome of CALR. By applying our previously established bioinformatics workflow, we will further identify any aberrations within the interactome of mutant CALR. Furthermore, we will compare the interactomes of type-1 and type-2 mutant CALR with each other to find altered interactions that might serve as an explanation of the phenotypic differences observed between the two mutants. Finally, a functional validation of candidate proteins that differ between the two interactomes will be performed.

Results:

We generated six constructs encoding for wild-type CALR, type-1 or type-2 mutant CALR fused to BirA* either at the N- or C-terminus. Next, we stably integrated these constructs into a HEK 293T cell line via site-directed Flp-FRT recombination. Expression of the fusion proteins was induced with doxycyclin and after confirming the induction, we treated the cells with biotin for 24 h serving as a substrate for the biotin ligase. Currently, we are evaluating the biotinylation "fingerprint" by immunoblotting and are determining the exact localization of our fusion proteins within the cells. The next step will be to perform a pulldown and proteomic analysis.

Conclusion:

The extensive BioID analysis will allow us to screen for altered protein-protein-interactions taking into account the metastable nature of CALR and the complex milieu of the cell. A more profound knowledge of how the interactomes influence the ET or MF phenotype will help identify therapeutic targets.

4096

S. Chaudron[1], K. Metzner[1], A. Marzel[1], J. Böni[2], S. Yerly[3], T. Klimkait[4], R. Kouyos[1], H. Günthard[1]

A molecular epidemiology approach to identify HIV-1 superinfection in the Swiss HIV Cohort study

Infectious Diseases and Hospital Epidemiology, University Hospital Zurich, Zurich[1], Institute of Medical Virology, University of Zurich, Zurich[2], Laboratory of Virology, Geneva University Hospital, Geneva[3], Department of Biomedicine, University of Basel, Basel[4]

Introduction:
HIV-1 superinfection (SI) is the infection of an HIV-1 seropositive individual with another viral strain. SI has been studied and associated with immune escape, viral recombination and disease progression. However, SI identification remains challenging: 1. SI strain may outcompete or be outcompeted by the first strain. 2. SI is difficult to discern from co-infection. 3. Intra-subtypes SI is difficult to prove, especially if caused by viruses from similar transmission clusters. 4. Finally, sampling frequencies are too low and systematic screenings of large populations to date are missing due to lack of needed longitudinal samples in untreated patients. Here we benefit from historic samples from >19,000 patients in the well characterized longitudinal Swiss HIV Cohort Study (SHCS). We thus aim to perform a large scale screen of the SHCS using longitudinal samples from patients and a molecular epidemiology approach to identify superinfection candidates.

Methods:
To do so, sequences of the HIV-1 pol gene from 11,738 patients in the SHCS drug resistance database were used for phylogenetic reconstruction. Patients having ≥2 longitudinal sequences available and belonging to non-monophyletic clusters were kept for the subsequent analysis. Then based on our dataset distribution 2 criteria emerged to select HIV-1 superinfected patients: 1. ≥20 patients must be included in the smallest cluster that includes all of the focal patient's sequences and 2. a genetic distance of ≥5% between the focal patient's sequences was also applied.

Results:
4,558 patients had ≥2 longitudinal sequences with 931 patients belonging to non-monophyletic clusters. Applying the 2 criteria described earlier; 330 candidates for HIV-1 superinfection were identified and will be further confirmed and studied.

Conclusion:
Based on these results; our molecular epidemiology approach is so far the largest screen to identify HIV-1 superinfection using longitudinal samples.

4098

J. Kresoja-Rakic[3], A. Szpenchcinski[2], F. Cerciello[2], M. Kirchner[1], M. Ronner[3], R. Stahel[2], W. Weder[1], E. Felley- Bosco[3]

Circulating non coding RNAs in liquid biopsies before and after chemotherapy reveals two groups of malignant pleural mesothelioma patients

Department of Thoracic Surgery, Univeristy Hospital of Zurich, Zurich[1], Clinic for Oncology, University Hospital Zurich, Zurich[2], Laboratory of Molecular Oncology, Division of Thoracic Surgery, University Hospital Zurich, Switzerland[3]

Introduction:
Circulating RNA are being explored in liquid biopsies for diagnostic and prognostic purposes. Our aim was to investigate the relationship between blood-borne miR-625-3p and long non-coding RNA GAS5, known to be overexpressed in malignant pleural mesothelioma (MPM) and compare their levels before and after chemotherapy.

Methods:
The present study included 36 patients with MPM, whose blood was available before and after chemotherapy and which was directly processed to obtain plasma. RNA was isolated from 100ul of the plasma using the miRNeasy Mini kit (Qiagen). MiRNAs were reverse transcribed into cDNA using poly-A tailing approach and quantified using miScript Primer Assay specific for each miRNA together with miScript SYBR Green PCR Kit (Qiagen). miR-16-5p was used as a reference gene when miRNAs were quantified. Since hemolysis can be a source of variation in miRNA profile, we quantified miR-451a and miR-23a-3p (ΔCt miR-23a – ΔCt miR-451 > 5 = hemolysis) in plasma samples. To demonstrate specificity of miScript Primer Assay against miR-625-3p, we cloned and sequenced the qPCR product. Total cDNA was prepared using QuantiTect Reverse Transcription kit (Qiagen) and lncRNA GAS5 and β-actin (used as reference gene) were detected by SybrGreen quantitative PCR.

Results:
Two samples had to be excluded because of hemolysis and two because of RNA degradation. Therefore, for only 32 patients paired plasma samples before and after chemotherapy were further analyzed. Coefficient of variation of both references genes miR-16-5p and β-actin in all samples was 5.4% and 5.8%, respectively, demonstrating little variation and stability between plasma samples. Quantification of miR-625-3p levels revealed a bimodal distribution. From each group, the qPCR product was cloned and sequenced demonstrating that SybrGreen method is detecting entire miR-625-3p population including isomiRs. Furthermore, we observed that in the group of patients with lower levels of circulating miR-625-3p, alterations in plasma level of miR-625-3p upon chemotherapy significantly inversely correlates with alterations of lncGAS5 in the same sample (p=0.0113) while in the group of patients expressing high miR-625-3p levels, a direct correlation (p=0.06) was observed.

Conclusion:
Our exploratory analysis revealed the value of circulating nucleic acids in defining two groups with a potentially different tumor biology.

4099

D. Heuberger[1], A. Franchini[1], R. Schüpbach[1]

Monitoring of proinflammatory mediators NF-κB and IL-8 in a human overexpression system

Institute of Intensive Care Medicine, University and University Hospital Zurich, Zurich, Switzerland[1]

Introduction:
One of the major role of human proteases is the regulation of the innate immune response to inflammation-associated tissue damage. The specific regulators of inflammation and tissue repair during this process are protease-activated receptors (PARs). Thrombin, the key procoagulatory and proinflammatory clotting protease cleaves and activates PAR1 for example to regulate the endothelial permeability and platelet activation. Recently, we showed for the first time that the thrombin/thrombomodulin (TM) complex could cleave PAR2. To test our hypothesis that thrombin activates PAR2 leading to proinflammatory responses we investigated the activation of NF-κB (Nuclear Factor- KappaB) which is a prototypical proinflammatory mediator involved in stress as well as inflammatory and immune responses. In unstimulated cells, IkB proteins inhibit NF-κB. Activation of the IkB kinase leads to lkB degradation and to a translocation of the NF-κB complex to the nucleus where the NF-κB complex binds on DNA response elements to induce target gene transcription. An NF-κB luciferase reporter plasmid was transfected together with a PAR1 or PAR2 construct into human embryonal kidney cells (HEK 293T) to investigate whether NF-κB DNA binding activity is induced by thrombin. The level of IL-8 secretion was observed to confirm the proinflammatory signaling upon thrombin activation. The intracellular signaling pathway of NF-κB activation was assessed by the inhibition of different pathway kinases (ERK1/2, p38, PI3K).

Methods:
To determine whether proinflammatory signaling was induced by thrombin cleavage, pGL4.32[*luc2P*/NF-κB-RE/Hygro] was transfected into HEK 293T cells together with a pcDNA3.1 plasmid containing PAR1, PAR2 or TM construct. Two days after lipofection, cells were stimulated with inhibitors and/or agonists for 6 hours and the NF-κB DNA binding activity was quantified by a luciferase assay. Quantification of secreted IL-8 was done with a human IL-8 ELISA according to manufacturer's protocol.

Results:
The NF-κB DNA binding activity was strongly induced by thrombin in cells transfected with PAR1 and *luc2P*/NF-κB-RE or PAR2 and TM together with *luc2P*/NF-κB-RE compared to the media control. Upon thrombin stimulation IL-8 was significantly induced in cells transfected with PAR1 or PAR2 and TM, which mirrors the induction of the NF-κB DNA binding activity.

Conclusion:
We were able to show in a human overexpression system for the first time that the cleavage of PAR2 by the thrombin/thrombomodulin complex leads to a clear proinflammatory response of NF-κB activation and IL-8 secretion. The NF-κB activation induction by thrombin via PAR1 could be confirmed in the established overexpression system. This well-established system can be used in a multitude of studies to test the activation of various overexpressed receptors by different pro-or anti-inflammatory mediators.

4100

A. Van Ransbeeck[1], A. Budilivski[2], D. Spahn[1], L. Macrea[1], F. Giuliani[2], K. Maurer[1]

Pain Assessment Discrepancies: A Cross- Sectional Study Highlights the Amount of Underrated Pain

Institute of Anesthesiology, University Hospital Zurich[1], Department of Quality Management & Patient Safety, University Hospital Zurich[2]

Introduction:
Inadequately treated postoperative pain can lead to longer healing processes, longer hospital stays, and the development of chronic pain. In a 900-bed university hospital in Switzerland, pain scores were assessed systematically. The study's primary aim was to define whether the routine pain assessment on the ward is accurate and reproducible. Subsequently the obtained data were used for a benchmark analysis to determine the hospital's performance in pain assessment quality compared with similar centers.

Methods:
During a 3-month period, PAIN OUT questionnaires were used for patients' interviews. Patients were included randomly according to the daily surgical schedule. Pain scores were assessed routinely by nursing staff on the wards and compared to PAIN OUT data. The ascertained data were analyzed by descriptive statistics as well as the Wilcoxon test for nonparametric values using IBM SPSS.

Results:
658 patients were included in the study. Comparing routine pain measurements with PAIN OUT results revealed that within the first 24 hours on the ward, pain scores were significantly lower than measured with PAIN OUT questionnaires. This difference increased with increasing pain scores.
The quality of pain management of the hospital in which this study was performed ranged around the 50th percentile when compared to similar centers.

Conclusion:
The cross-sectional data comparison of pain assessment by the ward staff and by interviews with the PAIN OUT questionnaire showed a large gap of underrated pain. The benchmark analysis with the method of PAIN OUT suggests a decent pain management among reference groups.

4101

M. Kölling[1], C. Genschel[2], T. Kaucsar[3], A. Hübner[2], S. Rong[4], R. Schmitt[4], I. Soerensen-Zender[4], G. Haddad[1], A. Kistler[5], H. Seeger[1], JT. Kielstein[6], D. Fliser[7], H. Haller[4], R. Wüthrich[1], M. Zörnig[8], T. Thum[2], J. Lorenzen[1]

Hypoxia-induced long non-coding RNA Malat1 is dispensable for renal ischemia/reperfusion-injury

Department of Nephrology, University Hospital Zürich, Switzerland[1], Institute of Molecular and Translational Therapeutic Strategies (IMTTS), Hannover Medical School, Germany[2], Semmelweis University, Budapest, Hungary[3], Department of Nephrology, Hannover Medical School, Germany[4], Department of Internal Medicine, Cantonal Hospital Frauenfeld, Switzerland[5], Department of Nephrology, Städtisches Klinikum Braunschweig GmbH, Braunschweig, Germany[6], Saarland University Medical Centre, Homburg/Saar, Germany[7], Georg-Speyer-Haus, Institute for Tumor Biology and Experimental Therapy, Frankfurt, Germany[8]

Introduction:
Renal ischemia/reperfusion (I/R) injury represents a major socioeconomic health problem. Non-coding RNA are crucially involved in pathophysiology. Long non-coding RNA *Malat1* (Metastasis Associated Lung Adenocarcinoma Transcript 1) was upregulated in renal I/R injury. We elucidated the functional role of *Malat1 in vitro* and its potential contribution to kidney injury *in vivo*.

Methods:
In patients, kidney biopsies and plasma samples were collected.

In vivo, *Malat1* knockout- (KO) and wild-type (WT) mice were subjected to unilateral and bilateral I/R. Histopathology-, gene expression-, kidney function- and survival studies were performed.

In vitro, *Malat1* was silenced by antisense oligonucleotides in endothelial cells (EC) and tubular epithelial cells (TEC) subjected to hypoxia/reoxygenation. Transcriptional activation- and functional studies were implemented. Genome-wide RNA analysis was performed.

Results:
Malat1 was upregulated in human kidney biopsies and plasma and in murine kidney tissue, EC and TEC and mainly nuclear-chromatin associated.

In vitro, *Malat1* inhibition reduced EC in the S-phase of the cell cycle. Proliferation decreased. Less EC were apoptotic after *Malat1* silencing. TEC were not functionally altered. *Malat1* was transcriptionally activated in EC and TEC by Hypoxia-inducible factor 1-alpha.

In vivo, *Malat1* KO- and WT mice showed similar degrees of tubular epithelial injuries and proliferating cells. Capillary rarefaction was not affected. Kidneys of *Malat1* KO- and WT mice expressed more pro-inflammatory (IL-1beta, IL-6, MIP2a, MCP-1) and pro-fibrotic (Col1a2, Col III, TGF-beta) genes. Similar amounts of macrophage-, T-cell infiltration and tubulointerstitial collagen were detected. mRNA- and smallRNA expressions showed only minor differences. The reduced kidney function was not altered by *Malat1* KO. *Malat1* KO mice showed no survival benefit.

Conclusion:
Malat1 plays a pivotal role in hypoxia/reoxygenation induced endothelial cell pathology. Even though previous studies have suggested a prominent role of *Malat1* in the induction of disease, we did not confirm an effect of *Malat1* loss on the progression of renal I/R-inury.

4102

F. Romano[1], D. Straumann[1], G. Bertolini[1]

The role of visual inputs on vestibular Cross-coupling stimulus

Neurology Department, University Hospital Zürich, Zürich[1]

Introduction:
Vestibular cross-coupling (CC) stimulus occurs when an individual tilts his head during an ongoing rotation in darkness. It induces tumbling sensation and motion sickness. Our aim was to investigate whether visual information decreases CC sensation by preserving the rotational sensation.

Methods:
Eleven healthy subjects were rotated (30°/s and 60°/s) around an earth-vertical yaw axis. CC stimulus was induced by an active head tilt of 45°. Such trial was executed four times: 1) in darkness; 2) in light, staring (not fixating) at a static optokinetic (OK) drum 3) in light, staring at an OK drum rotating in the opposite direction; 4) in darkness. After each head tilt, subject scored (0-20) the strength of the CC sensation respect to the first trial (defined as score=10).

Results:
Visual information reduced the CC sensation in all subjects. With static OK drum, CC sensation score was half at 30°/s, while 2/3 at 60°/s. An increase of OK velocity did not induce a further decrease CC sensation in 6/11 subjects (both at 30°/s and 60°/s).

Conclusion:
Our findings suggest: 1) Vection induced by OK drum partially decreases the CC sensation; 2) The reduction of CC by vection is less effective with stronger vestibular stimulations; 3) Vection twice as strong as the vestibular stimuli causes no further decrease in CC sensation in certain subjects, suggesting a possible saturation effect.

4103

JH. Jang[1], M. Haberecker[2], A. Curioni [3], F. Janker[1], A. Soltermann[2], W. Weder[1], W. Jungraithmayr[1]

The expression pattern of CD26/DPP4 in human lung cancer

Thorcic Surgery, University of Zurich,Zurich[1], Pathology, Institute of Clinical Pathology, University Hospital Zurich, Zurich[2], Oncology Department, Universitätsspital Zürich, Zürich[3]

Introduction:
Lung cancer is the leading cause of death among cancers. Despite improved surgical and novel radiation improvements, the overall prognosis remains poor. CD26/dipeptidyl peptidase 4 (DPP4) is a ubiquitously expressed transmembrane exopeptidase on the cell surfaces of many different cells including malignancies of breast, colon, and mesothelioma. Our group found previously that the activity of CD26/DPP4 of lung adenocarcinoma (Adeno-CA) patients is four times higher than in normal tissue and the inhibition of CD26/DPP4 decreased the growth of lung tumors in experimental models. These data prompted us to analyze the expression of CD26/DPP4 in samples from lung cancer patients to unravel the role of CD26/DPP4 as a biomarker for lung cancer and a target for inhibition to reduce lung cancer burden.

Methods:
To identify CD26/DPP4 by immunohistochemistry (IHC), we tested multi-organ tissue micro array (TMA) with 4 antibodies from Abcam, R/D systems, and Cell signaling technology. We selected the antibody provided by Cell signaling technology. For the analysis of CD26/DPP4 by IHC, TMAs constructed from the samples of non-small cell lung cancer patients were used. The cohort consisted of 475 patients (Adeno-CA: 223; Squamous carcinoma: 252). The intensity of the staining was scored from 0 to 3 in a blinded manner. Lung Adeno-CA cell lines (A549, H460, Gon8, Mai9) derived from advanced stage patients were used to assess the expression of CD26/DPP4. To quantify CD26/DPP4 in the human lung Adeno-CA cell lines, ELISA was performed.

Results:
IHC scores revealed that Adeno-CA expresses significantly more CD26/DPP4 compared to squamous carcinoma ($p<0.0001$). Consistent with our previous findings, early stage cancer (IA) scores significantly higher than other stages IIB ($p=0.0012$), IIIA ($p=0.0019$), and IV ($p=0.02$) among Adeno-CA samples. We could find secreted CD26/DPP4 from human Adeno-CA cell lines in supernatant, which reaches high level with variation (A549: 40pg/ml; H460: 161pg/ml; Gon8: 74pg/ml; Mai9: 648pg/ml).

Conclusion:
CD26/DPP4 expression was significantly higher at early stages of Adeno-CA samples when compared to advanced stages, supporting our previous findings. From the human cell line data, we suggest that advanced cancer secretes CD26/DPP4 more actively than early stage cancers. CD26/DPP4 seems to be a substantial target for inhibition of human Adeno-CA.

4104

I. Besmens[1], M. Calcagni[1], T. Giesen[1]

Reducing the immobilization period after DIP arthroplasty through a new dorsal approach

Klinik für Plastische Chirurgie und Handchirurgie, UniversitätsSpital Zürich, Zürich[1]

Introduction:
Degenerative changes of the distal interphalangeal (DIP) joints can be painful, disabling and disfiguring. Swanson spacers are primarily used in PIP and MP joints, but there are also many reports about their use at the DIP as an alternative to arthrodesis especially in high demand patients.
The standard approach for Swanson spacer implantation at the DIP joint involves transecting the extensor tendon close to its insertion. This necessitates a six weeks period of postoperative immobilization, which comes with the risk of losing some joint motion.
A second possible DIP approach involves sparing the extensor tendons as already published.
This approach has the potential risk of an extra anatomical implantation of the prosthesis and is technically demanding.
Interestingly both techniques lead to a similar range of motion of the replaced DIP joints of approximately 30° with a mean extensor lag of 12.
We present a novel approach for DIP joint arthroplasty with division of the extensor tendon in zone 2 with only two weeks of postoperative immobilization.

Methods:
From 2015-2017 we implanted 8 Swanson Spacers in DIP joints in 4 patients with the described approach: After an H-shaped skin incision with proximal slightly longer legs over the DIP joint the extensor tendon is incised in zone 2 just distal to the central slip insertion and the extensor tendon is flipped distally. The Swanson spacer is afterwards implanted as it is standard. After implantation the extensor tendon is sutured with two crossed sutures, one per slip.
Postoperatively patient received a DIP splint in slight hyperextension for two weeks and started mobilizing the joint without protective casting after 2 weeks. The DIP joint range of motion was measured at 2, 6 and 12 weeks postoperatively.

Results:
We reviewed all our patients with a follow up of at least 3 months.
At 12 months postoperative we measured extension lags between 0° and 20°. Median DIP flexion was 51°.

Conclusion:
Degenerative alterations in the hand including the DIP joint are a common problem with advanced age. Nowadays these patients tend to have a high demand for hand function for example for playing musical instruments or just using computers. Many patients will thus opt against DIP arthrodesis. Optimizing the motion preserving operative approaches is thus of value. Our postoperative results do not differ from the postoperative range of motion published in the literature for both tendon sparing and standard approach. But our approach is technically easy and requires only a significantly shorter time of immobilization.

4105

S. Motta[1], E. Fioretta[1], P. Dijkman[1], V. Lintas[1], L. Behrendt[2], S. Hoerstrup[1], M. Emmert[3]

Development of an Off-the-Shelf Tissue Engineered Sinus Valve for Transcatheter Pulmonary Valve Replacement: A Proof-of-Concept Study

Institute for Regenerative Medicine, University of Zurich, Zurich, Switzerland[1], Institute Mutualiste Montsouris (IMMR), Paris, France[2], Heart Center Zurich, University Hospital Zurich, Zurich, Switzerland[3]

Introduction:
Transcatheter technologies have evolved as a valid option for the treatment of heart valve disease. However, current artificial prostheses are associated to continuous degeneration and thus do not provide a long-term solution for young adults and children. Hence, tissue-engineered heart valves (TEHVs) with self-repair and regeneration properties may overcome this problem. We recently demonstrated the feasibility of off-the-shelf TEHVs transcatheter delivery in sheep. However, one limitation of these TEHVs was the absence of physiological Valsalva sinuses, resulting in non-physiological flow and maladaptive remodeling. Here, we describe the development and in-vivo proof-of-concept of such next-generation regenerative TEHVs using a custom-made sinus stent for transcatheter pulmonary valve replacement.

Methods:
Ovine cell-derived off-the-shelf TEHVs were manufactured in-vitro, sewn onto a sinus stent and implanted transapically (via thoracotomy) into adult sheep in an acute fashion and for 16 weeks. Valve performance was assessed by angiography and follow-up echocardiography. Valve remodeling was assessed by histology and immunofluorescence.

Results:
Transapical delivery of ovine-derived sinus TEHVs was successful. The valves showed a good acute and short-term performance with proper mobility and coaptation (mild insufficiency) for up to 8 weeks, however it then worsened towards severe regurgitation at 16 weeks. This was most likely due to a non-optimized in-vitro valve design, leading to a non-physiological hemodynamic loading and finally to negative leaflet remodeling.

Conclusion:
Here we demonstrate the development of a clinically relevant off-the-shelf tissue engineered transcatheter sinus valve. While acute and short-term performance of the acute design is encouraging, further geometry optimization is needed to ensure long-term functionality.

4106

I. Besmens[1], T. Giesen[1], O. Politikou[1], M. Calcagni[1]

Finger reconstruction with dorsal metacarpal and dorsal finger flaps based on the dorsal branches of the palmar digital arteries. 40 consecutive cases.

Klinik für Plastische Chirurgie und Handchirurgie, UniversitätsSpital Zürich, Zürich[1]

Introduction:
The aim of this study is to report our experience in finger reconstruction with reverse island flaps based on the dorsal branches of the palmar digital artery with particular emphasis on complications and their correlation with the vascularization pattern.

Methods:
In the years 2007-2017 we treated 40 patients for long finger injuries with reverse flow island flaps from the dorsal aspect of the distal hand or finger, based on the dorsal collateral branches of the palmar digital arteries.
The lesions were located on the index finger in 11 patients, on the middle finger in 8, on the ring finger in 6 and on the small finger in 10. The soft tissue defect was found at the distal part of the proximal phalanx in 12 cases, over the PIP joint or middle phalanx in 9 cases and over the DIP joint up to the nail bed in 14 cases.
The defects were located on the index finger in 10 patients, on the middle finger in 10, on the ring finger in 11 and on the small finger in 9 patients. The skin lesions were located as far distal as the dorsal aspect of the proximal phalanx in 18 cases up to the dorsal side of the PIP joint and/or middle phalanx in 10 cases and over the DIP joint and/or up to the nail bed in 12 cases. In 8 patients the defect was located (at least partially) on the palmar side of the digit.
The flaps were harvested from the second inter-metacarpal space in 18 cases, from the third in 13 and from the fourth in 9 cases. In all other cases the donor area was located at the dorso-lateral side of the proximal phalanx.
The patients were analysed in terms of flap survival, reconstruction achievement and subjective satisfaction. Flap necrosis was measured as percentage of the total original flap surface area.

Results:
The flap size ranged from 1x1cm to 4x1.5cm. The pedicle was tunnelized in the defect in 5 cases and was left exteriorized in 4. In all other cases it was possible to close the skin over the pedicle without tension. We did not note any significant venous insufficiency in the flaps, despite the fact that their venous drainage was usually via flimsy venae comitantes and by reversed flow.
Of the 40 flaps, 36 survived completely and 4 survived partially.
The complications were observed in flaps transferred to more distal defects. In all cases a conservative treatment led to secondary healing without additional surgery.
Average time for flap dissection was 30 minutes and all patients were discharged the day after surgery. The donor site was always primarily closed.

Conclusion:
In conclusion defect coverage with flaps from the dorsum of the hand or fingers is a straightforward single-stage procedure for defects up to the distal phalanx as well palmar as dorsal. Our results and data from the literature indicate that these flaps can be safely used for coverage on both palmar and dorsal aspect of the long fingers as they are thin, pliable and with a low donor site morbidity.

4107

M. Kölling[1], H. Seeger[1], G. Haddad[1], A. Kistler[3], A. Nowak[5], R. Faulhaber-Walter[2], H. Haller[2], D. Fliser[4], T. Mueller[1], R. Wüthrich[1], J. Lorenzen[1]

Circular RNAs in critically ill patients with acute kidney injury

Department of Nephrology, University Hospital Zürich, Switzerland[1], Department of Nephrology, Hannover Medical School, Germany[2], Department of Internal Medicine, Cantonal Hospital Frauenfeld, Switzerland[3], Saarland University Medical Centre, Homburg/Saar, Germany[4], Department of Internal Medicine, University Hospital Zürich, Switzerland[5]

Introduction:
Circular RNAs (circRNAs) have recently been described as novel non-coding regulators of gene expression. In particular, they might be master regulators of microRNA expression by their sponging activity. The detectability and stability in blood of these RNA transcripts has been demonstrated in patients with cancer and cardiovascular disease. We tested the hypothesis, that circulating circRNAs in plasma of critically ill patients with acute kidney injury at inception of renal replacement therapy may also be dysregulated and associate with patient survival.

Methods:
We performed a global circRNA expression analysis using RNA isolated from plasma of patients with acute kidney injury as well as healthy controls. Samples were depleted of linear RNAs by Rnase R treatment. Patients with Fabry Disease (FD) served as disease controls. This global screen revealed several dysregulated circRNAs in plasma samples of patients with acute kidney injury. CircRNA-array-based alterations were confirmed in plasma of 109 patients with acute kidney injury, 30 age-matched healthy controls and 42 disease controls by quantitative realtime-PCR.

Results:
Circulating concentrations of the novel circRNA *hsa_circ_103410* were up- regulated in plasma of patients with acute kidney injury as compared to healthy controls and disease controls. Cox regression and Kaplan-Meier curve analysis revealed circRNA as an independent predictor of 28-day survival ($p<0.01$).

Conclusion:
The alteration of circulating concentrations of circRNAs in patients with acute kidney injury supports *hsa_circ_103410* as a predictor of mortality in this patient cohort.

4108

P. Pagella[1], C. Cantù[2], G. Russo[3], M. Schwab[4], T. Mitsiadis[1]

Nogo-A is a gate-keeper of stem cell niches

Institute of Oral Biology, Department of Craniofacial Development and Regeneration, University of Zurich[1], Institute of Molecular Life Sciences, University of Zurich, Zurich[2], Functional Genomics Center, University and ETH Zürich, Switzerland[3], Brain Research Institute, University of Zurich and Department of Health Sciences and Technology, Swiss Federal Institute of Technology (ETH) Zurich, Zurich, Switzerland.[4]

Introduction:
Tissue homeostasis and regeneration are obtained via precise regulation of stem cell proliferation and differentiation, and migration of differentiated progeny. To investigate these processes we used the mouse incisor, which grows continuously thanks to highly regulated waves of cell proliferation, differentiation, migration and maturation/mineralization.

Methods:
We combined transgenic mouse models, in vivo lineage tracing, 3D-imaging, transcriptomics and proteomics approaches to investigate the mechanisms that regulate stem cell niche dynamics in the continuously growing mouse incisor.

Results:
Here we show that Nogo-A, a key modulator of axonal plasticity and regeneration, is expressed in a subset of cells within the dental epithelial stem cell niche. Nogo-A deletion affects the behavior of dental epithelial stem cells, leading to the formation of defective enamel. RNA sequencing analysis revealed that Nogo-A deletion affects the expression of genes involved in the regulation of the cell cycle and of cell adhesion within the stem cell compartment. Genetic lineage tracing analyses showed that neutralization of Nogo-A boosts proliferation of stem cells and the expansion of their progeny, accelerating the rhythm of incisors' growth, both *in vitro* and *in vivo*. Nogo-A is also expressed in stem cell niches of other tissues and organs, such as the hair follicles, indicating similar functions in these compartments.

Conclusion:
Overall, our data reveal that Nogo-A acts as a gatekeeper of stem cell niches, fine-tuning and modulating the rhythm of stem cells proliferation and differentiation.

4109

F. Romano[1], D. Straumann[1], G. Bertolini[1]

Impact of alcohol on self-motion perception and reflexive eye movements

Neurology Department, University Hospital Zürich, Zürich[1]

Introduction:
Acute alcohol intoxication is well known to alter the performances of visual and vestibular systems at different levels, from reflexive responses to spatial orientation. Despite the number of reports on such alterations, little is known about how alcohol interferes with the processing of the visual-vestibular integration.
We hypothesized that alcohol-induced disorientation and drop of navigation performance are due to detuning of the multisensory integration process responsible for merging visual and vestibular self-motion cues. To test this hypothesis, we investigated the effect of alcohol on the processing of self-motion sensory inputs comparing reflexive (eye movements) and perceptual responses to either visual or vestibular stimuli.

Methods:
Twelve healthy subjects underwent two tests: 1) A test for vestibulo-ocular reflex (VOR) and perceived rotational velocity (PRV), consisting of a passive rotation at a constant angular velocity of 90°/s for 60s. 2) A test for the optokinetic after-nystagmus (OKAN) and the associated vection (illusion of self-rotation) generated by an optokinetic drum rotating around the subject 30°/s for 60s. Each test was performed before (baseline) and 30 minutes after intake of the estimated alcohol amount needed to reach a blood alcohol content (BAC) of 0.06%.
The reflexive responses were measured with video-oculography and analyzed quantifying the decay of the slow phase velocity of the nystagmus during the velocity step (VOR) and after the visual stimulation (OKAN), while the perception (PRV and Vection) were quantified with an analog method consisting of matching the rate of lever spinning with the perceived angular velocity.

Results:
The VOR time constant significantly decreased from 14.0 ±1.2s (mean ±sd) before alcohol intake to 9.5 ±1.9s after alcohol intake, while the PRV time constant was 13.1 ± 2.1 s before alcohol and 11.1 ± 2.0 s after alcohol. Conversely, the OKAN was enhanced by alcohol consumption. The area under the curve (AUC) of the OKAR showed an increase from 174.4 ±36.0deg before alcohol to 206.0 ±76.2deg after alcohol. The AUC of the vection, instead, decreased from 19.8 ±27.4#round before to 8.1 ±11.0#round after alcohol intake.

Conclusion:
Our results suggested that alcohol affects visuo-vestibular processing of self-motion signals in a coherent way by altering the cerebellar velocity storage mechanism (VSM), i.e. the common process for integration and elaboration of self-motion information. A similar pattern has been observed in some of the patients with cerebellar degeneration, further corroborating the hypothesis that the effect of alcohol on self-motion perception depends on its alteration of the vestibule-cerebellum.

4110

A. Eijkenboom[1], L. Ebert[2], J. Plock[1], R. Schweizer[1], P. Kamat[1]

Automated vessel recognition and vessel wall analysis in tissue sections using deep learning

Department of Plastic Surgery and Hand Surgery, University Hospital Zurich, Zurich[1], Institute of Forensic Medicine, University of Zurich[2]

Introduction:
Deep learning, a subset of machine learning, utilizes artificial neural networks to automatically learn from given training datasets. The advantage is that these types of algorithms are more robust on complex data and faster than conventional, task specific algorithms.. Neural networks and deep learning have been applied to various fields, such as speech recognition and bioinformatics, but can also be used in the medical field. Deep learning technology can facilitate batch analysis of histopathological sections by not only classifying tissues, cells and structures, but also analyzing them. In this study, we focused on automation of vessel recognition and distinction between intima and media layer of the vessel wall for assessment of vascular pathologies such as e.g. intimal proliferation. Future applicability might include assessment of intimal thickening during chronic rejection in transplantation.

Methods:
Tissue specimens of skin, muscle and large arteries were harvested from rats at sacrifice after experimental hind-limb allotransplantation. Tissue sections were stained for Elastin van Gieson (EvG) to visualize the elastic interna and pictures were taken with a Leica DM6000B (Leica Microsystems, Wetzlar, Germany) at 20x and 40x magnification. The images were then assessed by measuring intima and media thickness. The Deep learning software Cognex ViDi Suite (Cognex, Natick, MA, USA), originally dedicated to industrial image analysis, was used to analyze the histologic images. A total of 66 images were used. The analysis consisted of 3 steps: 1. vessel recognition; 2. vessel classification as “vessel” or “no vessel”; 3. Segmentation of intima and media wall layer. For all steps, 70% of the images were used for training and 30% for validation.

Results:
The neural network was able to successfully classify vessels (Recall 90.5, Precision 76.4, F-score 82.8) and recognize the intimal and media wall layer accordingly. Validation in new, non-trained images confirmed this: media layers were recognized from surrounding tissue and the intima was separated from detritus and artifacts in the vessel lumen.

Conclusion:
This is the first study showing that deep learning has potential for automated vessel recognition and breakdown of their component when applied to histological images.

4111

F. Feldmann[1], G. Natalucci[2]

Association between development of early cortical activity on amplitude integrated EEG and 5-years neurodevelopmental outcome in the preterm infant

Child Development Centre, University Children's Hospital Zurich, Switzerland[1], Department of Neonatology, University Children's Hospital Zurich, Switzerland[2]

Introduction:
Background: Cerebral function monitoring with amplitude integrated electroencephalogram (aEEG) has been shown to be predictive of neurodevelopmental outcome up to 3 years of age in preterm born infants. However, the predictive value for outcome at early school age has not been investigated yet. **Objective:** To evaluate the predictive value of early aEEG monitoring for the neurodevelopmental outcome at early school age.

Methods:
Prospective cohort study on preterm born infants with gestational age (GA) <32.0 weeks, undergoing continuous aEEG recording during the first 3 days of life. aEEG characteristics were semiquantitatively (maturity and cycling score according to Burdjalov et al. 2003) and quantitatively (maximum and minimum aEEG amplitude) evaluated at 24, 48 and 72 hours of life. Neurodevelopmental outcome at 5 years of age was assessed by neurological examination and the Kaufman Assessment Battery for Children. Outcome at 5 years was defined as abnormal in case of cerebral palsy (CP) or IQ performance <85 and IQ was separately considered as continuous outcome. Multivariate linear and logistic regression models were used to analyse the predictive value of aEEG parameters during the first three days of life for neurodevelopmental outcome. Models were adjusted for GA, socioeconomic status (SES), small for GA, major brain lesions, score for neonatal acute physiology perinatal extension-II and sedation.

Results:
Among 120 monitored preterm infants (48% female) with mean GA (range) 29.4 (24.4-31.9) weeks and birth weight 1245 (570-2120) grams, 94 infants were assessed at a mean corrected age of 68.2 (45-87) months. Four infants died and 22 infants were lost to follow-up (follow-up rate 82%). The median IQ (IQR) was 100 (89-108), IQ below 85 occurred in 15% and CP in 2.5%. All four aEEG measures were not associated with abnormal outcome at 5 years. In multivariate linear regression only SES was significantly associated with IQ, (strongest association with the minimal aEEG amplitude at 24 h: R^2 .40, B 2.3, 95%CI 1.1-3.4, p<.001).

Conclusion:
In this cohort of preterm born infants, neurodevelopmental outcome at 5 years was not predicted by early aEEG, but was associated with SES. In contrast to previous reports this data cannot confirm the predictive value for the long-term neurodevelopmental outcome of preterm infants. This might be due to the short period of early functional cerebral monitoring of this cohort with relatively favourable outcome.

4112

G. Natalucci[1], A. Adams[1]

Two-year outcome of extremely preterm infants < 26 weeks of gestation born in Switzerland: is intensity of perinatal care associated with increased neurodevelopmental impairment?

Department of Neonatology, University Children's Hospital Zurich, Switzerland[1]

Introduction:
In Switzerland, neonatal survival of extremely low gestational age neonates (ELGANs) with gestational age <26 weeks improved following the publication of the 2002 Swiss guidelines for the perinatal care of infants born at the limit of viability, with no increase in the rate of short-term complications. A substantial centre-to-centre difference in neonatal mortality persisted after the guidelines' publication. This study aimed to compare survival and neurodevelopmental impairment rates at 2 years of corrected age among ELGANs born alive in the 9 Swiss level III perinatal centres; and to investigate the impact of centre-specific levels of perinatal interventional activity on these outcomes.

Methods:
Prospective population-based study including all ELGANs without major congenital malformations born alive in Switzerland in 2006-2013 with gestational age <26 weeks.
Perinatal interventional activity was graded as low, medium and high based on 3 obstetric and 4 neonatal key indicators. Outcomes at 2 years were mortality, survival with unfavourable (i.e. one of following: cerebral palsy with GMFCS >1; equivalent of a developmental test score <2SD from the respective norm; hearing loss; uni- or bilateral blindness) and favourable outcome (none of the above). Crude and risk-adjusted standardized outcome ratios (SOR, 95%-CI) based on the centre-specific level of perinatal interventional activity were calculated with regression models using 5-fold imputed data.

Results:
Among 927 included infants, 564 (61% of cohort) died before discharge and 319 (88% of survivors) were assessed at 2 years corrected age [46% females, mean (SD) gestational age 25.1 (0.5) weeks]. Favourable and unfavourable outcomes were observed in 75% and 25% of survivors, respectively. After risk adjustment (for gestational age, birth weight z-score, male sex, multiple birth, outborn rate and socioeconomic status), mortality was significantly higher (1.33, 1.30-1.36) and favourable outcome significantly lower (0.76, 0.74-0.79) in centres with low perinatal interventional activity compared to other centres. In centres with high perinatal interventional activity, mortality was significantly lower (0.84, 0.80-0.90) and favourable outcome significantly higher (1.07, 1.07-1.13) compared to other centres.

Conclusion:
There are significant differences in 2-year outcome of ELGANs between the 9 Swiss level III perinatal centres. The level of perinatal interventional activity for ELGANs is negatively correlated with mortality and positively correlated with favourable outcome.

4113

U. Karakus[1], J. Lam[1], O. Boyman[1]

Development of Treg cell-stimulating IL-2/anti-IL-2 antibody complexes

Department of Immunology, University Hospital Zurich, Zurich, Switzerland[1]

Introduction:
Interleukin-2 (IL-2) is crucial for the homeostasis and activation of the immune system by playing an essential role in immune tolerance and ensuring optimal T cell responses. In particular, IL-2 is crucial for $CD4^+$ regulatory T (T_{REG}) cells, which are controlled by the transcription factor forkhead box P3 (FoxP3) and govern peripheral immune tolerance. Survival and suppressive capacity of T_{REG} cells relies greatly on IL-2 availability, mirrored by their high expression of the high affinity trimeric IL-2 receptor, which includes the IL-2 receptor alpha (CD25). Hence, T_{REG} cells can be selectively stimulated by providing recombinant IL-2 bound to a specific anti-IL-2 monoclonal antibody (mAb), which delivers IL-2 to the trimeric IL-2 receptor, resulting in the selective stimulation of $CD25^{high}$ T_{REG} cells. The advantage of such cytokine/anti-cytokine mAb complexes, besides increased half-life *in vivo*, is the preferential action on T_{REG} cells compared to free IL-2, as the latter shows dose-dependent activation of memory $CD8^+$ T cells and natural killer cells in addition to T_{REG} cells. Currently, we are investigating the in vivo properties of CD25-directed IL-2 complexes, which we have developed recently, and are characterizing their mode of interaction with the IL-2 receptor to unveil the molecular mechanism behind the observed selectivity.

Methods:
By flow cytometry, we have characterized binding profiles of IL-2 complexes to human embryonic kidney (HEK) 293T cells transiently expressing single subunits of the IL-2 receptor, or combinations thereof, forming dimeric or trimeric IL-2 receptors.T_{REG} cell levels in C57BL/6 mice that received a short-term treatment of three intraperitoneal IL-2 complex injections were analyzed by flow cytometry. Furthermore, serum IL-2 levels were measured by enzyme-linked immunosorbent assay (ELISA) to estimate the *in vivo* half-life of CD25-directed IL-2 complexes.

Results:
We have recently developed CD25-directed IL-2 complexes, composed of human IL-2 and a specific anti-human IL-2 mAb, which selectively stimulate T_{REG} cells. Besides elevated *in vivo* serum half-life, we have found that CD25-directed IL-2 complexes specifically associate with the trimeric but not with the dimeric IL-2 receptor *in vitro*.

Conclusion:
T_{REG} cell-stimulating IL-2 complexes preferably stimulate $CD25^{high}$ T_{REG} cells via their high affinity, trimeric IL-2 receptor and therefore could potentially treat T_{REG} cell-deficient pathologies, including autoimmune diseases (e.g. type 1 diabetes, multiple sclerosis and systemic lupus erythematosus) and allotransplant-related disorders.

4114

AE. Serra Roma[1], M. Gualandi[1], A. Siebenhuener[1], M. Manz[1], O. Shakhova[1]

Generation of neuroendocrine organoids

Department of Hematology and Oncology, University Hospital Zurich, Wagistrasse 14, 8952 Schlieren[1]

Introduction:
Neuroendocrine tumors are a very heterogeneous group of tumors that can arise in the lungs, adrenal glands, among others. The neuroendocrine system is diffused along the body and is responsible for the secretion of multiple proteins important for the regulation of different physiological activities. Such secretory capacity upon excitation, together with the expression of neural markers, could reveal the neural origin of these cells. Nevertheless, although is known that such cells arise from the ectoderm, there is still a debate whether these cells are epithelial or neural crest derived. In the recent years, organoids have risen as a scientific tool not only for the study of the biology behind different systems, with the best well-known example of the intestinal and cerebral organoids, but also for the testing of new therapeutics and drug combinations, in order to improve the patients outcome. Therefore, in order to elucidate the biology behind the neuroendocrine tumours and to evaluate new therapeutics for neuroendocrine tumours, we aimed to establishing a new neuroendocrine organoids culture system using adrenal glands as a starting point.

Methods:
We used a single cell culture approach of adrenal glands from wildtype and Sox10-Cre; TdTomato mice. The originated organoids were stained for neuroendocrine markers.

Results:
In a first approach, the culture of adrenal glands from wild type mice resulted in the growth of organoid structures. When stained for chromogranin A, a chromaffin cell marker, these structures show few stained cells. Moreover, when adrenal glands from *Sox10-Cre, TdTomato* mice are cultured, the generation of fluorescent organoids is observed.

Conclusion:
These evidences indicates a possible medullary origin of such structures, supporting the possibility of generation of neuroendocrine organoids.

4115

HC. Wong[1], S. Isringhausen[1], M. Manz[1], C. Nombela-Arrieta[1], A. Müller[1]

Characterization of Bone Marrow GVHD post Allogeneic Hematopoietic Cell Transplantation in Mice

Klinik für Hämatologie, Universitätsspital Zürich, Schmelzbergstrasse 12, 8091, Zürich Switzerland[1]

Introduction:
Graft-vs-Host Disease (GVHD) – common complication post allogeneic hematopoietic cell transplantation (allo-HCT). In contrast to classical target organs alloreactivity directed against hematopoietic (HC) and non-hematopoietic (NHC) bone marrow (BM) structures has been poorly characterized, even though HC dysfunction following allo-HCT is frequently observed.

Methods:
Using MHC-matched, minor-antigen-mismatched HCT models (C3H.SWàC57BL/6 (B6)), effects of lethal total body irradiation (TBI) and HCT of HSC ($cKIT^+Sca1^+Lin^-$) alone or in combination with T cells (Tc)/Tc subsets ($CD4^+$/$CD8^+$/Total (CD4+CD8) Tc) on the HC and NHC compartment of BM. Bones and marrow were analyzed by flow cytometry and 3D-imaging.

Results:
At 2w post allo-HCT recipients given pure HSC had significantly higher BM cellularity with prompt recovery of B-cells and granulocytes compared with HSC+Tc/Tc subset. Likewise, alloreactive (but not congenic) Tc severely disrupted NHC: HSC recipients showed prompt recovery of BM endothelial (EC; $CD45^-Ter119^-CD31^+$), and CXCL12-abundant reticular (CAR; $CD45^-Ter119^-CD31^-CD140B^+$) cells. In contrast, HSC+Tc recipients significantly delayed recovery with lower EC and CAR cell counts. 3D-imaging revealed rapid recovery of extracellular matrix and sinusoidal vascular structures, with simultaneous disappearance of adipocytes at 2w post allo-HCT in HSC group, whereas HSC+Tc recipients displayed severe disruption of structural integrity with impaired recovery of BM microvessels and occupation of space by adipocytes. Using B6.CXCL12-GFP recipients to visualize CAR cells by 3D-imaging, CAR cell regeneration was impaired by HSC+Tc, but not pure HSC recipients. To address the question whether alloreactive Tc exert direct GVH-related damage to NHC structures, or alternatively, only recipient's HC is attacked whereas suppression of EC and CAR cells results from the inflammatory milieu. We generated chimeras by transplanting C3H.SW-BM into TBI-B6 recipients: C3H.SW (HC) and B6 (NHC). In a 2nd HCT HSC+/-Tc were transplanted from (i) C3H.SW (allo to NHC, congenic to HC) or (ii) B6 (congenic to NHC, allo to HC) donors into these chimeras. (i) At 2w post-2nd HCT BM cellularity, EC and CAR cell numbers were decreased when donor Tc were allo to NHC, but congenic to HC. NHC populations were normal in number when pure allo HSC were given. (ii) B6 donor (allo to HC, congenic to NHC) Tc grafts given at 2w post-2nd HCT had no effect on EC numbers. CAR cell numbers were reduced, but less severe compared with transfer of allo HSC+Tc. Together, these findings suggest, EC is a direct target of alloreactive Tc; CAR cells are affected by both alloreactive Tc and inflammatory conditions generated by attack of HC. Finally, to test influence of GVH-related cytokines on NHC we used B6.$TNF\alpha R^{-/-}$ and B6.$IFN\gamma R^{-/-}$ mice as recipients of C3H.SW HSC+/-Tc. Recovery of HC and NHC was identical in WT and $TNF\alpha R^{-/-}$ recipients of C3H.SW grafts. In contrast, $IFN\gamma R^{-/-}$ recipients of allo HSC+CD4 grafts had significantly higher CAR cell counts compared with WT recipients (but lower than pure HSC recipients). These results support the hypothesis that CAR cells are also susceptible to inflammatory damage.

Conclusion:
In clinical HCT delayed HC reconstitution presents a major problem contributing to increased morbidity and mortality. GVH reactions of the BM have been poorly characterized. Our data show that not only host hematopoiesis, but also NHC stromal and vascular compartments of BM are affected by both alloreactivity of donor Tc and their inflammatory microenvironment, even in the absence of clinical GVHD.

4116

R. Chen[1], Th. Hornemann[2,4,5], W. Yu[2], S. Camarago[3], R. Graf[1,5], S. Sonda[1,5]

1-Deoxy-Sphingolipids, novel biomarkers of diabetes, are cytotoxic for exocrine pancreatic cells

Swiss Hepato-Pancreatico-Biliary(HPB) Centre, Division of Surgical Research, Department of Visceral & Transplantation Surgery, University Hospital Zurich[1], Institute for Clinical Chemistry, University Hospital Zurich[2], Institute of Physiology, University of Zurich[3], Competence Centre for Systems Physiology and Metabolic Diseases, Zurich[4], Centre for Integrative Human Physiology, University of Zurich[5]

Introduction:
Exocrine pancreatic insufficiency and exocrine function alterations are characteristics of pancreatitis. They are frequent in diabetes mellitus (DM) patients with a prevalence up to 50%. Although reduced levels of insulin may explain many of the proposed mechanisms of pancreatic dysfunction following DM, the same phenotype is also detected in insulin-independent DM. This highlights the concept that additional factors are likely to contribute to the pathophysiology of acinar cells.
We recently discovered that 1-deoxy-sphingolipids (1-deoxySLs), the levels of which increase in DM and metabolic syndrome are cytotoxic for beta cells. Our preliminary results showed that 1-deoxySLs are also cytotoxic for acinar cells *in vitro*. Furthermore, the high level of 1-deoxySLs in diabetic animal model aggravated acinar cell damage whereas lowering levels of 1-deoxySLs improved cell deterioration. In this research, we investigate molecular and cellular factors that contribute to compromise acinar cell functionality in the context of DM. Based on the endocrine and exocrine pancreas crosstalk, we hypothesize that elevated 1-dSeoxyLs levels affect directly the pancreatic exocrine compartment by compromising pancreatic acinar cells in DM, thus increasing its predisposition to develop exocrine pancreatic diseases.

Methods:
In this study, we used *in vivo* mouse models with STZ-induced diabetes and cerulein-induced pancreatitis. Reduction of 1-deoxySLs synthesis was achieved by oral L-serine supplementation. Disease severity was assessed with biochemical and immunohistochemical methods. Molecular mechanisms of 1-deoxySL-dependent toxicity were evaluated *in vitro* on AR42J pancreatic acinar cells and primary acinar cells.

Results:
DM induction resulted in increased 1-deoxySL levels but also atrophy and fibrosis of pancreatic parenchyma. Reduction of 1-deoxySL synthesis by oral L-serine supplementation ameliorated the damage of the exocrine pancreatic tissue, without restoring insulin production in beta cells. This suggests that elevated 1-deoxySLs rather than insulin deficiency contribute to the exocrine damage in DM. *In vitro* studies showed that treatment with 1-deoxysphinganine, one of the early products of 1-deoxySLs synthesis at low concentration reduced replication and promoted cytotoxicity in pancreatic acinar cells. In addition, this 1-deoxySL-mediated cytotoxicity was associated with mitochondrial dysfunction and endoplasmic reticulum stress.

Conclusion:
Our work revealed that 1-deoxySLs are cytotoxic for exocrine pancreatic cells, suggesting a role for these lipids in the exocrine dysfunctions following DM. Oral L-serine supplementation could be a therapeutic treatment for ameliorating exocrine pancreatic diseases in diabetic patients.

Keywords: **Diabetes mellitus; 1-deoxysphingolipids; pancreatitis; acinar cells**

4117

E. Malagola[1], R. Chen[1], M. Bombardo[1], E. Saponara[1], T. Reding[1], R. Graf[1], S. Sonda[1]

Deiodinase type 3 (DIO3) limits acinar cell proliferation following acute pancreatitis

Swiss-HPB Center, Department of Visceral and Transplantation Surgery, University Hospital Zurich[1]

Introduction:
Deiodinases are a class of enzymes that regulate thyroid hormones' (TH) availability within the cells. Deiodinase type 3 (DIO3) in particular is responsible for inactivation of TH. Thyroid hormones have been shown to exert a mitogenic effect on pancreatic acinar cells. In the present study we asked whether acinar cell proliferation following acute pancreatitis is dependent on TH action and is restricted by DIO3 activity.

Methods:
Pharmacological approaches were used to alter TH availability *in vivo*. Acinar specific inducible DIO3 KO mice were generated ($DIO3^{fl/fl}$ x $ELACreERT^{+/fl}$). Mice received serial injections of cerulein to induce pancreatitis. Levels of acinar cell proliferation and inflammation were investigated through immunohistochemistry as well as gene expression analysis. Serum TH levels were quantified by biochemical analyses.

Results:
Manipulation of TH levels by pharmacological or genetic strategies did not alter the initial damage incurred through cerulein application. However, the regenerative response to damage was altered. In particular, gene expression analysis revealed a pancreas specific regulation of DIO transcript levels within the acinar cells following acute pancreatitis. Pharmacological manipulation of TH levels *in vivo* demonstrated a direct correlation between circulating TH levels and acinar cell proliferation. Furthermore, genetic ablation of DIO3 in DIO3KO animals significantly increased the number of proliferating acinar cells.

Conclusion:
Our results underline that acinar cell proliferation following pancreatitis depends on TH availability. Furthermore, we observed an important role of DIO3, the TH inactivating enzyme, in restricting acinar cell proliferation following acute pancreatitis.

4118

Ph. Knobel[1], M. Pruschy[1]

The BioID method: Opportunity for translational research

Laboratory for Molecular Radiobiology, Department of Radiation Oncology, University Hospital Zürich[1]

Introduction:
The BioID-method is a relatively new molecular tool to identify protein-protein interactions due to proximity-dependent labeling of proteins by a promiscuous biotin protein (BirA) ligase in vitro and in vivo. Cellular expression of a protein of interest (bait) fused to the biotin ligase enables biotinylation of proximate proteins within approximately 10 nm. This protein labeling is initiated by the addition of biotin over a defined period to generate substantial labeling of proximal interacting proteins and therefore creating a history of protein-protein interactions. Following cell lysis and protein denaturation, biotinylated proteins are captured by affinity purification for identification by mass spectrometry. There are several advantages to normally used techniques such as immunoprecipitation.

1) The BioID-method can be applied in vitro and in vivo.
2) The proximity-dependent labeling of proteins is applied over a defined period and therefore identifies additionally low abundant, fast and transient interactors.
3) Due to mild washing conditions, weak protein interactors and protein interactor complexes are preserved.

In the laboratory for Molecular Radiobiology, we are generating a functional BioID system in a clinically relevant orthotopic lung tumor model in immune competent mice in order to reveal a history of protein-protein interactions in the tumor microenvironment. This leads to additional druggable targets in a clinically relevant tumor model.

Methods:
1) Fusion of the BirA enzyme with the gene of interests. 2) Expression of the fusion protein in cell lines that will be used in cell cultures and mouse tumor models. 3) Analysis of correct localization and functionality using western blot and immunofluorescence technique. 4) Preparation of the cell lines in culture or in an ortothopic lung tumor model. After administering biotin, the BirA ligase biotinylates over a defined period all proteins that are in close proximity to your protein of interest. 5) Biotinylated proteins isolated from the cell lines or the tumors are lysed, purified and identified by mass spectrometry.

Results:
Others and we have successfully established and applied the BirA method and shown that it represents a strong tool for the identification of protein-protein interaction networks. New interactors could be identified that were not detectable with other techniques such as immunoprecipitation.

Conclusion:
The BioID method has been applied to study protein-protein interactions and therefore explore new molecular mechansims in distinct subcellular locations in many organisms such as mammalian cells *in vitro* and *in vivo*, unicellular organisms such as Trypanosoma brucei, Toxoplasma gondii, Dictyostelium discoideum and Plasmodium berghei or host-pathogen systems such as Viral and Bacterial infection. A future step is applying the BioID method in clinically relevant tumor models in order to understand the plasticity of protein-protein interactions in the tumor microenvironment and discover new druggable targets that can be tested in clinical trials.

4119

C. Pothmann[1]; H.-C. Pape[1], H.-P. Simmen[1], V. Neuhaus[1]

Does the immunosuppressive therapy influence postoperative fracture healing after organ transplantation?

Department of Trauma Surgery, University Hospital Zürich[1]

Introduction:
Within the last years, the number of people with transplanted organs, as well as their lifetime and quality of life after organ transplantation (TPL) increased. They actively participate in everyday life and suffer fractures. Do patients after TPL and under immunosuppressive therapy show impaired fracture healing?

Methods:
A retrospective analysis of the trauma database of a level one trauma centre was made. Immunosuppressed patients after TPL treated with an osteosynthesis between 2004 and 2016 were included. Patients had regular radiological and clinical follow-up. The fracture healing time was assessed and compared with patients without immunosuppressive therapy of this hospital and of standard surgical reference works. The reference group was matched and paired by age at the time of fracture, gender, type/location of fracture and technique of osteosynthesis.

Results:
29 patients (15 male, 14 females, mean age 43 years) after TPL with overall 40 fractures were included in the analysis. 13 kidney-TPL, 6 lung-TPL, 5 liver-TPL, 3 heart-TPL, 2 kidney/pancreas-TPL. All patients got treated with at least two immunosuppressive drugs. The age of the reference group was comparable (paired t-test 0.753). Cause of accident: 37.5% sports/leisure, 35% work/household, 12.5% traffic accidents, 5% without trauma. The operation was performed under perioperative long-term antibiosis, often with a combination of two or three drugs. Patients were hospitalized for an average duration of 11.3 days and were also examined by the particular organ specialists. Osteosynthesis: in 90% primary operative fracture treatment, in 10% two-step procedure. 11 plates distal radius and ulna [healing period (h) 14 weeks (w)], 3 plates tibia [h 20 w], 3 plates fibula [h 11 w], 9 nails femur [h 51 w], 3 plates clavicle [h 51 w], 4 spondylodesis spinal column [h 24 w], 3 plates/screws pelvis/sacrum [h 7 w], 1 tension band wiring patella [h 49 w], 3 plates humerus [h 34 w]. Compared to the paired references the time of fracture healing was significantly prolonged ($p<0.001$). Complications: 1 wound infection, 2 hematomas, 1 non-union, 2 persistent pains, 2 secondary displacement/lysis/material breakage; 3 operative revisions.

Conclusion:
The fracture healing under immunosuppressive therapy after TPL was significantly delayed. The immunosuppressive therapy may be responsible for these problems. We recommend surgical standard techniques should be applied, rehabilitation of movement and weight bearing has to be adapted.

Conference Location

University Hospital Zurich
Grosser Hörsaal Ost
Rämistrasse 100
8091 Zürich

Contact Address

Prof. Dr. med. Gabriela Senti
Direktorin Forschung und Lehre
UniversitätsSpital Zürich
Rämistrasse 100 / MOU 2
8091 Zürich

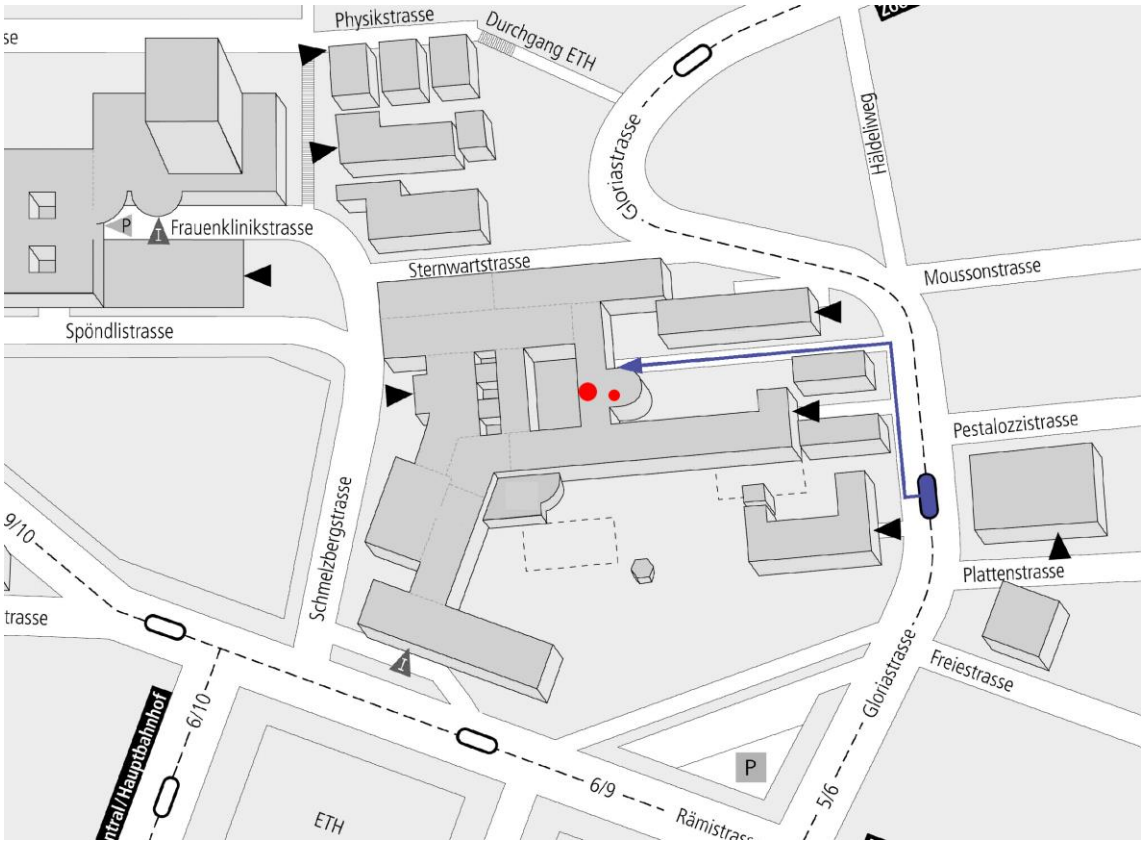

UniversitätsSpital
Zürich